ENGINEERING *SACCHAROMYCES CEREVISIAE* WITH ENHANCED SUPPLY OF PRECURSOR METABOLITES FOR EFFICIENT PRODUCTION OF FUELS AND CHEMICALS

BY

JIAZHANG LIAN

DISSERTATION

Submitted in partial fulfillment of the requirements
for the degree of Doctor of Philosophy in Chemical Engineering
in the Graduate College of the
University of Illinois at Urbana-Champaign, 2015

Urbana, Illinois

Doctoral Committee:

Professor Huimin Zhao, Chair
Associate Professor Christopher Rao
Associate Professor Charles Schroeder
Associate Professor Yong-Su Jin

Abstract

Saccharomyces cerevisiae has been widely established as a platform microorganism for industrial production of a wide variety of products including but not limited to ethanol, organic acids, amino acids, enzymes, and therapeutic proteins, owing to its high tolerance to harsh industrial conditions, such as low pH, high sugar concentration and growth inhibitors in the biomass hydrolysate, as well as resistance to phage infection. However, one of the major challenges for high level production of value-added compounds other than ethanol is the strong fluxes for ethanol formation even under aerobic condition, a phenomenon known as Crabtree effect. Notably, a wide variety of products with industrial interest are derived from a few precursor metabolites, such as 2,3-butanediol (BDO) and *iso*-butanol from pyruvate, *n*-butanol, polyhydroxybutyrate, and isoprenoids from acetyl-CoA, and free fatty acids, fatty alcohols, and fatty acid ethyl esters from long chain acyl-CoAs. Therefore, metabolic engineering and synthetic biology approaches were applied to engineer *S. cerevisiae* with enhanced supply of these precursor metabolites for efficient production of fuels and chemicals. More importantly, these engineering efforts can be integrated to construct a platform yeast cell factory, since pyruvate is the direct precursor for acetyl-CoA generation and enhanced acetyl-CoA levels will provide a driving force for acyl-CoAs pool engineering.

To construct a pyruvate overproducing yeast strain, three structural genes encoding pyruvate decarboxylases, *PDC1*, *PDC5*, and *PDC6* were deleted to completely eliminate ethanol production. Followed by overexpression of *MTH1* and adaptive evolution, the resultant Pdc^- yeast strain grew on glucose as the sole carbon source with pyruvate as the major product. Subsequent introduction of a BDO biosynthetic pathway resulted in the production of BDO at a

yield over 70% of the theoretical value and a titer higher than 100 g/L using fed-batch fermentation.

To engineer acetyl-CoA pool in *S. cerevisiae*, alternative acetyl-CoA biosynthesis routes were characterized using synthetic biology approaches and metabolic engineering was applied to redirect the metabolic fluxes towards acetyl-CoA biosynthesis. Acetyl-CoA biosynthetic pathways from *Escherichia coli* (pyruvate dehydrogenase, PDH) and *Yarrowia lipolytica* (ATP-dependent citrate lyase, ACL) were found to enable the growth of the Acs^- (*acs1*Δ *acs2*Δ) strain on glucose as the sole source. To construct a functional PDH in the cytosol of yeast, different lipoylation pathways were introduced and engineered. Besides the naturally existing scavenging pathway and *de novo* biosynthetic pathway, we also designed a semi-synthetic lipoylation pathway based on the acyl-ACP synthetase (AasS). The scavenging pathway resulted in a functional PDH that enabled the growth of Acs^- strain to a similar level of the wild-type strain. The *de novo* biosynthetic lipoylation pathway was hindered by the difficulty in reconstituting a functional type II fatty acid synthase (FAS) in the cytosol to provide the precursor (octanoyl-ACP) for protein lipoylation. The introduction of the semi-synthetic lipoylation pathway (Vh*AasS*-cyto*ACP1*-cyto*PPT2*) resulted in functional PDH and rescued the growth of the Acs- strain when octanoic acid was supplementated. Based on these results, a *de novo* biosynthetic lipoylation pathway was re-designed and proposed. Then these heterologous biosynthetic pathways were combined with host engineering to design and construct acetyl-CoA overproducing yeast strains. By deleting *ADH1*, *ADH4*, *GPD1*, and *GPD2* involved in ethanol and glycerol formation, the glycolytic flux was redirected towards this precursor metabolite, resulting in a 4 fold improvement in *n*-butanol production. Subsequent introduction of alternative acetyl-CoA biosynthetic pathways, the production of *n*-butanol was further increased. Although

significant improvement of *n*-butanol production was achieved, the final titer was still much lower than that of ethanol and the resultant yeast strains suffered from accumulation of the toxic intermediates such as acetaldehyde and acetate. Therefore, more efforts were put into the engineering of acetyl-CoA pools in the Pdc^- strain, where ethanol production was completely eliminated and pyruvate was accumulated to high levels.

To engineer acyl-CoAs levels in *S. cerevisiae*, a new biosynthesis platform based on the reversal of β-oxidation cycle was constructed using synthetic biology approaches. Compared with the conical FAS, which is ATP, ACP, and NADPH dependent, the reversed β-oxidation pathway is featured for its ATP and ACP independence and CoA and NADH dependence. The energetic benefits of ATP independence and availability of CoA and NADH versus ACP and NADPH confer advantages for acyl-CoAs biosynthesis. Reversed β-oxidation pathways were constructed and found to produce *n*-butanol, decanoic acid, and ethyl decanoate, indicating the functional reversal of β-oxidation cycle at least 4 turns.

To facilitate the engineering in *S. cerevisiae*, new synthetic biology tools was also developed. First, plasmids with step-wise increased copy numbers (20-100 copies per cell) were constructed by engineering the expression level of selection marker proteins, including both auxotrophic and dominant markers. More importantly, the copy number of the plasmids with engineered dominant markers (5-100 copies per cell) showed a positive correlation with the concentration of antibiotics supplemented to the growth media. Based on this finding, a new and simplest synthetic biology approach named induced pathway optimization by antibiotic doses (iPOAD) was developed to optimize the performance of multi-gene biosynthetic pathways by different combination of antibiotic concentrations in *S. cerevisiae*. To demonstrate this approach, iPOAD was applied to optimize the lycopene and n-butanol biosynthetic pathways, with the

production of lycopene and *n*-butanol increased by 10- and 100-fold, respectively. Finally, the iPOAD optimized pathway was integrated to chromosomes to increase the strain stability and eliminate the requirement of antibiotic supplementation, by taking advantage of the iPOAD and CRISPR-Cas9 technologies for multiplex pathway integration.

To My Family

Acknowledgements

First and foremost, I would like to thank my advisor Huimin Zhao for his guidance on these projects. He not only trained my experimental skills, but also the essence to be a good researcher. He is also acknowledged for persuading me to join the University of Illinois at Urbana-Champaign and his group to start my academic life and his continuous help in preparing for my future career. I would also like to thank my committee members, Professor Christopher Rao, Professor Charles Schroeder, and Professor Yong-Su Jin for their insightful input, constructive suggestions, and generous help.

I am also very thankful to all Zhao Group members for their helpful discussions, friendship, and assistance, especially Yongbo Yuan, Ran Chao, Tong Si, Xueyang Feng, Sijin Li, Jing Du, Byoungjin Kim, Sam Hamedi Rad, Dan Coursolle, Meng Wang, and Dawn Eriksen to work together as a team in the Energy Biosciences Institute. For the pyruvate pool engineering project, I would like to thank Ran Chao for his help in setting up bioreactors for fed-batch fermentation. For the acetyl-CoA pool engineering project, I would like to thank Tong Si and Nikhil U. Nair for their preliminary but essential results. For the acyl-CoAs engineering project, I would like to thank Ran Chao and Zehua Bao for their help in cloning FOX2 homologs from different yeast species. For the iPOAD project, I would like to thank my undergrad researcher, Jin Run, who did most of cloning and characterization of the plasmids with different copy numbers, and Dr. Sijin Li for her help in flow cytometry. Dr. Xueyang Feng is acknowledged for the collaboration on the fatty alcohol project. Dr. Han Xiao is appreciated for her help and suggestions on the design of Di-CRISPR. I would like to thank Dr. Mingzi Zhang from the Zhao Group @Singapore (Metabolic Engineering Research Lab, A*STAR, Singapore) for her insightful discussion and collaboration in the BDO project. I would like to thank Dr. Alvaro

Hernandez from Roy J. Carver Biotechnology Center at the University of Illinois at Urbana-Champaign for his help in next generation sequencing. I would like to thank Mohammad (Sam) Hamedi Rad for his help in the CDT2 engineering project, which is not presented in this thesis though. I also would like to thank Dr. Mayandi Sivaguru from the Core Facilities at the Institute for Genomic Biology at the University of Illinois at Urbana-Champaign for his help with the confocal microscopy, although these results were not presented in the thesis either.

I would like to thank Prof. John Cronan from our campus to share the Vh*AasS* containing plasmid (pYFJ84), Prof. Jens Nielsen from Chalmers University of Technology to provide pIYC08 (acetyl-CoA engineering plasmid) and pJC2 (NADPH engineering plasmid), Prof. Christer Larsson from Chalmers University of Technology to provide the MEK and 2-butanol producing plasmids, and Dr. Mingzi Zhang to share the *meso*-BDO biosynthetic pathway.

Finally, I would like to express my most sincere gratitude to my wife Jiewen Zhou, my son Lucas Lian, my parents, and my friends for their constant support and unconditional love.

Table of Contents

Chapter 1 Introduction

1.1 Yeast Cell Factory

Biological conversion of renewable feedstock into fuels and chemicals has been intensively investigated due to increasing concerns on sustainability and global climate change (1). Many chemicals, such as lactic acid, succinic acid, and *iso*-butanol, used to be produced by chemical processes are synthesized biologically with microbial fermentation. Microorganisms are able to convert a wide range of substrates, such as plant biomass and agricultural waste, to value-added chemicals and fuels, promising a low carbon economy and sustainable future. Biofuels and chemicals are preferred to be produced at large scales using industrially friendly hosts such as *Escherichia coli* and *Saccharomyces cerevisiae*. Besides these two model microorganisms, cyanobacteria (2) and oleaginous yeasts (3) have also been explored as cell factories. Compared with its counterparts, *S. cerevisiae* is more industrially relevant thanks to the well-studied genetic and physiological background, the availability of a large collection of genetic tools, the compatibility of high-density and large-scale fermentation, the resistance to phage infection, and the high tolerance against toxic inhibitors and products (4). Therefore, *S. cerevisiae* is one of the most popular cell factories and has been successfully used in modern fermentation industry to produce a wide variety of products including but not limited to ethanol, organic acids, amino acids, enzymes, and therapeutic proteins (1, 4).

Compared with ethanol, the production of other molecules, especially advanced biofuels and low value-added chemicals, using yeast cell factories is less successful, in terms of the titer, yield, and productivity. One major reason is due to the well-known Crabtree effect: most of the glycolytic fluxes going through ethanol formation even under respiration conditions. Thus,

various metabolic engineering strategies have been applied to redirect the metabolic fluxes from ethanol to the desired products, such as the inactivation of the alcohol dehydrogenases (*ADH*s) (5) or the pyruvate decarboxylases (*PDC*s) (6, 7). Notably, a wide variety of products with industrial interests are derived from a few precursor metabolites, such as lactate, 2,3-butanediol (BDO), and *iso*-butanol from pyruvate, *n*-butanol, polyhydroxybutyrate (PHB), and isoprenoids from acetyl-CoA, and free fatty acids (FFAs), fatty alcohols (FALs), alkanes, and fatty acid ethyl esters (FAEEs) from long chain acyl-CoAs (Figure 1.1). Therefore, the design and construction of *S. cerevisiae* strains with enhanced supply of these precursor metabolites, including pyruvate, acetyl-CoA, and acyl-CoAs, will develop this yeast as a platform cell factory for efficient production of biofuels and chemicals besides ethanol.

1.2 Engineering Pyruvate Metabolism

As an end product of glycolysis, pyruvate is the branch point to control the flow of metabolic fluxes, especially for respiration and fermentation. In addition, pyruvate is the precursor for the production of a wide range of fuel and chemical molecules, such as ethanol, *iso*-butanol, 2,3-butanediol, lactate, malate, and succinate (7). In *S. cerevisiae*, there are three major fates of pyruvate metabolism, pyruvate decarboxylase (PDC) mediated ethanol fermentation, pyruvate dehydrogenase (PDH) mediated acetyl-CoA generation and respiration, and pyruvate carboxylase (PYC) initiated gluconeogenesis (8).

1.2.1 Distribution of glycolytic fluxes at the pyruvate branch

How the carbon flow is controlled at the pyruvate branch is an interesting and ongoing study. Although the K_M of PDH (0.6 mM at pH8.1 and 0.2 mM at pH6.5) (9) and PYC (c.a. 0.8 mM) (10) towards pyruvate is an order of magnitude lower than that of pyruvate decarboxylase

(c.a. 5 mM, 1-3 mM in the absence of phosphate, fourfold higher in the presence of 25 mM phosphate, while normal intracellular phosphate concentration in *S. cerevisiae* is 5-15 mM) (11), most of the metabolic fluxes go through ethanol fermentation even under aerobic conditions. The first explanation of such dilemma is due to glucose repression (also known as Crabtree effect), meaning that the expression or enzymatic activities of respiratory proteins are inhibited by the presence of glucose (12). Another explanation lies in the higher capacity (V_{max}) of PDC. It is estimated that the capacity of mitochondrial pyruvate oxidation is at least ten-fold lower than that of pyruvate decarboxylase (8).

1.2.1.1 Pyruvate dehydrogenase (PDH)

The PDH complex consists of three major catalytic components, El, E2, and E3, which are encoded by *PDA1* and *PDB1*, *LAT1*, and *LPD1*, respectively. A fourth component X encoded by *PDX1* does not have any catalytic function but may be involved in the assembly of the complex (9). In the first step, pyruvate is covalently linked to thiamine pyrophosphate (TPP), the cofactor of El, to form acetaldehyde-TPP (the active aldehyde). Then the acetaldehyde group is oxidized and the resulting acetyl moiety is coupled to the lipoamide cofactor of E2, which is subsequently transferred to CoA. During the oxidation of the active aldehyde, the E2 lipoamide group is reduced to dihydrolipoamide, whose reoxidation is catalyzed by E3 using NAD^+ as the electron acceptor. Overall, one acetyl-CoA molecule and an NADH reducing force are generated from one pyruvate molecule. The disruption of the PDH structural genes, including *PDA1*, *PDB1*, *LAT1*, and *PDX1*, results in complete loss of pyruvate dehydrogenase activity. Interestingly, these Pdh^- strains do not have significant growth defects compared with the wild-type strain, indicating that acetyl-CoA generated by the PDH-bypass pathway in the cytosol is sufficient for cellular demands.

1.2.1.2 Pyruvate decarboxylase (PDC)

PDC catalyzes the TPP- and Mg^{2+} -dependent decarboxylation of pyruvate to acetaldehyde and CO_2. The pyruvate decarboxylation activity results from the expression of three structural genes, *PDC1*, *PDC5*, and *PDC6*, whose expression levels are dependent on the transcription factor, Pdc2p (13). While *PDC1* is highly expressed under most of the conditions tested, the expression level of *PDC5* is much higher in the *PDC1* deletion strain, suggesting an auto-regulation system of the expression of PDC genes (14). Interestingly, although the PDC6 sequence has a high similarity with PDC1 and PDC5, its expression is not detectable in the wild-type *S. cerevisiae* strain. The disruption of all three structural genes (*pdc1*Δ *pdc5*Δ *pdc6*Δ) completely abolishes PDC activity. The resulting Pdc^- strain cannot grow in defined medium with glucose as the sole carbon source, although its growth on ethanol is not affected (15). Since PDC activity is required for acetyl-CoA generation in the cytosol, the growth of the Pdc^- strain in glucose minimal medium is possible only when a C_2 compound such as acetate or ethanol is supplemented. It is suggested that the inability of the Pdc^- strain to grow in glucose minimal medium might result from two factors, glucose repression of the expression of respiratory genes and a lack of route to generate cytosolic acetyl-CoA.

1.2.1.3 Pyruvate carboxylase (PYC)

Pyruvate carboxylase, encoded by *PYC1* and *PYC2* in *S. cerevisiae*, catalyzes the anaplerotic synthesis of oxaloacetate from pyruvate (10). Oxaloacetate produced by PYC is an important intermediate, which plays a crucial role in gluconeogenesis and lipogenesis. Gluconeogenesis, a metabolic pathway for the generation of glucose from non-carbohydrate carbon substrates, begins with the formation of oxaloacetate by the carboxylation of pyruvate at

the cost of one ATP molecule. PYC is stimulated by high levels of acetyl-CoA and inhibited by high levels of ADP and glucose. Although PYC in higher eukaryotes is located in the mitochondria, both Pyc1p and Pyc2p are completely cytosolic in *S. cerevisiae*. When both *PYC1* and *PYC2* are disrupted, the resulting Pyc^- strain cannot grow in glucose as the sole carbon source. Growth of this pyruvate carboxylase-negative (Pyc^-) mutant is possible when aspartate instead of ammonium is provided as the primary nitrogen source, thus by-passing the anaplerotic function of pyruvate carboxylase (16). Although oxaloacetate can also be synthesized by the glyoxylate cycle, the inability of Pyc^- strains to grow on glucose indicates that the glyoxylate-cycle enzymes (such as the isocitrate lyase) are repressed or even inactivated in the presence of glucose. Interestingly, a dominant suppressor mutation (*DGT1-1*), which causes a reduced uptake of glucose and thus alleviates glucose catabolite repression, has been isolated which allows Pyc^- strain to grow on glucose defined medium (17).

1.2.2 Engineering at the pyruvate branch for biosynthesis

As mentioned above, since most of the glycolytic fluxes go through ethanol fermentation even under aerobic conditions, PDC is often chosen as the major target for metabolic engineering. Unfortunately, the Pdc^- strain (either *pdc2*Δ or *pdc1*Δ *pdc5*Δ *pdc6*Δ) is notorious for its inability to grow on glucose as the sole carbon source and the requirement of a C_2 compound (acetate or ethanol) supplementation to synthesize cytoplasmic acetyl-CoA (15). Inverse metabolic engineering revealed that an internal deletion in the *MTH1* coding sequence enabled the growth of Pdc^- strain on glucose (18, 19). In another study, a mutation in the Mth1p coding sequence (Ala81Pro) was also found in the evolved Pdc^- strain that was able to grow on glucose as the sole carbon source (20). Mth1p is a transcription factor involved in glucose sensing which can inhibit the expression of hexose transporter genes (*HXT*s), thus the uptake of glucose. The internal

deletion or single amino acid mutation increases the stability of Mth1p by removing the putative sites related to protein degradation (19), maintaining the intracellular glucose concentration to a low level and alleviating glucose repression.

However, how cytosolic acetyl-CoA is generated in the evolved Pdc$^-$ strain is still an interesting question. Previously work indicated that acetaldehyde generated by the cleavage of threonine, a reaction catalyzed by threonine aldolase (encoded by *GLY1*), might serve as a precursor for the synthesis of cytosolic acetyl-CoA (21). A recent study (22) also confirmed that Ach1p, the acetyl-CoA hydrolase (later renamed as CoA transferase) located in the mitochondria, might function as the acetyl-CoA shuttle between the mitochondria and the cytosol in the form of acetate. In wild-type *S. cerevisiae* strain, the expression of *ACH1* was repressed in the presence of glucose; while in the evolved Pdc$^-$ strain, glucose repression was alleviated and Ach1p was functionally expressed. Acetyl-CoA was hydrolyzed by Ach1p in the mitochondria to release acetate, which could freely exit mitochondria and be re-activated by acetyl-CoA synthetase to form acetyl-CoA in the cytosol.

Since pyruvate is accumulated to a level as high as 135 g/L (6), the Pdc$^-$ strain can be developed into an important platform cell factory to produce a wide range of biofuels and value-added chemicals other than ethanol, including but not limited to *iso*-butanol, 2,3-butanediol, lactate, malate, succinate, and glycerol. Lactate with a titer up to 110 g/L could be obtained in a Pdc$^-$ strain expressing an *LDH* gene from *Lactobacillus casei* in 1 L fermenter under aerobic conditions (7). High titer and yield production of 2,3-butanediol was also reported using an evolved Pdc$^-$ strain overexpressing an acetolactate synthase (*alsS*) and acetolactate decarboxylase (*alsD*) from *Bacillus subtilis* as well as the endogenous butanediol dehydrogenase (*BDH1*) from various carbon sources, such as glucose (20), cellobiose (23), and xylose (24). The highest

production was achieved using glucose fed-batch fermentation, with a titer and yield as high as 96.2 g/L and 0.28 g/g, respectively (20). Fermentative production of malate using the Pdc$^-$ strain was also attempted by combined overexpression of a pyruvate carboxylase (*PYC2*), a cytosolically located malate dehydrogenase (*MDH3ΔSKL*) and a malate transporter from *Schizosaccharomyces pombe* (Sp*MAE1*). Malate titer of up to 59 g/L was reached with a yield of 0.42 mol/mol glucose in shake flask fermentation (25). Recently, the malate producer was further engineered to produce succinate. Under optimal conditions in a bioreactor, the engineered strain produced around 13 g/L succinate with a yield of 0.21 mol/mol glucose at low pH (26). Although glycerol is not directly derived from pyruvate, the elimination of ethanol formation in the Pdc$^-$ strain may redirect the metabolic fluxes to glycerol formation, especially under low-oxygen or anaerobic conditions. By further engineering cytosolic NADH availability and overexpressing *GPD2*, glycerol titer of higher than 50 g/L and yield as high as 1.08 mol/mol glucose were achieved in aerobic and glucose-limited chemostat cultures with formate co-feeding (27).

1.3 Engineering Acetyl-CoA Metabolism

As a central metabolite, acetyl-CoA plays important roles in a series of cellular functions. It's also a key precursor in the biosynthesis of sterols, amino acids, fatty acids, and polyketides. In *S. cerevisiae*, acetyl-CoA metabolism occurs in various compartments, including mitochondria, peroxisomes, nucleus, and cytosol (28). In the cytosol where biosynthesis generally occurs, acetyl-CoA is generated via the PDH-bypass pathway, from pyruvate to acetaldehyde and then to acetate, which is activated to acetyl-CoA by the acetyl-CoA synthetase (ACS) at the cost of two ATP equivalents (Figure 1.3). Due to the feedback inhibition of ACS and high energy input requirement, the activation of acetate is a rate-limiting step. In addition, due to the Crabtree effect, the glycolytic fluxes mainly go through ethanol formation and the

supply of acetyl-CoA is very limited. Several metabolic engineering strategies have been attempted to boost the availability of acetyl-CoA in the cytosol of yeast, such as to redirect the metabolic fluxes to acetyl-CoA biosynthesis, to inactivate the competing pathways, and to introduce heterologous biosynthetic pathways with higher efficiency and lower energy input requirement (Figure 1.3).

1.3.1 Metabolic engineering to redirect the metabolic fluxes

Due to the Crabtree effect, most of the metabolic fluxes go through ethanol formation during glucose fermentation in *S. cerevisiae*, which means that the central metabolism of yeast should be engineered to redirect the metabolic fluxes to acetyl-CoA biosynthesis. As shown in Figure 1.3, acetaldehyde is the branch point to control the flux distribution between ethanol and acetyl-CoA. Therefore, the inactivation of alcohol dehydrogenases (*ADH*s) was chosen as first the metabolic engineering target. By the deletion of *ADH1*, a major *ADH* responsible for ethanol fermentation, 1.9-fold improvement in FFAs production was achieved in a fatty acids producing host (29). The major concerns with *ADH* inactivation are the poor growth of the resultant yeast strain resulted from the accumulation of the toxic intermediates [acetaldehyde and acetate] and the residual production of ethanol as the major product due to the redundancy of *ADH*s in the *S. cerevisiae* genome (5, 30).

Since most of the acetyl-CoA involved reactions are essential to maintain cellular functions, there were not many successful examples by eliminating the acetyl-CoA consuming pathways. Most current efforts targeted toward the glyoxylate shunt, which contributes to the transport and consumption of cytosolic acetyl-CoA in yeast (28, 31). The glyoxylate shunt can be disrupted by knocking out *CIT2* or *MLS1*, which encodes peroxisomal citrate synthase and

cytosolic malate synthase, respectively (31). Compared with the reference strain with an intact glyoxylate shunt, the inactivation of *CIT2* or *MLS1* increased the production of α-santalene by 1.36- and 2.27-fold (32), 3-hydroxypropionic acid (3-HP) by 1.19- and 1.20-fold (33), and *n*-butanol by 1.58- and 1.36-fold (34), respectively. Interestingly, it was found that the production of polyhydroxybutyrate (PHB) was impaired in the *cit2*Δ or *mls1*Δ yeast strain (35).

In terms of the acetyl-CoA consuming pathways that are essential for cell survival, such as the biosynthesis of sterols and amino acids down regulating the expression of genes encoding the initial or rate-limiting enzymes of these biosynthetic pathways, such as *ERG10* and *HMG1* in the sterols pathway, will be more desirable rather than completely eliminating the enzyme activity by gene knockout. Basically, the expression of essential genes can be knocked down by replacing the endogenous promoter with a very weak or inducible/repressible one (36). A more powerful and flexible strategy is to reconstruct the RNA interference (RNAi) machinery in *S. cerevisiae* and knock down the targeted genes with the customized small interfering RNA (37-39).

1.3.2 Synthetic biology for alternative acetyl-CoA biosynthetic pathways

Due to feedback inhibition and high energy input requirement, the endogenous PDH-bypass pathway suffered from low efficiency for acetyl-CoA biosynthesis. To overcome such limitations, a feedback inhibition insensitive ACS mutant from *Salmonella enterica* ($SeAcs^{L641P}$) (32, 34, 35, 40) and/or alternative acetyl-CoA biosynthetic pathways with less energy input requirement (Figure 1.3) have been introduced to boost the availability of acetyl-CoA in yeast (41, 42). Notably, improved production of amorphadiene (40), α-santalene (32), PHB (35, 41), *n*-butanol (34), 3-HP (33), and FFAs (42) were achieved by engineering the acetyl-CoA pool in *S.*

cerevisiae. Considering the significance of acetyl-CoA in cellular metabolism, nature has evolved various routes to synthesize acetyl-CoA under different conditions. The biosynthetic routes of acetyl-CoA from central metabolites, such as pyruvate, acetate, and citrate, and their (potential) applications in improved production of fuels and chemicals in yeast are discussed below.

1.3.2.1 Engineered PDH-bypass pathway

Although ACS was determined to be rate-limiting, the overexpression of the endogenous *ACS1* or *ACS2* led to no or limited improvement in acetyl-CoA levels in yeast (40). It was found that ACS was post-translationally deactivated via acetylation (43). In other words, ACS is subject to feedback inhibition by acetyl-CoA. A point mutation at the acetylation position could maintain ACS at the active form and increase the acetyl-CoA supply, one such example is the feedback inhibition insensitive ACS mutant from *Salmonella enterica* ($SeAcs^{L641P}$). In wild-type yeast strains, the supply of acetate was found to limit acetyl-CoA biosynthesis as well. Thus, upstream genes including ethanol dehydrogenase (*ADH2*) and/or aldehyde dehydrogenase (*ALD6*) were co-expressed with $Se\mathit{Acs}^{L641P}$ to direct the metabolic fluxes to acetate and then acetyl-CoA biosynthesis. By introducing the engineered PDH-bypass pathway, the production of α-santalene was increased by 1.75-fold (32), amorphadiene by 1.22-fold (40), 3-HP by about 1.50-fold (33), PHB by 18-fold (35), and *n*-butanol by 3.10-fold (34), respectively. In another study, the production of FALs could be increased from 140 mg/L to 236 mg/L by introducing such an acetyl-CoA boosting pathway into the engineered yeast strain with increased fluxes to fatty acid biosynthesis (FAB).

1.3.2.2 Pyruvate dehydrogenase (PDH), pyruvate:ferrodoxin oxidoreductase (PFO), and pyruvate:$NADP^+$ oxidoreductase (PNO)

PDH catalyzes the oxidative degradation of pyruvate to generate acetyl-CoA in an ATP-independent manner (Figure 1.3), which is the most widely existed and probably the most efficient route for acetyl-CoA generation. Unfortunately, PDHs are only found in prokaryotes and eukaryotic organelles. By expressing the mitochondrial PDH structural genes without the mitochondrial targeting sequences (*PDA1-PDB1-PDX1-LAT1-LPD1*) or the bacterial PDH genes (*lpdA-aceE-aceF*), a new route of acetyl-CoA biosynthesis can be constructed in the cytosol of yeast. As mentioned above, TPP, FAD, NAD^+, and lipoic acid are used as cofactors for PDH catalyzed reactions. TPP, FAD, and NAD^+ are readily available in the cytosol of yeast, while lipoic acid is only present in the mitochondria. Recently, functional expression of PDH complex in the cytosol of yeast was achieved by co-expressing PDH structural genes (*pdhA pdhB aceF lpd*) and protein-lipoate ligase genes (*lplA lplA2*) from *Enterococcus faecalis*. When lipoic acid was supplemented to the growth medium, functional PDH complex can fully replace the endogenous pathway for cytosolic acetyl-CoA synthesis, with a growth rate similar to the wild-type yeast strain (44). Although it has been validated by growth complementation, functional PDH in the cytosol has not been used for metabolic engineering applications yet.

Rather than PDH, some anaerobic fungi use pyruvate:ferrodoxin oxidoredutase (PFO) (45) or pyruvate:$NADP^+$ oxidoreductase (PNO) (46) for oxidative degradation of pyruvate to generate acetyl-CoA. Instead of NADH, reduced ferrodoxin and NADPH are released as reducing agents by PFO and PNO, respectively (Figure 1.3). Compared with other routes for acetyl-CoA generation, PNO possesses several advantages to construct an acetyl-CoA overproducing strain for FAB, since it supplies both acetyl-CoA and NADPH and functions

under anaerobic conditions in an ATP-independent manner (46). Interestingly, PNO is a fusion protein with an N-terminal PFO domain fused to a C-terminal flavoprotein domain, which transports electrons from the FeS clusters of the PFO domain to NADPH (47).

1.3.2.3 Pyruvate:formate lyase (PFL)

Pyruvate:formate lyase (PFL) was reported to be able to fully replace the endogenous pathway for cytosolic acetyl-CoA generation (48). PFL is generally found in prokaryotes for acetyl-CoA biosynthesis under anaerobic conditions, but also in some anaerobic eukaryotes. Different from PDH, PFO, or PNO, which generates acetyl-CoA via oxidative decarboxylation of pyruvate, PFL follows a radical chemistry to convert pyruvate into acetyl-CoA and formate (Figure 1.3). PFL was tested in the Ald$^-$ (*ald2*Δ *ald3*Δ *ald4*Δ *ald5*Δ *ald6*Δ) and/or Acs$^-$ (*acs1*Δ-*acs2*Δ) yeast strains as an alternative route for acetyl-CoA biosynthesis (48). Neither Ald$^-$ nor Acs$^-$ yeast strain can grow on glucose as the sole carbon source due to the lack of a route for cytosolic acetyl-CoA generation. The introduction of PFL rescued the growth on glucose as the sole carbon source under strictly anaerobic conditions, accompanied with the production of formate (48). The growth rate of the Ald$^-$ or Acs$^-$ strain with PFL was lower than that of the wild-type strain, and the application for the production of acetyl-CoA derived molecules has not been evaluated yet. Considering the accumulation of formate in the PFL containing yeast strain, NADH can be generated by co-expression of a formate dehydrogenase (*FDH*) (49) and used as a reducing force for biosynthesis.

1.3.2.4 Pyruvate oxidase (POX)

Pyruvate oxidase, also named as phosphate-dependent pyruvate oxidase, converts pyruvate directly to acetyl-phosphate, CO_2, and H_2O_2 under aerobic conditions. TPP and FAD

are the two cofactors involved in this enzymatic reaction. Although acetyl-CoA can be readily generated by PDH under aerobic conditions at higher efficiency and without the production of toxic compound, it is found that PoxB is used preferentially at low growth rates and that *E. coli* benefits from being able to convert pyruvate to acetyl-CoA by a seemingly wasteful route (50).

1.3.2.5 Acetylating aldehyde dehydrogenase (A-ALD)

The activation of acetate is so ATP intensive that it constrains the maximal yield of the acetyl-CoA derived products. In addition, the supply of acetyl-CoA is even more limited under anaerobic conditions, a preferred process for industrial applications. Many prokaryotes contain an acetylating acetaldehyde dehydrogenase (A-ALD), which catalyzes the reversible conversion of acetaldehyde and acetyl-CoA in an ATP-independent manner (Figure 1.3). As a proof of concept, A-ALD was also tested in the Ald^- and/or Acs^- yeast strains as an alternative route for acetyl-CoA biosynthesis (48). Among different bacterial A-ALDs, EutE from *E. coli* (EcEutE) was determined to possess the highest activity and enable the highest specific growth rate on glucose. Although A-ALD could fully replace the endogenous acetyl-CoA biosynthetic route, the engineered strains still grew more slowly than the wild-type yeast strain. In addition, the use of A-ALD was only demonstrated by growth complementation, and its energetic benefit for the synthesis of acetyl-CoA derived products still needs further evaluation. Recently, EcEutE was introduced into a fatty acids producing host but only marginal improvement was observed in FFAs production (29).

1.3.2.6 ATP-dependent citrate lyase (ACL)

ATP-dependent citrate lyase (ACL) uses a tricarboxylic acid (TCA) cycle intermediate citrate as the substrate (Figure 1.3), which is enzymatically converted to acetyl-CoA and

oxaloacetate at the cost of one ATP molecule (51). Notably, comparative genomic studies reveals the presence of *ACL* in oleaginous yeasts such as *Yarrowia lipolytica*, while not in non-oleaginous yeasts such as *S. cerevisiae* (52). Such difference may imply the significance of ACL in providing precursor metabolites for the biosynthesis of fatty acids and lipids. *ACL*s from oleaginous yeasts , plants (53), and mammalian cells (42, 54) have been functionally expressed in *S. cerevisiae* and were able to increase the production of FFAs by 1.17-fold (42, 54) and *n*-butanol by about 2-fold . In another study, *ACL* from *Arabidopsis thaliana* and *Y. lipolytica* were introduced into a yeast strain engineered for overproducing FALs, whose titer was increased from 140 mg/L to 217 mg/L and 330 mg/L, respectively (55).

Due to the Crabtree effect and compartmentalization of cellular metabolism, citrate concentration in the cytosol may be low and rate-limiting for ACL activity (Figure 1.3). To increase the intracellular citrate level, both metabolic engineering strategies and process optimization have been attempted. To decrease the consumption of citrate through TCA cycle, *IDH1* and/or *IDH2* were deleted and citrate level was increased about 5-fold (42). Under nitrogen-limited conditions, a 3-fold increase in intracellular citrate concentration was achieved (54). Accordingly, the introduction of an ACL to the citrate accumulating strain led to increased production of FFAs (42, 54).

1.3.2.7 Phosphoketolase (PK)

Phosphoketolase, which catalyzes the cleavage of D-xylulose-5-phosphate into acetyl phosphate and glyceraldehyde-3-phosphate, is generally found in some filamentous fungi for cytosolic acetyl-CoA biosynthesis, such as *Aspergillus nidulans* (56). The phosphoketolase pathway was originally introduced into *S. cerevisiae* for improved xylose utilization (57), and

later was found to enhance the synthesis of acetyl-CoA as well (41, 58, 59) (Figure 1.3). By heterologous expression of the phosphoketolase pathway in a yeast strain producing PHB, the production could be improved from 4 mg/g dry cell weight in the reference strain to 28 mg/g dry cell weight, while only 16 mg/g dry cell weight was produced in the same background strain with the engineered PDH-bypass pathway (41). The phosphoketolase pathway was also introduced to the FAEEs producing yeast strain, and the production of FAEEs was increased by 5.7-fold compared with the reference strain (59). Since the metabolic flux to pentose phosphate pathway is limited during glucose fermentation, the intracellular concentration of D-xylulose-5-phosphate can be rate-limiting for acetyl-CoA biosynthesis via the phosphoketolase pathway. On the contrary, xylose is consumed via D-xylulose-5-phosphate. Therefore, it will be interesting to test the production of acetyl-CoA derived fuels and chemicals from xylose using the *S. cerevisiae* strains containing the phosphoketolase pathway (Figure 1.3).

1.4 Engineering Fatty Acyl-CoAs Metabolism

In yeast, FAB is carried out by the type I fatty acid synthase (FAS) system with all functional domains organized in two polypeptides, Fas1p and Fas2p. Although the organization of the FAS system varies between different organisms, the individual enzymatic reactions of FAB are essentially the same (60, 61). FAB begins with the conversion of acetyl-CoA into malonyl-CoA by acetyl-CoA carboxylase (ACC) at the cost of ATP. Malonyl-CoA is then transferred to ACP by malonyl-CoA:ACP transacylase. The generated malonyl-ACP is used as an extender unit, condensing with acyl-ACP to form β-ketoacyl-ACP with two more carbon units. The extended β-ketoacyl-ACP is subject to an NADPH-dependent reduction to form β-hydroxyacyl-ACP, whose hydroxyl group is removed by β-hydroxyacyl-ACP dehydratase, leading to the formation of *trans*-2-enoyl-ACP. The double bond is then reduced in another

NADPH-dependent reaction by the *trans*-2-enoyl-ACP reductase. Each elongation cycle results in the synthesis of acyl-ACP with the fatty acyl chain extended by two carbon units (Figure 1.4A). Besides the canonical FAB mechanisms shared by most of organisms, nature also evolved several special mechanisms to synthesize fatty acids *de novo*, such as the elongase system (62, 63) (Figure 1.4B) and the fermentative pathway (64, 65) (Figure 1.4C). Although not widely distributed in nature, these special pathways possess significant advantages over the canonical ones, in terms of pathway efficiency and controllability of the fatty acids chain lengths. Since the endogenous FAS system suffer from low efficiency and high regulation (66), such as coordinated induction of FAB genes, feedback inhibition, and inositol-mediated repression (60, 67), fatty acids do not naturally accumulate to high levels. Therefore, the hijack of FAB regulatory network by engineering of the transcriptional factors and heterologous expression of FASs have been tried to overcome the limitations of the endogenous system.

1.4.1 Engineering of structural genes

To increase the metabolic fluxes to FAB, the most straightforward strategy is to overexpress *ACC1*, *FAS*1 and *FAS*2. By replacing the native promoters of *ACC1*, *FAS1*, and *FAS2* with strong and constitutive promoters, their expression levels were increased about 7- to 16-fold. Accordingly, the production of FFAs, FALs, and FAEEs were increased by about 11-, 2-, and 4-fold, respectively (68).

To improve the fatty acyl-CoA levels, competing pathways were also engineered in *S. cerevisiae*. For example, the β-oxidation cycle, contributing to the degradation of fatty-CoAs, can be disrupted by the deletion of *POX1*. Unfortunately, the disruption of β-oxidation cycle led to lower production of FALs and FAEEs (55, 68). Besides β-oxidation, a large fraction of fatty

acids are utilized to synthesize steryl esters (SEs) and triacylglycerols (TAGs) in *S. cerevisiae*. Compared with the wild-type strain, FFAs content was increased about 3-fold in a strain (*are1*Δ *dga1*Δ *are2*Δ *lro1*Δ) devoid of TAG and SE formation, 4-fold in a strain (*pox1*Δ) incapable of β-oxidation, and 5-fold in a strain (*are1*Δ *dga1*Δ *are2*Δ *lro1*Δ *pox1*Δ) lacking both TAG and SE biosynthesis and β-oxidation pathways (69). Highest FFAs production, 2.2 g/L with 32% of the theoretical yield, was achieved in a recent study (70) by combining the disruption of β-oxidation and fatty acid activation (*faa1*Δ *faa4*Δ *fat1*Δ *faa2*Δ *pxa1*Δ *pox1*Δ) and the overexpression of the diacylglycerol acyltransferase (*DGA1*) and the triacylglycerol lipase (*TGL3*).

1.4.2 Engineering of regulatory genes

Due to the limited success in improving the efficiency of FAB by engineering structural genes, another study targeted the transcriptional regulators involved in FAB to increase the production of FALs (55). By manipulating the structural genes in fatty acids synthesis and degradation pathways, the production of FALs was increased less than 1.6-fold. On the contrary, the disruption of the regulatory network by knocking out transcriptional factors improved the production of FALs by 1.6- to 2.7-fold. Specifically, the deletion of *RPD*3, a negative regulator of phospholipids metabolism, enabled the highest production of FALs at a titer around 122 mg/L. Since the phospholipids synthesis requires fatty acids as the precursors, the deletion of negative regulators of phospholipids metabolism can enhance the phospholipids production and create a driving force for FAB.

It is well known that FAB is also subject to feedback inhibition by fatty acyl-CoAs or fatty acyl-ACPs. In eukaryotes, acyl-CoA binding protein (encoded by *ACB1*) plays an important role in transporting fatty acyl-CoAs in different compartments and attenuating the feedback

inhibitory effect of acyl-CoAs on FAB enzymes, such as Acc1p, Fas1p, and Fas2p (71). A recent report found that overexpression of *ACB1* could enhance the supply of fatty acyl-CoAs and increase the production of FAEEs by around 1.2-fold (72). On the contrary, another study found that the deletion of *ACB1* could enhance the cytosolic acyl-CoAs and increase the production of FAEEs by 1.48-fold (73).

1.4.3 Synthetic biology for alternative FAS

1.4.3.1 Bacterial type I FAS (bFAS)

Due to their coordinated biosynthesis, type I FASs are generally considered to be kinetically more efficient than the dissociated type II FASs. However, FAS may still be rate-limiting for FAB in yeast, because of its highly regulated network. Type I FASs are mainly present in eukaryotes, but also found in some actinomycetes, such as *Mycobacterium* species (74). Considering the significant differences between prokaryotes and eukaryotes, heterologous expression of a bacterial type I FAS (bFAS) was proposed for efficient FAB in yeast, by taking the advantage of the type I FAS while bypassing the endogenous regulation. It was found that a bFAS (FAS-B) from *Brevibacterium ammoniagenes* (also known as *Corynebacterium ammoniagenes*) together with its activation protein (phosphopantetheinyl transferase, PptA) could complement the growth of a *fas*1Δ mutant on fatty acids free medium, indicating that *FAS-B* could be functionally expressed in yeast and synthesize all necessary fatty acids or fatty acyl-CoAs to maintain cellular functions (75). Subsequent introduction of a wax synthase gene redirected the additional FAB fluxes to the synthesis of FAEEs, whose titer was 6-fold higher than that in the wild-type strain. It was also shown that a FAS-B mutant (Y2226F), whose

ketoacyl-ACP reductase activity was eliminated by point mutation at the catalytic center, enabled the production of triacetic acid lactone (TAL) at a titer higher than 50 mg/L in *S. cerevisiae* (76).

1.4.3.2 *Homo sapiens* type I FAS (hFAS)

Considering the kinetics advantage of the type I FASs, another strategy is to use the *Homo sapiens* type I FAS (hFAS). Different with the yeast counterpart, whose structure is well organized and highly complex, hFAS is not constrained by a scaffolding structure and displays a remarkable degree of flexibility (77). Especially for the TE domain, this fatty acids cleaving unit is on the C-terminus and isolated from the core scaffold. It was found that the removal of the TE domain (hFASΔTE) eliminated the native TE activity, but had no negative effect on the activity of other domains (78). Coexpression of a short-medium chain specific *TE* (*FatB1* from *Cuphea palustris* or *TEII* from *Rattus norvegicus*) together with the engineered hFAS resulted in the shift of fatty acids profiles. C_6, C_8, and C_{10} fatty acids were detected at high levels in the engineered strain, and the production of the major fatty acid (C_8) was increased more than 17-fold compared with the wild-type strain. By replacing the native TE domain, the short-medium chain specific TEs were linked to hFAS and the closer proximity of TE and FAS domains resulted in a 4- to 9-fold increase in C_8 fatty acid levels over the unlinked counterparts and a 64-fold increase over the wild type strain (78). The flexibility, high activity, and probably feedback inhibition insensitivity make hFAS a promising platform to produce fatty acids derived molecules with different chain lengths.

1.4.3.3 Elongase

As mentioned above, the traditional FAS system utilizes malonyl-ACP as the extender unit and NADPH as the reducing force to elongate the acyl chains, highlighting the ATP,

NADPH, and ACP dependence (60). A different *de novo* FAS system, the microsomal elongase, was described in *Trypanosoma brucei*, a eukaryotic human parasite that causes sleeping sickness (62, 63). Genome sequence indicates the presence of a putative type II FAS system, but experimental results suggest that the type II FAS is not responsible for *de novo* FAB. For example, 1) the components are membrane associated proteins, while soluble proteins are generally found for a type II FAS system. 2) Several type II FAS inhibitors, such as triclosan and cerulenin, which inhibit *trans*-2-enoyl-ACP reductase and β-ketoacyl-ACP synthase (79), respectively, will not affect FAB. 3) RNA interference (RNAi) silencing of ACP, a key component of type II systems, has no effect on *de novo* FAB either. Later, the system was characterized to use three elongases instead of a type II FAS (Figure 1.4B).

In this microsomal elongase system, malonyl-CoA serves as the extender unit and CoA is the acyl chain carrier (Figure 1.4B). In other words, this system is ATP, NADPH, and CoA dependent. In addition, trypanosomes have different fatty acids requirements during their life cycle, as they encounter various growth environments (62). It is found that the fatty acids requirement was achieved via the chain specificity of elongases, with ELO1 converting C_4 to C_{10}-CoA, ELO2 extending C_{10} to C_{14}-CoA, and ELO3 elongating C_{14} to C_{18}-CoA (Figure 1.4B). The modular feature of the elongase system will allow the accessibility for chain length engineering. For example, if only ELO1 is included together with the cyanobacterial alkane biosynthetic pathway, C_7 and C_9 alkanes will be the major products, which are the same as gasoline. Compared with *E. coli*, *S. cerevisiae* possess the intracellular membrane network and may be a better host for functional reconstitution of the elongase system, whose components are membrane associated proteins.

1.4.3.4 Fermentative pathway via the reversed β-oxidation cycle

Another special mechanism for *de novo* FAB is described in the mitochondria of *Euglena gracilis* (64, 65). So far, five different FAS systems have been reported for *E. gracilis*, two type II FAS localized in the chloroplasts, one type I FAS in the cytosol, one microsomal FAS, and one mitochondrial FAS. The mitochondrial system is involved in anaerobic wax ester fermentation. This fermentative pathway is malonyl-CoA (or ATP) independent, and has the ability to synthesize fatty acids directly from acetyl-CoA as both starter and extender units (64). In addition, NADH, instead of NADPH, serves as the reducing power (Figure 1.4C). Due to the ATP and ACP independence and CoA and NADH dependence, the fermentative FAB proceeds by reversal of the β-oxidation cycle. Compared with the canonical FAB, the fermentative pathway is advantageous for its energetic benefits of ATP independence and availability of CoA and NADH versus ACP and NADPH inside the cell (Figure 1.4C). Although genes coding the fermentative fatty acid synthesis pathway are not well characterized yet, the availability of the genome sequence of *E. gracilis* will definitely help to decipher the genetic code and benefit in designing efficient fatty acids derived biofuel synthetic pathways.

The advantages of such system were demonstrated in recent reports to reverse the β-oxidation cycles for efficient production of a series of fatty acids derived fuels and chemicals with different chain lengths (80, 81). By manipulating several global transcriptional regulators involved in fatty acids metabolism and carbon catabolite repression, all β-oxidation enzymes were constitutively expressed under anaerobic conditions even with the absence of fatty acids and presence of glucose (80). The resultant strain could reverse the β-oxidation cycle to produce *n*-butanol, long chain alcohols, and FFAs at much higher titers and yields than previous studies. Similarly, functional reversal of the β-oxidation cycle was achieved via a synthetic biology

approach by overexpressing all the structural genes of the β-oxidation cycle (81). Although the efficiency of the latter system was much lower than the former one, it represented a well-defined platform that could be readily transferred to other hosts, such as *S. cerevisiae*.

1.5 Project Overview

This thesis focuses on design and engineering of *S. cerevisiae* for efficient production of advanced biofuels and chemicals using metabolic engineering and synthetic biology approaches. One of the major challenges for high level production of value-added compounds other than ethanol in *S. cerevisiae* is the strong fluxes for ethanol formation even under aerobic conditions. Since many of the molecules of interest are derived from a few precursor metabolites, such as pyruvate, acetyl-CoA, and acyl-CoAs, this work aims to enhance the supply of these precursor metabolites in *S. cerevisiae* for efficient production of fuels and chemicals. Notably, the aims of this research can be integrated to construct a platform yeast cell factory, meaning that pyruvate is the direct precursor for acetyl-CoA generation and enhanced acetyl-CoA levels will provide a driving force for acyl-CoAs pool engineering.

In the second chapter of this thesis, a pyruvate overproducing yeast strain was constructed by deleting three structural genes encoding pyruvate decarboxylases, *PDC1*, *PDC5*, and *PDC6*. The resulting Pdc^- strain could not grow on glucose as the sole carbon source and required C_2 (ethanol or acetate) supplementation to synthesize cytosolic acetyl-CoA (6, 15). Followed by overexpression of *MTH1* and adaptive evolution, the resultant yeast grew on glucose as the sole carbon source with pyruvate as the major product. Interestingly, the evolved Pdc^- strain was found to enable simultaneous consumption of glucose and galactose, the two major components of red algae. Subsequent introduction of a BDO biosynthetic pathway consisting of the cytosolic acetolactate synthase (cyto*ILV2*), an acetolactate decarboxylase from

Bacillus subtilis (Bs*AlsD*), and the endogenous butanediol dehydrogenase (*BDH1*) resulted in the production of enantiopure (*2R,3R*)-butanediol (*R*-BDO). A yield over 70% of the theoretical value was achieved in the shaker flask. Using fed-batch fermentation, more than 100 g/L *R*-BDO (1100 mM) was synthesized from a mixture of glucose and galactose. The high titer and yield of the enantiopure *R*-BDO produced and the ability to co-ferment glucose and galactose make our engineered yeast strain a superior host for cost-effective production of bio-based BDO from renewable resources. In addition, further metabolic engineering was applied to construct a yeast strain that produced high levels of enantiopure *meso*-BDO, whose further conversion to 2-butanone (methyl ethyl ketone, MEK) and 2-butanol was also attempted.

Chapter 3 and Chapter 4 mainly focus on acetyl-CoA pool engineering in *S. cerevisiae*. In Chapter 3, alternative acetyl-CoA routes were characterized using synthetic biology approaches. Acetyl-CoA biosynthetic pathways from *E. coli* and *Yarrowia lipolytica* were introduced and found to complement the growth of Acs$^-$ (*acs1*Δ *acs2*Δ) strain on glucose as the sole source. These results indicated that the heterologous pathways were functional in *S. cerevisiae* and could fully replace the endogenous ACS-dependent pathway for acetyl-CoA generation in the cytosol. By co-expressing PDH structural genes and a lipoate-protein ligase gene in the Acs$^-$ strain, growth rate similar to the wild-type yeast strain could be achieved, if lipoic acid was supplemented to the growth medium. To eliminate the lipoic acid auxotroph, *de novo* lipoic acid biosynthesis and lipoylation machinery were also reconstituted in the cytosol of yeast, together with the PDH structural components. Due to the difficulty in reconstituting a functional type II fatty acid synthase (FAS) system, a semi-synthetic lipoylation pathway was designed to provide the precursor (octanoyl-ACP) of protein lipoylation, by co-expressing the acyl-ACP synthetase from *Vibrio harveyi* (VhAasS), free ACP (cytoACP1), and ACP activator (cytoPPT2). The

growth complementation of the Acs$^-$ strain indicated that PDH was lipoylated by the semi-synthetic pathway and functional, when octanoic acid was supplemented. Based on these results, a *de novo* biosynthetic lipoylation pathway was re-designed.

In the 4th chapter of this thesis, the characterized acetyl-CoA biosynthetic pathways in the previous chapter were used for metabolic engineering applications, with the aim to design and construct acetyl-CoA overproducing yeast strains. Combined strategies of disrupting competing pathways and introducing heterologous biosynthetic pathways were carried out to enhance acetyl-CoA levels, with the CoA-dependent *n*-butanol production as the reporter. By deleting *ADH1, ADH4, GPD1,* and *GPD2* involved in ethanol and glycerol formation, the glycolytic flux was redirected towards this precursor metabolite, resulting in a 4 fold improvement in *n*-butanol production. Subsequent introduction of heterologous acetyl-CoA biosynthetic pathways, including pyruvate dehydrogenase (PDH), ATP-dependent citrate lyase (ACL), and PDH-bypass further increased the production of *n*-butanol. Although significant improvement of *n*-butanol production was achieved, the final titer was still much lower than that of ethanol. In addition, the resultant yeast strains suffered from accumulation of the toxic intermediates, acetaldehyde and acetate, as well as the residual production of ethanol as the major product due to the redundancy of *ADH*s in the *S. cerevisiae* genome (5, 30). Therefore, more efforts were put into the engineering of acetyl-CoA pools in the Pdc$^-$ strain (constructed in Chapter 2), where ethanol production was completely eliminated.

Different from pyruvate and acetyl-CoA as general precursor metabolites for a series of biological reactions, acyl-CoAs are the direct substrates of many fuels and chemicals, such as FFAs, FALs, and FAEEs. Thus, the goal of Chapter 5 is to construct a new biosynthesis platform for acyl-CoAs in *S. cerevisiae* based on the reversal of β-oxidation cycle. Compared with the

traditional FAB, which is ATP, ACP, and NADPH dependent, the reversed β-oxidation pathway is featured for its ATP and ACP independence and CoA and NADH dependence. The energetic benefits of ATP independence and availability of CoA and NADH versus ACP and NADPH confer advantages for efficient FAB. Recent reports to synthesize a series of chemicals and fuels were achieved by reversing β-oxidation cycles in *E. coli* via systems biology and synthetic biology approaches. The advantage of such system was demonstrated by the highest reported titer of fuels and chemicals produced. Taking the merits of yeast for biofuel production into account, we sought to develop a platform for advanced biofuel production based on the reversal of β-oxidation cycles in *S. cerevisiae*. Using synthetic biology approaches, reversed β-oxidation pathways were constructed and found to produce *n*-butanol, decanoic acid, and ethyl decanoate, indicating the functional reversal of β-oxidation cycle at least 4 turns.

In the last chapter of this thesis, I focused on the development of new synthetic biology tools for engineering in *S. cerevisiae*. First of all, plasmids with different copy numbers (20-100 copies per cell) were constructed by engineering the expression level of selection marker proteins, including both auxotrophic and dominant markers. More importantly, the copy number of the plasmids with engineered dominant markers (5-100 copies per cell) showed a positive correlation with the concentration of antibiotics supplemented to the growth media. Based on this finding, a new and simplest synthetic biology approach, named induced pathway optimization by antibiotic doses (iPOAD), to improve the performance of multi-gene biosynthetic pathways in *S. cerevisiae* was developed through modular optimization of multi-gene pathways by different combinations of antibiotic concentrations. To demonstrate this approach, iPOAD was applied to optimize the lycopene and *n*-butanol biosynthetic pathways, with the production of lycopene and *n*-butanol increased by 10- and 100-fold, respectively. Finally, the iPOAD optimized pathways

were integrated to the chromosome to increase the strain stability and eliminate the requirement of antibiotic supplementation, by taking advantage of the CRISPR-Cas9 technology for multiplex pathway integration.

1.6 References

1. **Du J, Shao Z, Zhao H.** 2011. Engineering microbial factories for synthesis of value-added products. J. Ind. Microbiol. Biotechnol. **38:**873-890.
2. **Lu X.** 2010. A perspective: photosynthetic production of fatty acid-based biofuels in genetically engineered cyanobacteria. Biotechnol. Adv. **28:**742-746.
3. **Ageitos JM, Vallejo JA, Veiga-Crespo P, Villa TG.** 2011. Oily yeasts as oleaginous cell factories. Appl. Microbiol. Biotechnol. **90:**1219-1227.
4. **Hong KK, Nielsen J.** 2012. Metabolic engineering of *Saccharomyces cerevisiae*: a key cell factory platform for future biorefineries. Cell Mol. Life Sci. **69:**2671-2690.
5. **de Smidt O, du Preez JC, Albertyn J.** 2012. Molecular and physiological aspects of alcohol dehydrogenases in the ethanol metabolism of *Saccharomyces cerevisiae*. FEMS Yeast Res. **12:**33-47.
6. **van Maris AJ, Geertman JM, Vermeulen A, Groothuizen MK, Winkler AA, Piper MD, van Dijken JP, Pronk JT.** 2004. Directed evolution of pyruvate decarboxylase-negative *Saccharomyces cerevisiae*, yielding a C_2-independent, glucose-tolerant, and pyruvate-hyperproducing yeast. Appl. Environ. Microbiol. **70:**159-166.
7. **Abbott DA, Zelle RM, Pronk JT, van Maris AJA.** 2009. Metabolic engineering of *Saccharomyces cerevisiae* for production of carboxylic acids: current status and challenges. FEMS Yeast Res. **9:**1123-1136.
8. **Pronk JT, Yde Steensma H, Van Dijken JP.** 1996. Pyruvate metabolism in *Saccharomyces cerevisiae*. Yeast **12:**1607-1633.
9. **Kresze GB, Ronft H.** 1981. Pyruvate dehydrogenase complex from baker's yeast. 1. Purification and some kinetic and regulatory properties. Eur. J. Biochem. **119:**573-579.
10. **Ruiz-Amil M, De Torrontegui G, Palacian E, Catalina L, Losada M.** 1965. Properties and function of yeast pyruvate carboxylase. J. Biol. Chem. **240:**3485-3492.
11. **van Urk H, Schipper D, Breedveld GJ, Mak PR, Scheffers WA, van Dijken JP.** 1989. Localization and kinetics of pyruvate-metabolizing enzymes in relation to aerobic alcoholic fermentation in *Saccharomyces cerevisiae* CBS 8066 and *Candida utilis* CBS 621. Biochim. Biophys. Acta **992:**78-86.
12. **Postma E, Verduyn C, Scheffers WA, Van Dijken JP.** 1989. Enzymic analysis of the crabtree effect in glucose-limited chemostat cultures of *Saccharomyces cerevisiae*. Appl. Environ. Microbiol. **55:**468-477.
13. **Hohmann S.** 1993. Characterisation of *PDC2*, a gene necessary for high level expression of pyruvate decarboxylase structural genes in *Saccharomyces cerevisiae*. Mol. Gen. Genet. **241:**657-666.
14. **Hohmann S, Cederberg H.** 1990. Autoregulation may control the expression of yeast pyruvate decarboxylase structural genes *PDC1* and *PDC5*. Eur. J. Biochem. **188:**615-621.
15. **Flikweert MT, de Swaaf M, van Dijken JP, Pronk JT.** 1999. Growth requirements of pyruvate-decarboxylase-negative *Saccharomyces cerevisiae*. FEMS Microbiol. Lett. **174:**73-79.
16. **Stucka R, Dequin S, Salmon JM, Gancedo C.** 1991. DNA sequences in chromosomes II and VII code for pyruvate carboxylase isoenzymes in *Saccharomyces cerevisiae*: analysis of pyruvate carboxylase-deficient strains. Mol. Gen. Genet. **229:**307-315.

17. **Gamo FJ, Lafuente MJ, Gancedo C.** 1994. The mutation *DGT1-1* decreases glucose transport and alleviates carbon catabolite repression in *Saccharomyces cerevisiae*. J. Bacteriol. **176:**7423-7429.
18. **van Maris AJA, Geertman JMA, Vermeulen A, Groothuizen MK, Winkler AA, Piper MDW, van Dijken JP, Pronk JT.** 2004. Directed evolution of pyruvate decarboxylase-negative *Saccharomyces cerevisiae*, yielding a C_2-independent, glucose-tolerant, and pyruvate-hyperproducing yeast. Appl. Environ. Microbiol. **70:**159-166.
19. **Oud B, Flores CL, Gancedo C, Zhang X, Trueheart J, Daran JM, Pronk JT, van Maris AJ.** 2012. An internal deletion in *MTH1* enables growth on glucose of pyruvate-decarboxylase negative, non-fermentative *Saccharomyces cerevisiae*. Microb. Cell Fact. **11:**131.
20. **Kim SJ, Seo SO, Jin YS, Seo JH.** 2013. Production of 2,3-butanediol by engineered *Saccharomyces cerevisiae*. Bioresour. Technol. **146:**274-281.
21. **van Maris AJ, Luttik MA, Winkler AA, van Dijken JP, Pronk JT.** 2003. Overproduction of threonine aldolase circumvents the biosynthetic role of pyruvate decarboxylase in glucose-limited chemostat cultures of *Saccharomyces cerevisiae*. Appl. Environ. Microbiol. **69:**2094-2099.
22. **Chen Y, Zhang Y, Siewers V, Nielsen J.** 2015. Ach1 is involved in shuttling mitochondrial acetyl units for cytosolic C2 provision in *Saccharomyces cerevisiae* lacking pyruvate decarboxylase. FEMS Yeast Res.**:**DOI: 10.1093/femsyr/fov1015.
23. **Nan H, Seo SO, Oh EJ, Seo JH, Cate JH, Jin YS.** 2014. 2,3-butanediol production from cellobiose by engineered *Saccharomyces cerevisiae*. Appl. Microbiol. Biotechnol. **98:**5757-5764.
24. **Kim SJ, Seo SO, Park YC, Jin YS, Seo JH.** 2014. Production of 2,3-butanediol from xylose by engineered *Saccharomyces cerevisiae*. J. Biotechnol. **192:**376-382.
25. **Zelle RM, de Hulster E, van Winden WA, de Waard P, Dijkema C, Winkler AA, Geertman JM, van Dijken JP, Pronk JT, van Maris AJ.** 2008. Malic acid production by *Saccharomyces cerevisiae*: engineering of pyruvate carboxylation, oxaloacetate reduction, and malate export. Appl. Environ. Microbiol. **74:**2766-2777.
26. **Yan D, Wang C, Zhou J, Liu Y, Yang M, Xing J.** 2014. Construction of reductive pathway in *Saccharomyces cerevisiae* for effective succinic acid fermentation at low pH value. Bioresour. Technol. **156:**232-239.
27. **Geertman JM, van Maris AJ, van Dijken JP, Pronk JT.** 2006. Physiological and genetic engineering of cytosolic redox metabolism in *Saccharomyces cerevisiae* for improved glycerol production. Metab. Eng. **8:**532-542.
28. **Strijbis K, Distel B.** 2010. Intracellular acetyl unit transport in fungal carbon metabolism. Eukaryot. Cell **9:**1809-1815.
29. **Li X, Guo D, Cheng Y, Zhu F, Deng Z, Liu T.** 2014. Overproduction of fatty acids in engineered *Saccharomyces cerevisiae*. Biotechnol. Bioeng. **111:**1841-1852.
30. **Ida Y, Furusawa C, Hirasawa T, Shimizu H.** 2012. Stable disruption of ethanol production by deletion of the genes encoding alcohol dehydrogenase isozymes in *Saccharomyces cerevisiae*. J. Biosci. Bioeng. **113:**192-195.
31. **Chen Y, Siewers V, Nielsen J.** 2012. Profiling of cytosolic and peroxisomal acetyl-CoA metabolism in *Saccharomyces cerevisiae*. PLoS One **7:**e42475.
32. **Chen Y, Daviet L, Schalk M, Siewers V, Nielsen J.** 2013. Establishing a platform cell factory through engineering of yeast acetyl-CoA metabolism. Metab. Eng. **15:**48-54.

33. **Wang Y, Chen H, Yu O.** 2014. A plant malonyl-CoA synthetase enhances lipid content and polyketide yield in yeast cells. Appl. Microbiol. Biotechnol. **98:**5435-5447.
34. **Krivoruchko A, Serrano-Amatriain C, Chen Y, Siewers V, Nielsen J.** 2013. Improving biobutanol production in engineered *Saccharomyces cerevisiae* by manipulation of acetyl-CoA metabolism. J. Ind. Microbiol. Biotechnol. **40:**1051-1056.
35. **Kocharin K, Chen Y, Siewers V, Nielsen J.** 2012. Engineering of acetyl-CoA metabolism for the improved production of polyhydroxybutyrate in *Saccharomyces cerevisiae*. AMB Express **2:**52.
36. **Ozaydin B, Burd H, Lee TS, Keasling JD.** 2013. Carotenoid-based phenotypic screen of the yeast deletion collection reveals new genes with roles in isoprenoid production. Metab. Eng. **15:**174-183.
37. **Drinnenberg IA, Weinberg DE, Xie KT, Mower JP, Wolfe KH, Fink GR, Bartel DP.** 2009. RNAi in budding yeast. Science **326:**544-550.
38. **Crook NC, Schmitz AC, Alper HS.** 2014. Optimization of a yeast RNA interference system for controlling gene expression and enabling rapid metabolic engineering. ACS Synth. Biol. **3:**307-313.
39. **Si T, Luo Y, Bao Z, Zhao H.** 2015. RNAi-assisted genome evolution in *Saccharomyces cerevisiae* for complex phenotype engineering. ACS Synth. Biol. **4:**283-291.
40. **Shiba Y, Paradise EM, Kirby J, Ro DK, Keasling JD.** 2007. Engineering of the pyruvate dehydrogenase bypass in *Saccharomyces cerevisiae* for high-level production of isoprenoids. Metab. Eng. **9:**160-168.
41. **Kocharin K, Siewers V, Nielsen J.** 2013. Improved polyhydroxybutyrate production by *Saccharomyces cerevisiae* through the use of the phosphoketolase pathway. Biotechnol. Bioeng. **110:**2216-2224.
42. **Tang X, Feng H, Chen WN.** 2013. Metabolic engineering for enhanced fatty acids synthesis in *Saccharomyces cerevisiae*. Metab. Eng. **16:**95-102.
43. **Starai VJ, Escalante-Semerena JC.** 2004. Acetyl-coenzyme A synthetase (AMP forming). Cell Mol. Life Sci. **61:**2020-2030.
44. **Kozak BU, van Rossum HM, Luttik MA, Akeroyd M, Benjamin KR, Wu L, de Vries S, Daran JM, Pronk JT, van Maris AJ.** 2014. Engineering acetyl coenzyme A supply: functional expression of a bacterial pyruvate dehydrogenase complex in the cytosol of *Saccharomyces cerevisiae*. MBio **5:**e01696-01614.
45. **Ragsdale SW.** 2003. Pyruvate ferredoxin oxidoreductase and its radical intermediate. Chem. Rev. **103:**2333-2346.
46. **Inui H, Ono K, Miyatake K, Nakano Y, Kitaoka S.** 1987. Purification and characterization of pyruvate:$NADP^+$ oxidoreductase in *Euglena gracilis*. J. Biol. Chem. **262:**9130-9135.
47. **Muller M, Mentel M, van Hellemond JJ, Henze K, Woehle C, Gould SB, Yu RY, van der Giezen M, Tielens AG, Martin WF.** 2012. Biochemistry and evolution of anaerobic energy metabolism in eukaryotes. Microbiol. Mol. Biol. Rev. **76:**444-495.
48. **Kozak BU, van Rossum HM, Benjamin KR, Wu L, Daran JM, Pronk JT, van Maris AJ.** 2013. Replacement of the *Saccharomyces cerevisiae* acetyl-CoA synthetases by alternative pathways for cytosolic acetyl-CoA synthesis. Metab. Eng. **21C:**46-59.
49. **Overkamp KM, Kotter P, van der Hoek R, Schoondermark-Stolk S, Luttik MA, van Dijken JP, Pronk JT.** 2002. Functional analysis of structural genes for NAD^+-dependent formate dehydrogenase in *Saccharomyces cerevisiae*. Yeast **19:**509-520.

50. **Abdel-Hamid AM, Attwood MM, Guest JR.** 2001. Pyruvate oxidase contributes to the aerobic growth efficiency of *Escherichia coli*. Microbiology **147:**1483-1498.
51. **Zaidi N, Swinnen JV, Smans K.** 2012. ATP-citrate lyase: a key player in cancer metabolism. Cancer Res. **72:**3709-3714.
52. **Vorapreeda T, Thammarongtham C, Cheevadhanarak S, Laoteng K.** 2012. Alternative routes of acetyl-CoA synthesis identified by comparative genomic analysis: involvement in the lipid production of oleaginous yeast and fungi. Microbiology **158:**217-228.
53. **Fatland BL, Ke J, Anderson MD, Mentzen WI, Cui LW, Allred CC, Johnston JL, Nikolau BJ, Wurtele ES.** 2002. Molecular characterization of a heteromeric ATP-citrate lyase that generates cytosolic acetyl-coenzyme A in *Arabidopsis*. Plant. Physiol. **130:**740-756.
54. **Tang X, Chen WN.** 2014. Investigation of fatty acid accumulation in the engineered *Saccharomyces cerevisiae* under nitrogen limited culture condition. Bioresour. Technol. **162:**200-206.
55. **Feng X, Lian J, Zhao H.** 2015. Metabolic engineering of *Saccharomyces cerevisiae* to improve 1-hexadecanol production. Metab. Eng. **27:**10-19.
56. **Panagiotou G, Andersen MR, Grotkjaer T, Regueira TB, Hofmann G, Nielsen J, Olsson L.** 2008. Systems analysis unfolds the relationship between the phosphoketolase pathway and growth in *Aspergillus nidulans*. PLoS One **3:**e3847.
57. **Sonderegger M, Schumperli M, Sauer U.** 2004. Metabolic engineering of a phosphoketolase pathway for pentose catabolism in *Saccharomyces cerevisiae*. Appl. Environ. Microbiol. **70:**2892-2897.
58. **Papini M, Nookaew I, Siewers V, Nielsen J.** 2012. Physiological characterization of recombinant *Saccharomyces cerevisiae* expressing the *Aspergillus nidulans* phosphoketolase pathway: validation of activity through 13C-based metabolic flux analysis. Appl. Microbiol. Biotechnol. **95:**1001-1010.
59. **de Jong BW, Shi S, Siewers V, Nielsen J.** 2014. Improved production of fatty acid ethyl esters in *Saccharomyces cerevisiae* through up-regulation of the ethanol degradation pathway and expression of the heterologous phosphoketolase pathway. Microb. Cell Fact. **13:**39.
60. **Tehlivets O, Scheuringer K, Kohlwein SD.** 2007. Fatty acid synthesis and elongation in yeast. Biochim. Biophys. Acta **1771:**255-270.
61. **Chan DI, Vogel HJ.** 2010. Current understanding of fatty acid biosynthesis and the acyl carrier protein. Biochem. J. **430:**1-19.
62. **Lee SH, Stephens JL, Paul KS, Englund PT.** 2006. Fatty acid synthesis by elongases in trypanosomes. Cell **126:**691-699.
63. **Lee SH, Stephens JL, Englund PT.** 2007. A fatty-acid synthesis mechanism specialized for parasitism. Nat. Rev. Microbiol. **5:**287-297.
64. **Inui H, Miyatake K, Nakano Y, Kitaoka S.** 1984. Fatty acid synthesis in mitochondria of *Euglena gracilis*. Eur. J. Biochem. **142:**121-126.
65. **Hoffmeister M, Piotrowski M, Nowitzki U, Martin W.** 2005. Mitochondrial trans-2-enoyl-CoA reductase of wax ester fermentation from *Euglena gracilis* defines a new family of enzymes involved in lipid synthesis. J. Biol. Chem. **280:**4329-4338.
66. **Lennen RM, Pfleger BF.** 2012. Engineering *Escherichia coli* to synthesize free fatty acids. Trends Biotechnol. **30:**659-667.

67. **Chirala SS.** 1992. Coordinated regulation and inositol-mediated and fatty acid-mediated repression of fatty acid synthase genes in *Saccharomyces cerevisiae*. Proc. Natl. Acad. Sci. U. S. A. **89:**10232-10236.
68. **Runguphan W, Keasling JD.** 2014. Metabolic engineering of *Saccharomyces cerevisiae* for production of fatty acid-derived biofuels and chemicals. Metab. Eng. **21:**103-113.
69. **Valle-Rodriguez JO, Shi SB, Siewers V, Nielsen J.** 2014. Metabolic engineering of *Saccharomyces cerevisiae* for production of fatty acid ethyl esters, an advanced biofuel, by eliminating non-essential fatty acid utilization pathways. Appl. Energ. **115:**226-232.
70. **Leber C, Polson B, Fernandez-Moya R, Da Silva NA.** 2015. Overproduction and secretion of free fatty acids through disrupted neutral lipid recycle in *Saccharomyces cerevisiae*. Metab. Eng. **28:**54-62.
71. **Knudsen J, Jensen MV, Hansen JK, Faergeman NJ, Neergaard TB, Gaigg B.** 1999. Role of acyl-CoA binding protein in acyl-CoA transport, metabolism and cell signaling. Mol. Cell Biochem. **192:**95-103.
72. **Shi S, Valle-Rodriguez JO, Siewers V, Nielsen J.** 2014. Engineering of chromosomal wax ester synthase integrated *Saccharomyces cerevisiae* mutants for improved biosynthesis of fatty acid ethyl esters. Biotechnol. Bioeng. **111:**1740-1747.
73. **Thompson RA, Trinh CT.** 2014. Enhancing fatty acid ethyl ester production in *Saccharomyces cerevisiae* through metabolic engineering and medium optimization. Biotechnol. Bioeng. **111:**2200-2208.
74. **Gago G, Diacovich L, Arabolaza A, Tsai SC, Gramajo H.** 2011. Fatty acid biosynthesis in actinomycetes. FEMS Microbiol. Rev. **35:**475-497.
75. **Eriksen DT, HamediRad M, Zhao H.** 2014. Orthogonal fatty acid biosynthetic pathway improves fatty acid ethyl ester production in *Saccharomyces cerevisiae*. ACS Synth. Biol.**:**DOI: 10.1021/sb500319p.
76. **Zha W, Shao Z, Frost JW, Zhao H.** 2004. Rational pathway engineering of type I fatty acid synthase allows the biosynthesis of triacetic acid lactone from D-glucose *in vivo*. J. Am. Chem. Soc. **126:**4534-4535.
77. **Leibundgut M, Maier T, Jenni S, Ban N.** 2008. The multienzyme architecture of eukaryotic fatty acid synthases. Curr. Opin. Struct. Biol. **18:**714-725.
78. **Leber C, Da Silva NA.** 2014. Engineering of *Saccharomyces cerevisiae* for the synthesis of short chain fatty acids. Biotechnol. Bioeng. **111:**347-358.
79. **Lu JZ, Lee PJ, Waters NC, Prigge ST.** 2005. Fatty acid synthesis as a target for antimalarial drug discovery. Comb. Chem. High T. Scr. **8:**15-26.
80. **Dellomonaco C, Clomburg JM, Miller EN, Gonzalez R.** 2011. Engineered reversal of the β-oxidation cycle for the synthesis of fuels and chemicals. Nature **476:**355-359.
81. **Clomburg JM, Vick JE, Blankschien MD, Rodriguez-Moya M, Gonzalez R.** 2012. A synthetic biology approach to engineer a functional reversal of the β-oxidation cycle. ACS Synth. Biol. **1:**541-554.

1.7 Figures

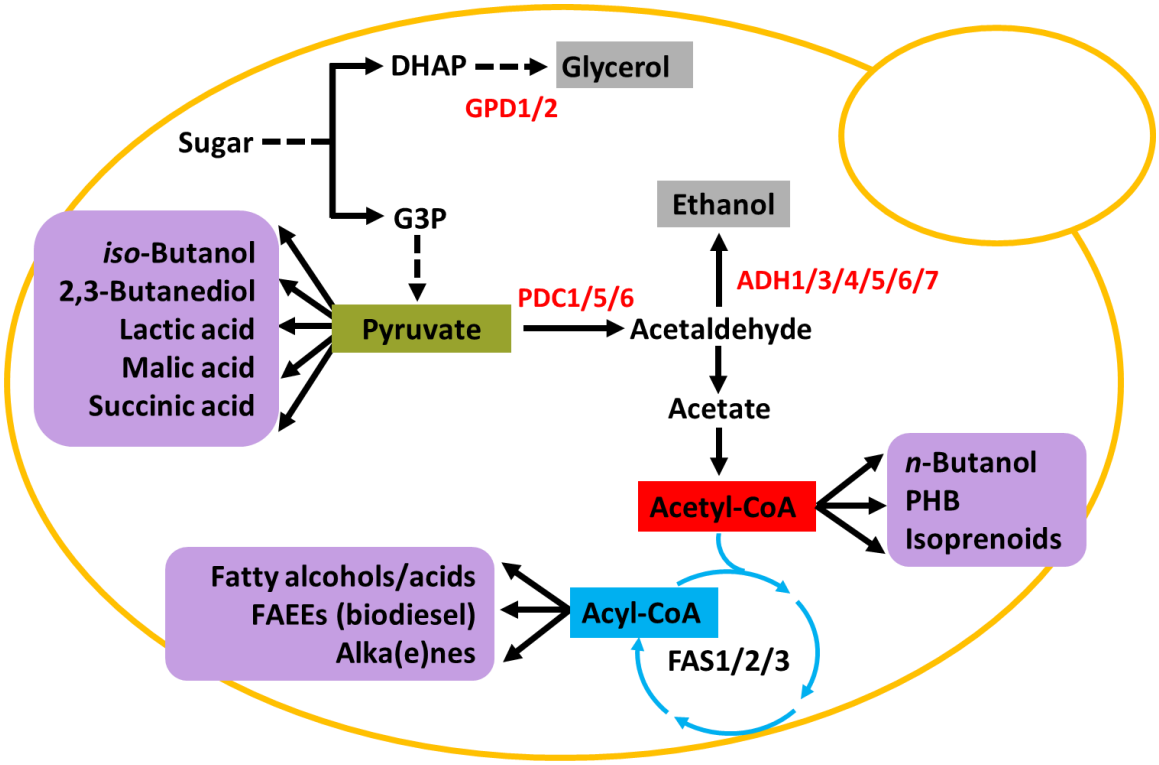

Figure 1.1 Overview of yeast cell factory for high-level production of biofuels and chemicals via engineering the supply of precursor metabolites. A wide range of biofuels and value-added chemicals (shown in purple) are derived from a few precursor metabolites (shown in box), such as pyruvate, acetyl-CoA, and acyl-CoAs. Metabolic engineering targets to enhance precursor supply by decreasing or eliminating undesirable by-product formation are shown in red.

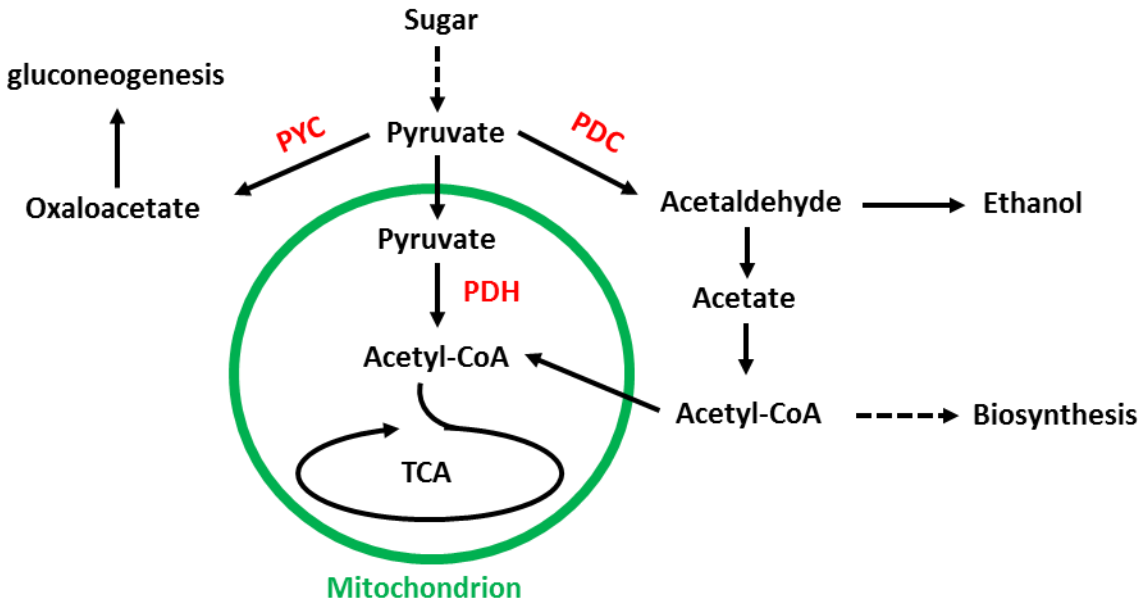

Figure 1.2 Control of yeast metabolism at the pyruvate branch point. The metabolic fluxes are mainly divided to fermentation (PDC for ethanol formation), respiration (PDH for TCA cycle), and gluconeogenesis (PYC).

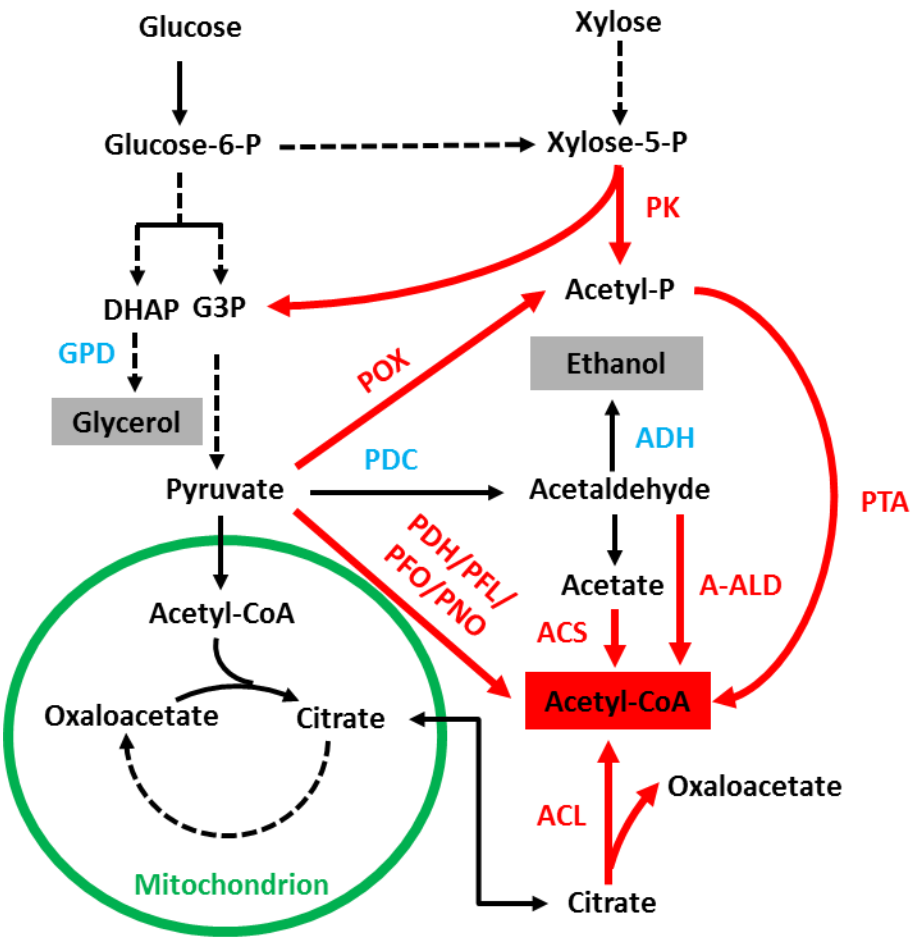

Figure 1.3 Design and construction of acetyl-CoA overproducing yeast strains via synthetic biology and metabolic engineering strategies. The metabolic engineering targets (glycerol production and ethanol formation) to redirect the glycolytic fluxes to acetyl-CoA biosynthesis are shown in blue. Heterologous pathways, including pyruvate dehydrogenase (PDH), pyruvate:formate lyase (PFL), pyruvate:ferrodoxin oxidoreductase (PFO), pyruvate:$NADP^+$ oxidoreductase (PNO), engineered PDH-bypass pathway, ATP-dependent citrate lyase (ACL), acetylating aldehyde dehydrogenase (A-ALD), pyruvate oxidase (POX) pathway, and phosphoketolase pathway (PK), which demonstrate higher efficiency and/or lower energy input requirement and may enhance the acetyl-CoA level in the cytosol of yeast, are shown in red. ACS: acetyl-CoA synthetase; PTA: phosphotransacetylase.

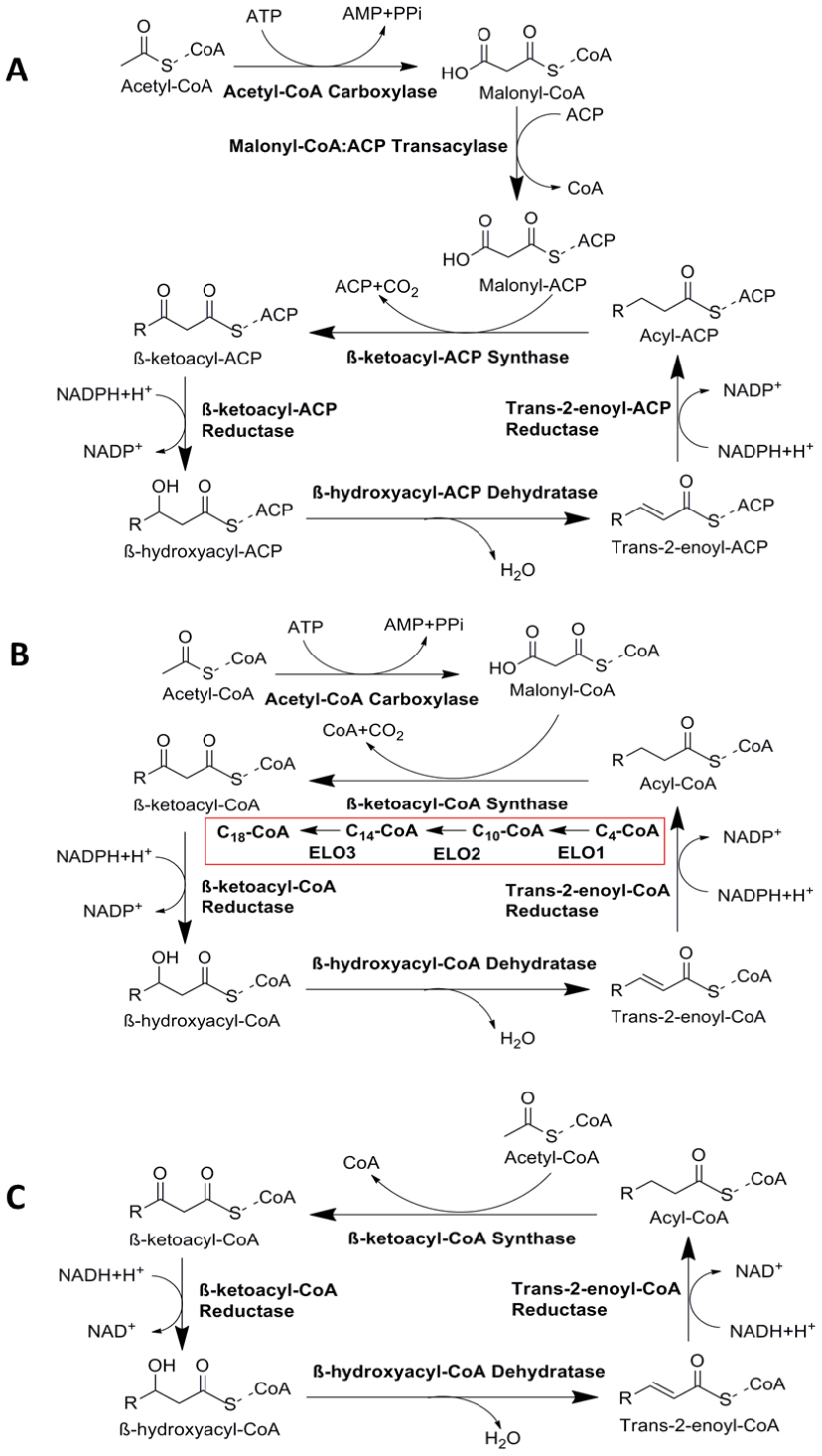

Figure 1.4 Overview of the general and two non-canonical schemes for fatty acid biosynthesis. Fatty acyl chain is extended by two carbon units after each elongation cycle including condensation, reduction, dehydration, and reduction. Different with the canonical scheme (A), which shows ATP/malonyl-CoA, ACP, and NADPH dependence, the elongase system (B) is ATP, CoA, and NADPH dependent (ACP independent), while the fermentative pathway (C) is CoA and NADH dependent (ATP, ACP, and NADPH independent).

Chapter 2 Pyruvate Pool Engineering and its Application in Efficient Production of 2,3-Butanediol

2.1 Introduction

As an end product of glycolysis and a central metabolite, pyruvate is the entry point of many cellular reactions and the branch point to control the flow of metabolic fluxes, especially for respiration and fermentation. Notably, several of the pyruvate involved reactions will lead to the synthesis of a wide range of fuel and chemical molecules, such as ethanol, *iso*-butanol, 2,3-butanediol, lactate, malate, and succinate (1). In *Saccharomyces cerevisiae*, most of the glycolytic fluxes go through ethanol fermentation even under aerobic conditions, known as Crabtree effect. To redirect the metabolic flux from ethanol to the synthesis of other pyruvate derived products, pyruvate decarboxylases (PDCs), the branch point controlling enzymes to convert pyruvate to ethanol, were chosen as the target for metabolic engineering. The pyruvate decarboxylation activity results from the expression of three structural genes, *PDC1*, *PDC5*, and *PDC6*. However, the Pdc^- strain (*pdc1*Δ *pdc5*Δ *pdc6*Δ) cannot grow on glucose as the sole carbon source and requires C_2 (acetate or ethanol) supplementation to synthesize cytoplasmic acetyl-CoA (2), which makes it not ideal for industrial applications. Inverse metabolic engineering revealed that an internal deletion or a single mutation in the Mth1p coding sequence enabled the growth of the Pdc^- strain on glucose (3). Mth1p is a transcription factor involved in glucose sensing which can inhibit the expression of hexose transporter genes (*HXT*s) to retard glucose uptake. The internal deletion increased the stability of Mth1p by removing the putative sites related to protein degradation (3), maintaining the intracellular glucose concentration to a low level and alleviating glucose repression.

To demonstrate the utility of the pyruvate overproducing yeast strain, biological production of 2,3-butanediol (BDO) was chosen as a case study. BDO is an important chemical with extensive industrial applications (4-6). Due to its low freezing point, BDO can be used as an antifreeze agent. A more important application is its potential to produce 1,3-butanediene, the monomer of synthetic rubber. In addition, BDO derivatives, such as methyl ethyl ketone and diacetyl, have found applications in fuel and food industries (4). BDO exists in three isomeric forms, *(*2*S*,3*S)*-butanediol (*S*-BDO), *meso*-butanediol (*meso*-BDO), and *(*2*R*,3*R)*-butanediol (*R*-BDO). Many native hosts such as *Klebsiella* and *Enterobacter* species can accumulate BDO to high levels. Nevertheless, these native producers are pathogenic and synthesize a mixture of BDO stereoisomers, which prevents their commercial application (5). Therefore, the development of an industrially friendly host for biological production of BDO from renewable resources is highly desirable.

Recently, the use of marine macroalgae as a renewable feedstock has attracted increasing attention mainly because the lack of lignin makes the hydrolysis of seaweed rather simple and straightforward (7, 8). Among several different types of marine macroalgae, the red algae, such as *Gelidium amansii*, are known for high carbohydrate content and abundance in nature. The major carbohydrate components of red algae are glucose and galactose, which are mainly released from cellulose and agarose, respectively (9). To make a biorefinery process based on a renewable feedstock economically feasible, the producing host should be able to utilize all sugars efficiently and simultaneously (10). However, catabolite repression is widely found in microorganisms, which means glucose is the preferred carbon source and the utilization of other carbon sources will be inhibited until glucose is depleted. As a result, sequential utilization or diauxic growth is observed during mixed sugar fermentation, leading to low yield and

productivity of the final products (11). A cellobiose utilization pathway consisting of a cellodextrin transporter and a β-glucosidase was recently introduced into *S. cerevisiae* to overcome glucose repression (12, 13), which enabled the consumption of cellobiose and galactose simultaneously (14). Nevertheless, the cellobiose consumption rate is much slower than that of glucose even after intensive protein engineering and pathway optimization (15-19), making co-utilization of glucose and galactose still a preferred process.

In this chapter, a pyruvate overproducing *S. cerevisiae* strain was engineered and applied to produce BDO at high titer and yield. The growth of the Pdc$^-$ strain on glucose was restored through the introduction of the internal truncated *MTH1* (*MTH1*T) followed by adaptive evolution. In the presence of an *R*-BDO biosynthetic pathway, efficient production of enantiopure *R*-BDO was achieved by completely eliminating ethanol production (Figure 2.1). In addition, an enantiopure *meso*-BDO producing yeast strain was constructed and the further conversion of *meso*-BDO to 2-butanol was attempted as well. Moreover, the engineered Pdc$^-$ strain showed glucose-derepressed properties, enabling co-fermentation of glucose and galactose. Notably, this strain has the potential to be further engineered for simultaneous utilization of a mixture of sugars derived from other renewable resources, such as brown macroalgae and cellulosic biomass, for cost-effective production of fuels and chemicals. Notably, a major part of this chapter is adapted from one of my research articles published in *Metabolic Engineering* (20).

2.2 Results

2.2.1 Construction of a pyruvate overproducing yeast strain

To redirect the flux from ethanol to the desired products, the three structural genes encoding pyruvate decarboxylase, *PDC1*, *PDC5*, and *PDC6*, were knocked out consecutively

using the classic *loxP-KanMX-loxP* method (21). As expected, the Pdc$^-$ strain could not grow on hexose (such as glucose or galactose) as the sole carbon source, while the growth on ethanol was not affected. The introduction of an internal truncated *MTH1* was reported to enable the growth of Pdc$^-$ strain on glucose (3, 22). Since the truncated Mth1p was claimed to have increased intracellular stability and abundance to better repress glucose uptake, a similar strategy was carried out by over-expressing *MTH1* on a multi-copy plasmid in this study. Accordingly, the overexpression of either the full length *MTH1* or the truncated version (*MTH1*T) could rescue the growth in the medium with low glucose concentration, where Pdc$^-$/MTH1T grew slightly better (Figure 2.2A). These results in turn supported the assumption that the internal deletion in Mth1p alleviated glucose repression by interfering degradation of this transcriptional regulator protein.

Nevertheless, the growth on higher sugar concentration was still poor. To make this strain more suitable for industrial applications, adaptive evolution was carried out to improve the cell growth rate on high glucose concentrations. After 10 rounds of serial transfer in SC medium containing 20 g/L glucose, three single clones, Pdc$^-$/MTH1T-e1 (E10), Pdc$^-$/MTH1T-e2, and Pdc$^-$/MTH1T-e3, were isolated and the cell growth rate of the evolved strains was found to be significantly improved (Figure 2.2B).

The whole genomes of the parent strain Pdc$^-$/MTH1T and the three evolved strains were sequenced to identify the mutations that might be responsible for the improved growth on high concentrations of glucose. Approximately 30 SNVs unique to each of the evolved strain relative to the parent strain were identified, and a majority of the SNVs were intergenic (non-coding regions). Four out of five non-synonymous SNVs were shared by all the evolved strains (Table 2.1). *YHR094C* (*HXT1*) encodes a low affinity hexose transporter induced only at high glucose concentration, and the loss of function would decrease the glucose uptake rate when its

concentration was high (23, 24). *YML088W* (*UFO1*) encodes a subunit of the SCF ubiquitin ligase complex responsible for the ubiquitination and subsequent degradation of regulatory and signaling proteins (25), and the inactivation might enhance the intracellular stability of Mth1p. The mechanisms of *YER046W* and *YLR412C* mutations in the evolved phenotype remain unclear. Notably, about 25% of the SNVs were found in the mitochondrial DNA (Table 2.1), which agreed with the requirement of mitochondrial activity for cell growth in the Pdc^- strain. Since the phenotypes of the three evolved strains were similar, Pdc^-/MTH1T-e1 (E10) was chosen for further studies.

2.2.2 Simultaneous utilization of glucose and non-glucose carbon sources by the pyruvate overproducing yeast strain

2.2.2.1 Co-utilization of glucose and galactose

Since the overexpression of *MTH1* released glucose repression, we hypothesized that this engineered strain (E10) might enable the utilization of glucose and non-glucose sugars simultaneously. To test this hypothesis, co-fermentation of glucose and galactose, which are the major carbohydrate components of red algae, was carried out. Although *S. cerevisiae* can consume galactose efficiently using the endogenous Leloir pathway, its utilization is completely inhibited with the presence of glucose in the wild-type strain (14). Interestingly, glucose and galactose were consumed simultaneously in the Pdc^- strain, without any glucose repression phenomena observed (Figure 2.3A). 10 g/L glucose and 10 g/L galactose were metabolized in 20 hours after inoculation, and the specific consumption rate of glucose and galactose was rather similar.

2.2.2.2 Co-utilization of glucose, galactose, and acetate

Although acetate was not reported to be present in the hydrolysate of red seaweed at high concentration, acetic acid hydrolysis was proposed to be a better method than the traditional sulfuric acid hydrolytic technology (26, 27). Therefore, co-fermentation of glucose and galactose was also carried out in the presence of acetate. As shown in Figure 2.3B, all three components, 10 g/L glucose, 10 g/L galactose, and 2 g/L acetate, were consumed nearly at the same rate. Interestingly, the sugar consumption rate was even higher with the presence of acetate, which may serve as a source to generate cytosolic acetyl-CoA for lipid and hormone biosynthesis. Similar growth and sugar consumption rates were observed if acetate is supplemented to the medium in the range of 5% to 15% of total sugar (data not shown). In other words, acetate, the previously reported inhibitor (28), can unexpectedly enhance the cell growth and sugar consumption rates of the engineered strain at the concentration range typically found in the biomass hydrolysate (5-10% of total sugar) (29).

*2.2.3 Co-fermentation of glucose and galactose to produce enantiopure (2*R,3R*)-butanediol at high titer and yield*

2.2.3.1 BDO production in the evolved Pdc$^-$ strain

By introducing a BDO biosynthetic pathway into the Pdc$^-$ strain, glycolytic flux was redirected into BDO fermentation (Figure 2.1). Notably, better cell growth and enhanced sugar consumption were observed in the strain containing the BDO pathway (E10/RBDO) when the oxygen level was low (Figure 2.4). Particularly, BDO fermentation enabled the growth and sugar utilization of the engineered Pdc$^-$ strain under anaerobic condition. In other words, the introduction of the BDO pathway could partially restore anaerobic growth of the Pdc$^-$ yeast strain.

Acetoin was accumulated to a high level under aerobic condition, while glycerol was the major byproduct under anaerobic condition (Figure 2.4 and Table 2.2). In addition, higher BDO yield and productivity were achieved in YP medium than those in SC medium (Table 2.2). Therefore, subsequent BDO fermentation studies were carried out under oxygen-limited condition in a rich medium. In YP medium supplemented with 10 g/L glucose and 10 g/L galactose, the BDO yield was higher than 70% of the theoretical value (Figure 2.5A and Table 2.2).

2.2.3.2 Chirality of BDO produced in the evolved Pdc$^-$ strain

Interestingly, only one peak for BDO was detected in the HPLC chromatogram of the fermentation broth, indicating the production of enantiopure BDO in strain E10/RBDO. To determine the chirality of the BDO produced, enantiopure *R*-BDO and *meso*-BDO were loaded to the column. Using the HPLC method mentioned in Methods and Materials, acetoin, *meso*-BDO and *R*-BDO can be separated (Figure 2.6A, B, C, and D). Owing to the stereospecificity of the yeast BDH, *R*-BDO and *meso*-BDO are synthesized from *R*-acetoin and *S*-acetoin, respectively (30). Thus, *S*-BDO was not included in this study. Accordingly, it could be concluded that only *R*-BDO, with *R*-acetoin as the intermediate, was synthesized in the Pdc$^-$ yeast strain (Figure 2.6E, F, and G). As a comparison, in our previous work to redirect the flux from ethanol to BDO by inactivating *ADH*s, a mixture of *R*-BDO and *meso*-BDO were produced at low yield and productivity, and the production of ethanol as the major product as well as the accumulation of acetate were observed (Figure 2.6H).

2.2.3.3 Fed-batch fermentation to improve BDO production

Similar to previously reported results (3, 22), sugar utilization was severely impaired after complete disruption of *PDC*s. Although the Pdc$^-$ strain was engineered for better growth on

glucose via introduction of *MTH1* and adaptive evolution, the sugar consumption rate and BDO productivity were decreased at higher sugar concentrations (Table 2.3). Thus fed-batch fermentation was carried out to produce more BDO in a fermentor. By feeding the same concentration of glucose and galactose continuously to the bioreactor, BDO continued to be synthesized in up to 300 hours, and more than 100 g/L (roughly 1100 mM) was produced at the end of fermentation (Figure 2.5B). Moreover, the concentration of glucose and galactose in the bioreactor was maintained relatively constant, indicating the simultaneous utilization of glucose and galactose during the whole fermentation process.

2.2.4 Construction of an enantiopure meso*-BDO producer and its further conversion to MEK and 2-butanol*

2.2.4.1 Construction of an enantiopure *meso*-BDO producer

Although *R*-BDO has advantages to be used as an anti-freeze agent, *meso*-BDO will be desired in some cases, such as the further biological conversion to methyl ethyl ketone (MEK, also known as 2-butanone) and 2-butanol. A *meso*-BDO biosynthetic pathway containing the acetolactate synthase gene from *Bacillus licheniformis* (Bl*BudB*), the acetolactate decarboxylase gene from *Enterobacter cloacae* (Ec*BudA*), and the *meso*-butanediol dehydrogenase gene from *E. cloacae* (Ec*BudC*) was introduced into E10 to construct E10/mBDO, which produced a mixture of *R*-BDO and *meso*-BDO. This results indicated that the endogenous (2*R*,3*R*)-butanediol dehydrogenases (*R*-BDHs), encoded by *BDH1* and *BDH2*, were sufficient for *R*-BDO production. Since only *meso*-BDO could be biologically converted to MEK and 2-butanol, both *BDH1* and *BDH2* were disrupted to construct PB, a strain deficient in both PDC and BDH activities. As

expected, introduction of the *meso*-BDO pathway into strain PB allowed the production of enantiopure *meso*-BDO (Figure 2.6I), which has not been reported in literature yet.

2.2.4.2 Further conversion of *meso*-BDO to MEK and 2-butanol using B_{12}-dependent diol dehydratases

The production of MEK and 2-butanol from *meso*-BDO was first described in Lactobacilli and the biosynthetic pathway (Figure 2.7) was proposed as a two-step process, dehydration of *meso*-BDO to MEK by a diol dehydratase and hydrogenation of MEK to 2-butanol by a secondary alcohol dehydrogenase (Sadh) (31). Later it was found that the diol dehydratase was induced by the presence of a diol substrate, such as 1,2-propanediol and *meso*-BDO (32), indicating its involvement in the conversion of *meso*-BDO. Naturally, diol dehydratase is involved in fucose utilization with 1,2-propanediol as the native substrate (33), but has been widely used for 1,3-propanediol production from glycerol (34) (named glycerol dehydratase or GDH in this case). Although the activity towards BDO has been reported, the use of diol dehydratase for MEK and 2-butanol production is rather limited. Recently, MEK or 2-butanol production from *meso*-BDO was reported in both *Escherichia coli* (35) and *S. cerevisiae* (36). In the former work, diol dehydratase (*dhaB123*, also named as *pduCDE*) and its reactivator genes (*orfz* and *orfB2*, also known as *pduGH*) from *Klebsiella pneumonia* were introduced into *E. coli*, which was able to produce 13.2 mg/L MEK from 5g/L *meso*-BDO. When the MEK pathway was combined with a *meso*-BDO pathway, the new strain could produce up to 151 mg/L MEK from glucose directly. In the latter work, a diol dehydratase and its reactivator genes (*pdcCDEGH*) from *Lactobacillus reuterii* and a *Sadh* gene from *Gordonia sp.* were introduced into a *gpd1*Δ *gpd2*Δ *S. cerevisiae* strain, which was able to produce small amount of MEK and 2-butanol under anaerobic condition (36).

Based on these studies, diol dehydratase and its re-activator genes from both *K. pneumonia* (Kp*PduCDEGH*) and *L. reuterii* (Lr*PduCDEGH*) were cloned and tested in our enantiopure *meso*-BDO producing yeast. Since MEK is rather volatile, the production of 2-butanol was attempted first, by co-expressing a *Sadh*. First of all, several endogenous ADHs and those from *E. coli* were tested for their activity to reduce MEK to 2-butanol. Unfortunately, except that Adh2p and FucO from *E. coli* showed little activity, none of these ADHs showed much higher activity than the control strain (Figure 2.8). Then a *Sadh* gene from *Achromobacter xylosoxidans* (Ax*Sadh* or Ax*Bdh*) was codon-optimized and cloned using two gBlocks. Indeed, significant MEK reducing activity was detected in Ax*Bdh* containing yeast strain, which was then used for following 2-butanol production studies.

The production of 2-butanol was tested in the wild-type strains expressing either Kp*PduCDEGH* or Lr*PduCDEGH* with *meso*-BDO supplementation (butanediol to 2-butanol, B2B). Unfortunately, none of the recombinant yeast strains (CEN/KpB2B, CEN/LrB2B, and CEN/LrB2B2) could produce any detectable levels of MEK or 2-butanol. Since the intracellular concentration of *meso*-BDO for bioconversion might be limited by its uptake rate, especially when glucose was present, it was desirable to test the production of 2-butanol in the *meso*-BDO producing strains (glucose to 2-butanol, D2B). Since glycerol was produced at high levels under anaerobic condition and proposed to be a competitive inhibitor for BDO dehydration, *GPD1* and *GPD2* responsible for glycerol formation were further deleted in the iPB strain to construct iGPB (Figure 2.9), a strain deficient in GPD, PDC, and BDH activities. As expected, no glycerol formation was observed in the iGPB/mBDO strain, which still produced enantiopure *meso*-BDO (Figure 2.6J). Again, no MEK or 2-butanol could be detected in all recombinant yeast strains (iGPB/KpD2B and iGPB/LrD2B) under all tested conditions, probably due to a lack of

coenzyme B_{12} uptake system in *S. cerevisiae*, which was a required cofactor for diol dehydratases from both *K. pneumonia* and *L. reuterii*. Although the production of MEK and 2-butanol using the diol dehydratase from *L. reuterii* was reported, the titer was extremely low and the identities of MEK or 2-butanol were not further confirmed by MS (36).

2.2.4.3 B_{12}-independent diol dehydratases for *meso*-BDO conversion

Besides B_{12}-dependent ones, there are also B_{12}-independent diol dehydratases in nature, which are oxygen-sensitive and require S-adenosylmethionine (SAM) as a cofactor. Since SAM is a natural metabolite in *S. cerevisiae* and anaerobic fermentation is preferred for industrial applications, we then switched to B_{12}-independent diol dehydratases. Although the importance for cost-effective production of 1,3-propanediol, there have been only a few B_{12}-independent diol dehydratases reported so far, such as those from *Clostridium butyricum* (37), *Clostridium phytofermentans* (38), and *Roseburia inulinivorans* (33). In this work, genes encoding the diol dehydratase (Ri*GdhA*) and its activator (Ri*GdhB*) from *R. inulinivorans* were codon-optimized for expression in *S. cerevisiae* and cloned into high copy number plasmids with *HIS3* and *LEU2* selection marker, respectively, by DNA2.0. Unfortunately, there was still no production of MEK and 2-butanol either in the wild-type strain with *meso*-BDO supplementation (CEN/RiB2B) or the *meso*-BDO producing strain (iGPB/RiD2B).

2.2.4.4 Diol dehydratase-mediated *n*-propanol production from 1,2-propanediol

As mentioned above, 1,2-propanediol is the natural substrate of diol dehydratases. To confirm that diol dehydratases could be functionally expressed in *S. cerevisiae*, 1,2-propanediol was fed to the growth medium instead of *meso*-BDO, which might result in the production of *n*-propanol. However, no production of *n*-propanol was detected. Although vacuum and nitrogen

purge was repeated several cycles, the presence of small amount of oxygen in the medium could still completely abolish the B_{12}-independent diol dehydratase activities. Therefore, high cell density fermentation was used for *n*-propanol production, assuming that small amount of oxygen could be consumed by yeast metabolism. Interestingly, a small peak with the same retention time as *n*-propanol standard was detected by GC-MS (Figure 2.10). Although the MS fragmentation patterns were not exactly the same, all characteristic MS fragments of *n*-propanol (m/z 31, 42, and 59) were identified. The peak was so small that the additional noisy fragments might result from the background. Although we tried to optimize the GC-MS program, the separation of the "*n*-propanol peak" and the "background peak" was not successful. In addition, the area of this peak was positively correlated with the exogenously added SAM (Figure 2.10F), a cofactor of B_{12}-independent diol dehydratase, further confirming that it was indeed the *n*-propanol peak. Considering the low production of *n*-propanol and the much lower activity of diol dehydratase towards *meso*-BDO, the conversion of *meso*-BDO to MEK and 2-butanol was not further attempted.

2.3 Discussions

Unlike many BDO native producers, *S. cerevisiae* is an industrially friendly cell factory for the production of bio-based fuels and chemicals (39). During normal alcoholic fermentation, several endogenous pathways in *S. cerevisiae*, mainly the PDC-dependent pathway and acetolactate synthase-dependent pathway, lead to the formation of a small amount of BDO (30). Although at a low concentration around 1 mM, the BDO produced by the wild-type yeast constitutes a mixture of 67% *R*-BDO and 33% *meso*-BDO, derived from (*3R*)-acetoin and (*3S*)-acetoin, respectively (30). Metabolic engineering, which has been widely used to redirect the metabolic flux to the desired products in various hosts (40-43), was also applied to the

production of BDO in *S. cerevisiae*. By disrupting the pyruvate decarboxylases and introducing a BDO biosynthetic pathway (Figure 2.1), BDO was produced at high titer and yield. Moreover, only one enantiopure form (*R*-BDO) was produced in the Pdc$^-$ strain (Figure 2.6), indicating the important role of PDCs in the biosynthesis of *meso*-BDO. For certain applications where enantiopure BDO is needed, e.g. the use of *R*-BDO as an antifreeze agent, the yeast strain constructed in this study should be advantageous compared to other reported engineered yeast strains and the native BDO producers.

Many renewable feedstocks contain different sugar components, such as glucose and xylose from cellulosic biomass, glucose and galactose from red algae, and glucose and mannitol from brown algae. To increase the productivity of the fermentation process, it is desirable to engineer a yeast strain capable of consuming a mixture of sugars simultaneously. Although intensive studies have contributed to understanding the mechanisms of catabolite repression, the construction of a glucose-derepressed yeast strain has never been achieved, probably due to the complex regulation of the glucose signaling network (11, 44). In the present work, the Pdc$^-$ strain was found to enable co-utilization of glucose and galactose, with or without the presence of acetate (Figure 2.3). Therefore, the constructed strain would be an ideal host to produce bio-based fuels and chemicals from red algae-derived sugar mixtures. To use lignocellulose as a feedstock, a yeast strain that can consume glucose and xylose efficiently and simultaneously needs to be engineered, which is a more challenging task. However, the COMPACTER method (15) developed in our lab, which allowed rapid optimization of host-specific metabolic pathways by fine-tuning the expression levels of multiple genes simultaneously, can be applied to construct an efficient xylose utilization pathway in the Pdc$^-$ strain. Simultaneous utilization of glucose and

xylose may be achieved in the glucose derepressed host with an optimized xylose utilization pathway.

Due to the net generation of one NADH molecule in BDO biosynthesis from glucose, glycerol is produced as the major byproduct (Figures 2.1 and 2.6E), especially under low oxygen level or anaerobic conditions. Although the deletion of *GPD1* and *GPD2* was able to completely abolish glycerol production, the host was reported to have no growth under anaerobic conditions because of the lack of an electron sink to re-oxidize the generated NADH molecule (45). Recently, acetate was proposed to be used as an electron sink in *S. cerevisiae* by introducing the *E. coli mhpF* gene, an acetylating NAD^+-dependent acetaldehyde dehydrogenase, which converts acetyl-CoA to acetaldehyde then to ethanol by the endogenous ADHs (45). Compared with the glycerol sink, there are several advantages to use acetate as the electron acceptor. First of all, acetate is a cheap substrate and widely existed in biomass hydrolysates (28, 29). In addition, two NADH molecules will be re-oxidized per ethanol molecule produced from acetate, while only one NADH molecule will be re-oxidized per glycerol molecule produced from glucose.

Another strategy to overcome the glycerol accumulation issue is to further convert *meso*-BDO to 2-butanol, whose biosynthesis from glucose is NADH neutral. Another advantage of 2-butanol production over BDO production is the lower cost of separation from fermentation broth. Since BDO is miscible with water, the separation cost is one of the major challenges that hinder the commercialization of Bio-BDO (5). Although diol dehydratases could be functionally expressed in *S. cerevisiae* when 1,2-propanediol was supplemented as the substrate, neither B_{12}-dependent nor B_{12}-independent diol dehydratases showed any activity towards *meso*-BDO and enabled 2-butanol production. As for the B_{12}-dependent system, the capability of coenzyme B_{12} uptake by yeast cells together with its high cost were the major concerns, and the construction of

a B_{12} producing yeast strain was rather desirable. As for the B_{12}-independent system, the diol dehydratases were extremely sensitive to oxygen, and the whole fermentation process should be performed under strictly anaerobic condition. Because *meso*-BDO is not the natural substrate for diol dehydratases, protein engineering (46) must be performed for both B_{12}-dependent and B_{12}-independent diol dehydratases to increase their activity and/or specificity towards BDO.

2.4 Conclusions and Perspectives

In summary, a pyruvate overproducing yeast strain was constructed by complete disruption of pyruvate decarboxylase activity, and the growth on glucose was restored by the overexpression of *MTH1* followed by adaptive evolution. Due to the glucose-derepressed properties, the engineered strain enabled co-fermentation of glucose and non-glucose carbon sources, such as galactose and galactose/acetate. After the introduction of an *R*-BDO biosynthetic pathway, enantiopure *R*-BDO was produced at high titer and yield from a mixture of glucose and galactose. By feeding glucose and galactose continuously, more than 100 g/L *R*-BDO was produced, which is the highest BDO titer ever reported in yeast. Future work will focus on engineering of the yeast strains to simultaneously consume sugar mixtures from other renewable resources, such as glucose and xylose from lignocellulosic biomass. Similarly, a yeast strain that could produce enantiopure *meso*-BDO was also constructed and its further conversion to MEK and 2-butanol was attempted. Currently, the diol dehydratase catalyzed reaction was the rate-limiting step for the production of MEK and 2-butanol, which required the involvement of protein engineering to improve their activity and/or specificity towards BDO. In addition, the pyruvate overproducing strain constructed will be a good start point for acetyl-CoA pool engineering, another important precursor metabolite that can be generated from pyruvate.

2.5 Materials and Methods

2.5.1 Strains, media, and cultivation conditions

All engineered strains used in this chapter are based on *S. cerevisiae* CEN.PK2-1C strain. *E. coli* strain DH5α was used to maintain and amplify plasmids. Yeast strains were cultivated in complex medium consisting of 2% peptone and 1% yeast extract supplemented with the corresponding carbon source, such as glucose (YPD), galactose (YPG), and/or ethanol (YPE). Recombinant strains were grown on complete synthetic (SC) medium consisting of 0.17% yeast nitrogen base, 0.5% ammonium sulfate, and the appropriate amino acid drop out mix (CSM-HIS-TRP-LEU-URA, MP Biomedicals, Solon, OH), supplemented with the corresponding carbon source. *E. coli* strains were cultured at 37^{o}C in Luria-Bertani broth containing 100 μg/mL ampicillin. *S. cerevisiae* strains were cultured at 30^{o}C and 250 rpm for aerobic growth, and 30^{o}C and 100 rpm for oxygen limited fermentation. For anaerobic fermentation, anaerobic culture tubes with butyl rubber stoppers and aluminum seals (Chemglass Life Sciences, Vineland, NJ) were vacuumed and purged with nitrogen to remove the residual oxygen and 480 mg/L Tween-80 and 10 mg/L ergosterol were supplemented as anaerobic growth factors. Coenzyme B_{12} was supplemented at a final concentration of 0.5 g/L when B_{12}-dependent diol dehydratases were included. All restriction enzymes, Q5 polymerase, and the *E. coli - S. cerevisiae* shuttle plasmids were purchased from New England Biolabs (Ipswich, MA). All chemicals were purchased from either Sigma-Aldrich or Fisher Scientific.

2.5.2 DNA manipulation

The yeast homologous recombination based DNA assembler method (47) was used to construct the recombinant plasmids used in this chapter, which were listed in Table 2.4. Briefly,

DNA fragments sharing homologous regions to adjacent DNA fragments were generated via polymerase chain reaction (PCR). The desired DNA fragments were purified with a QIAquick Gel Extraction Kit (Qiagen, Valencia, CA) and co-transformed into *S. cerevisiae* along with the linearized backbone to assemble several elements in a single step manner. The *MTH1* gene was amplified from the genomic DNA of CEN.PK2-1C strain. To construct the internal truncated *MTH1* (*MTH1*T) (3), the N-terminal fragment (1-168 bp) and C-terminal fragment (394-1302 bp) were amplified separately and pieced together using the DNA assembler method. For the construction of the *R*-BDO pathway (Figure 2.1), the endogenous acetolactate synthase gene without the mitochondrial targeting sequence (cyto*ILV2*, 271-2064 bp, predicted by MITOPROT (48)), the *Bacillus subtilis* acetolactate decarboxylase gene (Bs*AlsD*, NCBI Accession No. NP_391481.1), and the endogenous butanediol dehydrogenase (*BDH1*) gene were PCR-amplified from their corresponding genomic DNAs and assembled into the 2μ multiple copy plasmid, pRS426. Wizard Genomic DNA Purification Kit (Promega, Madison, WI) was used to extract the genomic DNA from both bacteria and yeast, according to the manufacturer's protocol. To confirm the correct clones, yeast plasmids were isolated using a Zymoprep Yeast Plasmid Miniprep II Kit (Zymo Research, Irvine, CA) and re-transformed into *E. coli*. Plasmids were isolated using a QIAprep Spin Miniprep Kit (Qiagen) and confirmed using both diagnostic PCR and restriction digestion. A *meso*-BDO biosynthetic pathway (pRS416-mBDO), containing the acetolactate synthase gene from *Bacillus licheniformis* (Bl*BudB*), the acetolactate decarboxylase gene from *Enterobacter cloacae* (Ec*BudA*), and the *meso*-butanediol dehydrogenase gene from *E. cloacae* (Ec*BudC*), was kindly provided by Dr. Mingzi Zhang (Metabolic Engineering Research Lab, A*STAR, Singapore). Plasmids pRS313-Lr*PduCDE*, pUC57-Lr*PduGH*, and pRS315-*Sadh* were a gift from Prof. Christer Larsson from Chalmers University of Technology (Gothenburg,

Sweden) (36). *TDH3p(GPDp)-PduG PduH-ADH1t* cassette in pUC57-Lr*PduGH*, an integrative plasmid, was sub-cloned into pRS414 and pRS415, respectively, at the *Sal*I and *Sac*I sites. Yeast strains were transformed using the LiAc/SS carrier DNA/PEG method (49), and transformants were selected on the appropriate SC plates.

2.5.3 Strain construction

All the strains used in this chapter were listed in Table 2.5. For the construction of Pdc^- strain, the *loxP-KanMX-loxP* method (21) was used for successive deletion of all three structural genes in the order of *PDC5-PDC6-PDC1*. The resultant Pdc^- strain was maintained in medium with ethanol as the sole carbon source. After restoring the growth on glucose, the *MTH1* containing strains (Pdc^-/MTH1 and Pdc^-/MTH1T) were maintained on low concentration glucose (5 g/L). To make the strain more suitable for practical use, adaptive evolution by serial transfer in 20 g/L glucose was carried out to improve the glucose consumption rate. The resultant strain (E10) was transformed with an *R*-BDO or *meso*-BDO biosynthetic pathway to construct strain E10/RBDO and E10/mBDO, respectively. *BDH1* and *BDH2* were knocked out in E10 strain using the same *loxP-KanMX-loxP* method (21) to construct strain PB. Further disruption of *GPD1* and *GPD2* was achieved using HI-CRISPR system (50) developed in our group in a single step, by introducing an 8bp deletion into the desired coding sequences (392-399 deletion in *GPD1* locus and 601-608 deletion in *GPD2* locus). The introduction of the desired deletion in both loci of strain iGPB was confirmed by DNA sequencing (Figure 2.9).

2.5.4 Flask and fed-batch fermentation

The recombinant yeast strains were pre-cultured in the appropriate SC medium, washed twice in ddH_2O, and then inoculated into YP medium supplemented with glucose and galactose

with an initial OD of 5, unless specified otherwise. To test the effect of acetate on the growth and product formation in the engineered Pdc^- strain, acetate was added into the medium at the concentration of 5% (16.7 mM), 10% (33.3 mM), or 15% (50 mM) of total sugar, respectively. For the engineered strains without the heterologous pathway, cells were cultured under aerobic condition, while oxygen limited condition was used for BDO fermentation.

Fed-batch fermentation was carried out in the Multifors Multiple Benchtop Bioreactors (Infors-HT, Bottmingen, Switzerland) with 0.5 L working volume. The temperature was controlled at 30°C and the pH of the culture media was maintained at 5.5 by controlled addition of 4N NaOH or 4N H_2SO_4. The dissolved oxygen concentration in the bioreactor was maintained at around 10-15% by controlling the air flow rate and agitation speed. Strain E10/RBDO was pre-cultured in SC-His-Ura medium and inoculated into 500 mL sterile YP medium supplemented with 10 g/L glucose and 10 g/L galactose with an initial OD of 5. After 16 hours of fermentation, glucose and galactose were fed simultaneously from sugar mixture stock containing 200 g/L glucose and 200 g/L galactose. Sugar feeding rate was micro-adjusted based on the sugar consumption rate, maintaining the sugar concentration in the fermentor at around 10 g/L.

2.5.5 Analytical methods

Cell growth was determined by measuring the absorbance at 600 nm using a Biotek Synergy 2 Multi-Mode Microplate Reader (Winooski, VT). For flask fermentation, samples were taken every 4 hours after inoculation. For fed-batch fermentation, samples were taken every 2-4 hours in the early stage to monitor sugar concentration in the fermentor and every 12 hours after reaching steady state. Extracellular metabolites, including glucose, galactose, acetate, and

butanediol, were detected and quantified using Shimadzu HPLC (Columbia, MD) equipped with an Aminex HPX-87H column (Bio-Rad, Hercules, CA) and Shimadzu RID-10A refractive index detector. The column was kept at 65ºC and 0.5 mM sulfuric acid solution was used as a mobile phase with a constant flow rate of 0.6 mL/min. Each data point represents the mean of at least duplicate samples.

2-Butanol was analyzed by a Shimadzu GCMS-QP2010 Plus GC-MS equipped with an AOC-20i+s autosampler (Shimadzu Inc., Columbia, MD) and a DB-Wax column with a 0.25 μm film thickness, 0.25 mm diameter, and 30 m length (Agilent Inc., Palo Alto, CA). Samples were extracted using the same volume of ethyl acetate containing 10 mg/L *n*-butanol as the internal standard and the top layer was analyzed by GC-MS. Injection port and interface temperature was set at 250 ºC, and the ion source was set to 230 ºC. The helium carrier gas was set at a constant flow rate of 2 mL/min. The oven temperature program was set as the following: a) hold at 50ºC for 3 min, b) increase at the rate of 15ºC min^{-1} to 120ºC, c) increase at the rate of 50ºC min^{-1} to 230ºC, d) and then hold at 230ºC for additional 2.5 min. The mass spectrometer was operated with a solvent cut time of 1.5 min, an event time of 0.2 s, a scan speed of 2500 from the range of 30-500 mass to charge (m/z) ratio.

2.5.6 Genome sequencing and single nucleotide variation (SNV) identification

Next generation sequencing of the whole genomes of Pdc^-/MTH1T, Pdc^-/MTH1T-e1 (E10), Pdc^-/MTH1T-e2, and Pdc^-/MTH1T-e3 was performed at the Roy J. Carver Biotechnology Center at the University of Illinois at Urbana-Champaign. The barcoded shotgun genomic DNA libraries were constructed with the TruSeq DNA Sample Preparation Kit (Illumina, San Diego, CA), and then quantitated by fluorometry (Qubit), a bioanalyzer (Agilent), and quantitative PCR.

Then the libraries were sequenced for 101 cycles from one end of the fragments (single-reads) for 100 nt on an Illumina HiSeq2000 using a TruSeq SBS Sequencing Kit version 3. FASTQ files were generated with Casava 1.8.3.

Each sample yielded approximately 25 million reads, and the average quality scores per base were higher than 30. High throughout sequencing data were analyzed using CLC Genomics Workbench version 6.5.1. Reads were trimmed based on quality scores, which were then mapped to an S288C reference sequence. SNVs were identified using the Probabilistic Variant Detection function. Then the Filter against Control Reads tool was used to remove the variants found in Pdc^-/MTH1T, generating the SNVs unique to Pdc^-/MTH1T-e1 (E10), Pdc^-/MTH1T-e2, and Pdc^-/MTH1T-e3.

2.6 References

1. **Abbott DA, Zelle RM, Pronk JT, van Maris AJA.** 2009. Metabolic engineering of *Saccharomyces cerevisiae* for production of carboxylic acids: current status and challenges. FEMS Yeast Res. **9:**1123-1136.
2. **Flikweert MT, de Swaaf M, van Dijken JP, Pronk JT.** 1999. Growth requirements of pyruvate-decarboxylase-negative *Saccharomyces cerevisiae*. FEMS Microbiol. Lett. **174:**73-79.
3. **Oud B, Flores CL, Gancedo C, Zhang X, Trueheart J, Daran JM, Pronk JT, van Maris AJ.** 2012. An internal deletion in *MTH1* enables growth on glucose of pyruvate-decarboxylase negative, non-fermentative *Saccharomyces cerevisiae*. Microb. Cell Fact. **11:**131.
4. **Celińska E, Grajek W.** 2009. Biotechnological production of 2,3-butanediol-current state and prospects. Biotechnol. Adv. **27:**715-725.
5. **Ji XJ, Huang H, Ouyang PK.** 2011. Microbial 2,3-butanediol production: a state-of-the-art review. Biotechnol. Adv. **29:**351-364.
6. **Syu MJ.** 2001. Biological production of 2,3-butanediol. Appl. Microbiol. Biotechnol. **55:**10-18.
7. **Wei N, Quarterman J, Jin YS.** 2013. Marine macroalgae: an untapped resource for producing fuels and chemicals. Trends Biotechnol. **31:**70-77.
8. **Wargacki AJ, Leonard E, Win MN, Regitsky DD, Santos CN, Kim PB, Cooper SR, Raisner RM, Herman A, Sivitz AB, Lakshmanaswamy A, Kashiyama Y, Baker D, Yoshikuni Y.** 2012. An engineered microbial platform for direct biofuel production from brown macroalgae. Science **335:**308-313.
9. **Wi SG, Kim HJ, Mahadevan SA, Yang DJ, Bae HJ.** 2009. The potential value of the seaweed Ceylon moss (*Gelidium amansii*) as an alternative bioenergy resource. Bioresour. Technol. **100:**6658-6660.
10. **Kim SR, Ha SJ, Wei N, Oh EJ, Jin YS.** 2012. Simultaneous co-fermentation of mixed sugars: a promising strategy for producing cellulosic ethanol. Trends Biotechnol. **30:**274-282.
11. **Vinuselvi P, Kim MK, Lee SK, Ghim CM.** 2012. Rewiring carbon catabolite repression for microbial cell factory. BMB Rep. **45:**59-70.
12. **Li S, Du J, Sun J, Galazka JM, Glass NL, Cate JH, Yang X, Zhao H.** 2010. Overcoming glucose repression in mixed sugar fermentation by co-expressing a cellobiose transporter and a β-glucosidase in *Saccharomyces cerevisiae*. Mol. Biosyst. **6:**2129-2132.
13. **Ha SJ, Galazka JM, Kim SR, Choi JH, Yang X, Seo JH, Glass NL, Cate JH, Jin YS.** 2011. Engineered *Saccharomyces cerevisiae* capable of simultaneous cellobiose and xylose fermentation. Proc. Natl. Acad. Sci. U. S. A. **108:**504-509.
14. **Ha SJ, Wei Q, Kim SR, Galazka JM, Cate J, Jin YS.** 2011. Cofermentation of cellobiose and galactose by an engineered *Saccharomyces cerevisiae* strain. Appl. Environ. Microbiol. **77:**5822-5825.
15. **Du J, Yuan Y, Si T, Lian J, Zhao H.** 2012. Customized optimization of metabolic pathways by combinatorial transcriptional engineering. Nucleic Acids Res. **40:**e142.

16. **Yuan Y, Zhao H.** 2013. Directed evolution of a highly efficient cellobiose utilizing pathway in an industrial *Saccharomyces cerevisiae* strain. Biotechnol. Bioeng. **110:**2874-2881.
17. **Eriksen DT, Hsieh PCH, Lynn P, Zhao H.** 2013. Directed evolution of a cellobiose utilization pathway in *Saccharomyces cervisiae* by simultaneously engineering multiple proteins. Microb. Cell Fact. **12:**61.
18. **Ha SJ, Galazka JM, Joong Oh E, Kordic V, Kim H, Jin YS, Cate JH.** 2013. Energetic benefits and rapid cellobiose fermentation by *Saccharomyces cerevisiae* expressing cellobiose phosphorylase and mutant cellodextrin transporters. Metab. Eng. **15:**134-143.
19. **Lian J, Li Y, HamediRad M, Zhao H.** 2014. Directed evolution of a cellodextrin transporter for improved biofuel production under anaerobic conditions in *Saccharomyces cerevisiae*. Biotechnol Bioeng **111:**1521-1531.
20. **Lian J, Chao R, Zhao H.** 2014. Metabolic engineering of a *Saccharomyces cerevisiae* strain capable of simultaneously utilizing glucose and galactose to produce enantiopure (2*R*,3*R*)-butanediol. Metab. Eng. **23:**92-99.
21. **Hegemann JH, Guldener U, Kohler GJ.** 2006. Gene disruption in the budding yeast *Saccharomyces cerevisiae*. Methods Mol. Biol. **313:**129-144.
22. **van Maris AJA, Geertman JMA, Vermeulen A, Groothuizen MK, Winkler AA, Piper MDW, van Dijken JP, Pronk JT.** 2004. Directed evolution of pyruvate decarboxylase-negative *Saccharomyces cerevisiae*, yielding a C_2-independent, glucose-tolerant, and pyruvate-hyperproducing yeast. Appl. Environ. Microbiol. **70:**159-166.
23. **Ozcan S, Johnston M.** 1995. Three different regulatory mechanisms enable yeast hexose transporter (*HXT*) genes to be induced by different levels of glucose. Mol. Cell. Biol. **15:**1564-1572.
24. **Scalcinati G, Knuf C, Partow S, Chen Y, Maury J, Schalk M, Daviet L, Nielsen J, Siewers V.** 2012. Dynamic control of gene expression in *Saccharomyces cerevisiae* engineered for the production of plant sesquitepene alpha-santalene in a fed-batch mode. Metab. Eng. **14:**91-103.
25. **Ivantsiv Y, Kaplun L, Tzirkin-Goldin R, Shabek N, Raveh D.** 2006. Unique role for the UbL-UbA protein Ddi1 in turnover of SCFUfo1 complexes. Mol. Cell. Biol. **26:**1579-1588.
26. **Kim HT, Yun EJ, Wang D, Chung JH, Choi IG, Kim KH.** 2013. High temperature and low acid pretreatment and agarase treatment of agarose for the production of sugar and ethanol from red seaweed biomass. Bioresour. Technol. **136:**582-587.
27. **Kim HT, Lee S, Kim KH, Choi IG.** 2012. The complete enzymatic saccharification of agarose and its application to simultaneous saccharification and fermentation of agarose for ethanol production. Bioresour. Technol. **107:**301-306.
28. **Himmel ME, Bayer EA.** 2009. Lignocellulose conversion to biofuels: current challenges, global perspectives. Curr. Opin. Biotechnol. **20:**316-317.
29. **Sedlak M, Ho NW.** 2004. Production of ethanol from cellulosic biomass hydrolysates using genetically engineered *Saccharomyces* yeast capable of cofermenting glucose and xylose. Appl. Biochem. Biotechnol. **113-116:**403-416.
30. **Gonzalez E, Fernandez M, Larroy C, Sola L, Pericas M, Pares X, Biosca J.** 2000. Characterization of a (*2R,3R*)-2,3-butanediol dehydrogenase as the *Saccharomyces cerevisiae YAL060W* gene product. J. Biol. Chem. **275:**35876-35885.

31. **Speranza G, Corti S, Fontana G, Manitto P, Galli A, Scarpellini M, Chialva F.** 1997. Conversion of *meso*-2,3-Butanediol into 2-Butanol by Lactobacilli. Stereochemical and Enzymatic Aspects. J. Agric. Food Chem. **45:**3476-3480.
32. **Ghiaci P, Lameiras F, Norbeck J, Larsson C.** 2014. Production of 2-butanol through *meso*-2,3-butanediol consumption in lactic acid bacteria. FEMS Microbiol. Lett. **360:**70-75.
33. **Scott KP, Martin JC, Campbell G, Mayer CD, Flint HJ.** 2006. Whole-genome transcription profiling reveals genes up-regulated by growth on fucose in the human gut bacterium "*Roseburia inulinivorans*". J. Bacteriol. **188:**4340-4349.
34. **Nakamura CE, Whited GM.** 2003. Metabolic engineering for the microbial production of 1,3-propanediol. Curr. Opin. Biotechnol. **14:**454-459.
35. **Yoneda H, Tantillo DJ, Atsumi S.** 2014. Biological production of 2-butanone in *Escherichia coli*. ChemSusChem **7:**92-95.
36. **Ghiaci P, Norbeck J, Larsson C.** 2014. 2-Butanol and butanone production in *Saccharomyces cerevisiae* through combination of a B_{12} dependent dehydratase and a secondary alcohol dehydrogenase using a TEV-based expression system. PLoS One **9:**e102774.
37. **O'Brien JR, Raynaud C, Croux C, Girbal L, Soucaille P, Lanzilotta WN.** 2004. Insight into the mechanism of the B_{12}-independent glycerol dehydratase from *Clostridium butyricum*: preliminary biochemical and structural characterization. Biochemistry **43:**4635-4645.
38. **Petit E, LaTouf WG, Coppi MV, Warnick TA, Currie D, Romashko I, Deshpande S, Haas K, Alvelo-Maurosa JG, Wardman C, Schnell DJ, Leschine SB, Blanchard JL.** 2013. Involvement of a bacterial microcompartment in the metabolism of fucose and rhamnose by *Clostridium phytofermentans*. PLoS One **8:**e54337.
39. **Hong KK, Nielsen J.** 2012. Metabolic engineering of *Saccharomyces cerevisiae*: a key cell factory platform for future biorefineries. Cell. Mol. Life Sci. **69:**2671-2690.
40. **Yu M, Zhang Y, Tang IC, Yang ST.** 2011. Metabolic engineering of *Clostridium tyrobutyricum* for n-butanol production. Metab. Eng. **13:**373-382.
41. **Atsumi S, Cann AF, Connor MR, Shen CR, Smith KM, Brynildsen MP, Chou KJ, Hanai T, Liao JC.** 2008. Metabolic engineering of *Escherichia coli* for 1-butanol production. Metab. Eng. **10:**305-311.
42. **Cooksley CM, Zhang Y, Wang H, Redl S, Winzer K, Minton NP.** 2012. Targeted mutagenesis of the *Clostridium acetobutylicum* acetone-butanol-ethanol fermentation pathway. Metab. Eng. **14:**630-641.
43. **Lan EI, Liao JC.** 2011. Metabolic engineering of cyanobacteria for 1-butanol production from carbon dioxide. Metab. Eng. **13:**353-363.
44. **Rolland F, Winderickx J, Thevelein JM.** 2002. Glucose-sensing and -signalling mechanisms in yeast. FEMS Yeast Res. **2:**183-201.
45. **Guadalupe Medina V, Almering MJ, van Maris AJ, Pronk JT.** 2010. Elimination of glycerol production in anaerobic cultures of a *Saccharomyces cerevisiae* strain engineered to use acetic acid as an electron acceptor. Appl. Environ. Microbiol. **76:**190-195.
46. **Eriksen DT, Lian J, Zhao H.** 2014. Protein design for pathway engineering. J. Struct. Biol. **185:**234-242.

47. **Shao Z, Zhao H, Zhao H.** 2009. DNA assembler, an *in vivo* genetic method for rapid construction of biochemical pathways. Nucleic Acids Res. **37:**e16.
48. **Claros MG, Vincens P.** 1996. Computational method to predict mitochondrially imported proteins and their targeting sequences. Eur. J. Biochem. **241:**779-786.
49. **Gietz RD, Schiestl RH.** 2007. High-efficiency yeast transformation using the LiAc/SS carrier DNA/PEG method. Nat. Protoc. **2:**31-34.
50. **Bao Z, Xiao H, Liang J, Zhang L, Xiong X, Sun N, Si T, Zhao H.** 2014. Homology-integrated CRISPR-Cas (HI-CRISPR) system for one-step multigene disruption in *Saccharomyces cerevisiae*. ACS Synth. Biol.**:**DOI: 10.1021/sb500255k.

2.7 Tables

Table 2.1 SNVs identified in the coding sequences (CDS) of evolved strains as compared with Pdc$^-$/MTH1T

Non-synonymous SNVs in CDS	Pdc$^-$/MTH1T-e1	Pdc$^-$/MTH1T-e2	Pdc$^-$/MTH1T-e3
YER046W (SPO73)		Frame shift after Thr13	
YHR094C (HXT1)		Frame shift after Pro420	
YLR412C		Frame shift after Gly46	
YML088W (UFO1)		Stop codon after Glu600	
YNR038W (DBP6)	-	-	Leu605Ser
SNVs in CDS	4	4	5
SNVs in mitochondrial DNA	8	7	8
Total SNVs	32	34	38

Table 2.2 Effect of oxygen levels on the yield and productivity of *R*-BDO and the major by-products, acetoin and glycerol. The concentrations of glucose and galactose were maintained at the same initial level. The fermentation of E10/RBDO was carried out in SC or YP medium supplemented with 10 g/L glucose 10 g/L galactose under aerobic, oxygen-limited, and anaerobic conditions. For oxygen limited condition, different amounts of liquid media, 5 mL (10%v/v), 10mL (20% v/v), 15 mL (30% v/v), and 20 mL (40% v/v), were added to 50 mL unbaffled shake flasks.

BDO Yield (mM/mM Sugar)		SC			YP		
		R-BDO	Acetoin	Glycerol	*R*-BDO	Acetoin	Glycerol
Aerobic		0.21±0.01	0.26±0.01	0±0	0.20±0.05	0.26±0.01	0.03±0.00
Oxygen -limited	10% (v/v)	N.D.	N.D.	N.D.	0.56±0.03	0.16±0.01	0.03±0.00
	20% (v/v)	0.60±0.01	0.02±0.00	0.27±0.02	0.71±0.05	0.02±0.00	0.12±0.01
	30% (v/v)	N.D.	N.D.	N.D.	0.71±0.07	0±0	0.24±0.03
	40% (v/v)	N.D.	N.D.	N.D.	0.65±0.09	0±0	0.31±0.04
Anaerobic		0.46±0.01	0±0	0.42±0.01	0.58±0.01	0±0	0.61±0.01

BDO Productivity (mM/h)		SC			YP		
		R-BDO	Acetoin	Glycerol	*R*-BDO	Acetoin	Glycerol
Aerobic		1.68±0.03	1.61±0.01	0±0	1.48±0.03	1.96±0.02	0.19±0.02
Oxygen -limited	10% (v/v)	N.D.	N.D.	N.D.	3.70±0.12	1.05±0.07	0.18±0.03
	20% (v/v)	4.00±0.51	0.08±0.00	2.09±0.01	4.59±0.02	0.13±0.00	0.82±0.02
	30% (v/v)	N.D.	N.D.	N.D.	4.51±0.04	0±0	1.54±0.01
	40% (v/v)	N.D.	N.D.	N.D.	4.09±0.17	0±0	1.97±0.06
Anaerobic		0.54±0.04	0±0	0.49±0.02	1.71±0.03	0±0	1.75±0.02

Table 2.3 BDO yield and productivity using different sugar concentrations. The concentrations of glucose and galactose were maintained at the same initial level. The fermentation was carried out under oxygen-limited conditions.

Sugar Concentration (g/L)		BDO Productivity	BDO Yield (mM
Glucose	Galactose	(mM/h)	BDO/mM Total Sugar)
10	10	4.63±0.15	0.67±0.02
20	20	4.19±0.08	0.71±0.01
30	30	3.80±0.17	0.77±0.03

Table 2.4 Plasmids constructed in this chapter

Plasmid	Features
pRS414	CEN/ARS-based single copy plasmid with *TRP1* marker
pRS415	CEN/ARS-based single copy plasmid with *LEU2* marker
pRS423	2μ-based multi-copy plasmid with *HIS3* marker
pRS424	2μ-based multi-copy plasmid with *TRP1* marker
pRS425	2μ-based multi-copy plasmid with *LEU2* marker
pRS426	2μ-based multi-copy plasmid with *URA3* marker
pUG6	Template for *loxP-KanMX-loxP* gene deletion cassette
pSH47	*GAL1p-Cre* with *URA3* marker
MTH1	pRS423-*PGK1p-MTH1-HXT7t*
MTH1T	pRS423-*PGK1p-MTH1*T-*HXT7t*
RBDO	pRS426-*ENO2p*-cyto*ILV2-PGK1t-TPI1p*-Bs*AlsD-TPI1t-TEF1p-BDH1-TEF1t*
mBDO	pRS416-*ADH1p*-Bl*BudB-ADH1t-PGK1p*-Ec*BudA-CYC1t-PYK1p*-Ec*BudC-ADH2t*
RiGdhA	pD1237-*GPDp*-Ri*GdhA-CYC1t* (2μ, *HIS3*)
RiGdhB	pD1211-*TEF1p*-Ri*GdhB-CYC1t* (2μ, *LEU2*)
KpPduCDE	pRS426-*TPI1p*-Kp*PduC-TPI1t-TEF1p*-Kp*PduD-TEF1t-PGK1p*-Kp*PduE -HXT7t*
KpPduGH	pRS426-*GPDp*-Kp*PduG-CYC1t-ENO2p*-Kp*PduH-PGK1t*
LrPduCDE	pRS313-*TDH3p(GPDp)*-Lr*PduC PduD PduE-RPL18Bt-RPS19Bp-TEV-ADH1t* (36)
pUC57-LrPduGH	pUC57-*TDH3p(GPDp)*-Lr*PduG PduH-ADH1t* (36)
pRS414-LrPduGH	pRS414-*TDH3p(GPDp)-PduG PduH-ADH1t*
pRS415-LrPduGH	pRS415-*TDH3p(GPDp)-PduG PduH-ADH1t*
GoSadh	pRS315-*TDH3p(GPDp)-GoSadh-ADH1t* (36)
AxSadh	pRS424-*TEF1p*-Ax*Sadh-TEF1t*
ADH4	pRS425-*TEF1p-ADH4-TEF1t*
ADH5	pRS425-*TEF1p-ADH5-TEF1t*
ADH6	pRS425-*TEF1p-ADH6-TEF1t*
ADH7	pRS425-*TEF1p-ADH7-TEF1t*
YGL157W	pRS425-*TEF1p*-YGL157W-*TEF1t*
SOR1	pRS425-*TEF1p-SOR1-TEF1t*
XYL2	pRS425-*TEF1p-XYL2-TEF1t*
SFA1	pRS425-*TEF1p-SFA1-TEF1t*
BDH1	pRS425-*TEF1p-BDH1-TEF1t*
BDH2	pRS425-*TEF1p-BDH2-TEF1t*

Table 2.4 (Cont.)

Plasmid	Features
EcFucO	pRS425-*TEF1p*-Ec*FucO-TEF1t*
EcEutG	pRS425-*TEF1p*-Ec*EutG-TEF1t*
EcYiaY	pRS425-*TEF1p*-Ec*YiaY-TEF1t*
EcYqhD	pRS425-*TEF1p*-Ec*YqhD-TEF1t*
CaBdhB	pRS425-*TEF1p*-Ca*BdhB -TEF1t*
ADH2	pRS425-*TEF1p-ADH2-TEF1t*
ADH4s	pRS425-*TEF1p-ADH4s-TEF1t*
pCRCT-GPD1a-GPD2b	*GPD1* and *GPD2* crRNAs cloned into pCRCT (50)

Table 2.5 Strains used in this chapter

Strain	Phenotype
CEN.PK2-1C	*MATa ura3-52 trp1-289 leu2-3,112 his3Δ1 MAL2-8^C SUC2*
Pdc$^-$	CEN.PK2-1C *pdc5*Δ::*loxP pdc6*Δ::*loxP pdc1*Δ::*KanMX*
Pdc$^-$/MTH1	Pdc$^-$/ pRS423-MTH1
Pdc$^-$/MTH1T	Pdc$^-$/ pRS423-MTH1T
E10	Pdc$^-$/MTH1T, evolved for better growth on glucose
E10/RBDO	E10/pRS426-RBDO
E10/mBDO	E10/pRS416-mBDO
PB	E10 *bdh1-bdh2*Δ::*KanMX*
PB/mBDO	PB/pRS416-mBDO
iPdc$^-$	Pdc$^-$ *MTH1*::*MTH1T*
iE11	iPdc$^-$ evolved for better growth on glucose
iPB	iE11 *bdh1-bdh2*Δ::*KanMX*
iGPB	iPB *gpd1*Δ-*gpd2*Δ
CEN/KpB2B	CEN.PK2-1C/KpPduCDE+ AxSadh+ KpPduGH
CEN/LrB2B	CEN.PK2-1C/LrPduCDE+ AxSadh+ LrPduGH
CEN/LrB2B2	CEN.PK2-1C/LrPduCDE+pRS414-LrPduGH+ GoSadh
CEN/RiB2B	CEN.PK2-1C/RiGdhA+ AxSadh+ RiGdhB
iGPB/KpD2B	iGPB/KpPduCDE+ AxSadh+ KpPduGH+ mBDO
iGPB/LrD2B	iGPB/LrPduCDE+ AxSadh+pRS415-LrPduGH+ mBDO
iGPB/RiD2B	iGPB/RiGdhA+ AxSadh+ RiGdhB+ mBDO

2.8 Figures

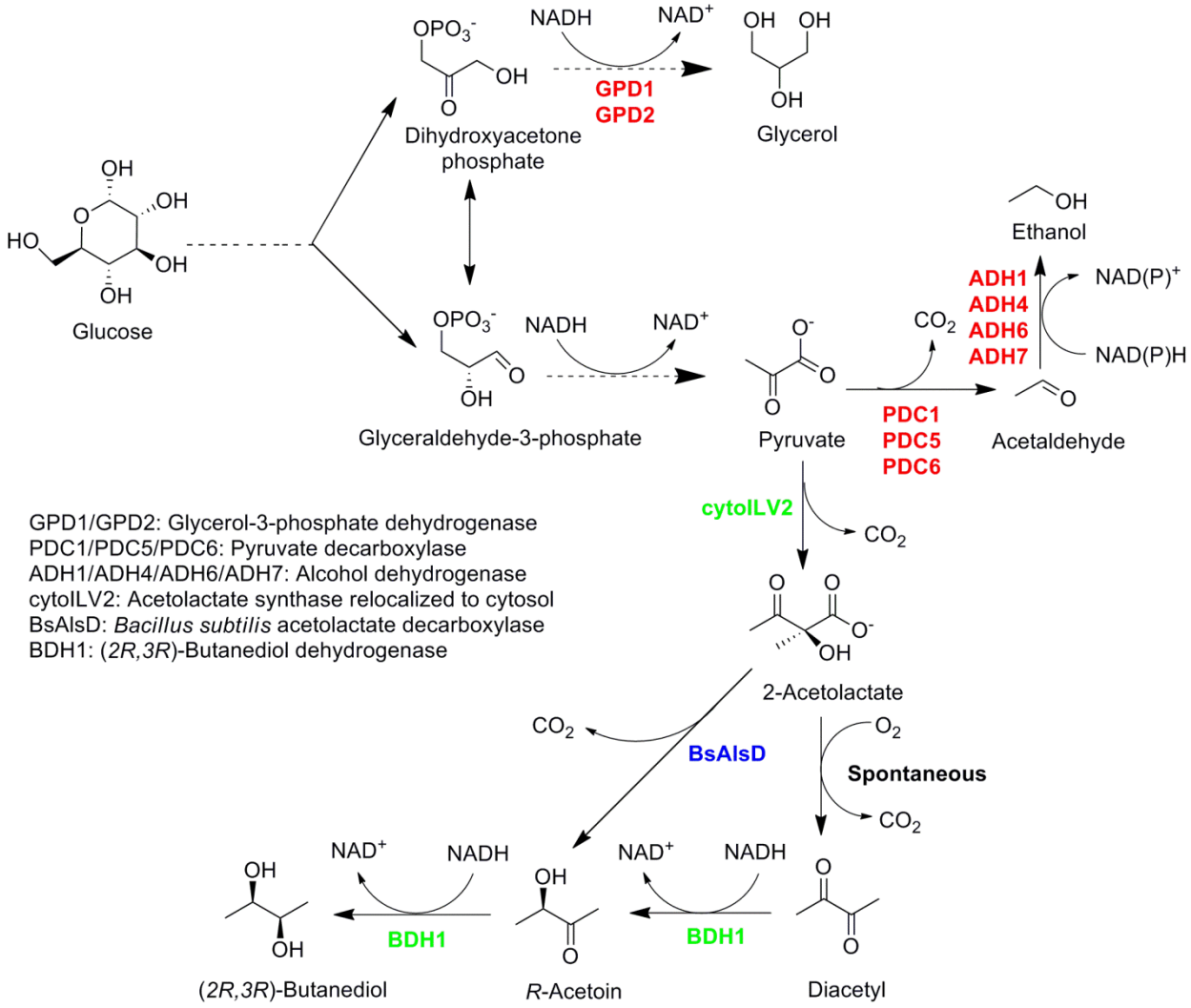

Figure 2.1 Metabolic pathway for the synthesis of (*2R,3R*)-butanediol in the engineered *S. cerevisiae* strain. The dashed arrows indicate several steps of enzymatic reactions. Genes in red represent the endogenous genes, which lead to the synthesis of major metabolites, such as ethanol and glycerol, and are targets to be inactivated to redirect the fluxes to BDO. As for the overexpressed BDO pathway, genes in green are cloned from *S. cerevisiae*, while the gene in blue indicates the heterologous *AlsD* gene.

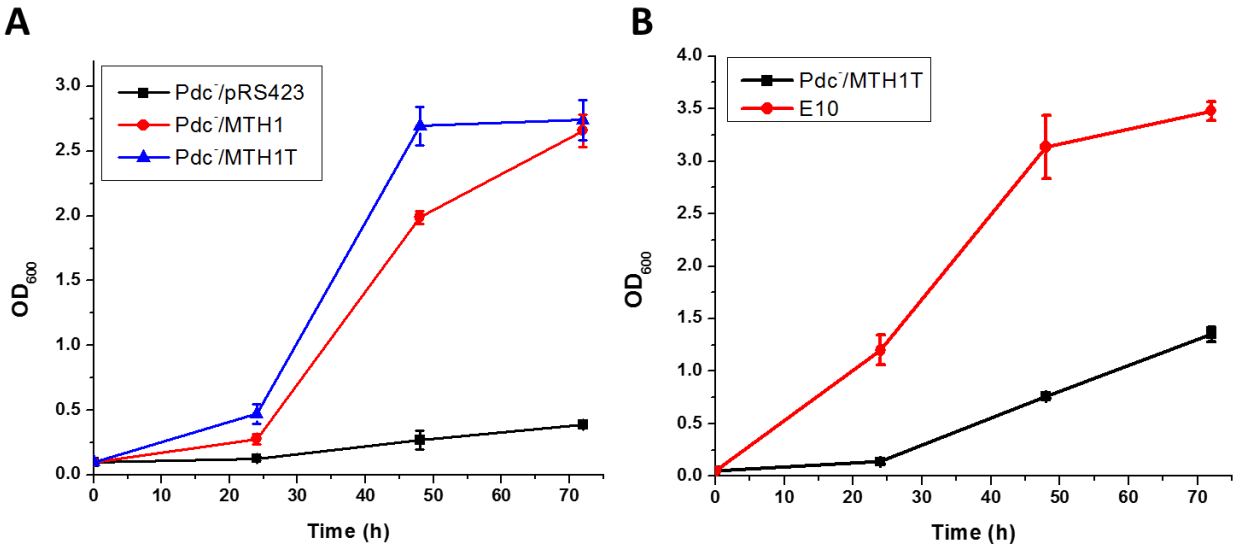

Figure 2.2 Construction of a Pdc$^-$ strain that can grow on glucose as the sole carbon source. A) Restoring the growth on glucose via the introduction of *MTH1* and *MTH1*T. B) Engineering better growth of strain Pdc$^-$/MTH1T on glucose via adaptive evolution. Yeast cells were pre-cultured on ethanol, inoculated into SC medium containing either 5 g/L (A) or 20 g/L (B) glucose with an initial OD of 0.05, and cultured under aerobic condition.

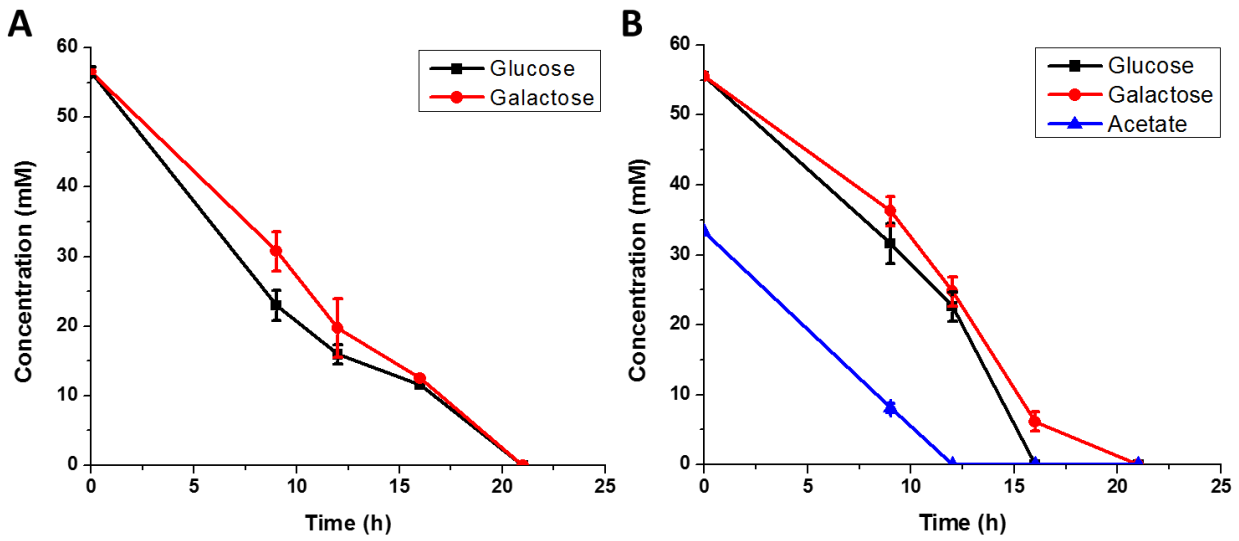

Figure 2.3 Co-utilization of glucose and non-glucose carbon sources in the engineered Pdc$^-$ yeast strain. A) Simultaneous consumption of glucose and galactose. B) Co-utilization of glucose and galactose with the presence of acetate at the concentration of 10% of total sugar.

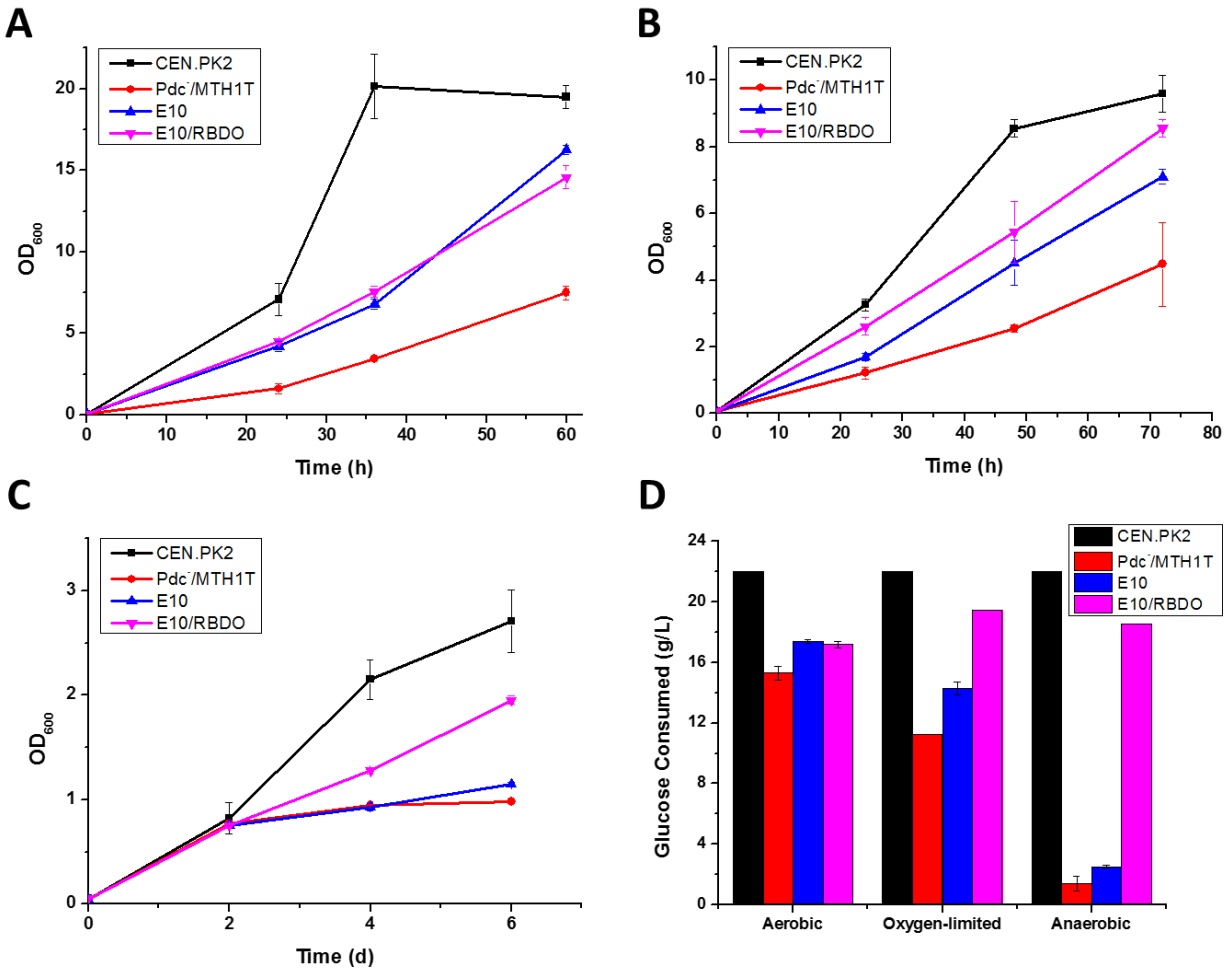

Figure 2.4 Comparison of the growth and sugar consumption of the evolved Pdc$^-$ strain with or without the BDO pathway. The wild-type strain (CEN.PK2), Pdc$^-$/MTH1T strain, evolved Pdc$^-$/MTH1T strain (E10), and the evolved strain with the BDO pathway (E10/RBDO) were cultured under aerobic (A), oxygen-limited (B), and anaerobic conditions (C). The amount of glucose consumed at the end of fermentation under these conditions was also compared (D). Yeast cells were pre-cultured on ethanol and inoculated into YPD media with an initial OD around 0.05.

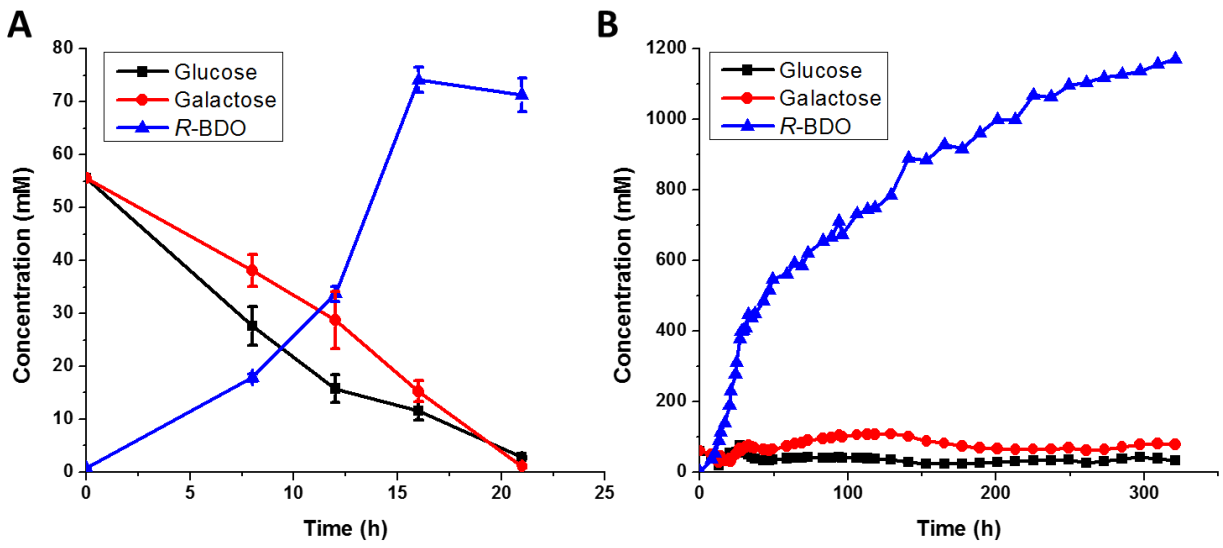

Figure 2.5 Co-fermentation of glucose and galactose for BDO production. A) BDO fermentation profile in shake flask with 10 g/L glucose and galactose under oxygen-limited condition. B) Fed-batch fermentation for BDO production. A mixture of sugars consisting of the same concentration of glucose and galactose was continuously fed to the bioreactor.

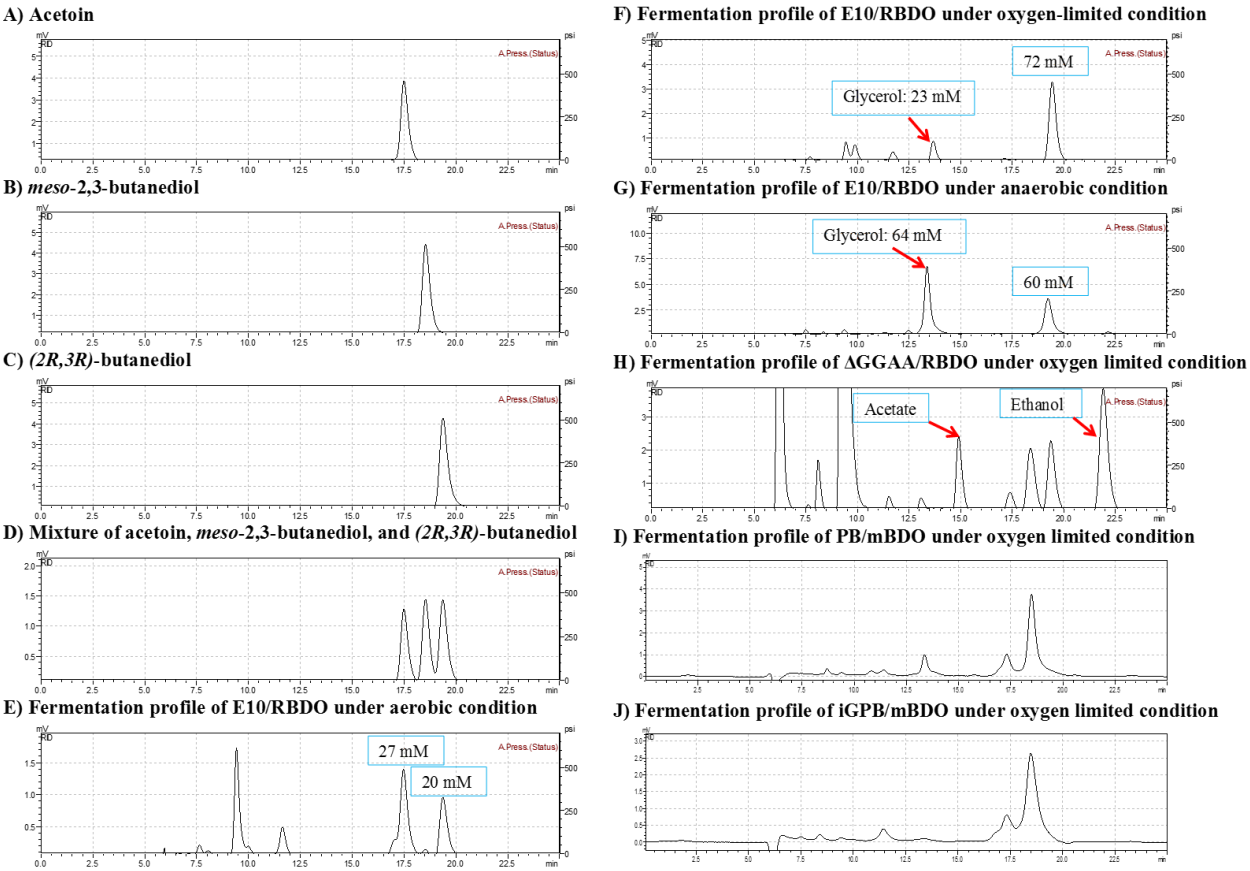

Figure 2.6 Separation of acetoin, *meso*-BDO and *R*-BDO via HPLC and BDO fermentation profiles. Since the yeast BDH is *R*-specific, which reduces *R*-acetoin and *S*-acetoin stereospecifically to *R*-BDO and *meso*-BDO, respectively, *S*-BDO is not included in this study.

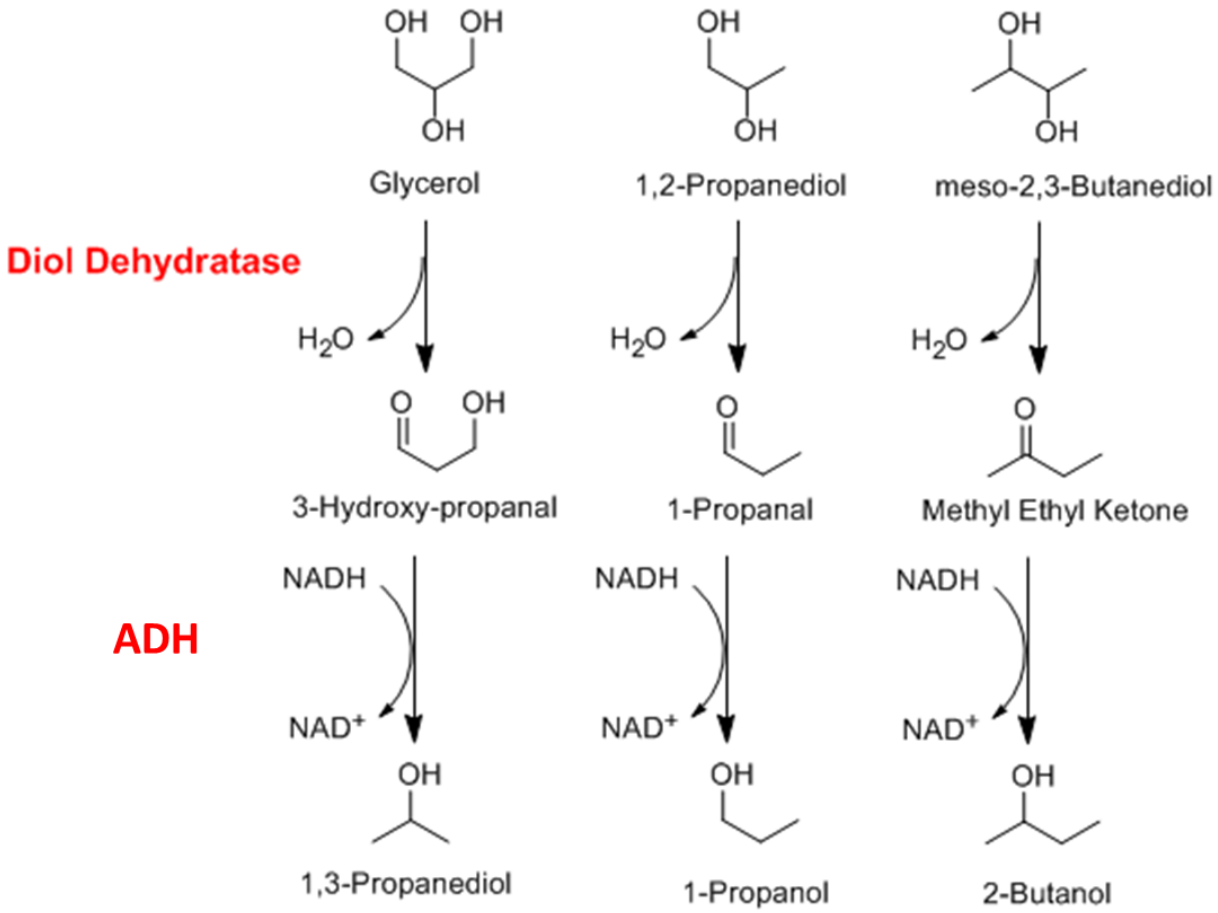

Figure 2.7 Diol dehydratase mediated 1,3-propanediol, 1-propanol, and 2-butanol production, with glycerol, 1,2-propanediol, and *meso*-BDO as the substrate, respectively. An ADH should also be included to reduce the corresponding aldehydes, with secondary alcohol dehydrogenase (Sadh) for 2-butanol production.

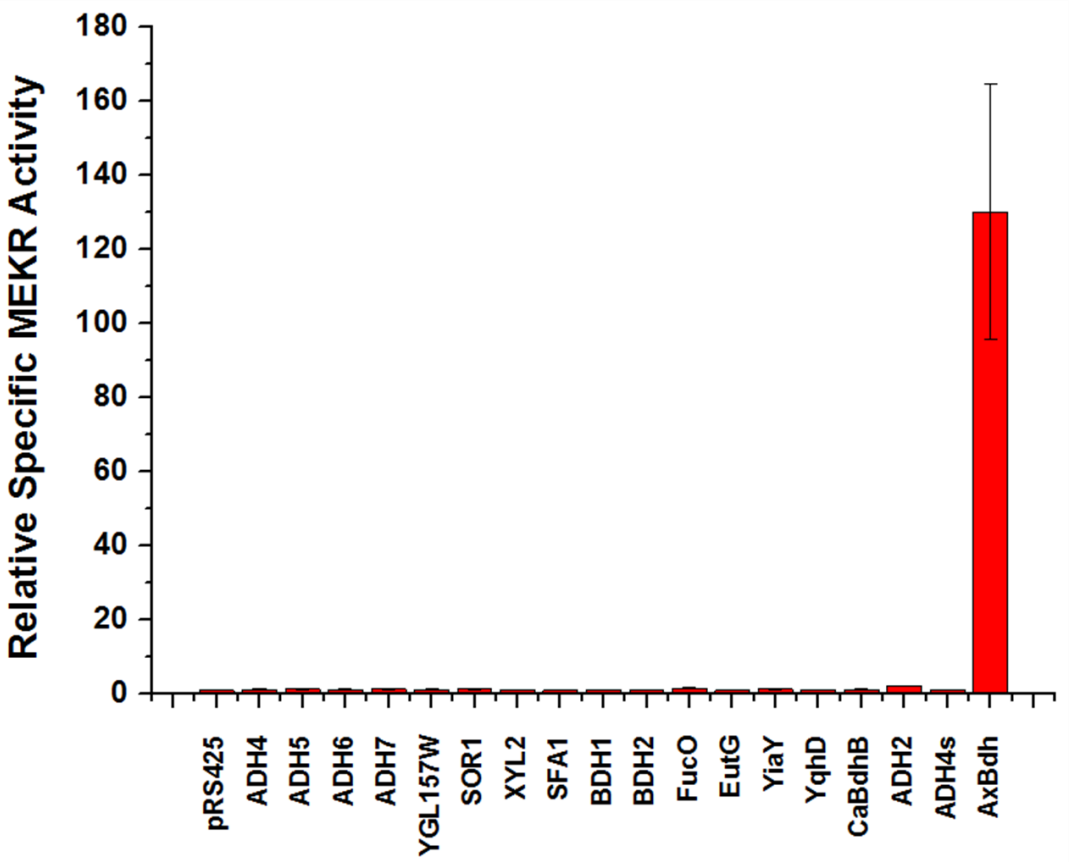

Figure 2.8 Secondary alcohol dehydrogenase (Sadh) or MEK reductase (MEKR) assay with MEK as the substrate. Several endogenous ADHs and ADHs from *E. coli* and *Achromobacter xylosoxidans* were cloned and transformed into CEN.PK2 strain to test the MEKR activities.

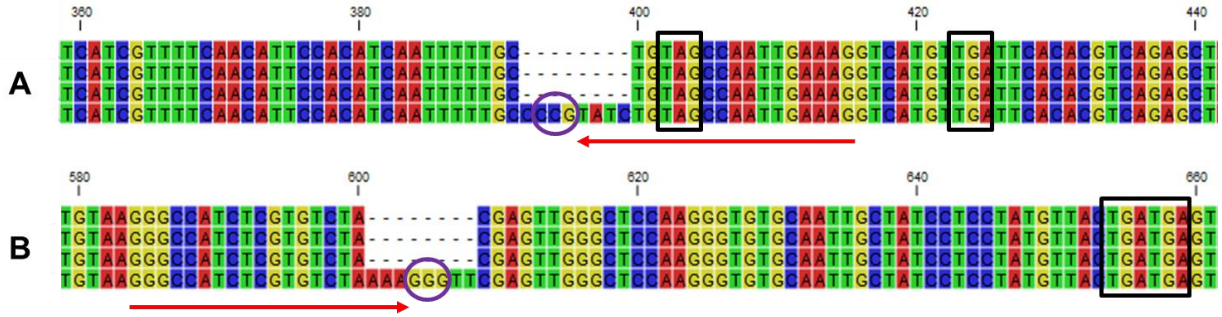

Figure 2.9 Confirmation of the disruption of both *GPD1* (A) and *GPD2* (B) using the HI-CRISPR system at the desired loci by DNA sequencing. The target sequences were marked with arrows, the corresponding PAMs were circled, and the introduced stop codons in the disrupted genes were boxed.

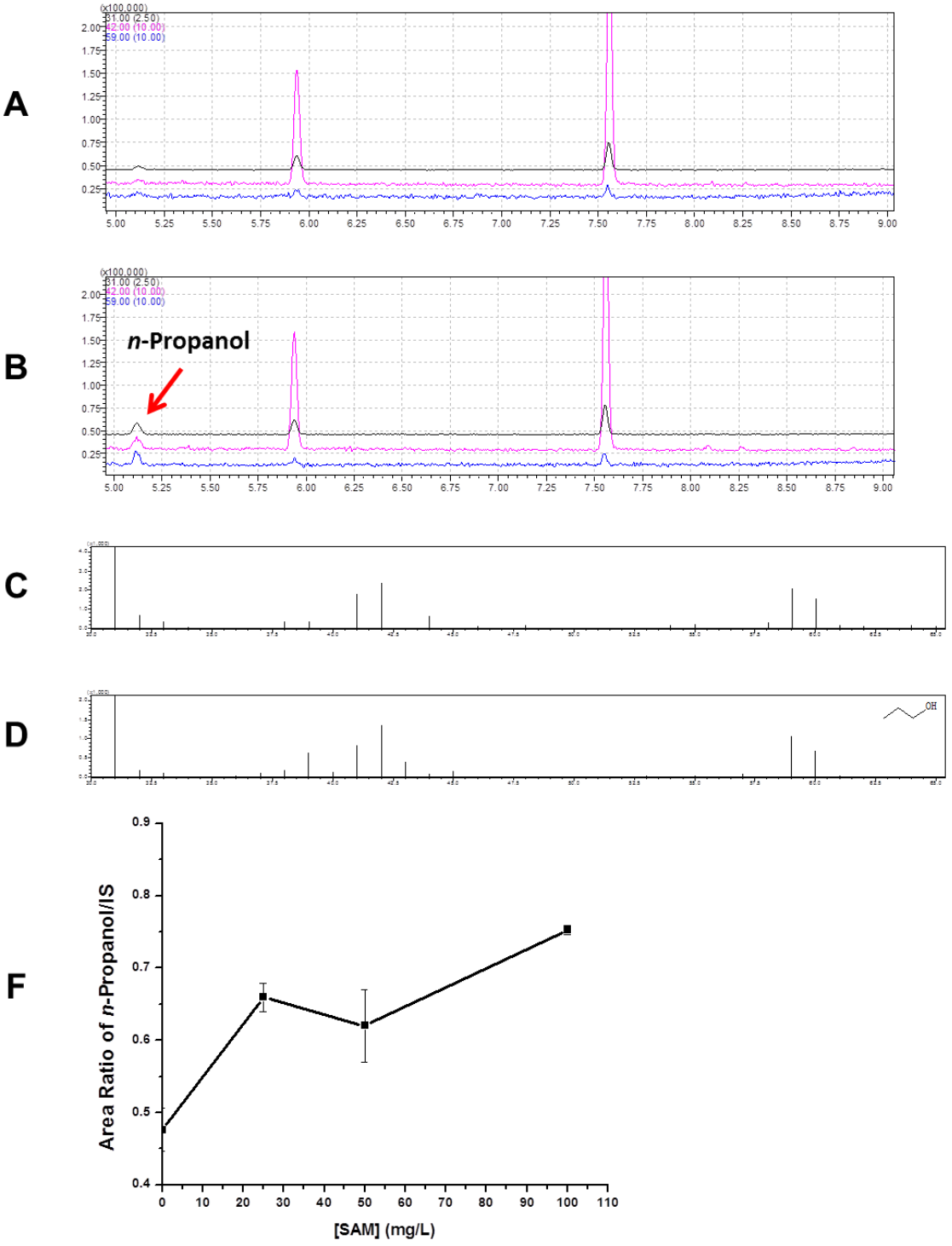

Figure 2.10 Detection of *n*-propanol by GC-MS (A, B, C, and D) and the effect of exogenous SAM supplementation on *n*-propanol production (E). GC chromatograph of fermentation profiles of CEN.PK2 and CEN/RiB2B with the supplementation of 1,2-propanediol using high cell density fermentation under anaerobic condition. MS fragmentation pattern of target (C) and *n*-propanol standard (D) were compared.

Chapter 3 Acetyl-CoA Pool Engineering via Synthetic Biology (I)

3.1 Introduction

Besides its significant role as a building block in cellular metabolism, acetyl-CoA is the key precursor for biological synthesis of a variety of fuel and chemical molecules, such as *n*-butanol, fatty acid ethyl esters (FAEEs), alkanes, polyhydroxybutyrate (PHB), and isoprenoid-derived drugs (1-5). However, *S. cerevisiae* is not optimized to synthesize acetyl-CoA, in terms of the titer and yield of acetyl-CoA derived molecules, if compared with those in *E. coli* and oleaginous yeasts. One explanation is the difference in acetyl-CoA metabolism. In *E. coli* (Figure 3.1A), acetyl-CoA is steadily synthesized from pyruvate by either pyruvate dehydrogenase (PDH) under aerobic conditions (6) or pyruvate:formate lyase (PFL) under anaerobic conditions (7). In eukaryotes, the metabolism of acetyl-CoA is separated into several compartments, including the mitochondria, peroxisomes, nucleus, and cytosol (8). Acetyl-CoA is mainly generated in the mitochondria by PDH, however, *S. cerevisiae* lacks the machinery to export the mitochondrial acetyl-CoA to the cytosol where the synthesis of desired products generally occurs (8). In the cytosol of yeast (Figure 3.1B), acetyl-CoA is generated via PDH-bypass, and the activation of acetate is the rate-limiting step, resulting from the low activity and high energy input requirement of the acetyl-CoA synthetase (ACS) (2). In addition, acetaldehyde is the branch point to control the flux to ethanol and acetyl-CoA, and most of the metabolic fluxes are going to ethanol during glucose fermentation due to the Crabtree effect and the fact that aldehyde dehydrogenases (ALDHs) have much lower affinity towards acetaldehyde than those of ADHs. Therefore, the ACS-dependent acetyl-CoA biosynthesis in the cytosol of *S. erevisiae* suffers from low metabolic fluxes and low efficiencies. On the contrary, cytosolic acetyl-CoA is mainly generated by ATP-dependent citrate lyase (ACL) in oleaginous yeasts such as *Yarrowia*

lipolytica (Figure 3.1C), which can accumulate fatty acids and lipids to high levels. ACL catalyzes a reversed reaction of citrate synthase, the first step of TCA cycle for acetyl-CoA assimilation. In other words, ACL functions as a shuttle to export the mitochondrial PDH-generated acetyl-CoA to the cytosol for biosynthesis.

As mentioned in Chapter 1, PDH catalyzes the oxidative degradation of pyruvate to generate acetyl-CoA in an ATP-independent manner, which is the most widely existed and probably the most efficient route for acetyl-CoA generation in nature. PDH is a huge multi-subunits protein complex, with TPP, FAD, NAD^+, and lipoic acid used as cofactors. Since TPP, FAD, and NAD^+ are readily available in the cytosol of yeast, the supply of lipoic acid as well as its attachment to PDH (lipoylation of E2 subunit) should be engineered together with the expression of PDH structural genes. In nature, two independent routes are probably synergistically used for protein lipoylation, the scavenging pathway and the *de novo* biosynthetic pathway. As for the scavenging pathway, exogenous lipoic acid will be assimilated by the host and attached to its protein targets by a lipoiate-protein ligase (Lpl). When exogenous lipoic acid is not available, it has to be synthesized *de novo* from octanoyl-ACP (Figure 3.2) by hijacking fatty acid biosynthesis. In *E. coli* (Figure 3.2A), where the lipoylation pathway is the most characterized and well-known, the *de novo* biosynthetic pathway proceeds by two consecutive reactions: in the first step the octanoyltransferase (LipB) transfers octanoyl moiety from endogenously produced octanoyl-ACP to the target apo-proteins; and in the second step the octanoyl moiety is converted to lipoic acid by the lipoyl synthase (LipA), which replaces a hydrogen atom on each of the octanoate C_6 and C_8 carbon atoms with a sulphur atom, to generate lipoylated proteins. In *Bacillus subtilis* (Figure 3.2B), a gram-positive bacterium, it is interesting to observe that a lipoylated protein (glycine cleavage system, GCV) is required for the

lipoylation of PDH E2 subunits. Later it is found that LipM is an octanoyltransferase that specifically transfers octanoyl moiety from octanoyl-ACP to GcvH, whereas LipL is an amido-transferase that transfers the octanoyl moiety from GcvH to PDH (9, 10). In *S. cerevisiae*, the lipoylation pathway is less understood, which is also found to be GCV-dependent (11-13). Therefore, a mechanism similar to that of *B. subtilis* is proposed: Lip2p (octanoyltransferase) specifically transfers octanoyl moiety from octanoyl-ACP to Gcv3p, and then Lip3p (amido-transferase) transfers the octanoyl moiety from Gcv3p to PDH. Currently, it is still not clear whether sulphur insertion (LipA or Lip5p) acts before or after octanoyl moiety transfer (LipL or Lip3p) from GCV (GcvH or Gcv3p). Both *B. subtilis* and *S. cerevisiae* require GCV (GcvH and Gcv3p) as an intermediate octanoyl moiety carrier, whereas *E. coli* does not (9). Notably, both LipM from *B. subtilis* and Lip3p from *S. cerevisiae* were characterized to have octanoyl-CoA transferase activity (13, 14), indicating that *B. subtilis* and *S. cerevisiae* can accept octanoyl-CoA as the substrate for protein lipoylation, although at a lower efficiency than that of octanoyl-ACP.

Considering the limitations of the endogenous ACS-dependent pathway for acetyl-CoA generation, this chapter aims to characterize alternative biosynthetic pathways with higher efficiency and lower energy input requirement via synthetic biology with a focus of PDH from *E. coli* and ACL from an oleaginous yeast, while Chapter 4 focuses on the improvement of metabolic fluxes towards acetyl-CoA biosynthesis via metabolic engineering. Currently, several metabolic engineering and synthetic biology strategies have been applied to boost the availability of acetyl-CoA in yeast, such as the use of an ACS mutant from *Salmonella enterica* (Se*Acs*^{L641P}) with increased activity (1-4) or the introduction of heterologous acetyl-CoA biosynthetic pathways with lower energy input requirement (5, 15). Notably, these engineering strategies have resulted in the improved production of isoprenoids (1, 2), polyhydroxybutyrate (PHB) (3, 5),

n-butanol (4), and fatty acids (15) in *S. cerevisiae*. Recently, functional expression of the PDH complex in the cytosol of yeast was achieved by co-expressing the PDH structural genes (*pdhA*, *pdhB*, *aceF*, and *lpd*) and the protein-lipoate ligase genes (*lplA* and *lplA2*) from *Enterococcus faecalis*. When lipoic acid was supplemented to the growth medium, a functional PDH complex could fully replace the endogenous ACS-dependent pathway for cytosolic acetyl-CoA synthesis (16). Although a growth rate similar to the wild-type yeast strain was achieved, the requirement of lipoic acid supplementation and its high cost hinder further application of such a system in industrial settings. Therefore, in this chapter, we focus more on the *de novo* biosynthesis and lipoylation pathway, besides the scavenging pathway, to reconstitute a functional PDH complex in the cytosol of yeast.

3.2 Results

3.2.1 Construction of helper plasmids to facilitate gene cloning and pathway assembly

In order to reconstitute a functional PDH in the cytosol of yeast, many genes and pathways have to be cloned and assembled, such as the PDH structural genes, a lipoylation pathway, and a type II fatty acid synthase (FAS). Thus, six helper plasmids with the whole promoter or terminator as the homology region with adjacent cassettes were constructed to facilitate gene cloning and pathway assembly. As shown in Figure 3.3 and Table 3.1, besides the eGFP cassette (promoter-eGFP-terminator), there was an additional promoter sequence at the 3' end of the terminator in each helper plasmid, serving as the homologous region for pathway assembly. Each eGFP sequence was flanked by a unique *Bam*HI site at 5' end and *Xho*I site at 3' end, which allowed the cloning of desired genes by replacing the eGFP sequence. In addition, unique restriction enzyme sites were also introduced to flank at both ends of each cassette, which conferred the flexibility to remove the whole cassette by restriction digestions. As shown in

Figure 3.3, the whole cassettes together with the downstream homologous sequences were PCR amplified and co-transformed into *S. cerevisiae* to assemble the whole pathway via the DNA assembler method (17).

3.2.2 Development of an in vivo *acetyl-CoA assay system*

Although several protocols for the detection of CoAs in biological systems have been developed, it is still rather tedious and labor intensive to do the extractions and assays (18, 19). Thus, an *in vivo* acetyl-CoA assay system was developed by disrupting the endogenous ACS-dependent acetyl-CoA biosynthesis. In *S. cerevisiae*, Acs1p and Acs2p were responsible for the activation of acetate at the cost of ATP consumption (ACS activities). While *ACS2* was found to be constitutively expressed under all conditions, the expression of *ACS1* was repressed by the presence of glucose. In other words, the disruption of *ACS2* would result in a yeast strain that could not grow on synthetic medium with glucose as the sole carbon source (Figure 3.4A). Since *ACS1* was expressed well under derepressed condition, the disruption of *ACS2* did not have a significant impact on the growth on ethanol containing medium (Figure 3.4A). Therefore, the acetyl-CoA biosynthetic pathways could be characterized by their ability to complement the growth of the *acs2*Δ *S. cerevisiae* strain (Table 3.2) on glucose synthetic medium. After restoring the growth with alternative acetyl-CoA biosynthetic pathways, *ACS1* should be further deleted to eliminate any possibility of host adaptation that might lead to the constitutive expression of *ACS1* when glucose was still present.

3.2.3 Growth complementation of the acs2*Δ strain by ACL*

Comparative genomics analysis revealed that one of the biggest differences between oleaginous yeast and non-oleaginous yeasts were the presence of ACL (20), a route to generate

cytosolic acetyl-CoA from citrate. Thus, ACL genes (*ACL1-ACL2*) from an oleaginous yeast *Y. lipolytica* were cloned and tested in the *acs2*Δ *S. cerevisiae* strain. The introduction of ACL rescued the growth of the *acs2*Δ strain on both solid (Figure 3.4A) and liquid synthetic media (Figure 3.4B) with glucose as the sole carbon source, although at a lower growth rate and biomass yield than the wild-type strain. Further deletion of *ACS1* in *acs2*Δ/ACL strain did not affect the growth significantly (data not shown), indicating that ACL from *Y. lipolytica* was functionally expressed in *S. cerevisiae* and could replace the endogenous pathway for acetyl-CoA biosynthesis.

3.2.4 Improving ACL performance via citrate supplementation and MDH and MAE co-expression

Although ACL could complement the growth of the Acs^- strain, the growth rate and biomass yield were much lower than the wild-type (Acs^+) strain. It was assumed that the cytosolic citrate concentration and/or the re-uptake of oxaloacetate by mitochondria might limit the activity of ACL in *S. cerevisiae*, especially when cultured on glucose. Therefore, citrate supplementation and co-expression with a malate dehydrogenase gene (*MDH*) and a malic enzyme gene (*MAE*) were carried out to further improve the activity of ACL. Oxaloacetate generated by ACL would be converted by MDH and MAE back to pyruvate, which could be efficiently re-assimilated by the mitochondria. While all MDHs were NADH specific, both NAD^+ and $NADP^+$ specific MAEs were existed in nature. Therefore, the endogenous *MDH3*, *Y. lipolytica MDH2*, *Y. lipolytia MAE1* (NAD^+ specific), and *Mortierella alpine MAE1* ($NADP^+$ specific) were cloned and assembled (Table 3.3). Either the mitochondrial targeting sequences or peroxisomal targeting sequences were removed in all MDHs and MAEs to express them in the cytosol of yeast. Among all ACL-MDH-MAE (AMM) systems tested, AMM2 worked the best

to increase the growth rate (Figures 3.5A). It was also found that the introduction of co-factor neutral pathways (AMM2 and AMM4) increased the ACL activity, while the pathways with transhydrogenase activity (AMM5 and AMM6) decreased the growth rate. Generally, citrate supplementation increased ACL activity, except for the wild-type strain (Figures 3.5C) and the AMM2 expressing strain (Figures 3.5E). The cytosolic acetyl-CoA biosynthesis was not related to citrate for the wide-type (Acs^+) strain; while for the AMM2 expressing Acs^- strain, the acetyl-CoA biosynthesis has been already improved by co-expressing *MAE-MDH*. These results indicated that citrate supplementation and *MDH-MAE* co-expression might follow a same mechanism to increase the acetyl-CoA biosynthesis capability of ACL. Notably, although the introduction of co-factor imbalanced AMM systems led to lower growth rate, they might be useful for metabolic engineering applications with enhanced supply of NADPH.

3.2.5 PDH with scavenging lipoylation pathway

Although PDH was only found in the mitochondria in eukaryotes, the expression of the bacterial counterpart genes, due to a lack of mitochondrial targeting sequences, will relocate the PDH enzymes to the cytosol. If they could be functionally reconstituted in this new compartment, a new route to generate acetyl-CoA directly from pyruvate could be created in the cytosol of yeast. Therefore, PDH structural genes from *E. coli* (Ec*LpdA*-Ec*AceE*-Ec*AceF*) and the lipoate-protein ligase genes from *E. coli* (Ec*LplA*) and *Bacillus subtilis* (Bs*LplJ*) were cloned. As shown in Figure 3.4A, co-expression of PDH structural genes and a lipoate-protein ligase gene could complement the growth of the *acs2*Δ *S. cerevisiae* strain on glucose synthetic medium, when lipoic acid was supplemented. Interestingly, the lipoate-protein ligase from *B. subtilis* (BsLplJ) performed better than that from *E. coli* (EcLplA), when co-expressed with the *E. coli* PDH structural genes (Figure 3.4B). Compared with the wild-type (Acs^+) strain, the growth rate and

biomass yield were quite similar, indicating that cytoPDH could fully replace the endogenous ACS-dependent pathway for acetyl-CoA biosynthesis in the cytosol of yeast. If lipoic acid was not supplemented to the growth medium, no cell growth could be observed (Figure 3.4A). In other words, the PDH containing Acs^- strain was lipoic acid auxotroph.

The *E. coli* PDH was reported to be subjected to feedback inhibition by NADH, which led to low or lack of activity under anaerobic condition (high ratio of $NADH/NAD^+$). Inverse engineering revealed a mutation in the LpdA coding sequence (E354K) resulted in an NADH feedback inhibition resistant PDH mutant (21). A following study on the saturation mutagenesis of the E354 site found more PDH mutants that were insensitive to NADH inhibition (22). In other words, these PDH mutants were functional under both aerobic and anaerobic conditions. Considering the reducing environment in the cytosol of yeast and the preference of anaerobic condition for industrial applications, two feedback inhibition insensitive PDH mutants with a mutation of E354K (PDHm1) and E354G (PDHm2), respectively, in the LpdA coding sequence were constructed. As shown in Figure 3.4C, no significant difference in the growth rate of the *acs2*Δ strains containing either the wild-type or the mutated PDHs was observed, indicating that PDH activity was not inhibited under aerobic condition. To test the advantage of using the NADH insensitive mutants, the PDH containing *acs2*Δ strains were cultured under micro-anaerobic condition. As shown Figures 3.6A and 3.6B, there was still no significant difference in the fermentation performance (glucose consumption and ethanol production) between these strains when the glucose concentration was low (20 g/L), indicating that the $NADH/NAD^+$ ratio was not high enough in the yeast cytosol to inhibit the activity of PDH or the activity of PDH was still high enough to provide sufficient amount of acetyl-CoA even under inhibited condition. Finally, fermentation with high concentration of glucose (100 g/L) was carried out under micro-

anaerobic condition, which resulted in slightly improved fermentation performance with the NADH insensitive mutants (Figures 3.6C and 3.6D). The results indicated that the re-oxidation of NADH via ethanol and glycerol formation was able to maintain the cytosolic NADH/NAD^+ ratio at a low level that would not inhibit the activity of PDH, even under micro-anaerobic condition. Nevertheless, since no significant difference between PDHwt, PDHm1, and PDHm2 under aerobic condition and the PDH mutants might be more active under anaerobic condition, especially in the engineered strains with impaired glycerol and ethanol fermentation, PDHm2 was chosen for all following studies to reconstitute the *de novo* lipoic acid biosynthesis and lipoylation machinery.

3.2.6 Development of the lipoic acid auxotrophic strain as an in vivo *acetyl-CoA assay system*

Although the *acs2*Δ *S. cerevisiae* strain has been used for *in vivo* acetyl-CoA assays, *ACS1* must be further deleted to confirm the functionality of the heterologous acetyl-CoA biosynthetic pathways. If the heterologous pathways were not very efficient in synthesizing acetyl-CoA, further disruption of *ACS1* in a poor growth strain could be challenging. Therefore, we switched to the use of the lipoic acid auxotrophic strain as the *in vivo* acetyl-CoA assay system. As shown in Figure 3.7, no cell growth was observed without lipoic acid supplementation, and the growth was increased gradually with higher lipoic acid concentrations. When the supplemented lipoic acid concentration was higher than 8 mg/L, a near wild-type growth rate could be achieved (Figure 3.7). Another advantage of the new acetyl-CoA assay system was the fast growth rate, compared with the *acs2*Δ *S. cerevisiae* strain, which had to be cultured on ethanol containing medium at an extremely slow growth rate. Except for the final step of acetyl-CoA assays, which would be carried out in lipoic acid free medium, all previous

steps including transformation and seed culture could be performed in a medium with lipoic acid supplementation.

3.2.7 PDH with a semi-synthetic lipoylation pathway

Although a functional PDH was reconstituted in the cytosol of yeast, its industrial application would still be hindered by the high cost of lipoic acid. Therefore, another goal of this chapter was to reconstitute the *de novo* lipoylation pathway. Octanoyl-ACP, an intermediate of fatty acid biosynthesis, was the natural substrate of lipoylation, although octanoyl-CoA was also reported to be acceptable at a much lower activity (13, 14). Unfortunately, the lipoylation enzymes had no access to octanoyl-ACP, which was constrained in the catalytic core of the type I FAS in the cytosol of yeast. In other words, a type II FAS should be functionally reconstituted in the cytosol for the *de novo* lipoylation machinery. To achieve this challenging goal step by step, a semi-synthetic lipoylation pathway was proposed and designed by taking advantage of the *Vibrio harveyi* acyl-ACP synthetase (VhAasS), a soluble enzyme that ligates free fatty acids to ACP to form acyl-ACPs (23). Interestingly, most of the acyl-ACP synthetases were membrane proteins, while VhAasS was a soluble cytosolic protein. As there is no free ACP in the cytosol of yeast, ACP and its activator must be included together with VhAasS. The first strategy was to relocate the mitochondrial proteins (encoded by *ACP1* and *PPT2*, respectively) to the cytosol by removing the mitochondrial targeting sequences (cyto*ACP1* and cyto*PPT2*). Another strategy was to use the *E. coli* counterparts (encoded by *acpP* and *acpS*, respectively), which possessed no mitochondrial targeting sequences. To test whether octanoyl-CoA could be accepted as the substrate, Faa2p (24), a medium chain fatty acyl-CoA synthetase, was relocated to the cytosol by removing the peroxisome targeting sequences, and the resultant cyto*FAA2* would be co-expressed with the lipoylation pathways. As mentioned above, the *E. coli* lipoylation pathway

was best characterized, and the lipoylation machinery from *B. subtilis* and *S. cerevisiae* mitochondria were able to accept octanoyl-CoA, besides octanoyl-ACP as the lipoylation precursor. Therefore, the lipoylation machineries from these three systems were cloned and assembled, and the resultant DNA constructs were named as EcLA (Ec*LipA*-Ec*LipB*), BsLA (Bs*GcvH*-Bs*LipL*-Bs*LipM*-Bs*LipA*), and ScLA (cyto*GCV3*-cyto*LIP2*-cyto*LIP3*-cyto*LIP5*), respectively. As for ScLA, the mitochondrial targeting sequences were removed to relocate the full pathway enzymes to the cytosol of *S. cerevisiae*.

As shown in Figures 3.8A, no cell growth was observed for all strains when octanoic acid was missing, indicating that the activity of VhAasS and cytoFaa2p was dependent on the presence of octanoate. If 10 mg/L octanoic acid was supplemented to the growth medium, readily cell growth was observed in the Acs$^-$/M2J strain expressing ScLA and VhEc (Vh*AasS*-Ec*AcpP*-Ec*AcpS*) or VhSc (Vh*AasS*-cyto*ACP1*-cyto*PPT2*); marginal growth was observed for EcLA; and no growth was observed for BsLA (Figure 3.8B). The results indicated that BsLA was not active; EcLA showed little activity; while ScLA was functional in the cytosol of yeast and could accept ACP from both *E. coli* and *S. cerevisiae* mitochondria. Under no circumstances would the growth of cyto*FAA2* expressing strain be detected, which indicated that either octanoyl-CoA could not be accepted as the lipoylation precursor or the lipoylation machinery was not active enough to activate apo-E2 subunit of PDH (Figure 3.8B). The cell growth of Acs$^-$/M2J strains with semi-synthetic lipoylation pathways was further confirmed in liquid medium containing 10 mg/L octanoic acid, which was also compared with the strain containing a scavenging pathway (Figure 3.8C). In addition, octanoic acid concentration of 10-30 mg/L was found to be optimal for cell growth: lower concentration led to low lipoylation efficiency and limited acetyl-CoA biosynthesis, while higher concentration resulted in cytotoxicity (Figure

3.8C). Since ScLA was the most active, it was used for the following studies to reconstitute a *de novo* synthetic lipoylation pathway.

3.2.8 PDH with a de novo *synthetic lipoylation pathway*

A final goal of this chapter was to design a *de novo* biosynthetic lipoylation pathway, meaning the reconstitution of functional PDH in synthetic medium without the supplementation of octanoic acid or lipoic acid. To achieve this, a type II FAS (Cem1p-Oar1p-Htd2p-Etr1p-Acp1p-Ppt2p-Mct1p) from the mitochondria of *S. cerevisiae* was relocated to the cytosol by removing the mitochondrial targeting sequences (cytoFAS1). Unfortunately, no cell growth was observed with the co-expression of M2J and ScLA in the Asc^- strain when cultured in synthetic medium with glucose as the sole carbon source, indicating a lack of enough octanoyl-ACP for lipoylation. One possibility lied on the poorly characterized property of Htd2p, whose mitochondrial targeting sequences could not be predicted by any publicly accessible program. Thus, the *E. coli* homologs, FabA and FabZ, which were confirmed to complement the *htd2*Δ strain, were included instead to construct cytoFAS2 and cytoFAS3. Unfortunately, still no growth was observed, indicating that the mitochondrial FAS system was not functional in the cytosol. Actually, the mitochondrial FAS is still not well characterized: for example, the enzyme and the corresponding substrate for the initial condensation step are still unknown, which is one major concern with this FAS system.

To verify whether FASs used in this chapter was functional in the cytosol of yeast, their activities were tested in the *fas1*Δ strain, whose endogenous pathway for fatty acid biosynthesis was disrupted. The growth of the *fas1*Δ strain was only possible when free fatty acid(s) was supplemented to the growth medium or an alternative FAS system was introduced. As shown in

Figure 3.9, the supplementation of C_{14} or C_{16} fatty acid could complement the growth of the *fas1*Δ strain, while the supplementation of a shorter chain fatty acid (such as C_{10} or C_{12}) or the introduction of FAS used in this chapter (including cytoFAS1, cytoFAS2, and cytoFAS3) could not enable the growth in a fatty acid free medium. These results confirmed that all the FAS systems used in this chapter were not functional in the cytosol of *S. cerevisiae*.

3.3 Discussion

As a central metabolite, acetyl-CoA plays an important role in a series of cellular functions involved in enzymatic acetyl transfer reactions. Acetyl-CoA is the starting compound of the tricarboxylic acid (TCA) cycle, and a key precursor in the biosynthesis of sterols, fatty acids and lipids, amino acids, and polyketides (20, 25-29). In addition, acetyl-CoA functions as the donor of acetyl group for post-translational acetylation reactions of histone and non-histone proteins. To accommodate the cellular requirement, nature has evolved a variety of routes for acetyl-CoA synthesis (Fig. S1), such as the oxidative decarboxylation of pyruvate (6), the oxidation of long-chain fatty acids (30), and the oxidative degradation of certain amino acids (20). In terms of the bulk synthesis of acetyl-CoA, the most common mechanism is the direct conversion from pyruvate, either by pyruvate dehydrogenase (PDH) under aerobic conditions (6), or by pyruvate ferredoxin oxidoreductase (PFO) (31), pyruvate $NADP^+$ oxidoreductase (PNO) (32), or pyruvate formate lyase (PFL) (7) under anaerobic conditions. Due to the compartmentalization of acetyl-CoA metabolism in eukaryotes, direct conversion of pyruvate to acetyl-CoA only happens in some organelles, such as mitochondria and chloroplasts. In the cytosol, two ATP consuming mechanisms are used to synthesize acetyl-CoA. One is PDH-bypass (2), i.e., from pyruvate to acetaldehyde and then to acetate, which is activated to acetyl-CoA by the acetyl-CoA synthetase (ACS) at the cost of two ATP molecules (33). PDH-bypass is

widely distributed in ethanogenic species, such as yeasts, filamentous fungi, and plants. The other is ATP-dependent citrate lyase (ACL), using a TCA cycle intermediate citrate as the substrate, which is enzymatically converted to acetyl-CoA and oxaloacetate at the cost of one ATP molecule (25). ACL is found in both ethanogenic and non-ethanogenic species such as fungi, plants, and animals. Notably, comparative genomics studies reveal that ACL is present in oleaginous yeasts such as *Y. lipolytica*, but not in non-oleaginous yeasts such as *S. cerevisiae* (20), indicating the significance of ACL in the supply of precursor metabolites to the biosynthesis of fatty acids and lipids. The phosphoketolase pathway is also reported to contribute to cytosolic acetyl-CoA generation in some fungal species (5).

There is a growing interest in developing *S. cerevisiae* as a cell factory for the production of biofuels and chemicals, owing to its high tolerance to harsh industrial conditions.(1, 34). Besides its essential role in numerous metabolic pathways and cellular functions, acetyl-CoA is the building block for the biosynthesis of many products of industrial interest. However, acetyl-CoA metabolism in yeast is rather complex and highly regulated. In addition, this precursor molecule is synthesized in various compartments and cannot be directly transported between these compartments. Due to the lack of ATP-dependent citrate lyase (ACL) and the carnitine shuttle when cultured in minimal medium (1), the activation of acetate is the only route to generate cytosolic acetyl-CoA in *S. cerevisiae*. This PDH-bypass route suffered from low enzyme activity and high energy input requirement. Therefore, the introduction of heterologous synthetic pathways with higher efficiency and lower energy input requirement should be able to enhance the availability of acetyl-CoA in the cytosol. In this chapter, PDH from *E. coli* and ACL from *Y. lipolytica* were characterized to enable the growth of the Acs^- strain on glucose synthetic medium. In other words, both PDH and ACL were functional to replace the endogenous ACS-

dependent pathway for acetyl-CoA biosynthesis. A similar strategy is to reconstruct the carnitine shuttle exporting mitochondrial acetyl-CoA to the cytosol in *S. cerevisiae*, as occurring in higher organisms (8). Interestingly, all components of the carnitine shuttle, such as the carnitine acetyltransferase and acetyl-carnitine translocase, exist in *S. cerevisiae* except for the *de novo* carnitine biosynthetic pathway (35). Due to the lack of carnitine in synthetic medium and its high cost, introducing a heterologous *de novo* carnitine biosynthetic pathway would be a viable option for industrial production of acetyl-CoA derived fuels and chemicals.

Considering the high cost of lipoic acid, a *de novo* lipoylation pathway should be included to construct a functional PDH in the cytosol of yeast, which was hindered by the challenge to reconstitute a functional type II FAS in the cytosol. Luckily, a semi-synthetic lipoylation pathway based on acyl-ACP synthetase (VhAasS) was constructed and could supply octanoyl-ACP for lipoylation when octanoic acid was supplemented to the growth medium. By combining with the reversed β-oxidation pathway, which was found to be able to produce octanoic acid when a medium chain thioesterase (CpFatB1) was co-expressed in Chapter 5, a *de novo* biosynthetic lipoylation pathway could be re-designed. As shown in Figure 3.10, octanoyl-CoA, an intermediate of the reversed β-oxidation pathway, could be thiolyzed by CpFatB1 to release octanoic acid, which could then be fed to the semi-synthetic lipoylation pathway to construct a functional PDH in the cytosol of yeast.

3.4 Conclusion and Future Work

Acetyl-CoA biosynthetic pathways from *E. coli* (PDH) and *Y. lipolytica* (ACL) were introduced into the cytosol of *S. cerevisiae* via synthetic biology approaches. Both ACL and PDH could replace the endogenous ACS-dependent pathway for acetyl-CoA biosynthesis. To construct a functional PDH in the cytosol of yeast, different lipoylation pathways were

introduced. Besides the naturally existing scavenging pathway and *de novo* biosynthetic pathway, we also designed a semi-synthetic lipoylation pathway based on the acyl-ACP synthetase (AasS). The scavenging pathway resulted in a functional PDH that enabled the growth of Acs^- strain to a similar level of the wild-type strain. While the *de novo* biosynthetic lipoylation pathway was hindered by the difficulty in reconstituting a functional type II FAS in the cytosol, the semi-synthetic lipoylation pathway could rescue the growth with octanoic acid supplementation although at a much lower growth rate and biomass yield. A new *de novo* biosynthetic lipoylation pathway was designed and proposed to combine the semi-synthetic lipoylation pathway and the reversed β-oxidation pathway. The next chapter will focus on the use of these alternative acetyl-CoA pathways for metabolic engineering applications: to increase the intracellular acetyl-CoA level with a goal to increase the titer and productivity of *n*-butanol and other value-added compounds.

3.5 Materials and Methods

3.5.1. Strains, media, and cultivation conditions

E. coli strain DH5α was used to maintain and amplify plasmids. *S. cerevisiae* CEN.PK2-1C was used as the host for homologous recombination based cloning, heterologous gene expression, and growth assays. Yeast strains were cultivated in complex medium consisting of 2% peptone and 1% yeast extract supplemented with either 2% glucose (YPD) or 2% ethanol (YPE). Recombinant strains were grown on synthetic complete (SC) medium consisting of 0.17% yeast nitrogen base, 0.5% ammonium sulfate, and 0.07% amino acid drop out mix (CSM-HIS-TRP-LEU-URA, MP Biomedicals, Solon, OH), supplemented with 2% glucose (SCD) or 2% ethanol (SCE). *E. coli* strains were cultured at 37ºC in Luria-Bertani broth containing 100 μg/mL ampicillin. *S. cerevisiae* strains were cultured at 30ºC and 250 rpm for aerobic growth, and 30ºC

and 100 rpm in un-baffled shaker flasks for oxygen limited fermentation. To select for antibiotic resistant *S. cerevisiae* strains, G418 was supplemented at a final concentration of 200 μg/mL. When necessary, lipoic acid was supplemented to the growth medium at a final concentration of 100 μg/L, unless specifically mentioned. All restriction enzymes, Q5 High Fidelity DNA polymerase, and the *E. coli* - *S. cerevisiae* shuttle vectors were purchased from New England Biolabs (Ipswich, MA). All chemicals were purchased from either Sigma-Aldrich or Fisher Scientific.

3.5.2 DNA manipulation

The yeast homologous recombination based DNA assembler method (17) was used to construct the helper plasmids, clone candidate genes and assemble the multiple-gene pathways. Recombinant plasmids constructed in this chapter were listed in Table 3.1. Briefly, polymerase chain reaction (PCR) was used to generate DNA fragments with homology arms at both ends, which were purified with a QIAquick Gel Extraction Kit (Qiagen, Valencia, CA) and co-transformed along with the linearized backbone into *S. cerevisiae*. All genetic elements, including promoters, coding sequences, and terminators, were PCR-amplified from their corresponding genomic DNAs. Wizard Genomic DNA Purification Kit (Promega, Madison, WI) was used to extract the genomic DNAs from both bacteria and yeasts, according to the manufacturer's protocol. To confirm the correct clones, yeast plasmids were isolated using a Zymoprep Yeast Plasmid Miniprep II Kit (Zymo Research, Irvine, CA) and re-transformed into *E. coli* DH5α or NEB Turbo competent cells. To construct NADH insensitive PDH mutants (PDHm1 and PDHm2), mutation at the E354 site of LpdA (E354K or E354G) was introduced by overlapped extension PCR and the resultant DNA fragment was cloned into the *Afe*I and *Pac*I sites of PDHwt. To construct cytoPDH and M2J, Bs*LplJ* cassette (*TEF1p*-Bs*LplJ*-*TEF1t*) was

cloned into the *Sal*I site of PDHwt and PDHm2, respectively, by the Gibson assembly method (New England Biolabs). To construct cytoFASs, cytoFAS0 was constructed first using the helper plasmid based DNA assembler method, then the *HTD2* cassette (*HXT7p-cytoHTD2-HXT7t*), the Ec*FabA* cassette (*HXT7p*-Ec*FabA-HXT7t*), and the Ec*FabZ* cassette (*HXT7p*-Ec*FabZ-HXT7t*) was cloned into the *Stu*I site of cytoFAS0 to construct cytoFAS1, cytoFAS2, and cytoFAS3, respectively. Ma*MAE* was synthesized by two gBLOCKs (Integrated DNA Technologies, Coralville, Iowa) and cloned into pH5. pYFJ84, the VhAasS containing plasmid, was kindly provided by Prof. John Cronan from the University of Illinois at Urbana-Champaign (36). Plasmids were isolated using a QIAprep Spin Miniprep Kit (Qiagen) and confirmed using both diagnostic PCRs and restriction digestions. Yeast strains were transformed using the LiAc/SS carrier DNA/PEG method (37), and transformants were selected on the appropriate SC plates.

3.5.3 Strain construction

All the strains used in this chapter were based on CEN.PK2-1C and listed in Table 3.2. The *Cre-loxP* method (38) was used to construct all knock-out strains. For the construction of *acs2*Δ strain, the *loxP*-Kl*URA3-loxP* cassette was PCR amplified with pUG73 as the template to include 40bp homology arms at both ends, and transformed into CEN.PK2-1C strain. The transformants were screened on SCE-URA plates and the resultant *acs2*Δ strain was maintained in medium with ethanol as the sole carbon source. After restoring the growth on glucose by ACL or PDH, *ACS1* was further deleted by transforming the *loxP-KanMX-loxP* cassette and selection on YPD plates supplemented with 200 mg/L G418. The resultant Acs$^-$ strains (*acs1*Δ *acs2*Δ) containing alternative acetyl-CoA pathways were maintained on glucose medium and used as an *in vivo* reporter of acetyl-CoA levels in the cytosol. The same method was used to knock out *FAS1*, encoding the β-subunit of fatty acid synthase, which was selected on YPD plates

containing 200 mg/L G418 and 0.05% C_{14} fatty acid. The resultant *fas1*Δ strain was maintained on glucose and free fatty acid containing medium and used as an *in vivo* reporter of fatty acid biosynthesis capabilities. The selection marker in the engineered strains was rescued by transforming the *Cre* expressing plasmid (pSH47, pSH62, or pSH63).

3.5.4 Growth assays

To test yeast cell growth on agar plates by spotting assays, *acs2*Δ yeast strains were pre-grown in the appropriate synthetic medium with 2% ethanol as the carbon source for about 5 days. Then yeast cells were collected by centrifugation, washed three times in sterile ddH_2O, and cells with appropriate dilutions (10^4, 10^3, 10^2, and 10^1 cells, assuming 10^7 cells/mL equivalent to OD_{600} of 1.0) were spotted into synthetic medium agar plates containing 2% ethanol, 2% glucose, and 2% glucose supplemented with 100 µg/L lipoic acid, respectively. Strains on glucose with lipoic acid plates were incubated at 30°C for 3 days, while those on ethanol and glucose plates were incubated at 30°C for 5 days. Liquid growth assays were performed using a Bioscreen C (Growth Curves USA, Piscataway, NJ) in four replicates. 4 µL of fully grown seeds were inoculated into 200 µL of the corresponding selection medium with an initial OD around 0.05. Tween80 or Brij58 was supplemented at a final concentration of 0.05%. The experiment was run at 30°C for 5 days with continuous shaking and sampling every 1h.

3.5.5 Prediction of the mitochondrial and peroxisomal targeting sequences

The mitochondrial targeting sequences of the candidate proteins were predicted using the MITOPROT online tool (http://ihg.gsf.de/ihg/mitoprot.html) (39). The peroxisomal targeting sequences were predicted using the PTSs predictor from PeroxisomeDB 2.0 (http://www.peroxisomedb.org/Target_signal.php) (40).

3.6 References

1. **Chen Y, Daviet L, Schalk M, Siewers V, Nielsen J.** 2013. Establishing a platform cell factory through engineering of yeast acetyl-CoA metabolism. Metab. Eng. **15:**48-54.
2. **Shiba Y, Paradise EM, Kirby J, Ro DK, Keasling JD.** 2007. Engineering of the pyruvate dehydrogenase bypass in *Saccharomyces cerevisiae* for high-level production of isoprenoids. Metab. Eng. **9:**160-168.
3. **Kocharin K, Chen Y, Siewers V, Nielsen J.** 2012. Engineering of acetyl-CoA metabolism for the improved production of polyhydroxybutyrate in *Saccharomyces cerevisiae*. AMB Express **2:**52.
4. **Krivoruchko A, Serrano-Amatriain C, Chen Y, Siewers V, Nielsen J.** 2013. Improving biobutanol production in engineered *Saccharomyces cerevisiae* by manipulation of acetyl-CoA metabolism. J. Ind. Microbiol. Biotechnol. **40:**1051-1056.
5. **Kocharin K, Siewers V, Nielsen J.** 2013. Improved polyhydroxybutyrate production by *Saccharomyces cerevisiae* through the use of the phosphoketolase pathway. Biotechnol. Bioeng. **110:**2216-2224.
6. **Guest JR, Angier SJ, Russell GC.** 1989. Structure, expression, and protein engineering of the pyruvate dehydrogenase complex of *Escherichia coli*. Ann. N. Y. Acad. Sci. **573:**76-99.
7. **Knappe J, Sawers G.** 1990. A radical-chemical route to acetyl-CoA: the anaerobically induced pyruvate formate-lyase system of *Escherichia coli*. FEMS Microbiol. Rev. **6:**383-398.
8. **Strijbis K, Distel B.** 2010. Intracellular acetyl unit transport in fungal carbon metabolism. Eukaryot. Cell **9:**1809-1815.
9. **Christensen QH, Martin N, Mansilla MC, de Mendoza D, Cronan JE.** 2011. A novel amidotransferase required for lipoic acid cofactor assembly in *Bacillus subtilis*. Mol. Microbiol. **80:**350-363.
10. **Martin N, Christensen QH, Mansilla MC, Cronan JE, de Mendoza D.** 2011. A novel two-gene requirement for the octanoyltransfer reaction of *Bacillus subtilis* lipoic acid biosynthesis. Mol. Microbiol. **80:**335-349.
11. **Schonauer MS, Kastaniotis AJ, Kursu VA, Hiltunen JK, Dieckmann CL.** 2009. Lipoic acid synthesis and attachment in yeast mitochondria. J. Biol. Chem. **284:**23234-23242.
12. **Marvin ME, Williams PH, Cashmore AM.** 2001. The isolation and characterisation of a *Saccharomyces cerevisiae gene* (*LIP2*) involved in the attachment of lipoic acid groups to mitochondrial enzymes. FEMS Microbiol. Lett. **199:**131-136.
13. **Hermes FA, Cronan JE.** 2013. The role of the *Saccharomyces cerevisiae* lipoate protein ligase homologue, Lip3, in lipoic acid synthesis. Yeast **30:**415-427.
14. **Christensen QH, Cronan JE.** 2010. Lipoic acid synthesis: a new family of octanoyltransferases generally annotated as lipoate protein ligases. Biochemistry **49:**10024-10036.
15. **Tang X, Feng H, Chen WN.** 2013. Metabolic engineering for enhanced fatty acids synthesis in *Saccharomyces cerevisiae*. Metab. Eng. **16:**95-102.
16. **Kozak BU, van Rossum HM, Luttik MA, Akeroyd M, Benjamin KR, Wu L, de Vries S, Daran JM, Pronk JT, van Maris AJ.** 2014. Engineering acetyl coenzyme A

supply: functional expression of a bacterial pyruvate dehydrogenase complex in the cytosol of *Saccharomyces cerevisiae*. MBio **5:**e01696-01614.

17. **Shao Z, Zhao H, Zhao H.** 2009. DNA assembler, an *in vivo* genetic method for rapid construction of biochemical pathways. Nucleic Acids Res. **37:**e16.
18. **Park JW, Jung WS, Park SR, Park BC, Yoon YJ.** 2007. Analysis of intracellular short organic acid-coenzyme A esters from actinomycetes using liquid chromatography-electrospray ionization-mass spectrometry. J. Mass Spectrom. **42:**1136-1147.
19. **Steen EJ, Chan R, Prasad N, Myers S, Petzold CJ, Redding A, Ouellet M, Keasling JD.** 2008. Metabolic engineering of *Saccharomyces cerevisiae* for the production of *n*-butanol. Microb. Cell Fact. **7:**36.
20. **Vorapreeda T, Thammarongtham C, Cheevadhanarak S, Laoteng K.** 2012. Alternative routes of acetyl-CoA synthesis identified by comparative genomic analysis: involvement in the lipid production of oleaginous yeast and fungi. Microbiology **158:**217-228.
21. **Kim Y, Ingram LO, Shanmugam KT.** 2008. Dihydrolipoamide dehydrogenase mutation alters the NADH sensitivity of pyruvate dehydrogenase complex of *Escherichia coli* K-12. J. Bacteriol. **190:**3851-3858.
22. **Sun Z, Do PM, Rhee MS, Govindasamy L, Wang Q, Ingram LO, Shanmugam KT.** 2012. Amino acid substitutions at glutamate-354 in dihydrolipoamide dehydrogenase of *Escherichia coli* lower the sensitivity of pyruvate dehydrogenase to NADH. Microbiology **158:**1350-1358.
23. **Byers DM, Holmes CG.** 1990. A soluble fatty acyl-acyl carrier protein synthetase from the bioluminescent bacterium *Vibrio harveyi*. Biochem. Cell Biol. **68:**1045-1051.
24. **Knoll LJ, Johnson DR, Gordon JI.** 1994. Biochemical studies of three *Saccharomyces cerevisiae* acyl-CoA synthetases, Faa1p, Faa2p, and Faa3p. J. Biol. Chem. **269:**16348-16356.
25. **Zaidi N, Swinnen JV, Smans K.** 2012. ATP-citrate lyase: a key player in cancer metabolism. Cancer Res. **72:**3709-3714.
26. **Zha W, Rubin-Pitel SB, Shao Z, Zhao H.** 2009. Improving cellular malonyl-CoA level in *Escherichia coli* via metabolic engineering. Metab. Eng. **11:**192-198.
27. **Tai M, Stephanopoulos G.** 2013. Engineering the push and pull of lipid biosynthesis in oleaginous yeast *Yarrowia lipolytica* for biofuel production. Metab. Eng. **15:**1-9.
28. **Xu P, Ranganathan S, Fowler ZL, Maranas CD, Koffas MA.** 2011. Genome-scale metabolic network modeling results in minimal interventions that cooperatively force carbon flux towards malonyl-CoA. Metab. Eng. **13:**578-587.
29. **Xu P, Gu Q, Wang W, Wong L, Bower AG, Collins CH, Koffas MA.** 2013. Modular optimization of multi-gene pathways for fatty acids production in *E. coli*. Nat. Commun. **4:**1409.
30. **Trotter PJ.** 2001. The genetics of fatty acid metabolism in *Saccharomyces cerevisiae*. Annu. Rev. Nutr. **21:**97-119.
31. **Ragsdale SW.** 2003. Pyruvate ferredoxin oxidoreductase and its radical intermediate. Chem. Rev. **103:**2333-2346.
32. **Inui H, Ono K, Miyatake K, Nakano Y, Kitaoka S.** 1987. Purification and characterization of pyruvate:$NADP^+$ oxidoreductase in *Euglena gracilis*. J. Biol. Chem. **262:**9130-9135.

33. **Starai VJ, Escalante-Semerena JC.** 2004. Acetyl-coenzyme A synthetase (AMP forming). Cell Mol. Life Sci. **61:**2020-2030.
34. **Runguphan W, Keasling JD.** 2014. Metabolic engineering of *Saccharomyces cerevisiae* for production of fatty acid-derived biofuels and chemicals. Metab. Eng. **21:**103-113.
35. **Franken J, Kroppenstedt S, Swiegers JH, Bauer FF.** 2008. Carnitine and carnitine acetyltransferases in the yeast *Saccharomyces cerevisiae*: a role for carnitine in stress protection. Curr. Genet. **53:**347-360.
36. **Jiang Y, Chan CH, Cronan JE.** 2006. The soluble acyl-acyl carrier protein synthetase of *Vibrio harveyi* B392 is a member of the medium chain acyl-CoA synthetase family. Biochemistry **45:**10008-10019.
37. **Gietz RD, Schiestl RH.** 2007. High-efficiency yeast transformation using the LiAc/SS carrier DNA/PEG method. Nat. Protoc. **2:**31-34.
38. **Hegemann JH, Guldener U, Kohler GJ.** 2006. Gene disruption in the budding yeast *Saccharomyces cerevisiae*. Methods Mol. Biol. **313:**129-144.
39. **Claros MG, Vincens P.** 1996. Computational method to predict mitochondrially imported proteins and their targeting sequences. Euro. J. Biochem. **241:**779-786.
40. **Schluter A, Real-Chicharro A, Gabaldon T, Sanchez-Jimenez F, Pujol A.** 2010. PeroxisomeDB 2.0: an integrative view of the global peroxisomal metabolome. Nucleic Acids Res. **38:**D800-D805.

3.7 Tables

Table 3.1 Plasmids constructed in this chapter

Plasmid	Construct
pH1	pRS425-*Stu*I-*PDC1p*-*Bam*HI-*eGFP*-*Xho*I-*ADH1t*-*Avr*II-*PYK1p*
pH11	pRS425-*Stu*I-*GPM1p*-*Bam*HI-*eGFP*-*Xho*I-*ADH1t*-*Avr*II-*PYK1p*
pH2	pRS425-*Avr*II-*PYK1p*-*Bam*HI-*eGFP*-*Xho*I-*CYC1t*-*Sbf*I-*ENO2p*
pH22	pRS425-*Avr*II-*ADH1t*-*GPDp*-*Bam*HI-*eGFP*-*Xho*I-*CYC1t*-*Sbf*I-*ENO2p*
pH3	pRS425-*Sbf*I-*ENO2p*-*Bam*HI-*eGFP*-*Xho*I-*PGK1t*-*Not*I-*TPI1p*
pH4	pRS425-*Not*I-*TPI1p*-*Bam*HI-*eGFP*-*Xho*I-*TPI1t*-*Sac*II-*TEFK1p*
pH5	pRS425-*Sac*II-*TEF1p*-*Bam*HI-*eGFP*-*Xho*I-*TEF1t*-*Xma*I
pH6	pRS425-*TEF1t*-*PGK1p*-*Bam*HI-*eGFP*-*Hind*III-*HXT7t*
pUG6	PCR template for *loxP*-*KanMX*-*loxP*
pUG73	PCR template for *loxP*-Kl*URA3*-*loxP*
pSH47	*GAL1p*-*Cre*-*CYC1t* containing plasmid with *URA3* marker
pSH62	*GAL1p*-*Cre*-*CYC1t* containing plasmid with *HIS3* marker
pSH63	*GAL1p*-*Cre*-*CYC1t* containing plasmid with *TRP1* marker
YlACL	pRS423-*TPI1p*-Yl*ACL1*-*TPI1t*-*TEF1p*-Yl*ACL2*-*TEF1t*
MM2	pRS425-*TPI1p*-cyto*MDH3*-*TPI1t*-*TEF1p*-cytoYl*MAE1*-*TEF1t*
MM4	pRS425-*TPI1p*-cytoYl*MDH2*-*TPI1t*-*TEF1p*-cytoYl*MAE1*-*TEF1t*
MM5	pRS425-*TPI1p*-cyto*MDH3*-*TPI1t*-*TEF1p*-cytoMa*MAE1*-*TEF1t*
MM6	pRS425-*TPI1p*-cytoYl*MDH2*-*TPI1t*-*TEF1p*-cytoMa*MAE1*-*TEF1t*
PDHwt	pRS414-*TEF1p*-Ec*LpdA*-*PGK1t*-*TPI1p*-Ec*AceE*-*GPDt*-*ENO2p*-Ec*AceF*-*TEF1t*
PDHm1	PDHwt with the mutation E354K of Ec*LpdA*
PDHm2	PDHwt with the mutation E354G of Ec*LpdA*
BsLplJ	pH5-Bs*LplJ*
EcLplA	pH5-Ec*LplA*
cytoPDH	PDHwt-*TEF1p*-Bs*LplJ*-*TEF1t*
M2J	PDHm2-*TEF1*p-Bs*LplJ*-*TEF1t*
BsLA	pRS425-*ENO2p*-Bs*GcvH*-*PGK1t*-*TPI1p*-Bs*LipA*-*TPI1t*-*TEF1p*- Bs*LipM*-*TEF1t*-*PGK1p*- Bs*LipL*-*HXT7t*
EcLA	pRS425-*TPI1p*-Ec*LipA*-*TPI1t*-TEF1p-Ec*LipB*-*TEF1t*
ScLA	pRS425-*ENO2p*-cyto*GCV3*-*PGK1t*-*TPI1p*-cyto*LIP5*-*TPI1t*-*TEF1p*-cyto*LIP3*-*TEF1t*-*PGK1p*-cyto*LIP2*-*HXT7t*
cytoFAA2	pRS423-*TEF1p*-*cytoFAA2*-*TEF1t*
cytoFAS0	pRS413-*GPM1p*-cyto*CEM1*-*ADH1t*-*PYK1p*-cyto*OAR1*-*CYC1t*-*ENO2p*-cyto*ETR1*-*PGK1t*-*TPI1p*-cyto*ACP1*-*TPI1t*-*TEF1p*-cyto*PPT2*-*TEF1t*-*PGK1p*-*cytoMCT1*-*HXT7t*
cytoFAS1	cytoFAS0-*HXT7p*-cyto*HTD2*-*HXT7t*
cytoFAS2	cytoFAS0-*HXT7p*-*EcFabA*-*HXT7t*
cytoFAS3	cytoFAS0-*HXT7p*-*EcFabZ*-*HXT7t*

Table 3.1 (cont.)

Plasmid	Construct
pYFJ84	pET16b-Vh*AasS* (36)
VhEc	pRS413-*TPI1p*-Ec*AcpP-TPI1t-TEF1p*-Ec*AcpS-TEF1t-PGK1p*-Vh*AasS-HXT7t*
VhSc	pRS413-*TPI1p*-cyto*ACP1-TPI1t-TEF1p*-cyto*PPT2-TEF1t-PGK1p*-Vh*AasS-HXT7t*

*Bs, *Baillus subtilis*; Ec, *Escherichia coli*; Ma, *Mortierella alpine*; Yl, *Yarrowia lipolytica*; Vh, *Vibrio harveyi*;

Table 3.2 Strains used in this chapter

Strain	Phenotype
CEN.PK2-1C	*MATa ura3-52 trp1-289 leu2-3,112 his3Δ1 MAL2-8^{C} SUC2*
*acs2*Δ	CEN.PK2-1C *acs2*Δ::*URA3*
*acs2*Δ/ACL	CEN.PK2-1C *acs2*Δ::*URA3*/YlACL
Acs^{-}/ACL	CEN.PK2-1C *acs2*Δ::*URA3 acs1*Δ::*KanMX*/YlACL
*acs2*Δ/M2J	CEN.PK2-1C *acs2*Δ::*URA3*/M2J
Acs^{-}/M2J	CEN.PK2-1C *acs2*Δ::*URA3 acs1*Δ::*KanMX*/M2J
Acs^{-}K/M2J	CEN.PK2-1C *acs2*Δ::*loxP acs1*Δ::*KanMX*/M2J
*fas1*Δ	CEN.PK2-1C *fas1*Δ::*KanMX*

Table 3.3 Co-factor specificities of MDHs and MAEs used in this chapter

	cytoYlMAE1	cytoMaMAE
cytoMDH3	AMM2 (NADH-NAD^+)	AMM5 (NADH-$NADP^+$)
cytoYlMDH2	AMM4 (NADH-NAD^+)	AMM6 (NADH-$NADP^+$)

3.8 Figures

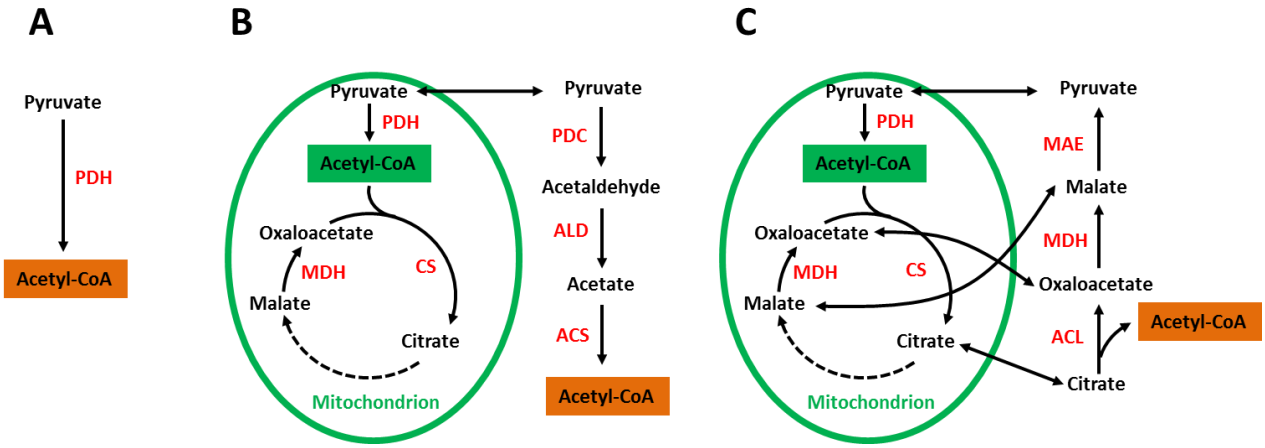

Figure 3.1 Acetyl-CoA biosynthesis in *E. coli* (A), *S. cerevisiae* (B), and *Y. lipolytica* (C).

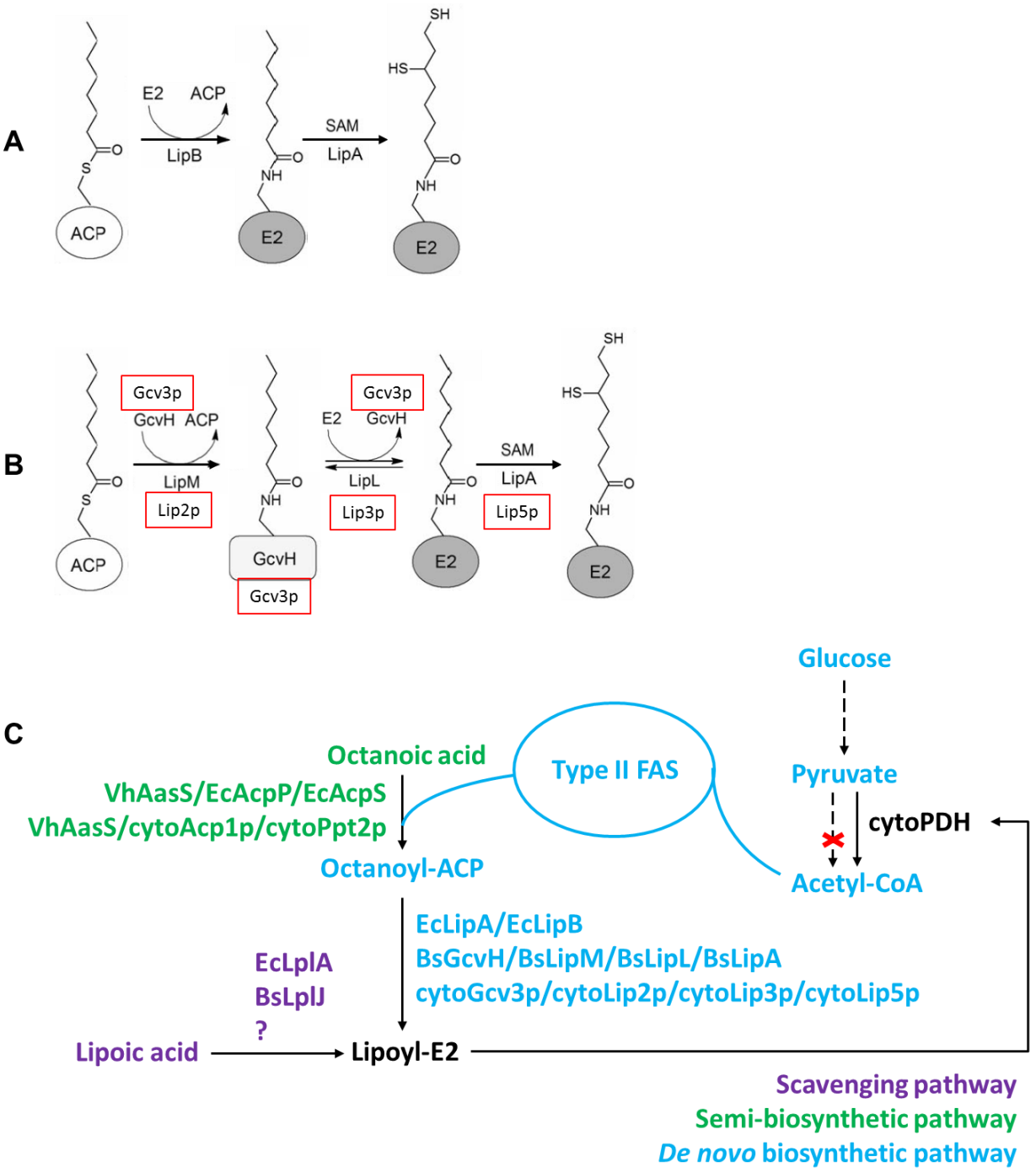

Figure 3.2 *De novo* lipoylation machineries in *E. coli* (A), *B. subtilis* (B), and *S. cerevisiae* (B, boxed). A functional PDH in the cytosol of yeast was designed and engineered with different lipoylation mechanisms, including the scavenging pathway, the semi-synthetic pathway, and the *de novo* biosynthetic pathway (C).

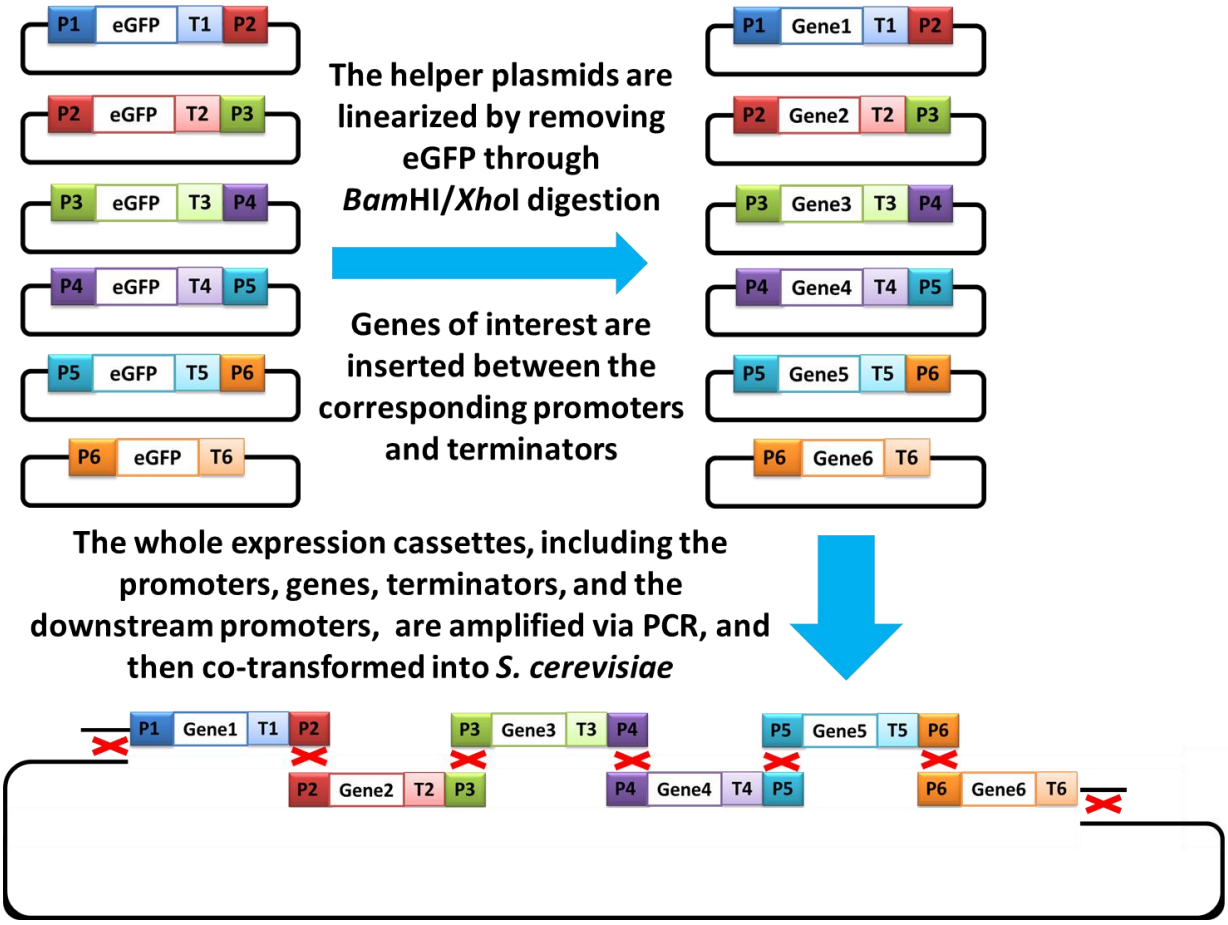

Figure 3.3 Schemes of gene cloning and pathway construction via DNA assembler using six helper plasmids.

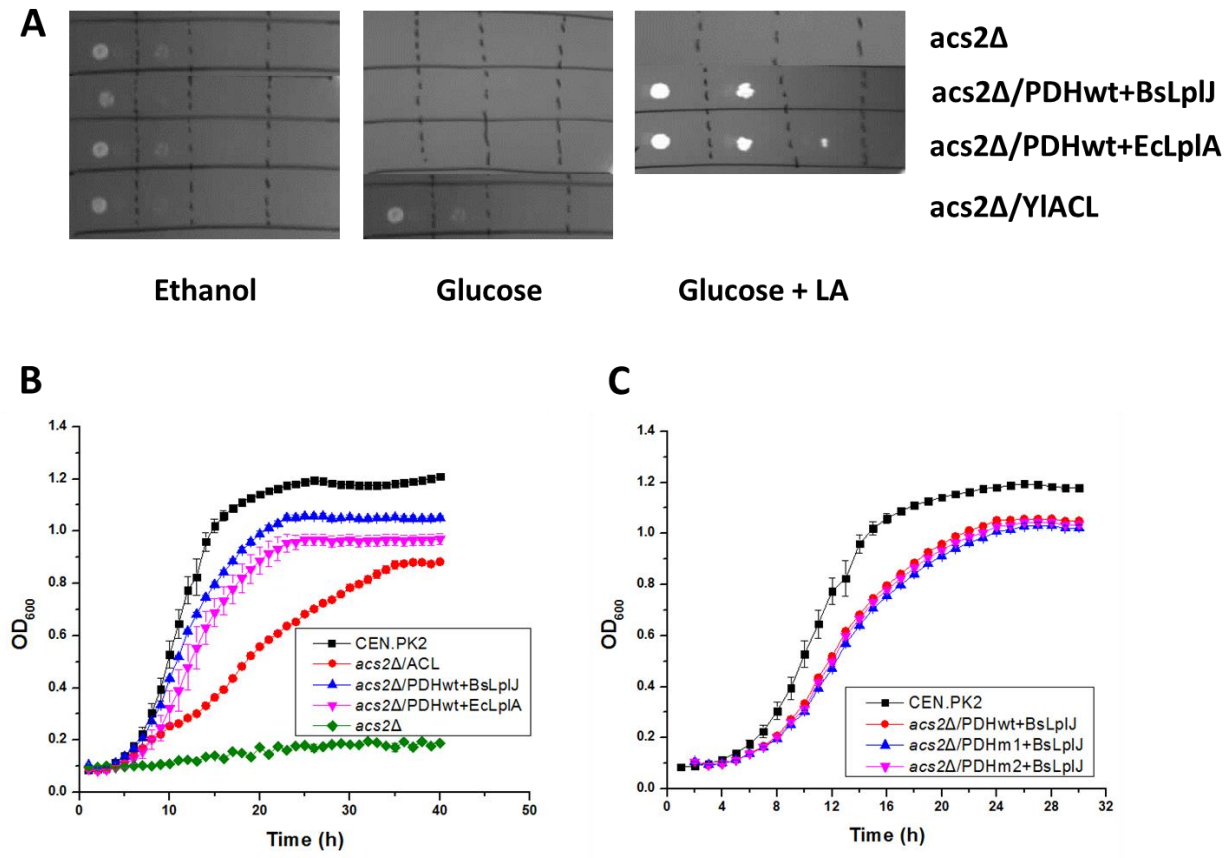

Figure 3.4 Complementation of the cell growth of *acs2*Δ yeast strain by introducing alternative acetyl-CoA biosynthesis, including ATP-dependent citrate lyase (ACL) and pyruvate dehydrogenase (PDH). The cell growth was determined by either spotting assays (A) on synthetic medium agar plates containing ethanol, glucose, and glucose with lipoic acid, respectively, or growth curves (B and C) in the corresponding liquid media (*acs2*Δ/ACL and CEN.PK2 on SCD, while all other strains on SCD supplemented with 100 µg/L lipoic acid) using the Bioscreen C.

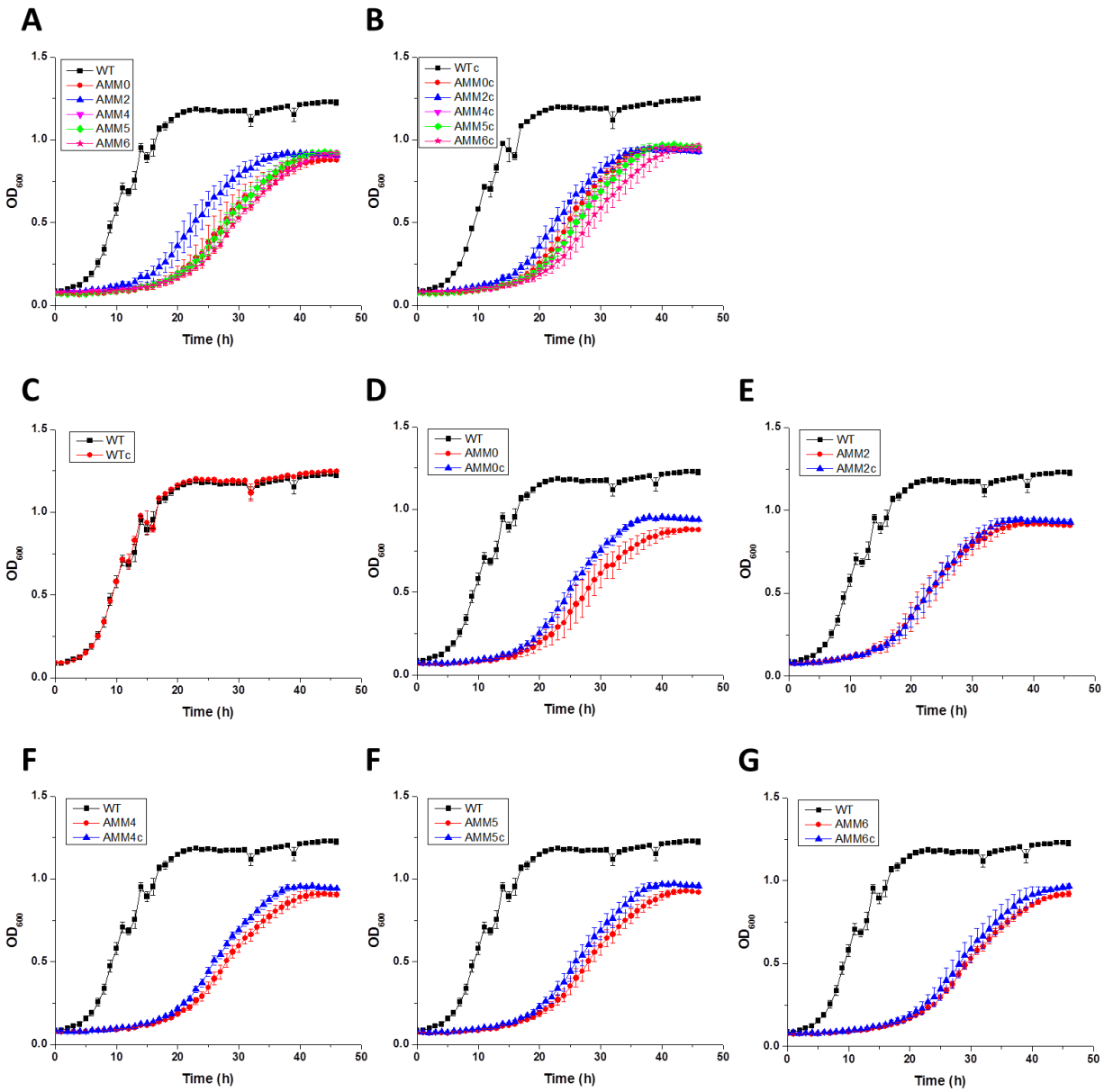

Figure 3.5 Improving the performance of ACL by citrate supplementation and *MDH-MAE* co-expression.

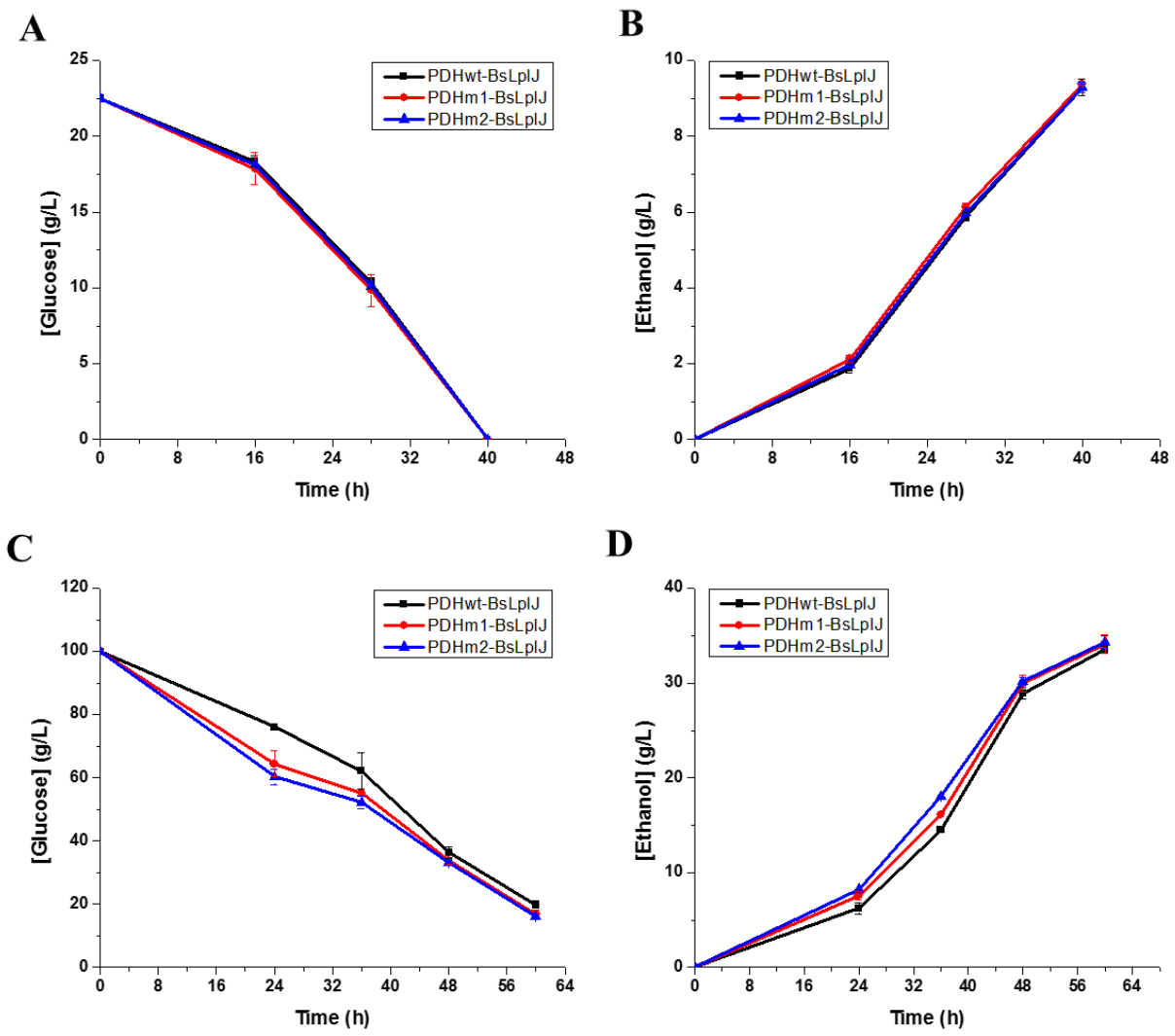

Figure 3.6 Fermentation performance of *acs2*Δ yeast strains containing PDH mutants with low (A and B) and high (C and D) glucose concentrations under micro-anaerobic condition.

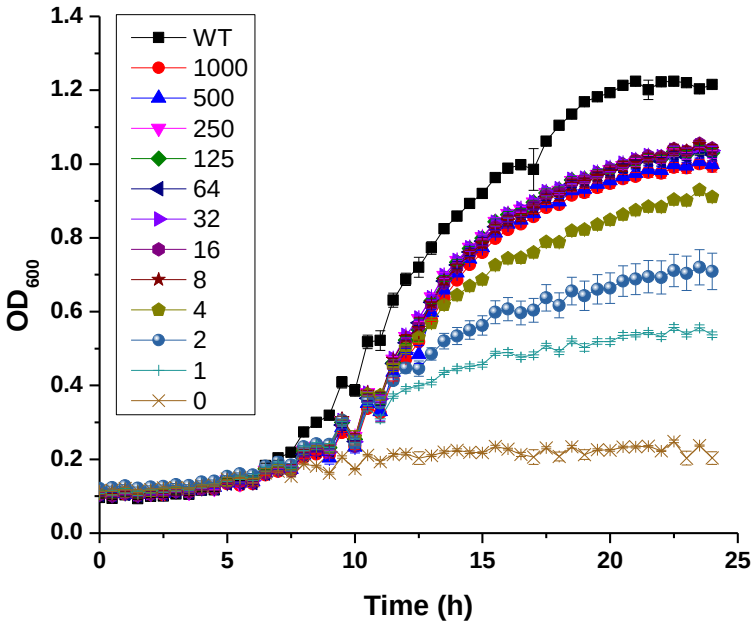

Figure 3.7 Growth dependence of Acs$^-$/M2J on lipoic acid concentration. Acs$^-$/M2J strain was pre-grown in SCD-WU medium supplemented with 100 µg/L lipoic acid until saturation and inoculated into fresh SCD-WU medium supplemented with lipoic acid at the indicated concentrations at an initial OD of 0.05. The growth of CEN.PK2 (WT) was measured under the same condition and included for comparison.

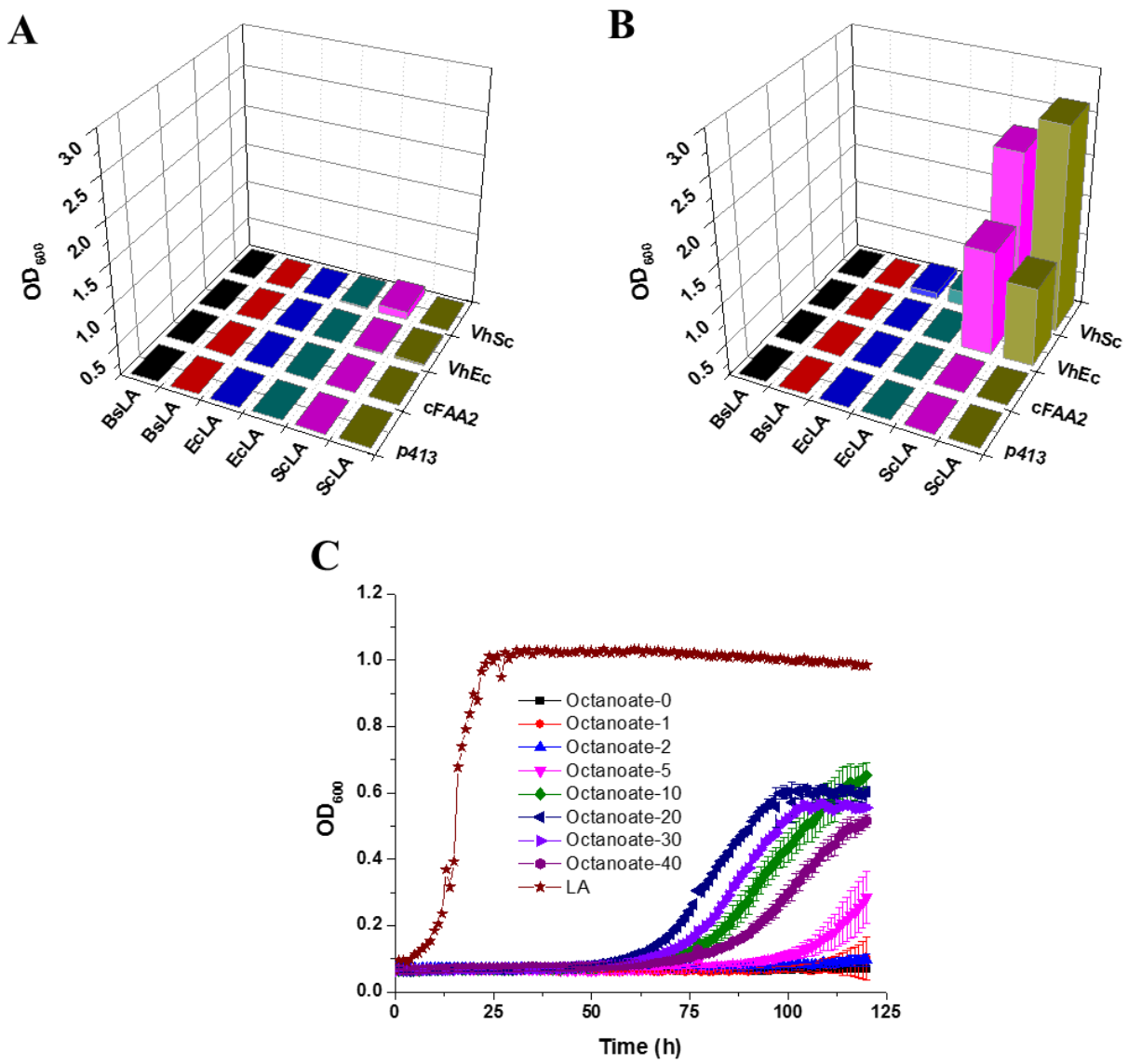

Figure 3.8 Reconstitution of a functional PDH by the semi-synthetic lipoylation pathway. Recombinant yeast strains were pre-cultured on SCD-HWLU medium supplemented with 100 µg/L lipoic acid, collected by centrifugation, washed three times in ddH_2O, and inoculated into fresh SCD-HWLU medium without (A) or with (B) the supplementation of 10 mg/L octanoic acid. Cell densities were measured 5 days after inoculation. The concentration of octanoic acid was optimized for the growth of Acs^-/M2J+ScLA+VhSc strain in SCD-HWLU medium (C). The growth of Acs^-/M2J+ScLA+VhSc strain in SCD-HWLU medium supplemented with 100 µg/L lipoic acid was included as a positive control.

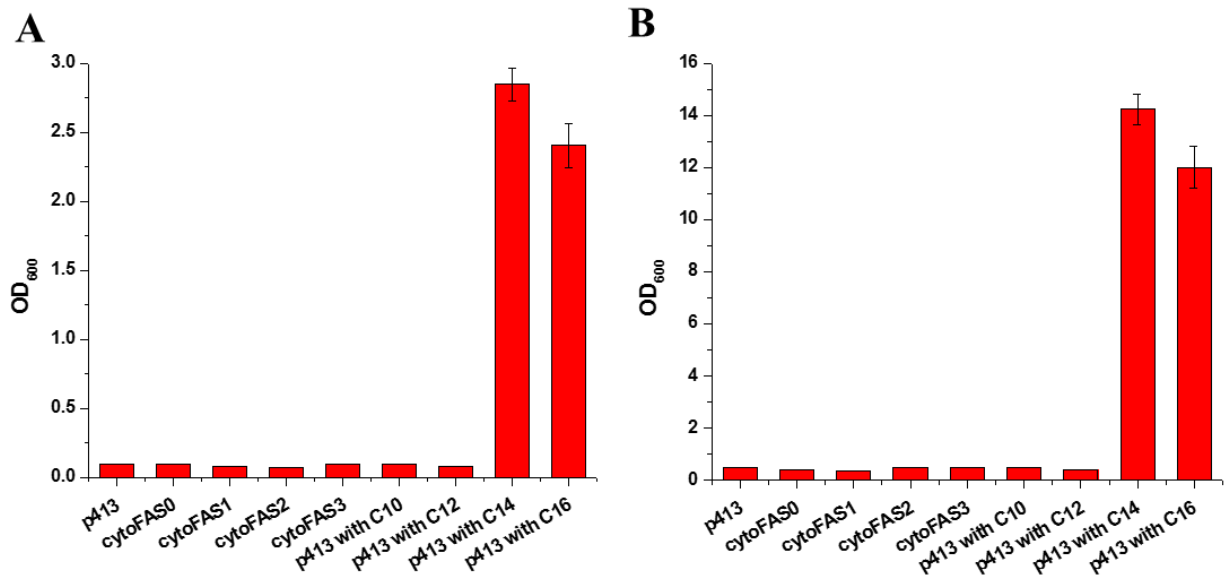

Figure 3.9 Growth complementation of *fas1*Δ strain by either introducing a type II FAS (cytoFAS1, cytoFAS2, cytoFAS3, and EcFAS1H) or supplementing free fatty acid (C_{10}, C_{12}, C_{14}, and C_{16}). Recombinant yeast strains were pre-grown in SCD-HIS medium supplemented with 200 mg/L G418 and 0.05% C_{14} fatty acid until saturation and then inoculated into fresh SCD-HIS (A) or YPD (B) medium supplemented with 200 mg/L G418 at an initial OD of 0.05. To test the growth complementation by free fatty acid supplementation, 0.05% fatty acid with the specifically mentioned chain length was added to the growth media.

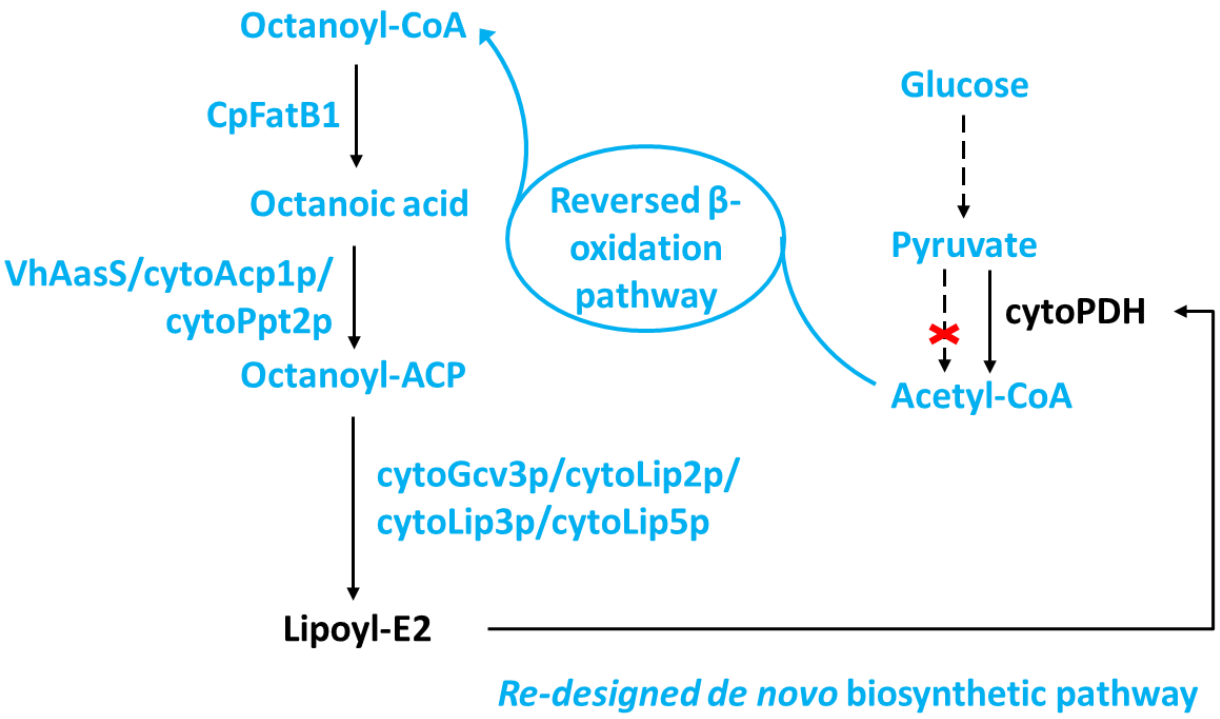

Figure 3.10 Re-designed *de novo* lipoylation pathway for functional PDH in the cytosol of yeast. Other than the use of a type II FAS, the semi-synthetic lipoylation pathway was combined with the reversed β-oxidation pathway to supply the lipoylation precursor, octanoyl-ACP.

Chapter 4 Acetyl-CoA Pool Engineering via Metabolic Engineering (II)

4.1 Introduction

In the previous chapter, the acetyl-CoA biosynthetic pathways from *Escherichia coli* (pyruvate dehydrogenase, PDH) and *Yarrowia lipolytica* (ATP-dependent citrate lyase, ACL), which showed higher catalytic activity and energetic benefits, were found to be functionally expressed in yeast and be able to replace the endogenous acetyl-CoA synthetase (ACS)-dependent system for acetyl-CoA biosynthesis in the cytosol. Although the expression of these two heterologous pathways as well as those reported in other studies (1, 2) complemented the growth of the Acs^- strain (*acs1*Δ *acs2*Δ), the use of these pathways to improve the production of acetyl-CoA derived value-added compounds has not been demonstrated yet, which was one of the major goals of this thesis. Therefore, this chapter mainly focuses on the application of these alternative acetyl-CoA biosynthetic pathways to improve the production of acetyl-CoA derived fuels and chemicals especially in the context of metabolic engineering.

Currently, most of the efforts on acetyl-CoA pool engineering in yeast were focused on the introduction of heterologous pathways, especially the PDH-bypass pathway with the ACS mutant (3-6). Due to its central role in cellular metabolism, acetyl-CoA is used as the substrate for a variety of enzymatic reactions. Therefore, host engineering to redirect the metabolic flux to acetyl-CoA can be as important as the introduction of heterologous acetyl-CoA biosynthetic pathways. As shown in Figure 4.1, acetaldehyde is the branch point to control the flux to ethanol and acetyl-CoA, and most of the metabolic fluxes are going to ethanol during glucose fermentation due to the Crabtree effect and much lower affinity of aldehyde dehydrogenases (ALDHs) towards acetaldehyde than that of alcohol dehydrogenases (ADHs). Thus the inactivation of ADHs would direct the flux to acetyl-CoA. However, previous reports indicated

that decreased ADH activity would lead to increased production of another major product glycerol (7), which also serves as one of the major electron sinks in *S. cerevisiae*. Therefore, simultaneous disruption of the glycerol pathway and the ethanol pathway would be necessary to enhance the acetyl-CoA levels. In *S. cerevisiae*, the transport of acetyl-CoA between different compartments is carried out by the glyoxylate shunt (8, 9), with several organic acids as the intermediates, such as citrate, malate, succinate, and oxaloacetate. The disruption of the glyoxylate shunt by knocking out *CIT2* or *MLS1*, encoding peroxisomal citrate synthase and cytosolic malate synthase, respectively, may enhance the levels of acetyl-CoA in the cytosol. The combined "push" and "pull" engineering may work synergistically to increase the cytosolic acetyl-CoA levels in yeast.

In this chapter, systematic evaluation of various metabolic engineering strategies for enhancing acetyl-CoA availability was carried out, including the disruption of competing pathways and the introduction of heterologous biosynthetic pathways with higher catalytic efficiency and lower energy input requirement. By inactivating the glycerol pathway and major ADHs involved in ethanol production, the metabolic flux was redirected to acetyl-CoA and the production of *n*-butanol was increased by 3-4 fold. Subsequent introduction of heterologous acetyl-CoA biosynthetic pathways, including the PDH-bypass pathways, cytosolic localized PDH (cytoPDH), and ACLs, into the engineered host further increased the production of *n*-butanol. Among these strategies, the cytoPDH worked the best, which increased the production of *n*-butanol by additional 3-4 fold. By combining the most effective acetyl-CoA pathways, *n*-butanol titer of as high as 100 mg/L could be achieved under high cell density fermentation, which is the highest *n*-butanol titer ever reported in *S. cerevisiae* using the CoA dependent pathway. Considering some limitations of the ADH (partially) deficient yeast strain, engineering

of acetyl-CoA levels in the Pdc$^-$ strain was also attempted. The acetyl-CoA overproducing strains constructed in this work would be useful for efficient production of a wide range of acetyl-CoA derived products. Note that a major part of this chapter is adapted from one of my research articles published in *Metabolic Engineering* (10).

4.2 Results

4.2.1 Construction of a n-butanol pathway as the reporter of cytosolic acetyl-CoA levels

Although several protocols for the detection of CoAs in biological systems have been developed, it is still rather tedious and labor intensive to do the extractions and assays (11, 12). Thus, the acetyl-CoA dependent *n*-butanol pathway from *Clostridium* was chosen as a model to study the effects of various metabolic engineering strategies on the acetyl-CoA pool in the cytosol of yeast. Thus, a pathway (HZ1982, Figure 4.2A) with the *Clostridium acetobutyrium* thiolase (CaThl), *C. acetobutyrium* β-hydroxybutyryl-CoA dehydrogenase (CaHbd), *Clostridium beijerinckii* crotonase (CaCrt), *Treponema denticola trans*-2-enoyl-CoA reductase (TdTer), *C. beijerinckii* butyraldehyde dehydrogenase (CbBad), and *C. acetobutyrium* butanol dehydrogenase B (CaBdhB) was constructed. However, no *n*-butanol production could be detected. Enzyme activity assay indicated the lack of Bad activity, while all other activities including Thl, Hbd, Crt, Ter, and Bdh were detected (Figure 4.2B). To have a functional *n*-butanol pathway, candidate genes with either putative Bad activity or bifunctional aldehyde/alcohol dehydrogenase (AdhE/Aad) activity were cloned from various organisms. Indeed, complementing HZ1982 with a functional Bad, such as MhpF, EutE, and AdhE from *E. coli* and Aad from *C. beijerinckii*, allowed the production of a small amount of *n*-butanol in yeast (Figure 4.2C). Among all the Bad or AdhE/Aad enzymes tested, EutE from *E. coli* gave the highest *n*-butanol production, which was cloned to replace the nonfunctional CbBad in HZ1982.

The resultant *n*-butanol pathway (BuPa28) was used as the reporter of the cytosolic acetyl-CoA levels. In the wild-type yeast strain with BuPa28, 2-3 mg/L *n*-butanol could be produced, a titer similar to those in previous reports (3, 12).

4.2.2 Host engineering to direct metabolic flux to acetyl-CoA

To redirect the glycolytic flux to acetyl-CoA, ethanol and glycerol biosynthetic pathways were partially or completely inactivated. In *S. cerevisiae*, glycerol-3-phosphate dehydrogenase was the rate-limiting enzyme for glycerol formation (Figure 4.1). Thus both of the structural genes, *GPD1* and *GPD2*, were deleted to eliminate glycerol production. As for the ethanol production, several alcohol dehydrogenases (ADHs), including but are not limited to Adh1p, Adh2p, Adh3p, Adh4p, Adh5p, Adh6p, and Adh7p, catalyze the NAD(P)H dependent reduction of acetaldehyde to ethanol (7), which directly compete with acetyl-CoA biosynthesis in the cytosol. Since Adh2p was glucose repressed at the transcription level, Adh3p and Adh5p were mainly localized in the mitochondrion, Adh6p and Adh7p were determined to be specific for medium chain and branched chain substrates, Adh1p and Adh4p were chosen as the targets to decrease ethanol production and redirect the flux to acetyl-CoA when cultured on glucose. The growth and sugar utilization were dramatically decreased when cultured the ΔGGAA (*gpd1*Δ *gpd2*Δ *adh1*Δ *adh4*Δ) strain on glucose, although no significant difference was observed for galactose fermentation (Figure 4.3). In addition, both acetaldehyde and acetate, the precursor for cytosolic acetyl-CoA, were accumulated to high levels after the inactivation of *ADH1* and *ADH4*. Accordingly, *n*-butanol titer was increased by more than 4 fold, compared with that in the wild-type strain (Figure 4.4). The productivity of *n*-butanol was only increased by about 2 fold, because of the impaired cell growth and sugar utilization.

The disruption of the competing acetyl-CoA consuming pathways, such as the glyoxylate shunt, was also carried out to enhance the availability of acetyl-CoA. As shown in Figure 4.4, *n*-butanol titer was increased by 2 fold by inactivating *CIT2* or *MLS1* in the wild-type strain. However, further deletion of *CIT2* or *MLS1* in the ΔGGAA strain led to decreased *n*-butanol production, probably caused by the accumulation of acetate to cytotoxicity levels (Figure 4.5). Therefore, ΔGGAA was chosen as the host for subsequent introduction of acetyl-CoA biosynthetic pathways.

4.2.3 Introduction of various acetyl-CoA biosynthetic pathways into the engineered host

4.2.3.1 Engineered PDH-bypass pathways

Concerning the low efficiency of the endogenous PDH-bypass pathway, heterologous acetyl-CoA biosynthetic pathways with higher efficiency and/or lower energy input requirement would be desirable. The most straightforward strategy was to overexpress the PDH-bypass pathway including the ACS mutant with much higher activity. However, the overexpression of the whole PDH-bypass pathway, which was demonstrated to improve the production of a series of acetyl-CoA derived molecules in wild-type yeast (3-6), nearly blocked the production of *n*-butanol in the engineered host (Figure 4.6A). Later it was found that low *n*-butanol production was accompanied with the accumulation of a large amount of acetate (Figure 4.5). To figure out the reason for low *n*-butanol production, additional recombinant plasmids containing *ALD6*-Se*Acs*^{L641P} or only Se*Acs*^{L641P} were constructed by gradually removing the upstream genes. Interestingly, the production of *n*-butanol was increased, with the highest titer produced by the engineered strain containing only ACS*. After codon optimization of this ACS mutant, the titer of *n*-butanol was further improved to about 20 mg/L. In contrast with the overexpression of the

Se*Acs* mutant, the overexpression of the endogenous *ACS1* and *ACS2* did not improve the production of *n*-butanol (Figure 4.6A), probably due to the low enzymatic activity or the post-translational deactivation.

4.2.3.2 Functional PDH in the cytosol (cytoPDH)

Although PDH was only found in the mitochondria of eukaryotes, the expression of the bacterial PDH genes, which lacked the mitochondrial targeting sequences, would create a new route to generate acetyl-CoA directly from pyruvate in the cytosol (cytoPDH). As demonstrated in the previous chapter of this thesis, cytoPDH containing the PDH structural genes from *E. coli* (Ec*LpdA*-Ec*AceE*-Ec*AceF*) and the lipoate-protein ligase gene from *Bacillus subtilis* (Bs*LplJ*) could fully replace the endogenous system for acetyl-CoA biosynthesis. Therefore, cytoPDH was also introduced into the engineered host (ΔGGAA), which resulted in additional three fold increase in *n*-butanol titer, a total of more than 12 fold improvement (Figure 4.6A).

4.2.3.3 ATP-dependent citrate lyase (ACL)

Comparative genomics analysis revealed that one of the biggest differences between oleaginous yeast and non-oleaginous yeasts were the presence of ACL (13), a route to generate cytosolic acetyl-CoA from citrate. Thus, ACL genes from an oleaginous yeast *Y. lipolytica* and the model plant *Arabidopsis thaliana* were cloned and introduced into the engineered *S. cerevisiae* strain. As shown in Figure 4.6A, the introduction of ACL from *Y. lipolytica* could increase the *n*-butanol titer by approximately two fold in the engineered host, while ACL from *A. thaliana* had no effect on improving the *n*-butanol titer, which was resulted from the low activity and/or poor expression of the plant genes in yeast (data not shown).

4.2.3.4 Function of the heterologous pathways in synthesizing cytosolic acetyl-CoA

To verify that the introduced acetyl-CoA pathways were functional and the increased *n*-butanol production was resulted from enhanced acetyl-CoA levels, acetyl-CoA concentration in various strains was determined using an Acetyl-CoA Assay Kit. As shown in Figure 4.6B, the deletion of *GPD1, GPD2, ADH1,* and *ADH4* increased the acetyl-CoA level by approximately 2 fold, and the introduction of heterologous acetyl-CoA pathways could further increase the acetyl-CoA level in *S. cerevisiae*. Although acetyl-CoA concentration was similar for the engineered strain with different acetyl-CoA pathways (Figure 4.6C), the amount of *n*-butanol produced was higher in the strain with cytoPDH than those with ACL or ACS. Since the activities of ACL and ACS are coupled to ATP consumption and PDH is ATP-independent, the increased *n*-butanol production might result from the energetic benefits of cytoPDH. In other words, the increased acetyl-CoA level and reduced energy input requirement lead to the highest *n*-butanol titer achieved in the cytoPDH harboring strain (Table 4.1). Another explanation lies on the fact that acetyl-CoA concentration in *S. cerevisiae* might be limited by the total CoA pool as well.

4.2.3.5 Combining the most effective Acetyl-CoA biosynthetic pathways

After verifying the activity of the acetyl-CoA biosynthetic pathways, we decided to combine the most effective and independent pathways in order to achieve maximal acetyl-CoA availability in the cytosol. As shown in Figure 4.7A, cytoPDH with ACS*Opt was the best combination, and could increase the titer of *n*-butanol by approximately six fold, compared with the engineered host with empty vectors. However, the total *n*-butanol titer was not significantly improved compared with the strain containing cytoPDH only, probably due to the burden of maintaining several plasmids, which was confirmed by the decreased *n*-butanol titer in the

control strain. Interestingly, the combination of ACS and ACL failed to increase the production of *n*-butanol, which might result from the energy input requirement for both enzymes. Thus, the combination of cytoPDH, ACL, and ACS was further attempted for *n*-butanol fermentation. To eliminate the plasmid burden issue, high cell density fermentation was carried out and the highest *n*-butanol titer over 100 mg/L could be achieved (Figure 4.7B).

4.2.3 Acetyl-CoA pool engineering in the unevolved Pdc⁻ strain

Considering the accumulation of acetaldehyde and acetate in the Adh⁻ strain, the inactivation of the upstream enzymes, the pyruvate decarboxylases (PDCs), was proposed to be a better strategy for efficient production of fuels and chemicals (14, 15). As mentioned in Chapter 2, the Pdc⁻ strain was incapable of growing on glucose as the sole carbon source and required C_2 supplementation to provide cytosolic acetyl-CoA (16). As an alternative to C_2 supplementation, introduction of acetyl-CoA biosynthetic pathways, such as cytoPDH and ACL, might enable the Pdc⁻ strain to grow on glucose as the sole carbon source.

Similar to the Acs⁻ strain lacking a route to generate cytosolic acetyl-CoA, the Pdc⁻ strain could be an ideal selection/screening platform to test the activity of the cytosolic acetyl-CoA pathways as well. As expected, the introduction of alternative acetyl-CoA pathways rescued the growth of the Pdc⁻ strain on low concentration glucose (5 g/L) as the sole carbon source (Figure 4.8A). Although the growth was still rather poor, protein engineering, pathway engineering, and even adaptive evolutionary engineering strategies (17) could be carried out to increase the activity of these pathways. Since the growth rate of the Pdc⁻ strain was the direct readout of acetyl-CoA levels in the cytosol, a high throughput selection/screening platform could be readily developed. As a proof of concept, adaptive evolution was carried out for the Pdc⁻ strain

containing cytoPDH by serial transfers in synthetic medium with 20 g/L glucose as the sole carbon source. After ten rounds of adaptive evolution, the growth rate of the evolved strain (Pdc^-/cytoPDHe) was quite similar to E10 (Figure 4.8B), an evolved Pdc^- strain containing *MTH1*T. Unfortunately, no *n*-butanol production could be detected after introducing the *n*-butanol biosynthetic pathway (data not shown), indicating that the acetyl-CoA level was still rather low in the evolved strain. To figure out the mechanisms of improved phenotype, the whole genomes of the evolved strains (Pdc^-/cytoPDH-e1 and Pdc^-/cytoPDH-e2) were sequenced (Table 4.1). Interestingly, a mutation in the Mth1p coding sequence (Ala81Pro) was observed in both of the evolved strains, indicating that the improved growth rate might result from alleviated glucose repression rather than enhanced acetyl-CoA supply. Notably, a previous study done by another group on the evolution of Pdc^- strain on glucose found the same mutation in Mth1p (Ala81Pro) (18). Recently, the similar study performed by a third group found a mutation at the same site of Mth1p (Ala81Asp) that contributed to the improved phenotype in synthetic medium with glucose as the sole carbon source (19). Since the mutation at the same site of Mth1p (Ala81) was obtained by several independent studies by different groups, it was confirmed that Ala81 contributed significantly to the activity or stability of Mth1p.

4.2.4 Acetyl-CoA pool engineering in the evolved Pdc^- strain

As the engineering of acetyl-CoA pool in the unevolved Pdc^- strain was unsuccessful, the evolved Pdc^- strain (iE11 constructed in Chapter 2) instead was used as the host, to eliminate the effects of host adaptation on acetyl-CoA pool engineering. Interestingly, a shift on the metabolite profiles was observed: alcohol fermentation (*iso*-butanol, *n*-butanol, 3-methyl-1-butanol) in Pdc^+ strain rather than acid fermentation (*iso*-butyrate, *n*-butyrate, 3-methyl-1-butyrate) in Pdc^- strain (Figure 4.9). Since the reduction of aldehydes to alcohols consumed one NADH molecule while

the oxidation to acids generated one NADPH molecule, it inferred a lack of NADPH and/or NADH in the Pdc$^-$ yeast strain. By introducing the cytoPDH and *n*-butanol biosynthetic pathway into iE11, the production of butyrate, instead of *n*-butanol, was detected by GC-MS, even without the supplementation of lipoic acid. Neither butyrate nor *n*-butanol was produced in iE11 strain containing only the *n*-butanol pathway, indicating that the PDH from *E. coli* possessed some background activity without lipoylation. When lipoic acid was supplemented to the fermentation medium, which would activate cytoPDH to generate more acetyl-CoA as well as NADH, the fermentation profiles shifted gradually back to alcohols. As shown in Figure 4.9, with the increasing concentration of lipoic acid, *iso*-butanol and 3-methyl-1-butanol were shifted from their acid form first and then *n*-butanol was generated. Different from *iso*-butanol and 3-methyl-1-butanol, only limited amount of *n*-butyrate was shifted to *n*-butanol, indicating that intracellular NADPH and/or NADH level was still rather low. Anyway, this was the first time to detect the production of *n*-butanol in the Pdc$^-$ yeast strain.

To investigate the effect of enhanced NADPH supply on fermentation performance of the iE11/cytoPDH strain to produce acetyl-CoA derived value added compounds, *n*-butanol in this case, three different strategies to boost NADPH level in yeast were tested. The first strategy (Figure 4.10A) was to overexpress *gapN*, encoding a non-phosphorylating glyceraldehyde-3-phosphate (G-3-P) dehydrogenase. Different from the G-3-P dehydrogenase in the glycolysis pathway, GAPN catalyzed an NADPH-dependent reaction. The second strategy (Figure 4.10B) was to overexpress *ZWF1*, encoding an enzyme that controls the entry point of the oxidative pentose phosphate pathway, which was the major source of NADPH in *S. cerevisiae*. The third strategy was to combine cytoPDH with the ACL-MDH-MAE system (Figure 4.10C), which not only functioned as an acetyl-CoA shuttle but also an NADH-NADPH shunt. Unfortunately, none

of these NADPH engineering strategies significantly changed the fermentation profiles and increased *n*-butanol production in the Pdc$^-$ Strain.

4.2.5 Further exploring ACL-MDH-MAE for metabolic engineering applications

As mentioned in Chapter 3, ACL-MDH-MAE system not only functions as an acetyl-CoA shuttle but also an NADH-NADPH shunt. In other words, ACL-MDH-MAE will not only provide acetyl-CoA but also NADPH, both of which are used as precursors by a wide range of biosynthetic pathways, such as fatty acid biosynthesis and 3-HP production. Besides biosynthetic pathways, ACL-MDH-MAE also has potential applications in catabolic pathways, such as xylose utilization. It is well known that the fungal redox pathway, which was generally introduced to *S. cerevisiae* to enable xylose utilization, suffers from co-factor imbalance problems, meaning NADPH consumption in the first step catalyzed by xylose reductase and NADH generation in the following step catalyzed by xylitol dehydrogenase (XDH). To demonstrate the application of the ACL-MDH-MAE system in both anabolic and catabolic pathways, xylose-based fatty alcohol production was carried out, based on an engineered yeast strain constructed in our previous study to produce fatty alcohol efficiently from glucose (20).

The introduction of an NADH-NADPH shunt into L34 (21), a xylose utilizing yeast strain constructed in our previous study, increased both the growth rate (Figure 4.11A) and xylose consumption rate (Figure 4.11B). Similarly, the enhanced supply of NADPH in XF3 (20), a fatty alcohol overproducing yeast strain constructed in our previous study, also further increased the production of fatty alcohol around 1.5 fold, with a final concentration of about 350 mg/L from 20 g/L glucose (Figure 4.11C). Notably, the titer of the control strain was not as high as that reported previously, probably due to the metabolic burden of introducing another multi-

copy plasmid. To investigate the potential synergy between catabolic and anabolic pathways, ACL-MDH-MAE was applied for xylose-based fatty alcohol production (Figure 4.11E and F). Although the consumption of xylose and the titer of fatty alcohols were both increased, the yield (g fatty alcohol per g xylose) was rather similar (Figure 4.11D), indicating that the increased fatty alcohol production was resulted from improved xylose utilization. In other words, we observed competition rather than synergy between the co-factor imbalanced (NADPH requiring) anabolic and catabolic pathways, with catabolism as the winner of the NADPH competition.

4.3 Discussions

There is a growing interest in developing *S. cerevisiae* as a cell factory for the production of biofuels and chemicals, owing to its high tolerance to harsh industrial conditions (3, 22). Besides its essential role in numerous metabolic pathways and cellular functions, acetyl-CoA is the building block for the biosynthesis of many products of industrial interest. However, acetyl-CoA metabolism in yeast is rather complex and highly regulated. In addition, this precursor molecule is synthesized in various compartments and cannot be directly transported between these compartments. In this chapter, the acetyl-CoA metabolism was engineered in *S. cerevisiae* to enhance the availability of this precursor metabolite in the cytosol.

Due to the lack of ATP-dependent citrate lyase (ACL) and the carnitine shuttle when cultured in minimal medium (3), the activation of acetate is the only route to generate cytosolic acetyl-CoA in *S. cerevisiae*. This PDH-bypass route suffered from low enzyme activity and high energy input requirement. Therefore, heterologous synthetic pathways with higher efficiency and lower energy input requirement were introduced to enhance the availability of acetyl-CoA in the cytosol. Among all acetyl-CoA pathways tested, cytoPDH from *E. coli* and ACL from *Y. lipolytica* worked the best to increase the production of *n*-butanol. In addition, although *n*-

butanol titer was different, acetyl-CoA concentration in the engineered strain containing ACS*Opt, cytoPDH, or YlACL was nearly the same, indicating that the synthesis of acetyl-CoA may also be limited by the total CoA pool. Engineering of CoA biosynthesis (23), especially the rate-limiting step catalyzed by pantothenate kinase, would further improve the concentration of acetyl-CoA in yeast. In terms of the compartmentalization of acetyl-CoA metabolism, the whole *n*-butanol pathway can be relocated to the same compartment as the precursor metabolite. Besides the enhanced availability of the precursor molecule, compartmentalization engineering was also found to have higher efficiency, as a result of increased local enzyme concentration and fewer competing pathways (24, 25).

Since most of the glycolytic flux goes to ethanol formation even under respiration conditions (the Crabtree effect), the flux towards acetyl-CoA is very limited. To redirect the metabolic flux towards acetyl-CoA, the synthesis of ethanol was decreased by deleting two major ADHs (*ADH1* and *ADH4*) in the cytosol, which was confirmed in part by the accumulation of acetaldehyde in the yeast cells. However, ethanol was still the major product, indicating the presence of other genes encoding enzymes with ADH activity in the yeast genome. Further disruption of an acetyl-CoA consuming pathway (the glyoxylate shunt) by the inactivation of *CIT2* or *MLS1* led to decreased *n*-butanol production, which was inconsistent with the results obtained in the wild-type yeast strain (Figure 4.4). This discrepancy might result from the effect of *ADH* deletion on acetate metabolism. In the wild-type strain, only a small amount of acetate was produced (Figure 4.3), which was considered as one of the rate-limiting factors for acetyl-CoA biosynthesis (4). Thus the disruption of the glyoxylate shunt would result in more acetate in the cytosol for acetyl-CoA biosynthesis (Figure 4.1). On the contrary, acetate was already accumulated to relative high levels in the ΔGGAA strain (Figures 4.3 and 4.5), and the

activity of ACS or the supply of ATP was rate-limiting for acetyl-CoA biosynthesis. Further disruption of the glyoxylate shunt in the ΔGGAA strain resulted in the accumulation of acetate to cytotoxic levels. The difference in acetate metabolism could also explain the observation that overexpression of the whole PDH-bypass pathway led to increased acetyl-CoA level in the wild-type strain while impaired the synthesis of acetyl-CoA derived products in the ΔGGAA strain.

Considering the accumulation of acetaldehyde and acetate in the Adh^- strain, the inactivation of the upstream enzymes, pyruvate decarboxylases (PDCs), was proposed to be a better strategy for efficient production of fuels and chemicals (14, 15). However, the Pdc^- strain was notorious for its inability to grow with glucose as the sole carbon source and required C_2 supplementation to provide cytosolic acetyl-CoA (16). As an alternative to C_2 supplementation, introduction of acetyl-CoA biosynthetic pathways, such as cytoPDH and ACL, was found to be able to rescue the growth on low concentrations of glucose (Figure 4.8A), which was similar to the work shown in Chapter 3 that these alternative acetyl-CoA biosynthetic pathways were able to complement the growth of an Acs^- (*acs1*Δ *acs2*Δ) *S. cerevisiae* strain. As ethanol production was completely eliminated and pyruvate was accumulated to high levels, the Pdc^- strain could be used as a good start point for acetyl-CoA pool engineering, especially for the cytoPDH. Since the growth was still rather poor and the growth rate of the Pdc^- strain was the direct readout of acetyl-CoA levels in the cytosol, a high throughput selection/screening platform based on growth rate could be readily developed. Unfortunately, the adaptive evolution results indicated the improved growth rate was resulted from glucose derepression (*MTH1* mutation) rather than enhanced acetyl-CoA levels. Then, we switched to engineer acetyl-CoA pool in the well evolved Pdc^- strain, as mentioned in chapter 2. Interestingly, a redistribution of the metabolic profiles was observed (Figure 4.9), from alcohol fermentation of the wild-type strain to acid fermentation of

Pdc$^-$ strain, which might indicate a cellular status lacking NADPH and/or NADH. Metabolic engineering efforts to combine NADPH engineering with acetyl-CoA engineering led to limited success. Therefore, a systematic understanding of the metabolism of the Pdc$^-$ strain would be required for the design and construction of an acetyl-CoA overproducing strain.

4.4 Conclusions and Perspectives

In summary, combined strategies of disrupting competing pathways to redirect the flux towards acetyl-CoA and introducing heterologous acetyl-CoA pathways with higher activity and lower energy input requirement were carried out to enhance the availability of acetyl-CoA in yeast. The yeast host was engineered to eliminate or decrease the formation of glycerol and ethanol and redirect the glycolytic flux to acetyl-CoA biosynthesis. Subsequent introduction of three independent acetyl-CoA biosynthetic pathways, with acetate (PDH-bypass), pyruvate (cytoPDH), and citrate (ACL) as the substrate, respectively, into the host increased the concentration of acetyl-CoA by approximately 3 fold. In terms of the accumulation of high level pyruvate and the function of cytoPDH to convert pyruvate to acetyl-CoA, the introduction of functional cytoPDHs into the Pdc$^-$ strain was also attempted to try to construct an acetyl-CoA overproducing yeast strain.

4.5 Materials and Methods

4.5.1 Strains, media, and cultivation conditions

All engineered strains used in this chapter are based on *S. cerevisiae* CEN.PK2-1C strain. *E. coli* strain DH5α was used to maintain and amplify plasmids, and recombinant strains were cultured at 37°C in Luria-Bertani (LB) broth containing 100 μg/mL ampicillin. Yeast strains were cultivated in complex medium consisting of 2% peptone and 1% yeast extract

supplemented with 2% glucose (YPD) or galactose (YPG). Recombinant strains were grown on synthetic complete medium consisting of 0.17% yeast nitrogen base, 0.5% ammonium sulfate, and the appropriate amino acid drop out mix, supplemented with 2% glucose (SCD) or galactose (SCG). The *adh1-adh4-* yeast strains were pre-cultured in galactose medium under aerobic conditions (30^{o}C and 250 rpm) and inoculated to glucose medium for *n*-butanol fermentation under oxygen-limited conditions (30°C and 100 rpm). All restriction enzymes, Q5 polymerase, and the *E. coli-S. cerevisiae* shuttle vectors were purchased from New England Biolabs (Ipswich, MA). All chemicals were purchased from Sigma-Aldrich (St. Louis, MO) unless otherwise specified.

4.5.2 DNA manipulation

The yeast homologous recombination based DNA assembler method was used to construct the recombinant plasmids (26). Briefly, DNA fragments sharing homologous regions to adjacent DNA fragments were co-transformed into *S. cerevisiae* along with the linearized backbone to assemble several elements in a single step. All recombinant plasmids constructed in this chapter are listed in Table 4.3. Wizard Genomic DNA Purification Kit (Promega, Madison, WI) was used to extract the genomic DNA from both bacteria and yeasts, according to the manufacturer's protocol. All acetyl-CoA biosynthetic pathways were first cloned into pRS424 or pRS414. In order to combine the overexpression of complementary acetyl-CoA pathways, PDH-bypass pathways were subcloned into pRS425, and ACLs were subcloned into pRS423. The acetyl-CoA and NADPH boosting plasmids, pIYC08 (3) and pJC2 (27), were kindly provided by Prof. Jens Nielsen from the Chalmers University of Technology. To confirm the correct clones, yeast plasmids were isolated using a Zymoprep Yeast Plasmid Miniprep II Kit (Zymo Research, Irvine, CA) and amplified in *E. coli* for verification.

4.5.3 Strain construction

All the strains used in this chapter are listed in Table 4.4. For the construction of *gpd1*Δ, *gpd2*Δ, *adh1*Δ, *adh4*Δ, *cit2*Δ, and/or *mls1*Δ strains, the *loxP*-KanMX-*loxP* method (28) was used for consecutive deletion of these genes. The Pdc^- strain was constructed chapter 2. The deletion of each gene was verified by diagnostic PCR. Yeast strains were transformed using the LiAc/SS carrier DNA/PEG method (29), and transformants were selected on the appropriate SCD or SCG plates. To construct the *trp1* deficient yeast strain, *trp1-289* was amplified from CEN.PK2 genome by PCR and then transformed into XF3. By counter selection on SCD plate supplemented with 0.5 g/L 5-fluoroanthranilic acid (5-FAA), the resultant strain (XF3w) was *trp1* deficient and could be transformed with pRS424 based recombinant plasmids.

4.5.4 n-Butanol fermentation and detection

A single colony from the newly transformed plate was inoculated into 3 mL of the appropriate SCD or SCG medium, and cultured under aerobic conditions for 36 h. Then 200 μL of seed culture was transferred into 10 mL of the corresponding SCD medium in a 50 mL unbaffled flask at an initial OD_{600} of about 0.05, and cultured under oxygen-limited conditions. Samples were taken every 24 h after inoculation until no further increase in *n*-butanol production was observed, and the highest titer detected was used to compare the effects of different metabolic engineering strategies on *n*-butanol production.

Samples were centrifuged at 14,000 rpm for 10 min and the resulting supernatant was analyzed using a Shimadzu GCMS-QP2010 Plus GC-MS equipped with an AOC-20i+s autosampler and a DB-Wax column with a 0.25 μm film thickness, 0.25 mm diameter, and 30 m length (Agilent Inc., Palo Alto, CA). Injection port and interface temperature was set at 250 °C,

and the ion source set to 230 °C. The helium carrier gas was set at a constant flow rate of 2 mL/min. The oven temperature program was set as the following: a) 3 min isothermal heating at 50 °C, b) increase at the rate of 15 °C min^{-1} to 120 °C, c) increase at the rate of 50 °C min^{-1} to 230 °C, d) and then isothermal heating at 230 °C for an additional 2.5 min. The mass spectrometer was operated with a solvent cut time of 1.5 min, an event time of 0.2 s, and a scan speed of 2500 from the range of 30-500 mass to charge (m/z) ratio. Concentrations were determined using standard curves, with 50 mg/L methanol as the internal standard. Each data point of the *n*-butanol titer represents the average of at least duplicates.

4.5.5 Acetyl-CoA assay

Yeast cells were pre-cultured, inoculated, and cultured under the same conditions as *n*-butanol fermentation. After growing to the mid-log phase, cell metabolism was quenched by adding 8 mL cells into 40 mL pre-chilled (-80 °C) methanol, and cells were harvested by centrifugation at 4,000 g for 5 min. Then 2 mL boiling ethanol was added to the cell pellets, followed by boiling for an additional 15 min to release intracellular metabolites. After centrifugation, the supernatant was vacuum dried and resuspended into 200 µL ddH_2O. The resultant solution containing acetyl-CoA was analyzed by the acetyl-Coenzyme A Assay Kit (Sigma-Aldrich). The concentration of acetyl-CoA was the average of biological duplicates and normalized by the dry cell weight.

4.5.6 Fatty alcohol fermentation and detection

A single colony from the fresh plate was inoculated into 5 mL appropriate SCD medium and cultured under aerobic conditions for 48 h. Then cells were collected, washed, and transferred into 5 mL the same SCD medium topped with 10% *n*-dodecane overlay in a 20 mL

glass tube at an initial OD_{600} of about 3. Fatty alcohol fermentation was performed under aerobic conditions for 48 h. The top *n*-dodecane layer was collected, diluted 100 fold in ethyl acetate containing 1 mg/L *n*-tridecane as an internal standard, and analyzed using the same GC-MS settings as mentioned above. The oven temperature program was set as the following: a) hold at 50ºC for 2 min isothermal heating, b) increase at the rate of 50ºC min^{-1} to 230ºC, c) and then hold at 230ºC for additional 15 min.

4.6 References

1. **Kozak BU, van Rossum HM, Benjamin KR, Wu L, Daran JM, Pronk JT, van Maris AJ.** 2013. Replacement of the *Saccharomyces cerevisiae* acetyl-CoA synthetases by alternative pathways for cytosolic acetyl-CoA synthesis. Metab. Eng. **21:**46-59.
2. **Kozak BU, van Rossum HM, Luttik MA, Akeroyd M, Benjamin KR, Wu L, de Vries S, Daran JM, Pronk JT, van Maris AJ.** 2014. Engineering acetyl coenzyme A supply: functional expression of a bacterial pyruvate dehydrogenase complex in the cytosol of *Saccharomyces cerevisiae*. MBio **5:**e01696-01614.
3. **Chen Y, Daviet L, Schalk M, Siewers V, Nielsen J.** 2013. Establishing a platform cell factory through engineering of yeast acetyl-CoA metabolism. Metab. Eng. **15:**48-54.
4. **Shiba Y, Paradise EM, Kirby J, Ro DK, Keasling JD.** 2007. Engineering of the pyruvate dehydrogenase bypass in *Saccharomyces cerevisiae* for high-level production of isoprenoids. Metab. Eng. **9:**160-168.
5. **Kocharin K, Chen Y, Siewers V, Nielsen J.** 2012. Engineering of acetyl-CoA metabolism for the improved production of polyhydroxybutyrate in *Saccharomyces cerevisiae*. AMB Express **2:**52.
6. **Krivoruchko A, Serrano-Amatriain C, Chen Y, Siewers V, Nielsen J.** 2013. Improving biobutanol production in engineered *Saccharomyces cerevisiae* by manipulation of acetyl-CoA metabolism. J. Ind. Microbiol. Biotechnol. **40:**1051-1056.
7. **de Smidt O, du Preez JC, Albertyn J.** 2012. Molecular and physiological aspects of alcohol dehydrogenases in the ethanol metabolism of *Saccharomyces cerevisiae*. FEMS Yeast Res. **12:**33-47.
8. **Chen Y, Siewers V, Nielsen J.** 2012. Profiling of cytosolic and peroxisomal acetyl-CoA metabolism in *Saccharomyces cerevisiae*. PLoS One **7:**e42475.
9. **Strijbis K, Distel B.** 2010. Intracellular acetyl unit transport in fungal carbon metabolism. Eukaryot. Cell **9:**1809-1815.
10. **Lian J, Si T, Nair NU, Zhao H.** 2014. Design and construction of acetyl-CoA overproducing *Saccharomyces cerevisiae* strains. Metab. Eng. **24:**139-149.
11. **Park JW, Jung WS, Park SR, Park BC, Yoon YJ.** 2007. Analysis of intracellular short organic acid-coenzyme A esters from actinomycetes using liquid chromatography-electrospray ionization-mass spectrometry. J. Mass Spectrom. **42:**1136-1147.
12. **Steen EJ, Chan R, Prasad N, Myers S, Petzold CJ, Redding A, Ouellet M, Keasling JD.** 2008. Metabolic engineering of *Saccharomyces cerevisiae* for the production of n-butanol. Microb. Cell Fact. **7:**36.
13. **Vorapreeda T, Thammarongtham C, Cheevadhanarak S, Laoteng K.** 2012. Alternative routes of acetyl-CoA synthesis identified by comparative genomic analysis: involvement in the lipid production of oleaginous yeast and fungi. Microbiology **158:**217-228.
14. **van Maris AJ, Geertman JM, Vermeulen A, Groothuizen MK, Winkler AA, Piper MD, van Dijken JP, Pronk JT.** 2004. Directed evolution of pyruvate decarboxylase-negative *Saccharomyces cerevisiae*, yielding a C_2-independent, glucose-tolerant, and pyruvate-hyperproducing yeast. Appl. Environ. Microbiol. **70:**159-166.
15. **Oud B, Flores CL, Gancedo C, Zhang X, Trueheart J, Daran JM, Pronk JT, van Maris AJ.** 2012. An internal deletion in *MTH1* enables growth on glucose of pyruvate-

decarboxylase negative, non-fermentative *Saccharomyces cerevisiae*. Microb. Cell Fact. **11:**131.

16. **Flikweert MT, de Swaaf M, van Dijken JP, Pronk JT.** 1999. Growth requirements of pyruvate-decarboxylase-negative *Saccharomyces cerevisiae*. FEMS Microbiol. Lett. **174:**73-79.
17. **Du J, Yuan Y, Si T, Lian J, Zhao H.** 2012. Customized optimization of metabolic pathways by combinatorial transcriptional engineering. Nucleic Acids Res. **40:**e142.
18. **Kim SJ, Seo SO, Jin YS, Seo JH.** 2013. Production of 2,3-butanediol by engineered *Saccharomyces cerevisiae*. Bioresour. Technol. **146:**274-281.
19. **Zhang YM.** 2015. Engineering cytosolic acetyl-CoA metabolism in *Saccharomyces cerevisiae*: Combining metabolic engineering and adaptive laboratory evolution. Ph.D. Thesis. Chalmers University of Technology, Göteborg, Sweden.
20. **Feng X, Lian J, Zhao H.** 2015. Metabolic engineering of *Saccharomyces cerevisiae* to improve 1-hexadecanol production. Metab. Eng. **27:**10-19.
21. **Li S, Du J, Sun J, Galazka JM, Glass NL, Cate JH, Yang X, Zhao H.** 2010. Overcoming glucose repression in mixed sugar fermentation by co-expressing a cellobiose transporter and a beta-glucosidase in *Saccharomyces cerevisiae*. Mol. Biosyst. **6:**2129-2132.
22. **Runguphan W, Keasling JD.** 2014. Metabolic engineering of *Saccharomyces cerevisiae* for production of fatty acid-derived biofuels and chemicals. Metab. Eng. **21:**103-113.
23. **Vadali RV, Bennett GN, San KY.** 2004. Cofactor engineering of intracellular CoA/acetyl-CoA and its effect on metabolic flux redistribution in *Escherichia coli*. Metab. Eng. **6:**133-139.
24. **Avalos JL, Fink GR, Stephanopoulos G.** 2013. Compartmentalization of metabolic pathways in yeast mitochondria improves the production of branched-chain alcohols. Nat. Biotechnol. **31:**335-341.
25. **Farhi M, Marhevka E, Masci T, Marcos E, Eyal Y, Ovadis M, Abeliovich H, Vainstein A.** 2011. Harnessing yeast subcellular compartments for the production of plant terpenoids. Metab. Eng. **13:**474-481.
26. **Shao Z, Zhao H, Zhao H.** 2009. DNA assembler, an *in vivo* genetic method for rapid construction of biochemical pathways. Nucleic Acids Res. **37:**e16.
27. **Chen Y, Bao J, Kim IK, Siewers V, Nielsen J.** 2014. Coupled incremental precursor and co-factor supply improves 3-hydroxypropionic acid production in *Saccharomyces cerevisiae*. Metab. Eng. **22:**104-109.
28. **Hegemann JH, Guldener U, Kohler GJ.** 2006. Gene disruption in the budding yeast *Saccharomyces cerevisiae*. Methods Mol. Biol. **313:**129-144.
29. **Gietz RD, Schiestl RH.** 2007. High-efficiency yeast transformation using the LiAc/SS carrier DNA/PEG method. Nat. Protoc. **2:**31-34.
30. **Kim B, Du J, Eriksen DT, Zhao H.** 2013. Combinatorial design of a highly efficient xylose-utilizing pathway in *Saccharomyces cerevisiae* for the production of cellulosic biofuels. Appl. Environ. Microbiol. **79:**931-941.

4.7 Tables

Table 4.1 Comparison of different acetyl-CoA biosynthetic pathways on the generation of energy (ATP) and co-factors (NADH/NADPH), as well as the *n*-butanol productivity and yield.

	Theoretical value/glucose[a]			Glucose consumption rate (g/L-h)	*n*-Butanol productivity (mg/L-h)	*n*-Butanol yield (mg/g glucose)
	ATP	NADH	NADPH			
NC	0	2	2	0.23±0.01	0.11±0.01	0.51±0.02
ACS*Opt	0	2	2	0.19±0.02	0.18±0.01	0.85±0.08
EcPDH	2	4	0	0.22±0.01	0.42±0.02	1.58±0.09
YlACL	1	4	0	0.20±0.02	0.26±0.04	1.23±0.18

[a]The numbers are the theoretical values for the heterologous acetyl-CoA biosynthetic pathways generated from one glucose molecule. A combination of the endogenous system and the heterologous system was used in the *n*-butanol fermentation process.

Table 4.2 SNVs identified in the coding sequences (CDS) of the evolved Pdc$^-$/cytoPDH strains

Non-synonymous SNVs in CDS	Pdc$^-$/cytoPDH-e1	Pdc$^-$/cytoPDH-e2
EIW11482.1 (Mth1p)		Ala81Pro
EIW10966.1 (Rph1p)		Gln715Lys
EIW07758.1 (Pdr10p)		Phe1381Ser
EIW12312.1 (Gem1p)	-	Ser489fs
EIW11030.1 (Unknown)	-	Val373fs
Total SNVs in CDS	4	5
Total SNVs	42	36

Table 4.3 Plasmids constructed in this chapter.

Plasmids	Description
pRS414	Single copy plasmid in *S. cerevisiae* with *TRP1* marker
pRS416	Single copy plasmid in *S. cerevisiae* with *URA3* marker
pRS423	Multiple copy plasmid in *S. cerevisiae* with *HIS3* marker
pRS424	Multiple copy plasmid in *S. cerevisiae* with *TRP1* marker
pRS425	Multiple copy plasmid in *S. cerevisiae* with *LEU2* marker
pRS426	Multiple copy plasmid in *S. cerevisiae* with *URA3* marker
pUG6	Template plasmid containing *loxP-KanMX-loxP* elements
pSH47	Cre containing plasmid for *loxP-KanMX-loxP* cassette recycle
HZ1982	pRS416-Ca*Thl*-Ca*Hbd*-Cb*Crt*-Td*Ter*-Cb*Bad*-Ca*BdhB*
EcMhpF	pRS425-Ec*MhpF*
EcEutE	pRS425-Ec*EutE*
EcAdhE	pRS425-Ec*AdhE*
CaAad	pRS423-Ca*Aad*
CaAdhE2	pRS423-Ca*AdhE2*
CbAad	pRS423-Cb*Aad*
CnBad	pRS423-Cn*Bad*
TeAad	pRS423-Te*Aad*
GlAad	pRS424-Gl*Aad*
BuPa28	pRS426-Ca*Thl*-Ca*Hbd*-Cb*Crt*-Td*Ter*-Ec*EutE*-Ca*BdhB*
HZ1983	pRS424-*PDC1-ALD6*-Se*Acs*^{L641P}
HZ2000	pRS424-*ALD6*-Se*Acs*^{L641P}
pIYC08	pRS423-*ADH2*- *ALD6*-Se*Acs*^{L641P}Opt-*ERG10* (3)
ACS1	pRS424-*ACS1*
ACS2	pRS424-*ACS2*
ACS*	pRS424-Se*Acs*^{L641P}
ACS*Opt	pRS424-Se*Acs*^{L641P}Opt
ACS*Opt-L	pRS425-Se*Acs*^{L641P}Opt
cytoPDH	pRS414-Ec*LpdA*-Ec*AceE*-Ec*AceF*-Bs*LplJ* (Chapter 3)
YlACL	pRS424-Yl*ACL1*-Yl*ACL2*
YlACL-H	pRS423-Yl*ACL1*-Yl*ACL2* (Chapter 3)
AtACL	pRS423-At*ACL1*-At*ACL2*
pJC2	pIYC04-*gapN* (27)
pJC2Z	pIYC04-*gapN-ZWF1*
MM5	pRS424-cyto*MDH3*-cytoMa*MAE* (Chapter 3)
MM6	pRS424-cytoYl*MDH2*-cytoMa*MAE* (Chapter 3)
TaFAR	pRS425-Ta*FAR* (20)
psXP	pRS416-Ps*XR*-Ps*XDH*-Ps*XDH* (30)

* At, *Arabidopsis thaliana*; Bs, *Bacillus subtilis*; Ca, *Clostridium acetobutylicum*; Cb, *Clostridium beijerinckii*; Cn, *Cupriavidus necator*; Ec, *Escherichia coli*; Gl, *Giardia lamblia*; Ps, *Pichia stiptis*; Se, *Salmonella enterica*; Td, *Treponema denticola*; Te, *Thermoanaerobacter ethanolicus*; Yl, *Yarrowia lipolytica*; Opt, codon optimized for expression in *S. cerevisiae*.

Table 4.4 Yeast strains used in this chapter.

Strains	Genotypes
CEN.PK2-1C	*MATa; ura3-52; trp1-289; leu2-3,112; his3Δ1; MAL2-8^C; SUC2*
BY4741	*MATa his3Δ1 leu2Δ0 met15Δ0 ura3Δ0*
ΔGGAA	CEN.PK2-1C *gpd1*Δ *gpd2*Δ *adh1*Δ *adh4*Δ
ΔCIT2	CEN.PK2-1C *cit2*Δ
ΔMLS1	CEN.PK2-1C *mls1*Δ
ΔGGAAC	ΔGGAA *cit2*Δ
ΔGGAAM	ΔGGAA *mls1*Δ
Pdc$^-$	CEN.PK2-1C *pdc1*Δ *pdc5*Δ *pdc6*Δ
E10	Pdc$^-$/MTH1T, evolved for better growth on glucose
iE11	Pdc$^-$/*MTH1*::*MTH1*T, evolved for better growth on glucose
L34	L2612-*ura3*::*URA3*-ps*XR*-ps*XDH*-ps*XKS* (21)
XF3	BY4741 *rpd3*Δ/*ACC1*+Ta*FAR*
XF3w	XF3 *trp1-289*

4.8 Figures

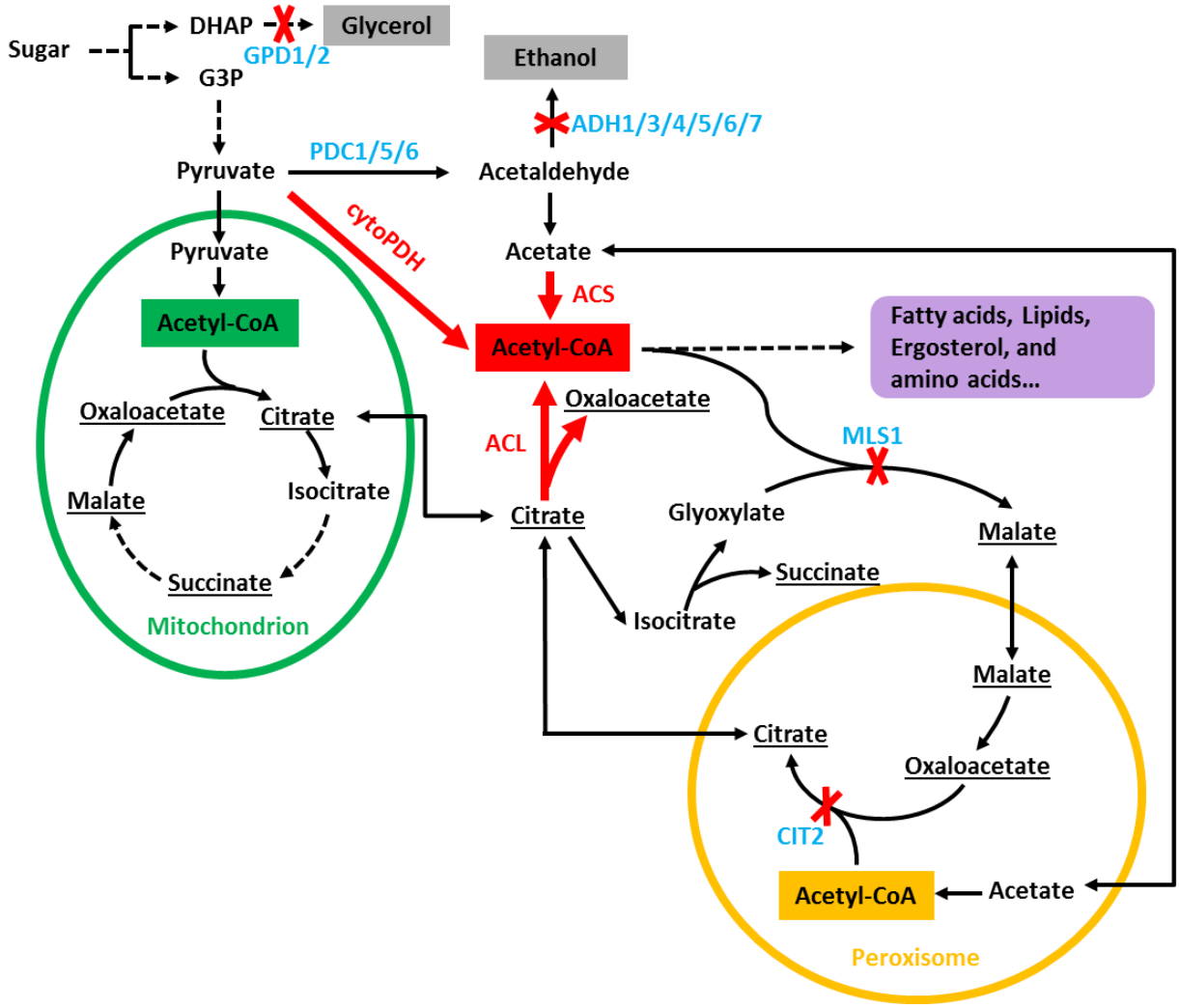

Figure 4.1 Overview of acetyl-CoA metabolism in *S. cerevisiae*, which happens in several compartments, including the mitochondria (green), peroxisomes (yellow), nucleus (not shown), and cytosol (red). Genes involved in the endogenous glycerol and ethanol pathways and the acetyl-CoA consuming glyoxylate shunt are shown in blue and chosen as the targets for deletion. The organic acids involved in the transport of acetyl-CoA in different compartments are underlined. The heterologous acetyl-CoA biosynthetic pathways tested in this study, including cytoPDH, ACS*, and ACL, are shown in red.

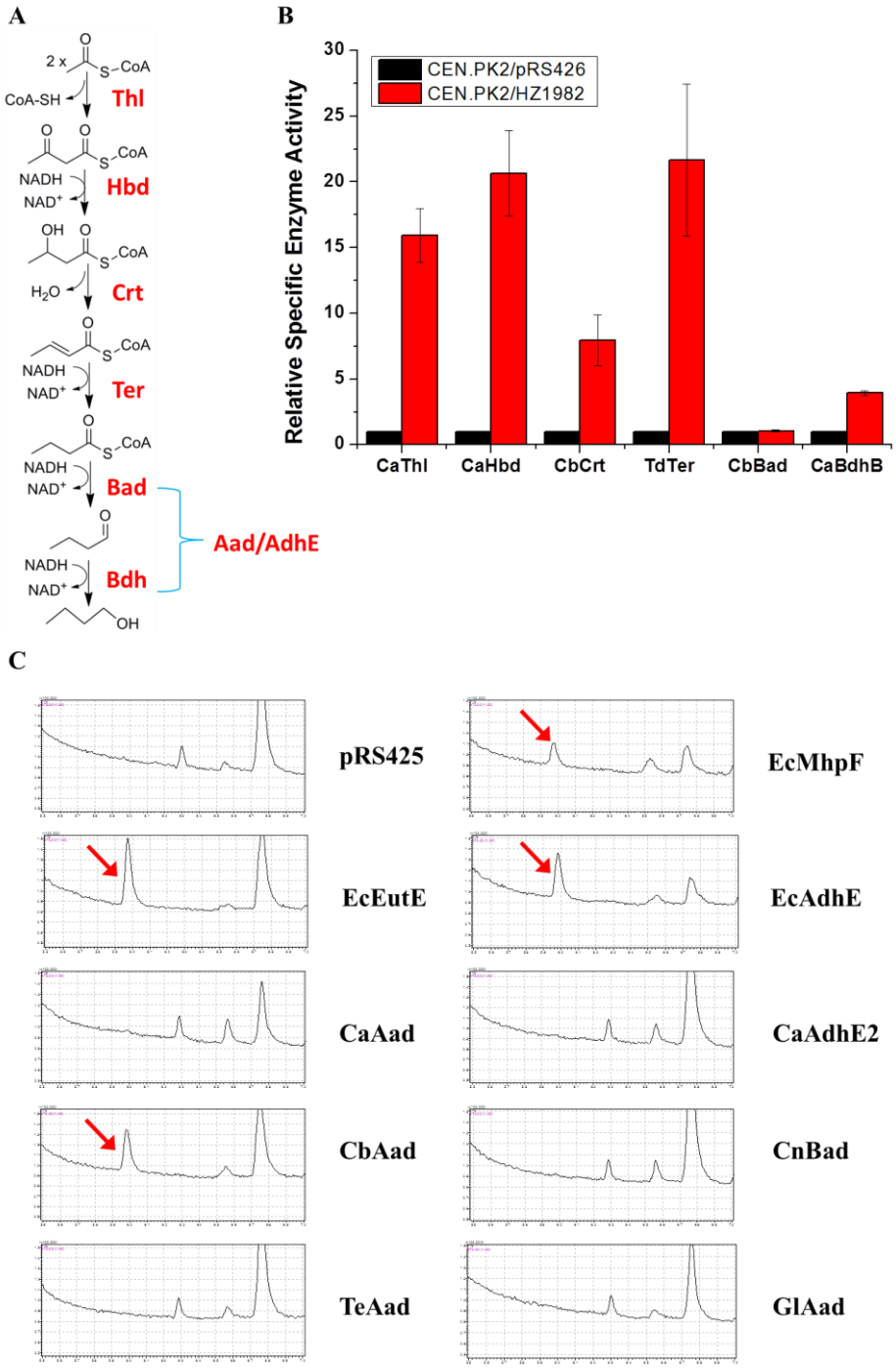

Figure 4.2 Construction of a CoA-dependent *n*-butanol pathway as the acetyl-CoA reporter. The Clostridia *n*-butanol biosynthetic pathway HZ1982 was constructed in our previous study (A) and the corresponding enzyme activity of each step in the pathway was determined by comparing with the control strain with an empty vector (B). The production of *n*-butanol by CEN.PK2/HZ1982 could be complementated by co-expressing a funtional Bad or AdhE/Aad (C). Candidate Bad or AdhE/Aad genes were cloned from various organisms, and transformed into ΔGGAA strain to test *n*-butanol production. Arrows indicated the peak for *n*-butanol.

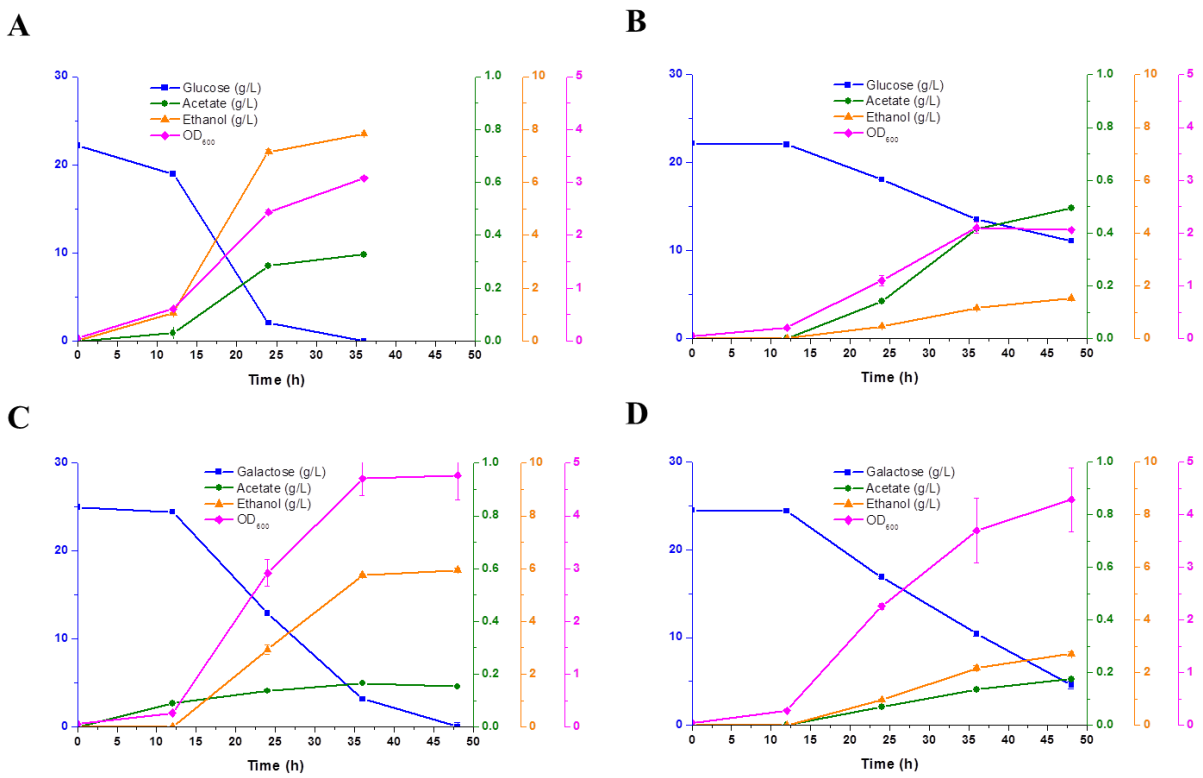

Figure 4.3 Fermentation performance of the wild-type (A and C) and the ΔGGAA (B and D) strains on glucose (A and B) and galactose (C and D) under oxygen-limited condition. The glucose consumption (blue), acetate production (green), ethanol formation (yellow), and cell growth (pink) were compared.

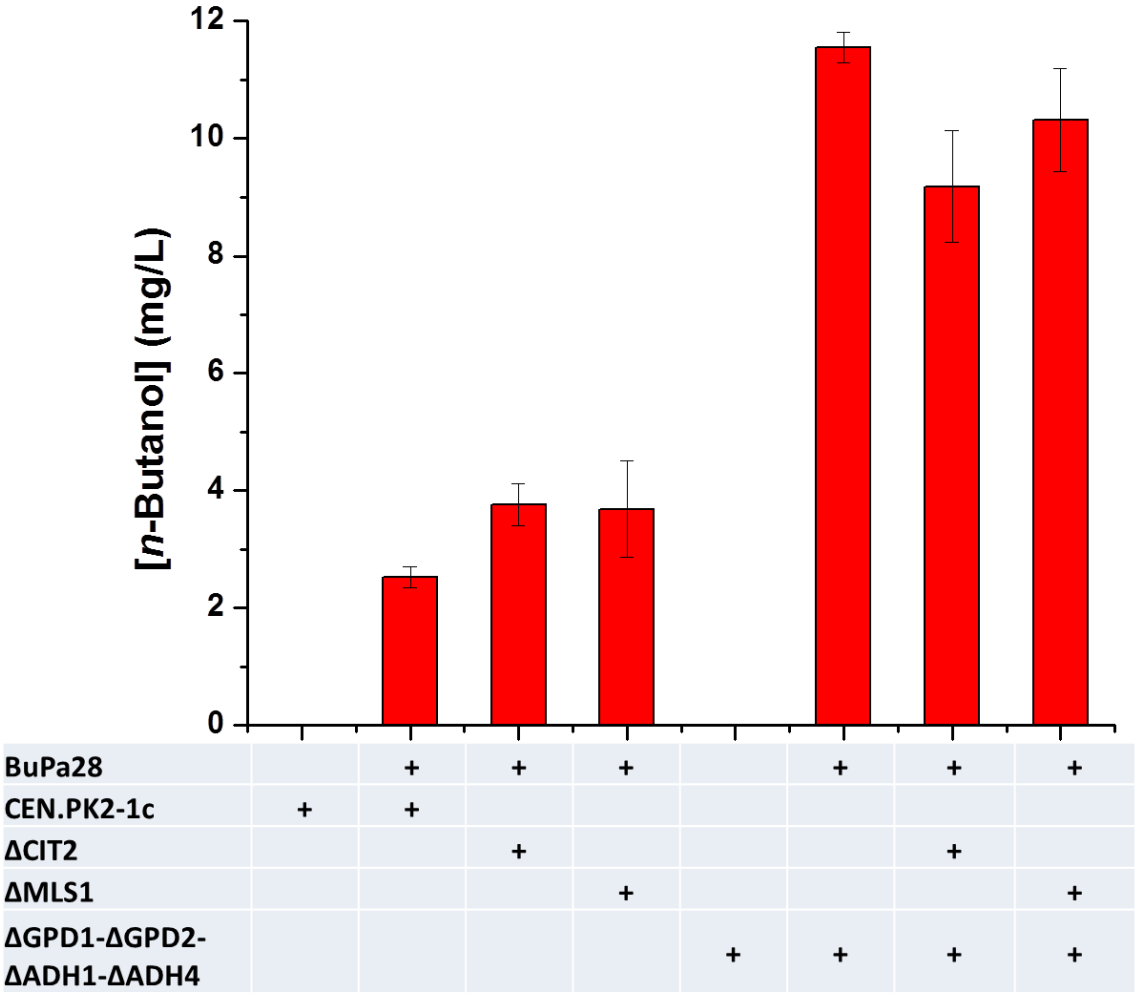

Figure 4.4 Host engineering to increase cytosolic acetyl-CoA levels in *S. cerevisiae*. GPD1 and GPD2 responsible for glycerol formation and ADH1 and ADH4 involved in ethanol production were inactivated to redirect the glycolytic flux to acetyl-CoA. *CIT2* and *MLS1* were deleted to disrupt the glyoxylate shunt contributing to the consumption of acetyl-CoA in the cytosol of yeast.

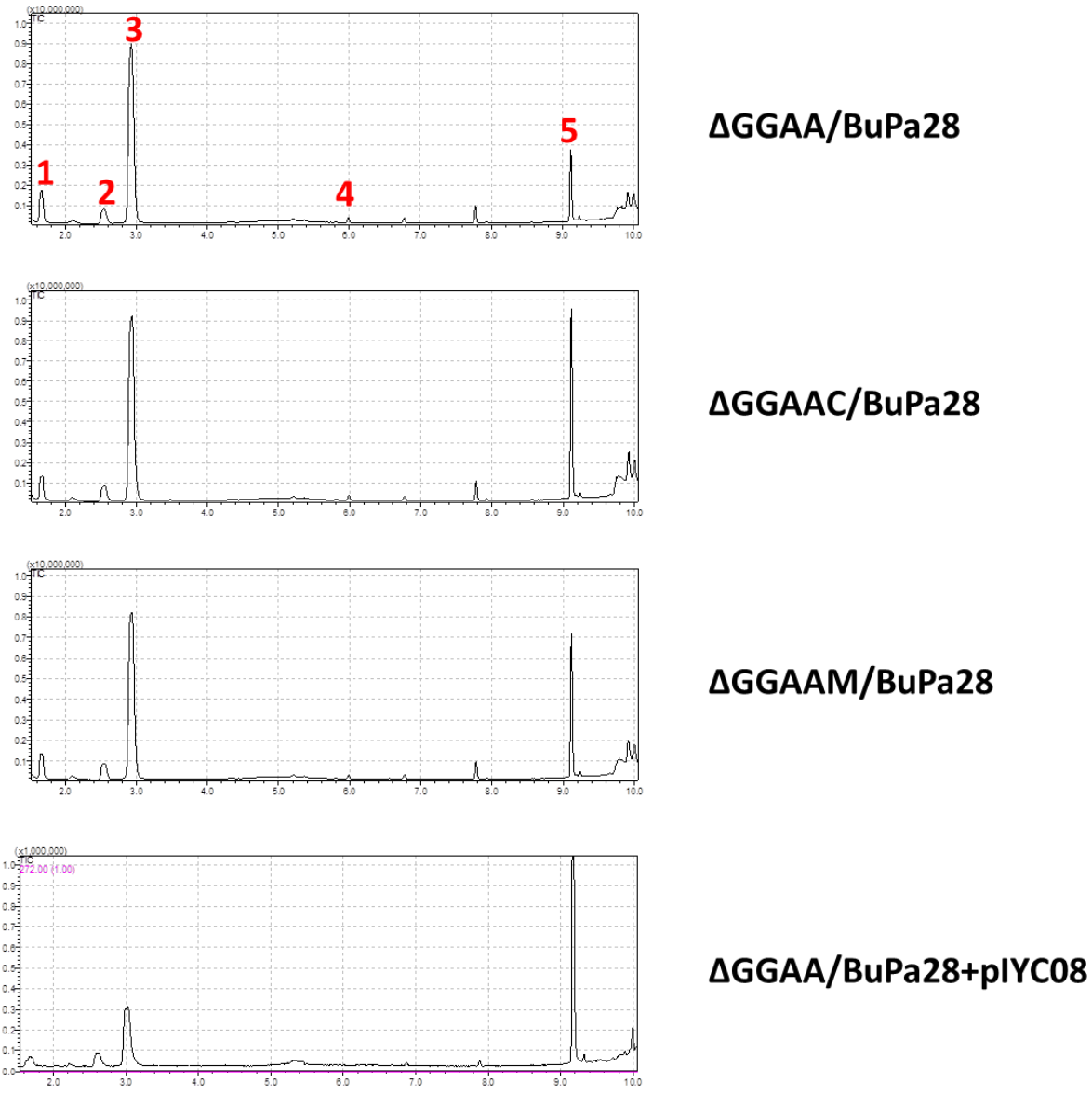

Figure 4.5 Fermentation profiles of the engineered yeast strains, analyzed by GC-MS. Peaks 1, 2, 3, 4, and 5 were acetaldehyde, methanol (internal standard), ethanol, *n*-butanol, and acetate, respectively.

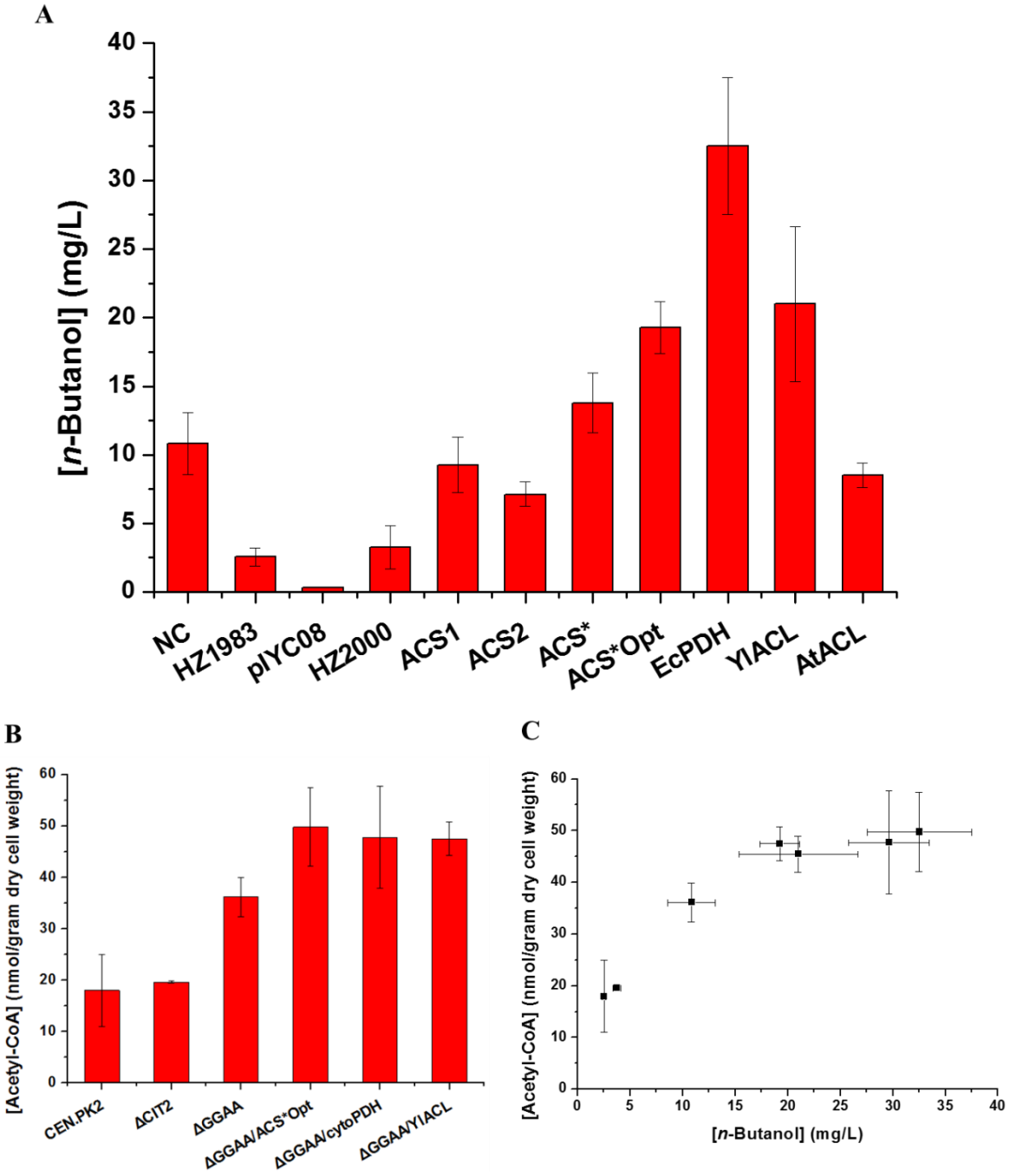

Figure 4.6 Enhancing acetyl-CoA levels via metabolic engineering, as demonstrated by increased *n*-butanol production (A) and increased acetyl-CoA concentration (B). Three series of complementary pathways, including the PDH-bypass, cytoPDH, and ACL, were introduced into the ΔGGAA *S. cerevisiae* strain to improve *n*-butanol production. The amount of *n*-butanol produced was plotted against the measured acetyl-CoA concentration.

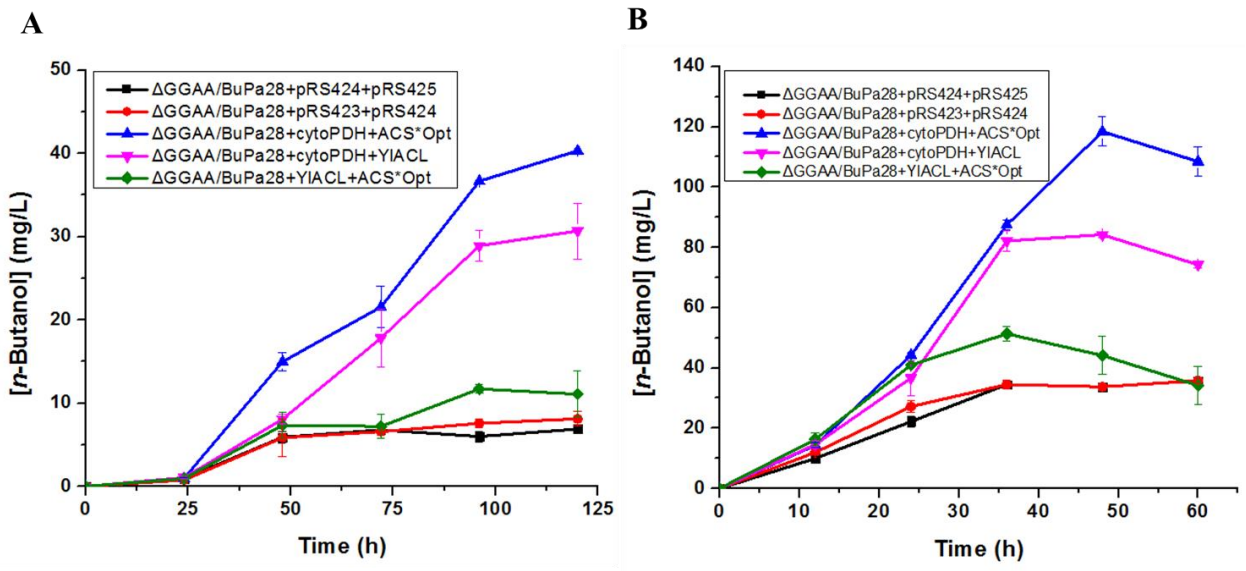

Figure 4.7 (A) Combination of the most effective and independent acetyl-CoA biosynthetic pathways for *n*-butanol production in the engineered yeast strains under oxygen-limited condition. (B) High cell density fermentation for *n*-butanol production with the combined acetyl-CoA pathways. The combination of EcPDH and ACS*Opt was found to be the most effective to boost acetyl-CoA levels in the engineered yeast strain.

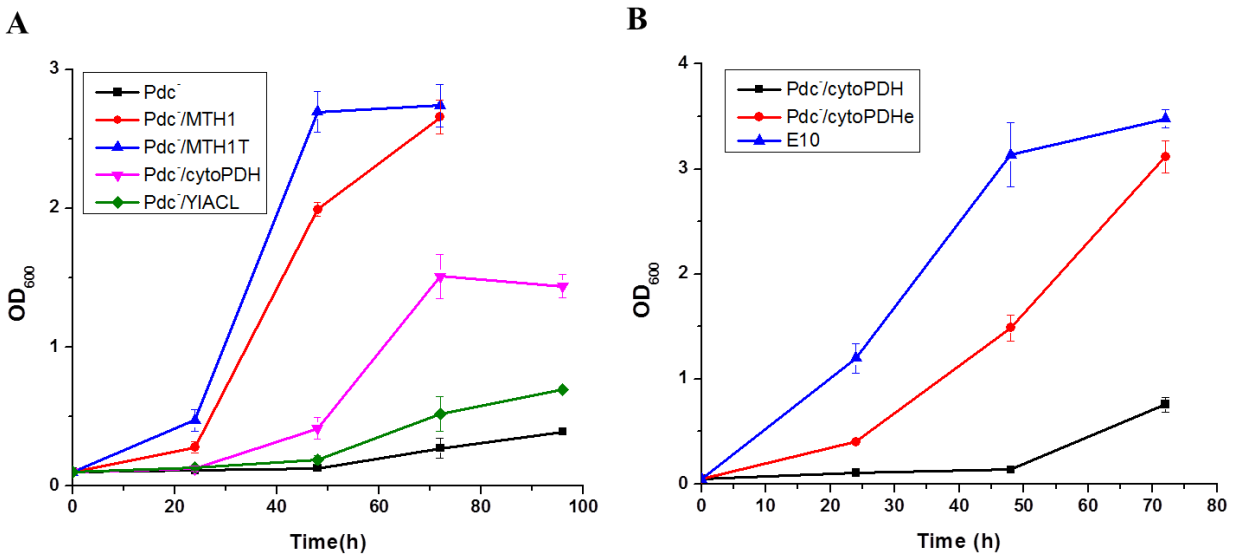

Figure 4.8 A) Restoring the growth of Pdc$^-$ strain on synthetic medium with low concentration glucose (5 g/L) as the sole carbon source via the introduction of alternative acetyl-CoA biosynthetic pathways. Pdc$^-$/MTH1 and Pdc$^-$/MTH1T constructed in Chapter 2 were included for comparison. B) Engineering better growth of strain Pdc$^-$/cytoPDH on glucose via adaptive evolution.

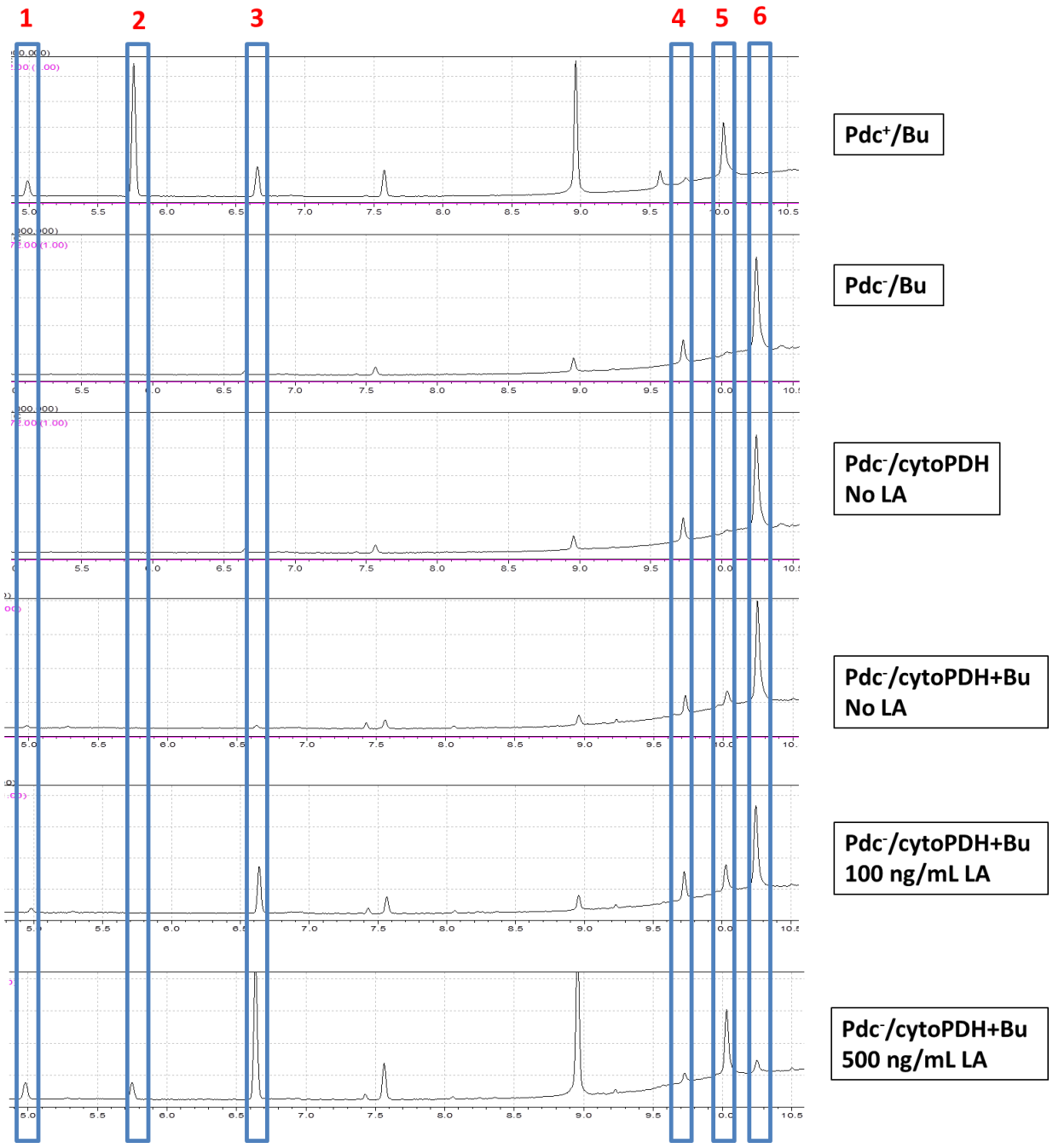

Figure 4.9 Redistribution of metabolic profiles in the evolved Pdc$^-$ yeast strain. Peaks 1, 2, 3, 4, 5, and 6 represented *iso*-butanol, *n*-butanol, *3*-methyl-1-butanol, *iso*-butyrate, *n*-butyrate, and *3*-methyl-1-butyrate, respectively.

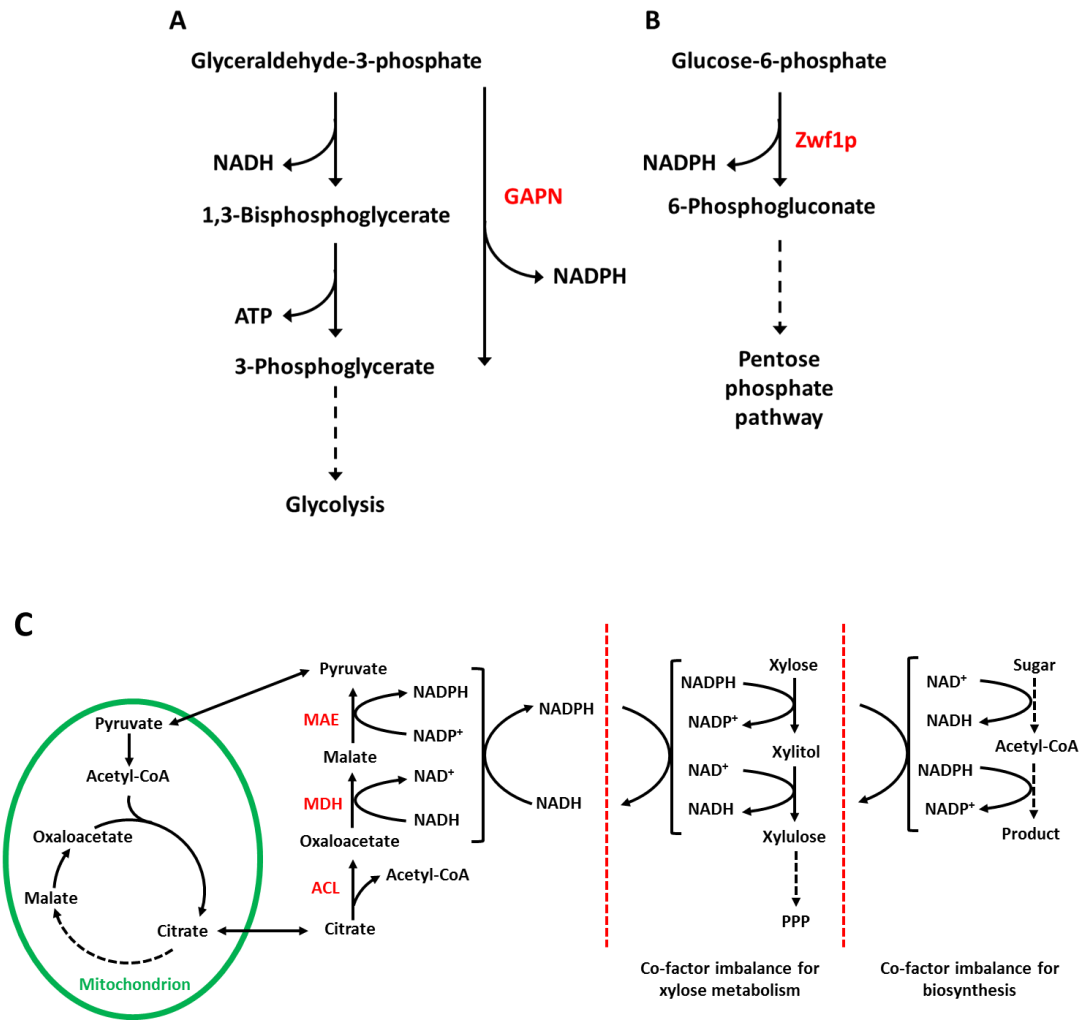

Figure 4.10 Strategies to enhance NADPH levels in *S. cerevisiae* investigated in this study. The first strategy (A) was to overexpress *gapN*, encoding a non-phosphorylating glyceraldehyde-3-phosphate (G-3-P) dehydrogenase. The second strategy (B) was to overexpress *ZWF1*, encoding an enzyme that control the entry point of oxidative pentose phosphate pathway. The third strategy was to use the ACL-MDH-MAE system, which showed (potential) metabolic engineering applications both anabolic and catabolic pathways.

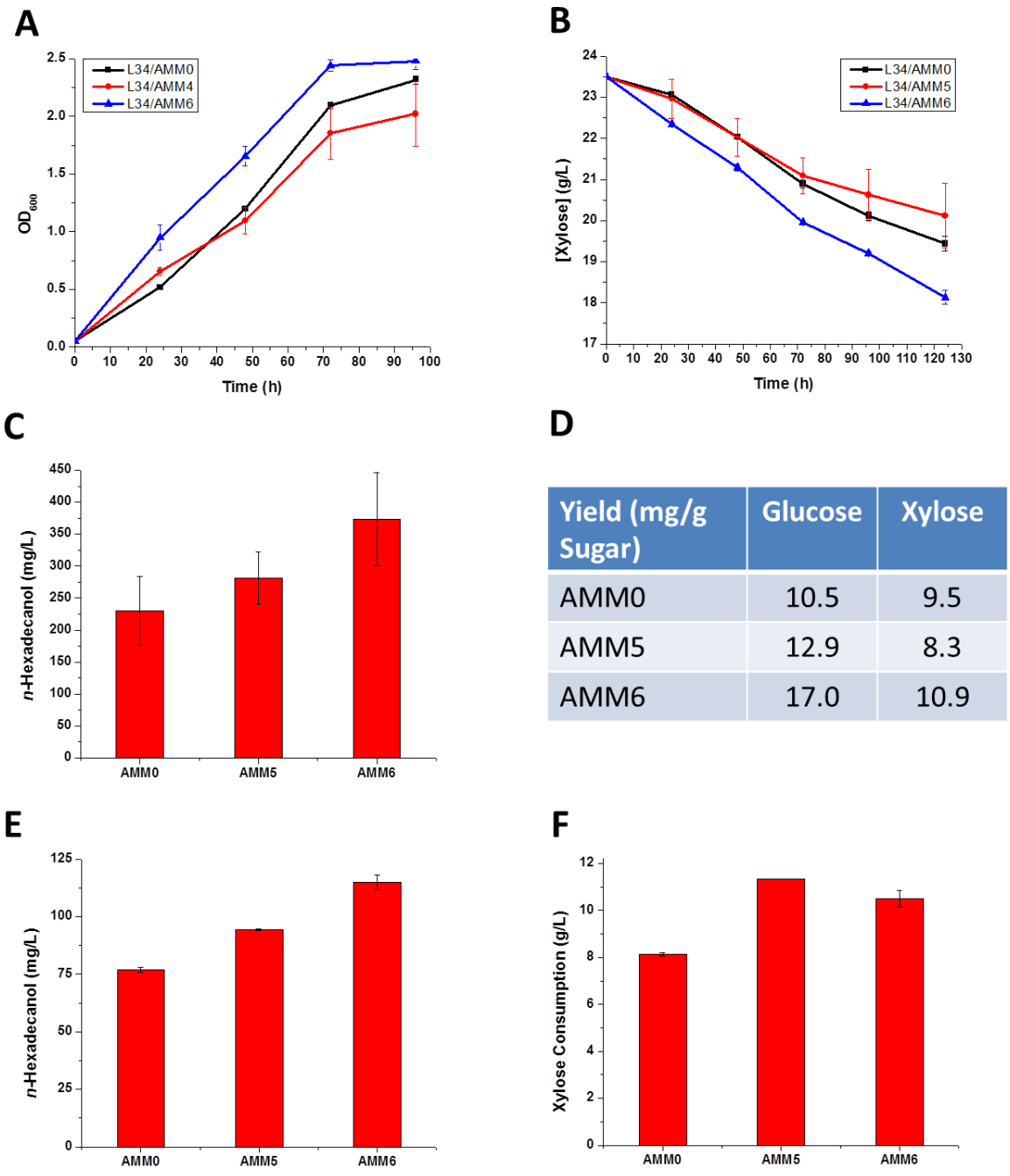

Yield (mg/g Sugar)	Glucose	Xylose
AMM0	10.5	9.5
AMM5	12.9	8.3
AMM6	17.0	10.9

Figure 4.11 Metabolic engineering applications of the ACL-MDH-MAE system for both catabolic (xylose utilization, A, B, and F) and anabolic pathways (fatty alcohol biosynthesis, C and E). Xylose-based fatty alcohol production (E and F) was carried out to investigate the relationship between catabolic and anabolic pathways, and the yield of fatty alcohol per sugar consumed was compared as well (D).

Chapter 5 Acyl-CoAs Pool Engineering via Functional Reversal of the β-Oxidation Cycle in *Saccharomyces cerevisiae*

5.1 Introduction

Biological conversion of plant-derived lignocellulosic materials into biofuels has been intensively investigated due to increasing concerns on energy security, sustainability and global climate change (1-3). Although commercial production of bioethanol has been achieved, ethanol has its intrinsic shortcomings such as low energy density, high corrosivity, and hydroscopicity. Thus, increasing effort has been devoted to produce advanced biofuels, such as *n*-butanol, long-chain alcohols, fatty acid ethyl esters (FAEEs or biodiesels), and alkanes, which have similar properties to current transportation fuels (4-6). Notably, most of the "drop-in" fuels are derived from fatty acids (fatty acyl-CoAs or fatty acyl-ACPs), which can be produced by the endogenous fatty acid biosynthetic pathways (FAB) (5). However, classic FAB suffers from high energy input and complicated regulation, which significantly hinders efficient and cost-effective production of advanced biofuels. Generally, FABs use malonyl-CoA which is activated from acetyl-CoA at the cost of ATP consumption as the starter unit, ACP as the acyl activation group, and NADPH as the reducing force (7-9). Interestingly, the fatty acid degradation pathway, i.e. so-called β-oxidation cycle, which happens in the opposite direction as that of FAB, proceeds in a much more efficient manner, as no ATP consuming reaction is involved and CoA and NADH are used as co-factors (10, 11).

To overcome the major limitation of FAB, a recent report demonstrated that the fatty acid degradation enzymes were functional in both degradative and synthetic directions and the *Escherichia coli* β-oxidation cycle could be functionally reversed to synthesize a series of

advanced fuels and chemicals, including short-, medium-, and long- chain alcohols and fatty acids (12, 13). Compared with the other engineering strategies, this novel platform has several advantages for advanced biofuel production, such as the high efficiency by avoiding the energy consuming and rate-limiting step to generate malonyl-CoA and the flexibility to produce alcohols and fatty acids with different carbon chain lengths. Although *E. coli* is currently the most popular host for metabolic engineering and synthetic biology studies, *Saccharomyces cerevisiae* has several advantages for industrial applications, such as the high tolerance to lignocellulose hydrolysate inhibitors and toxic products, the capability of high density fermentation, and the absence of phage contamination (1, 2). Although the reversal of β-oxidation for efficient fuel and chemical synthesis was firstly demonstrated in *E. coli* (12, 13), it might be extended to this eukaryotic system as well, owing to the ubiquitous nature of the β-oxidation process (10, 11). Therefore, we aimed to develop a new platform, based on the reversed β-oxidation pathway, to synthesize a wide variety of fuels and chemicals efficiently and cost-effectively in *S. cerevisiae*, including but not limited to fatty acids, fatty alcohols, FAEEs, alkanes, and even waxes (Figure 5.1).

Although the biochemistry is rather similar, the β-oxidation process in eukaryotes is more complicated than that in prokaryotes, mainly due to the compartmentalization of cellular metabolisms. Generally, eukaryotic β-oxidation of fatty acids happens in peroxisomes and/or mitochondria (14). In *S. cerevisiae*, peroxisomes are the only cellular compartment responsible for the complete degradation of medium- and long- chain fatty acids (10, 11). Due to the dependence on fatty acids for optimal activities and the lack of precursors and cofactors for biosynthesis, peroxisomes may be not a good location to reverse the β-oxidation cycle. Thus, we chose to construct the reversed β-oxidation pathway in the cytosol. To identify functional

pathway enzymes, a number of β-oxidation enzymes were cloned from various species and expressed in the cytosol of *S. cerevisiae*. As proof of concept, *n*-butanol was chosen as a reporter molecule because its synthesis requires the reversal of only one β-oxidation cycle. The ability to reverse the β-oxidation cycle for multiple times was then demonstrated by the synthesis of medium-chain fatty acids (MCFAs) and medium-chain fatty acid ethyl esters (MCFAEEs) in *S. cerevisiae*. To the best of our knowledge, this is the first report on the reversal of the β-oxidation cycle in a eukaryote. Note that most contents of this chapter are adapted from one of my research articles published in *ACS Synthetic Biology* (15).

5.2 Results

5.2.1 Cloning of Functional β-Oxidation Enzymes Expressed in the Cytosol of S. cerevisiae

To construct a reversed β-oxidation cycle in *S. cerevisiae*, a number of genes encoding the β-oxidation pathway from various species were cloned. The corresponding enzymes included: 1) *E. coli* and yeast β-oxidation enzymes (10, 11, 16, 17); 2) proteins sharing high homology with the *E. coli* reversed β-oxidation pathway enzymes (12); 3) putative enzymes that are predicted to have the desired functions or similar activities. Gene cloning and pathway assembly were performed using the helper plasmids (pH11, pH22, pH3, pH4, pH5, and pH6) constructed in Chapter 3, with the whole promoter or terminator as the homology arm between two adjacent cassettes.

Due to the availability of the commercial CoA substrates, enzyme activity assays were performed using C_4-CoAs, including acetoacetyl-CoA, β-hydroxybutyryl-CoA, and crotonoyl-CoA (*trans*-2-butenoyl-CoA). Considering the broad specificity of the β-oxidation enzymes, the enzyme assays using C_4-CoAs should be sufficient to represent the β-oxidation activities (18).

Since β-oxidation enzymes were localized either in the mitochondria and/or the peroxisomes in eukaryotes, the targeting sequences were predicted using the on-line tools (MITOPROT (19) for the mitochondrial targeting sequences and PeroxisomeDB 2.0 (20) for the peroxisomal targeting sequences) and removed in order to express the proteins in the cytosol of *S. cerevisiae*.

5.2.1.1 β-Ketoacyl-CoA synthase (KS)

The β-ketoacyl-CoA synthase (KS) activity was carried out in the thiolysis direction using acetoacetyl-CoA as the substrate. Several KS candidate genes were cloned from both *S. cerevisiae* and *E. coli* (Table 5.1). The thiolase from *Clostridium acetobutylicum* (CaThl), which is involved in the fermentative production of *n*-butanol (21), was used as the positive control. Both acetyl-transferase (Erg10p, EcAtoB and EcYqeF) and acyl-transferase (cytoFox3p and EcFadA) were included for analysis, which showed short-chain specificity (22) and broad specificity (17), respectively. As shown in Figure 5.2A, Erg10p showed the highest activity towards acetoacetyl-CoA among all enzymes tested, which was consistent with a previous report that Erg10p was optimal for *n*-butanol production in yeast (23). Unfortunately, none of the enzymes cloned from *E. coli* was functional. By removing the peroxisomal targeting sequences, Fox3p was relocalized to the cytosol and functionally expressed. Although the activity of cytoFox3p was lower than that of Erg10p, this β-oxidation enzyme was expected to exhibit broad specificity towards different chain length substrates (10, 11). Therefore, cyto*FOX3* was chosen to construct the reversed β-oxidation pathways.

5.2.1.2 β-Ketoacyl-CoA reductase (KR) and β-hydroxyacyl-CoA dehydratase (HTD)

The second and third steps of β-oxidation were carried out by a multi-functional enzyme, FadB in *E. coli* (16) and Fox2p in *S. cerevisiae* (17). Unfortunately, neither of them could be

functionally expressed in the cytosol of *S. cerevisiae* (Figure 5.2B). Therefore, more *FOX2* homologs were identified by BLAST search and cloned (Table 5.1). Unfortunately, although more than 20 candidate enzymes from different species were tested, none was found to possess either KR or HTD activities, towards acetoacetyl-CoA and crotonoyl-CoA, respectively. The difference of the protein folding environments between cytosol and peroxisomes might prevent all the *FOX2* homologs from being functionally expressed in the cytosol of *S. cerevisiae*. Different from *S. cerevisiae*, some oleaginous yeasts were found to have another set of β-oxidation system in the mitochondria in addition to the classic system in the peroxisomes (24). Therefore, the mitochondrial β-oxidation enzymes were cloned from *Yarrowia lipolytica*. The β-hydroxybutyryl-CoA dehydrogenase from *C. acetobutylium* (CaHbd) and crotonase from *C. beijerinckii* (CbCrt) (21, 25) were included as positive controls. There are two separate enzymes in the mitochondrial β-oxidation system to possess KR and HTD activities, encoded by *YALI0C08811* and *YALI0B10406*, respectively (24). This is different from the peroxisomal system, in which a multifunctional enzyme can catalyze the second and third steps of β-oxidation. As shown in Figure 5.2C, both of the mitochondrial β-oxidation enzymes could be functionally expressed in the cytosol of yeast, which showed comparable enzymatic activities with the clostridial equivalents. Thus, these two enzymes were chosen to construct the reversed β-oxidation pathways.

5.2.1.3 *Trans*-2-enoyl-CoA reductase (TER)

The first step of β-oxidation is the only irreversible step and carried out by fatty acid oxidase with the involvement of an oxygen molecule (10, 11). Instead, *trans*-2-enoyl-CoA reductases (TERs), which are involved in fatty acid biosynthesis (FAB) and only catalyze the reaction in the reduction direction, were included as the last step of the reversed β-oxidation

pathways. Several TERs, such as those from *Euglena gracilis* (EgTer) and *Treponema denticola* (TdTer), have been characterized (26-28) and determined to significantly improve the production of *n*-butanol (29, 30) and short-chain fatty acids (13) in *E. coli*. Therefore, TERs from *E. coli*, *S. cerevisiae*, *E. gracilis* and *T. denticola* and some homologs that shared high homology were cloned (Table 5.1). As shown in Figure 5.2D, several candidates involved in the biosynthesis of fatty acids, such as the endogenous Etr1p (cytoEtr1p), FabI from *E. coli* (EcFabI), TER from *E. gracilis* (EgTer), and TER from *T. denticola* (TdTer), were determined to possess the TER activity. Consistent with the previous work (26, 27), TdTer was found to have the highest activity when crotonoyl-CoA was used as the substrate. Therefore, cyto*ETR1* and Td*Ter* were chosen to construct the reversed β-oxidation pathways.

5.2.2 n-*Butanol Biosynthesis as Proof-of-concept*

After intensive cloning and screening by enzyme activity assays, several candidates were found to be functionally expressed in the cytosol of yeast with the desired activities, with at least one functional enzyme in each step of the β-oxidation cycle. Therefore, using the DNA assembler method (31, 32), a reversed β-oxidation pathway could be readily constructed. As a proof of concept, *n*-butanol biosynthesis that requires only one cycle reversal of β-oxidation was selected. Reversed β-oxidation pathways were constructed using *ERG10*/cyto*FOX3*-cytoYl*KR*-cytoYl*HTD*-Td*Ter*/cyto*ETR1*, based on the enzyme activity assay results. To synthesize *n*-butanol from butyryl-CoA, the CoA-acylating aldehyde dehydrogenase from *E. coli* (Ec*EutE*) (33, 34) and butanol dehydrogenase from *C. acetobutylium* (Ca*BdhB*) (21) were included in the reversed β-oxidation pathways. As shown in Figure 5.3, *n*-butanol, although at a very low titer, could be detected using the strains containing the reversed β-oxidation pathways, including rP31, rP32, rP34, and rP35. Currently, rP34 produced the highest amount of *n*-butanol, with a titer as

high as 20 mg/L in the wild-type yeast strain. Although the titer of *n*-butanol was still rather low compared with that in clostridia (25) and *E. coli* (12, 29, 30), it was approximately 10 fold higher than previous reports using the clostridial *n*-butanol fermentative pathway in yeast (23, 35), highlighting the high efficiency of the reversed β-oxidation pathways.

The assembled pathways containing functional β-oxidation enzymes could produce a small amount of *n*-butanol, indicating the successful reversal of the β-oxidation cycle. To ensure that the detected *n*-butanol was produced via the reversed β-oxidation pathway, pathway deletion and complementation were carried out (Figure 5.3). No *n*-butanol production was observed if cytoYl*KR* was replaced with *eGFP* (rP37 and rP38). Co-expression of cytoYl*KR* together with the "incomplete pathways" (rP37c and rP38c) could complement the production of *n*-butanol. In other words, the production of *n*-butanol was dependent on the presence of a functional reversed β-oxidation pathway in yeast.

5.2.3 Medium-chain Fatty Acids (MCFAs) Production

To show the reversal of more than one β-oxidation cycle, the production of alcohols with longer carbon chains, such as *n*-hexanol and *n*-octanol, should be achieved. Unfortunately, the CoA acylating aldehyde dehydrogenases or acyl-CoA reductases, which could reduce acyl-CoAs to the corresponding aldehydes, with the desired specificities were not available. On the contrary, thioesterases (TEs), catalyzing the release of free fatty acids from fatty acyl-CoAs, were well characterized and showed broad diversity, ranging from long-chain (C_{14}-C_{18}) and medium-chain (C_8-C_{12}) to short-chain (C_4-C_6) specificity.(36) In the present work, Cp*FatB1*, encoding a plant thioesterase with medium-chain specificity (37), was included in the reversed β-oxidation pathway. Using a modified protocol, all short- and medium- chain fatty acids could be readily

separated and detected by GC-MS (Figure 5.4B). In the control strain expressing the thioesterase (Cp*FatB1*) with a nonfunctional reversed β-oxidation pathway (rP38), only tiny amount of hexanoic acid (C_6) and octanoic acid (C_8) were detected (Figures 5.4C and 5.6A). The introduction of a functional reversed β-oxidation pathway (rP35) resulted in 6.1-fold improvement of octanoic acid production, with hexanoic acid production increased slightly as well (Figures 5.4D and 5.6A). Since acetyl-CoA served as both the starter and extender units for the reversed β-oxidation pathway, the same plasmids (rP35 and CpFatB1) were introduced into an acetyl-CoA overproducing host (ΔGGAA/ACS*) constructed in Chapter 4. The cellular acetyl-CoA level was increased by simultaneous disruption of the competing pathways (*GPD1* and *GPD2* for glycerol biosynthesis and *ADH1* and *ADH4* for ethanol formation) and overexpression of a feedback inhibition insensitive acetyl-CoA synthetase mutant from *Salmonella enterica* (Se*Acs*^{L641P}). In this acetyl-CoA overproducing strain, additional 3.2-fold in octanoic acid production was achieved (Figures 5.4E and 5.6A). In addition, the enhanced acetyl-CoA supply led to the production of decanoic acid (C_{10}), whose concentration was too low to be detected in the wild-type yeast strain (Figures 5.4 and 5.6A). On the other hand, these results indicated that acetyl-CoA was the rate-limiting factor for the efficiency of the reversed β-oxidation pathway.

The ability of the reversed β-oxidation pathway to accept odd-chain acyl-CoAs as substrates was demonstrated by supplementing propanoic acid to the medium. In *S. cerevisiae*, ACSs, encoded by *ACS1* and *ACS2*, contributed to the activation of propanoate to form propionyl-CoA,(38) which might be incorporated into the reversed β-oxidation cycle as well. As shown in Figure 5.4F, besides octanoic acid and decanoic acid, nonanoic acid (C_9) was also detected with propanoic acid supplementation. Interestingly, the production of heptanoic aicd (C_7)

was nearly un-detectable, probably due to the substrate specificity of the thioesterase used. Our current work demonstrated that the β-oxidation cycle was reversed at least 4 times to synthesize decanoyl-CoA and the reversed pathway could accept both even- and odd- chain substrates for carbon chain initiation and elongation.

5.2.4 Increased Production of Medium-chain Fatty Acid Ethyl Esters (MCFAEEs)

During sugar fermentation, *S. cerevisiae* produces a broad range of aroma-active substances, including ethyl octanoate and ethyl decanoate. The formation of MCFAEEs is catalyzed by acyl-CoA:ethanol *O*-acyltransferases, encoded by *EEB1* and *EHT1* (39, 40). Previous work indicated that the supply of MCFAs precursors was the rate-limiting factor for MCFAEEs biosynthesis (39, 40). Thus, it was assumed that the production of MCFAEEs would be increased if the β-oxidation cycle could be functionally reversed to provide more acyl-CoAs precursors. As expected, increased production of ethyl octanoate and ethyl decanoate was observed in the strain with a functional reversed β-oxidation pathway. The detection and quantification of ethyl octanoate and ethyl decanoate were achieved by GC-MS. As shown in Figure 5.5, the production of ethyl octanoate and ethyl decanoate was increased by 2.8- and 2.1-fold, respectively. Interestingly, although co-expressing *EEB1* or *EHT1* with the reversed β-oxidation pathway did not further increase the production of MCFAEEs (Figure 5.6B), the ratio of ethyl octanoate and ethyl decanoate was changed from 2:1 to around 1:1. These results might be caused by the dual functions of Eeb1p and Eht1p, with both acyltransferase (FAEE synthesis) and esterase activity (FAEE hydrolysis) (40). In addition, Eeb1p and Eht1p showed higher esterase activity towards octanoate ester than decanoate ester (40), whose overexpression might result in the hydrolysis of ethyl octanoate at a higher rate than that of ethyl decanoate. The production of FAEEs with alkyl chains longer than 10 was not detected under all conditions,

probably due to the specificity of the acyltransferases in *S. cerevisiae* (Eeb1p, Eht1p, and other unknown ones). These results also demonstrated that the β-oxidation cycle was reversed by at least 4 turns.

5.3 Discussions

The reversal of β-oxidation was confirmed by the production of *n*-butanol, MCFAs, and MCFAEEs in *S. cerevisiae*. The yeast β-oxidation enzymes show broad specificity towards short-, medium-, and long- chain substrates (10, 11), which represents a promising versatile platform for synthesis of a wide variety of fuel and chemical molecules with different chain lengths. Meanwhile, we also encountered the challenges to control the chain lengths of the final products. Currently, the chain lengths of the products were mainly controlled by the specificity of the terminal enzymes, such as the thioesterases and acyltransferases. Future work will be focused on protein engineering strategies to design the terminal enzymes with the desired product specificity (41).

The present study demonstrated that the β-oxidation cycle could be reversed by 4 times to synthesize decanoyl-CoA derived molecules, such as decanoic acid and ethyl decanoate. FAEEs with alkyl chain longer than 10 were not detected and no significant difference in the production of dodecanoic acid (C_{12}), tetradecanoic acid (C_{14}), and hexadecanoic acid (C_{16}) was observed between the strains with or without the reversed β-oxidation pathway (data not shown). These findings could result from the substrate specificities of the terminal enzymes used in this study and/or the efficiency of the β-oxidation cycle to be reversed by more than 4 times. The CoA acylating aldehyde dehydrogenase (EcEutE) showed short-chain specificity and only ethanol and *n*-butanol could be synthesized. The thioesterase (CpFatB1) showed medium-chain specificity and C_6-C_{10} fatty acids could be produced. There are no acyltransferases in *S. cerevisiae* that were

reported to be active towards the acyl chains longer than 10. In previous work, both system-level engineering approach and synthetic biology approach were applied to construct the functionally reversed β-oxidation pathways in *E. coli*. In the system-level engineering approach, several global transcriptional regulators were manipulated to enable the constitutive expression of all β-oxidation enzymes under anaerobic conditions with the absence of fatty acids and presence of glucose. The resultant strain could fully reverse the β-oxidation cycle to produce C_{16} and C_{18} fatty acids at a titer higher than 6 g/L (12). In the synthetic biology approach, all the structural genes of the β-oxidation cycle were overexpressed, without any manipulation on the transcriptional factors. Interestingly, overexpression of the structural genes only enabled the reversal of the β-oxidation cycle up to 5 turns to produce dodecanoic acid (C_{12}), whose titer was lower than 5 mg/L (13). The decreased number of reversed turns and the dramatically decreased titer for long-chain products indicated some limitations using the synthetic biology approach. Since the synthetic biology approach was used in the present study, we might encounter the same problems as the *E. coli* system. Alternatively, a similar system-level engineering approach can be applied to this eukaryotic system by manipulating the equivalent global regulators.

The high efficiency of the reversed β-oxidation pathway was characterized by its energetic benefits of the malonyl-CoA independence and the use of CoA and NADH instead of ACP and NADPH as cofactors (12). However, compared with the high efficiency of the reversed β-oxidation pathway in *E. coli*, this system seemed to not work well in yeast, as shown by the relatively low *n*-butanol and fatty acid productivity. One explanation for this observation is the difference in acetyl-CoA biosynthesis. In *E. coli*, acetyl-CoA is steadily synthesized from pyruvate by either pyruvate dehydrogenase (PDH) under aerobic conditions (42) and pyruvate-formate lyase (PFL) under anaerobic conditions (43). While in *S. cerevisiae*, acetyl-CoA is

mainly generated in the mitochondria, and the reversed β-oxidation pathway enzymes are localized in the cytosol. *S. cerevisiae* lacks the machinery to export the mitochondrial acetyl-CoA to the cytosol (44), making the situation even worse. Thus, due to the compartmentalization of acetyl-CoA metabolism, there is not enough driving force for the reversed β-oxidation pathway. In the cytosol of *S. cerevisiae*, acetyl-CoA is generated via the PDH-bypass pathway, from pyruvate to acetaldehyde and then to acetate, which is activated to acetyl-CoA by ACS at the cost of two ATP molecules (45). The activation of acetate is rate-limiting, due to the low activity of ACS and high energy input requirement. Several metabolic engineering strategies have been carried out to boost the availability of acetyl-CoA in yeast, such as the use of an ACS mutant with higher activity (35, 46-48) and the introduction of heterologous acetyl-CoA biosynthetic pathways with less energy input (49, 50). Notably, these strategies have been applied to improve the production of isoprenoids (46, 47), polyhydroxybutyrate (48, 49), *n*-butanol (35), and fatty acids (50) in *S. cerevisiae*. In the acetyl-CoA overproducing host, the production of octanoic acid was increased by 3.2-fold and the synthesis of decanoic acid was detected, indicating that the cellular acetyl-CoA level was indeed the rate-limiting factor of the reversed β-oxidation pathway. Therefore, the construction of an acetyl-CoA overproducing yeast may significantly enhance the efficiency of the reversed β-oxidation pathway for advanced biofuel production, not only increasing the titer but also diversifying the chain lengths of the final products. Considering the compartmentalization of acetyl-CoA metabolism, an alternative strategy is to relocate the reversed β-oxidation pathway to the same compartment as the precursor metabolite. By fusion with mitochondrial targeting sequences at N-termini, the engineered enzymes can be imported to the mitochondria (51, 52). Since the major β-oxidation

enzymes used in the present study originated from the mitochondria of *Y. lipolytica*, they should be functional in the mitochondria of *S. cerevisiae*.

5.4 Conclusions

To construct a functional reversed β-oxidation pathway, approximately 40 enzyme homologs were cloned from various species and at least one functional enzyme was obtained for each catalytic step. The production of *n*-butanol, MCFAs, and MCFAEEs indicated that the β-oxidation cycle was functionally reversed. More work should be done to further increase the intracellular acetyl-CoA level to push the β-oxidation cycle to be reversed more efficiently.

5.5 Methods

5.5.1 Strains, media, and cultivation conditions

E. coli strain DH5α was used to maintain and amplify plasmids. *S. cerevisiae* CEN.PK2-1C (*MATa ura3-52 trp1-289 leu2-3,112 his3Δ1 MAL2-8^C SUC2*, EUROSCARF) was used as the host for gene cloning and *n*-butanol, MCFAs, and MCFAEEs fermentation. Yeast strains were cultivated in complex medium consisting of 2% peptone and 1% yeast extract supplemented with 2% glucose (YPD). Recombinant strains were grown on synthetic complete medium consisting of 0.17% yeast nitrogen base, 0.5% ammonium sulfate, and 0.07% amino acid drop out mix without leucine and/or uracil (MP Biomedicals, Solon, OH), supplemented with 2% glucose (SCD-LEU, SCD-URA, OR SCD-LEU-URA). *E. coli* strains were cultured at 37ºC in Luria-Bertani broth containing 100 μg/mL ampicillin. *S. cerevisiae* strains were cultured at 30ºC and 250 rpm for aerobic growth, and 30ºC and 100 rpm in un-baffled shaker flasks for oxygen limited fermentation. All restriction enzymes, Q5 High Fidelity DNA polymerase, and the *E. coli* - *S. cerevisiae* shuttle vectors, including pRS425 and pRS426, were purchased from New

England Biolabs (Ipswich, MA). All chemicals were purchased from either Sigma-Aldrich (St. Louis, MO) or Fisher Scientific (Pittsburgh, PA).

5.5.2 DNA manipulation

The yeast homologous recombination based DNA assembler method (31, 32) was used to construct the helper plasmids, clone candidate genes and assemble the reversed β-oxidation pathways (Table 5.1). Briefly, polymerase chain reaction (PCR) was used to generate DNA fragments with homology arms at both ends, which were purified with a QIAquick Gel Extraction Kit (Qiagen, Valencia, CA) and co-transformed along with the linearized backbone into *S. cerevisiae*. All genetic elements including promoters, coding sequences, and terminators were PCR-amplified from their corresponding genomic DNAs. Wizard Genomic DNA Purification Kit (Promega, Madison, WI) was used to extract the genomic DNAs from both *E. coli* and various yeast species, according to the manufacturer's protocol. The sequence encoding the medium-chain thioesterase from *Cuphea palustris* (Cp*FatB1*) was synthesized by two gBlock fragments and cloned into pH5 via the DNA assembler method. To confirm the correct clones, yeast plasmids were isolated using a Zymoprep Yeast Plasmid Miniprep II Kit (Zymo Research, Irvine, CA) and re-transformed into *E. coli* DH5α competent cells. Plasmids were isolated using a QIAprep Spin Miniprep Kit (Qiagen) and confirmed by DNA sequencing. Yeast strains were transformed using the LiAc/SS carrier DNA/PEG (53) method, and transformants were selected on either SCD-LEU, SCD-URA, or SCD-LEU-URA plates.

5.5.3 Enzyme activity assays

To measure the activity of enzymes expressed in yeast, a single colony was inoculated into 5 mL SCD-LEU medium, and cultured under aerobic conditions for about 36 h. Then cells

were collected by centrifugation at 4,000 *g* for 5 min at 4°C, washed twice with pre-chilled water, and resuspended in 250 μL Yeast Protein Extraction Reagent (YPER). After incubation at 25°C with 700 rpm shaking in a thermomixer for 20 minutes, the supernatant containing all soluble proteins were separated by centrifugation at 14,000*g* for 10 min at 4°C and ready for enzyme activity assays. All the assays were performed in 96-well microplates at 30°C and the spectrophotometric changes were monitored using the Biotek Synergy 2 Multi-Mode Microplate Reader (Winooski, VT). The reaction was initiated by the addition of 10-20 μL cell extract, to a total volume of 200 μL. Enzyme activity was calculated using the initial reaction rate and normalized to the total protein concentration determined by the Bradford assay.

The KS activity was measured by monitoring the disappearance of acetoacetyl-CoA, corresponding to the thiolysis direction of the enzymatic reaction, which was monitored by the decrease in absorbance at 303 nm. The reaction mixture contained 100 mM Tris-HCl (pH 8.0), 10 mM $MgSO_4$, 200 μM acetoacetyl-CoA, and 200 μM free CoA.

The KR activity was measured by monitoring the decrease of absorption at 340 nm, corresponding to the consumption of NADH in the reducing direction of the reaction. The reaction mixture contained 100 mM potassium phosphate buffer (pH 7.3), 200 μM NADH, and 200 μM acetoacetyl-CoA.

The HTD activity was measured by the decrease of absorption at 263nm, corresponding to the disruption of the carbon-carbon double bond of crotonoyl-CoA. The assay mixture contained 100 mM Tris-HCl (pH 7.6) and 100 μM crotonoyl-CoA.

The TER activity was measured at 340 nm, corresponding to the consumption of NADH to reduce crotonoyl-CoA. The reaction mixture contained 100 mM potassium phosphate buffer (pH 6.2), 200 μM NADH, and 200 μM crotonoyl-CoA.

5.5.4 n-*Butanol fermentation and detection*

A single colony with the reversed β-oxidation pathway from the newly transformed plate was inoculated into 3 mL SCD-URA medium, and cultured under aerobic conditions for 36 h. Then 200 μL seed culture was transferred into 10 mL fresh SCD-URA medium in a 50 mL unbaffled shaker flask at an initial OD_{600} of about 0.05, and cultured under oxygen-limited conditions for *n*-butanol fermentation. Samples were taken every 24 h after inoculation until no further increase in *n*-butanol production was observed. The production of *n*-butanol was detected and quantified by GC-MS as described in section 4.5.4.

5.5.5 MCFAs fermentation and detection

A single colony with the reversed β-oxidation pathway and CpFatB1 was inoculated into 3 mL SCD-LEU-URA medium, and cultured under aerobic conditions for 36 h. Then 400 μL seed culture was transferred into 20 mL fresh SCD-LEU-URA medium in a 125 mL baffled shaker flask at an initial OD_{600} of about 0.05, and cultured under aerobic conditions for MCFAs fermentation for 48 h.

Fatty acids were analyzed using a previously described protocol with some modifications (37). A previous report indicated that the short- and medium- chain fatty acid methyl esters were rather volatile, leading to increased variability of the fatty acid analysis (37). Thus, *N*-(*t*-butyldimethylsilyl)-*N*-methyltrifluoroacetamide (MTBSTFA) was used to derivatize short- and medium- chain fatty acids in the present study (Figure 5.4A). The fatty acid *t*-butyldimethylsilyl

esters were less volatile, which would make the derivatization process more reproducible. 5 mg/L heptanoic acid was added as an internal standard. Extracellular fatty acids were extracted from 20 mL culture supernatant by adding 2 mL 1M HCl and 5 mL of a 2:1 chloroform:methanol mixture. The solution was vortexed and then centrifuged for 5 min at 4,000 rpm. The lower chloroform layer was recovered and evaporated in the chemical hood overnight. For derivatization, 100 μL MTBSTFA and 100 μL tetrahydrofuran (THF) were added to the dried sample, which was then incubated at 70ºC for 1 h. The THF layer was diluted 10-100 fold into THF and analyzed by a Shimadzu GCMS-QP2010 Plus GC-MS equipped with an AOC-20i+s autosampler (Shimadzu Inc., Columbia, MD) and a DB-Wax column with a 0.25 μm film thickness, 0.25 mm diameter, and 30 m length (Agilent Inc., Palo Alto, CA). Injection port and interface temperature was set at 250 ºC, and the ion source was set to 230 ºC. The helium carrier gas was set at a constant flow rate of 2 mL/min. The oven temperature program was set as the following: a) hold at 50ºC for 3 min, b) increase at the rate of 5ºC min^{-1} to 120ºC, c) increase at the rate of 50ºC min^{-1} to 230ºC, d) and then isothermal heating at 230ºC for additional 3 min.

5.5.6 MCFAEEs fermentation and detection

A single colony with the reversed β-oxidation pathway from the fresh plate was inoculated into 3 mL SCD-URA medium, and cultured under aerobic conditions for 36 h. Then 100 μL seed culture was transferred into 5 mL fresh SCD-URA medium topped with 10% *n*-dodecane overlay in a 20 mL glass tube at an initial OD_{600} of about 0.05, and cultured under aerobic conditions for MCFAEEs fermentation for 48 h.

The top *n*-dodecane layer was collected, diluted 100 fold in ethyl acetate containing 1 mg/L *n*-decanol as an internal standard, and analyzed using the same GC-MS settings as

mentioned above. The oven temperature program was set as the following: a) hold at 50ºC for 2 min isothermal heating, b) increase at the rate of 50ºC min^{-1} to 230ºC, c) and then hold at 230ºC for additional 15 min.

5.5.7 Prediction of the mitochondrial and peroxisomal targeting sequences

The mitochondrial targeting sequences of the candidate proteins were predicted using the MITOPROT online tool (http://ihg.gsf.de/ihg/mitoprot.html) (19). The peroxisomal targeting sequences were predicted using the PTSs predictor from PeroxisomeDB 2.0 (http://www.peroxisomedb.org/Target_signal.php) (20).

5.6 REFERENCES

1. **Du J, Shao Z, Zhao H.** 2011. Engineering microbial factories for synthesis of value-added products. J. Ind. Microbiol. Biotechnol. **38:**873-890.
2. **Hong KK, Nielsen J.** 2012. Metabolic engineering of *Saccharomyces cerevisiae*: a key cell factory platform for future biorefineries. Cell Mol. Life Sci. **69:**2671-2690.
3. **Kung Y, Runguphan W, Keasling JD.** 2012. From fields to fuels: recent advances in the microbial production of biofuels. ACS Synth. Biol. **1:**498-513.
4. **Zhang F, Rodriguez S, Keasling JD.** 2011. Metabolic engineering of microbial pathways for advanced biofuels production. Curr. Opin. Biotechnol. **22:**775-783.
5. **Handke P, Lynch SA, Gill RT.** 2011. Application and engineering of fatty acid biosynthesis in *Escherichia coli* for advanced fuels and chemicals. Metab. Eng. **13:**28-37.
6. **Harger M, Zheng L, Moon A, Ager C, An JH, Choe C, Lai YL, Mo B, Zong D, Smith MD, Egbert RG, Mills JH, Baker D, Pultz IS, Siegel JB.** 2013. Expanding the product profile of a microbial alkane biosynthetic pathway. ACS Synth. Biol. **2:**59-62.
7. **Chan DI, Vogel HJ.** 2010. Current understanding of fatty acid biosynthesis and the acyl carrier protein. Biochem. J. **430:**1-19.
8. **Lennen RM, Pfleger BF.** 2012. Engineering *Escherichia coli* to synthesize free fatty acids. Trends Biotechnol. **30:**659-667.
9. **Liu D, Xiao Y, Evans B, Zhang F.** 2015. Negative feedback regulation of fatty acid production based on a malonyl-CoA sensor-actuator. ACS Synth. Biol. **4:**132-140.
10. **van Roermund CW, Waterham HR, Ijlst L, Wanders RJ.** 2003. Fatty acid metabolism in *Saccharomyces cerevisiae*. Cell Mol. Life Sci. **60:**1838-1851.
11. **Trotter PJ.** 2001. The genetics of fatty acid metabolism in *Saccharomyces cerevisiae*. Annu. Rev. Nutr. **21:**97-119.
12. **Dellomonaco C, Clomburg JM, Miller EN, Gonzalez R.** 2011. Engineered reversal of the β-oxidation cycle for the synthesis of fuels and chemicals. Nature **476:**355-359.
13. **Clomburg JM, Vick JE, Blankschien MD, Rodriguez-Moya M, Gonzalez R.** 2012. A synthetic biology approach to engineer a functional reversal of the β-oxidation cycle. ACS Synth. Biol. **1:**541-554.
14. **Kunau WH, Dommes V, Schulz H.** 1995. β-Oxidation of fatty acids in mitochondria, peroxisomes, and bacteria: a century of continued progress. Prog. Lipid. Res. **34:**267-342.
15. **Lian J, Zhao H.** 2015. Reversal of the β-oxidation cycle in *Saccharomyces cerevisiae* for production of fuels and chemicals. ACS Synth. Biol. **4:**332-341.
16. **Campbell JW, Morgan-Kiss RM, Cronan JE.** 2003. A new *Escherichia coli* metabolic competency: growth on fatty acids by a novel anaerobic β-oxidation pathway. Mol. Microbiol. **47:**793-805.
17. **Hiltunen JK, Mursula AM, Rottensteiner H, Wierenga RK, Kastaniotis AJ, Gurvitz A.** 2003. The biochemistry of peroxisomal β-oxidation in the yeast *Saccharomyces cerevisiae*. FEMS Microbiol. Rev. **27:**35-64.
18. **Poirier Y, Antonenkov VD, Glumoff T, Hiltunen JK.** 2006. Peroxisomal β-oxidation--a metabolic pathway with multiple functions. Biochim. Biophys. Acta **1763:**1413-1426.
19. **Claros MG, Vincens P.** 1996. Computational method to predict mitochondrially imported proteins and their targeting sequences. Eur. J. Biochem. **241:**779-786.

20. **Schluter A, Real-Chicharro A, Gabaldon T, Sanchez-Jimenez F, Pujol A.** 2010. PeroxisomeDB 2.0: an integrative view of the global peroxisomal metabolome. Nucleic Acids Res **38:**D800-D805.
21. **Lutke-Eversloh T, Bahl H.** 2011. Metabolic engineering of *Clostridium acetobutylicum*: recent advances to improve butanol production. Curr. Opin. Biotechnol. **22:**634-647.
22. **Hiser L, Basson ME, Rine J.** 1994. ERG10 from *Saccharomyces cerevisiae* encodes acetoacetyl-CoA thiolase. J. Biol. Chem. **269:**31383-31389.
23. **Steen EJ, Chan R, Prasad N, Myers S, Petzold CJ, Redding A, Ouellet M, Keasling JD.** 2008. Metabolic engineering of *Saccharomyces cerevisiae* for the production of *n*-butanol. Microb. Cell Fact. **7:**36.
24. **Vorapreeda T, Thammarongtham C, Cheevadhanarak S, Laoteng K.** 2012. Alternative routes of acetyl-CoA synthesis identified by comparative genomic analysis: involvement in the lipid production of oleaginous yeast and fungi. Microbiology **158:**217-228.
25. **Lee SY, Park JH, Jang SH, Nielsen LK, Kim J, Jung KS.** 2008. Fermentative butanol production by Clostridia. Biotechnol. Bioeng. **101:**209-228.
26. **Tucci S, Martin W.** 2007. A novel prokaryotic trans-2-enoyl-CoA reductase from the spirochete *Treponema denticola*. FEBS Lett. **581:**1561-1566.
27. **Bond-Watts BB, Weeks AM, Chang MC.** 2012. Biochemical and structural characterization of the *trans*-enoyl-CoA reductase from *Treponema denticola*. Biochemistry **51:**6827-6837.
28. **Hoffmeister M, Piotrowski M, Nowitzki U, Martin W.** 2005. Mitochondrial trans-2-enoyl-CoA reductase of wax ester fermentation from *Euglena gracilis* defines a new family of enzymes involved in lipid synthesis. J. Biol. Chem. **280:**4329-4338.
29. **Bond-Watts BB, Bellerose RJ, Chang MCY.** 2011. Enzyme mechanism as a kinetic control element for designing synthetic biofuel pathways. Nat. Chem. Biol. **7:**222-227.
30. **Shen CR, Lan EI, Dekishima Y, Baez A, Cho KM, Liao JC.** 2011. Driving forces enable high-titer anaerobic 1-butanol synthesis in *Escherichia coli*. Appl. Environ. Microbiol. **77:**2905-2915.
31. **Shao Z, Zhao H, Zhao H.** 2009. DNA assembler, an *in vivo* genetic method for rapid construction of biochemical pathways. Nucleic Acids Res. **37:**e16.
32. **Shao Z, Rao G, Li C, Abil Z, Luo Y, Zhao H.** 2013. Refactoring the silent spectinabilin gene cluster using a plug-and-play scaffold. ACS Synth. Biol. **2:**662-669.
33. **Roof DM, Roth JR.** 1988. Ethanolamine utilization in *Salmonella typhimurium*. J. Bacteriol. **170:**3855-3863.
34. **Toth J, Ismaiel AA, Chen JS.** 1999. The ald gene, encoding a coenzyme A-acylating aldehyde dehydrogenase, distinguishes *Clostridium beijerinckii* and two other solvent-producing clostridia from *Clostridium acetobutylicum*. Appl. Environ. Microbiol. **65:**4973-4980.
35. **Krivoruchko A, Serrano-Amatriain C, Chen Y, Siewers V, Nielsen J.** 2013. Improving biobutanol production in engineered *Saccharomyces cerevisiae* by manipulation of acetyl-CoA metabolism. J. Ind. Microbiol. Biotechnol. **40:**1051-1056.
36. **Jing F, Cantu DC, Tvaruzkova J, Chipman JP, Nikolau BJ, Yandeau-Nelson MD, Reilly PJ.** 2011. Phylogenetic and experimental characterization of an acyl-ACP thioesterase family reveals significant diversity in enzymatic specificity and activity. BMC Biochem. **12:**44.

37. **Leber C, Da Silva NA.** 2013. Engineering of *Saccharomyces cerevisiae* for the synthesis of short chain fatty acids. Biotechnol. Bioeng. **111:**347-358.
38. **Pronk JT, van der Linden-Beuman A, Verduyn C, Scheffers WA, van Dijken JP.** 1994. Propionate metabolism in *Saccharomyces cerevisiae*: implications for the metabolon hypothesis. Microbiology **140:**717-722.
39. **Saerens SM, Delvaux F, Verstrepen KJ, Van Dijck P, Thevelein JM, Delvaux FR.** 2008. Parameters affecting ethyl ester production by *Saccharomyces cerevisiae* during fermentation. Appl. Environ. Microbiol. **74:**454-461.
40. **Saerens SM, Verstrepen KJ, Van Laere SD, Voet AR, Van Dijck P, Delvaux FR, Thevelein JM.** 2006. The *Saccharomyces cerevisiae EHT1* and *EEB1* genes encode novel enzymes with medium-chain fatty acid ethyl ester synthesis and hydrolysis capacity. J. Biol. Chem. **281:**4446-4456.
41. **Eriksen DT, Lian J, Zhao H.** 2014. Protein design for pathway engineering. J. Struct. Biol. **185:**234-242.
42. **Guest JR, Angier SJ, Russell GC.** 1989. Structure, expression, and protein engineering of the pyruvate dehydrogenase complex of *Escherichia coli*. Ann. N. Y. Acad. Sci. **573:**76-99.
43. **Knappe J, Sawers G.** 1990. A radical-chemical route to acetyl-CoA: the anaerobically induced pyruvate formate-lyase system of *Escherichia coli*. FEMS Microbiol. Rev. **6:**383-398.
44. **Strijbis K, Distel B.** 2010. Intracellular acetyl unit transport in fungal carbon metabolism. Eukaryot. Cell **9:**1809-1815.
45. **Starai VJ, Escalante-Semerena JC.** 2004. Acetyl-coenzyme A synthetase (AMP forming). Cell Mol. Life Sci. **61:**2020-2030.
46. **Shiba Y, Paradise EM, Kirby J, Ro DK, Keasling JD.** 2007. Engineering of the pyruvate dehydrogenase bypass in *Saccharomyces cerevisiae* for high-level production of isoprenoids. Metab. Eng. **9:**160-168.
47. **Chen Y, Daviet L, Schalk M, Siewers V, Nielsen J.** 2013. Establishing a platform cell factory through engineering of yeast acetyl-CoA metabolism. Metab. Eng. **15:**48-54.
48. **Kocharin K, Chen Y, Siewers V, Nielsen J.** 2012. Engineering of acetyl-CoA metabolism for the improved production of polyhydroxybutyrate in *Saccharomyces cerevisiae*. AMB Express **2:**52.
49. **Kocharin K, Siewers V, Nielsen J.** 2013. Improved polyhydroxybutyrate production by *Saccharomyces cerevisiae* through the use of the phosphoketolase pathway. Biotechnol. Bioeng. **110:**2216-2224.
50. **Tang X, Feng H, Chen WN.** 2013. Metabolic engineering for enhanced fatty acids synthesis in *Saccharomyces cerevisiae*. Metab. Eng. **16:**95-102.
51. **Avalos JL, Fink GR, Stephanopoulos G.** 2013. Compartmentalization of metabolic pathways in yeast mitochondria improves the production of branched-chain alcohols. Nat. Biotechnol. **31:**335-341.
52. **Farhi M, Marhevka E, Masci T, Marcos E, Eyal Y, Ovadis M, Abeliovich H, Vainstein A.** 2011. Harnessing yeast subcellular compartments for the production of plant terpenoids. Metab. Eng. **13:**474-481.
53. **Gietz RD, Schiestl RH.** 2007. High-efficiency yeast transformation using the LiAc/SS carrier DNA/PEG method. Nat. Protoc. **2:**31-34.

5.7 Tables

Table 5.1 List of plasmids constructed in this chapter.

Plasmid	Constructs
p426	pRS426, multi-copy plasmid with *URA3* marker
pH11	p425-GPM1p-*BamHI*-eGFP-*XhoI*-ADH1t
pH22	p425-ADH1t-GPDp-*BamHI*-eGFP-*XhoI*-CYC1t
pH3	p425-ENO2p-*BamHI*-eGFP-*XhoI*-PGK1t
pH4	p425-TPI1p-*BamHI*-eGFP-*XhoI*-TPI1t
pH5	p425-TEF1p-*BamHI*-eGFP-*XhoI*-TEF1t
pH66	pR25-TEF1t-PGK1p-*BamHI*-eGFP-*HindIII*-HXT7t
CaThl	pH11-Ca*Thl*
ERG10	pH11-*ERG10*
cytoFox3	pH11-cyto*Fox3*
EcAtoB	pH11-Ec*AtoB*
EcYqeF	pH11-Ec*YqeF*
EcFadA	pH11-Ec*FadA*
cytoFOX2	pH22-cyto*FOX2*
EcFadB	pH22-Ec*FadB*
cytoTdeFOX2	pH22-cytoTde*FOX2*
cytoCgFOX2	pH22-cytoCg*FOX2*
cytoNdFOX2	pH22-cytoNd*FOX2*
cytoVpFOX2	pH22-cytoVp*FOX2*
cytoNcFOX2	pH22-cytoNc*FOX2*
cytoKlFOX2	pH22-cytoKl*FOX2*
cytoTpFOX2	pH22-cytoTp*FOX2*
cytoZrFOX2	pH22-cytoZr*FOX2*
cytoAgFOX2	pH22-cytoAg*FOX2*
cytoPpFOX2	pH22-cytoPp*FOX2*
cytoPfFOX2	pH22-cytoPf*FOX2*
cytoHpFOX2	pH22-cytoHp*FOX2*
cytoCpFOX2	pH22-cytoCp*FOX2*
cytoPgFOX2	pH22-cytoPg*FOX2*
cytoCdFOX2	pH22-cytoCd*FOX2*
cytoCtrFOX2	pH22-cytoCtr*FOX2*
cytoSsFOX2	pH22-cytoSs*FOX2*
cytoLeFOX2	pH22-cytoLe*FOX2*
cytoCteFOX2	pH22-cytoCte*FOX2*
cytoYlFOX2	pH22-cytoYl*FOX2*
CaHbd	pH22-Ca*Hbd*
cytoYlKR	pH22-cytoYALI0C08811g
CbCrt	pH6-Cb*Crt*
cytoYlHTD	pH66-cytoYALI0B10406g

Table 5.1 (cont.)

Plasmid	Constructs
cytoETR1	pH3-cyto*ETR1*
ZTA1	pH3-*ZTA1*
cytoSPS19	pH3-cyto*SPS19*
YNL134C	pH3-YNL134C
YLR460C	pH3-YLR460C
YCR102C	pH3-YCR102C
EcYdiO	pH3-Ec*YdiO*
EcFabI	pH3-Ec*FabI*
EgTer	pH3-Eg*Ter*
TdTer	pH3-Td*Ter*
EcEutE	pH4-Ec*EutE*
CaBdhB	pH5-Ca*BdhB*
CpFatB1	pH5-Cp*FatB1*
EEB1	pH5-*EEB1*
EHT1	pH5-*EHT1*
rP31	p426-*ERG10*-cytoY*lKR*-cytoYl*HTD*-Td*Ter*-Ec*EutE*-Ca*BdhB*
rP32	p426-cyto*FOX3*-cytoYl*KR*-cytoYl*HTD*-Td*Ter*-Ec*EutE*-Ca*BdhB*
rP34	p426-*ERG10*-cytoYl*KR*-cytoYl*HTD*-cyto*ETR1*-Ec*EutE*-Ca*BdhB*
rP35	p426-cyto*FOX3*-cytoYl*KR*-cytoYl*HTD*-cyto*ETR1*-Ec*EutE*-Ca*BdhB*
rP37	p426-*ERG10-eGFP*-cytoYl*HTD*-Td*Ter*-Ec*EutE*-Ca*BdhB*
rP38	p426-cyto*FOX3-eGFP*-cytoYl*HTD*-Td*Ter*-Ec*EutE*-Ca*BdhB*

*Ag, *Ashbya gossypii*; Ca, *Clostridium acetobutylicum*; Cb, *Clostridium beijerinckii*; Cd, *Candida dubliniensis*; Cg, *Candida glabrata*; Cp, *Candida parapsilosis*; Cte, *Candida tenuis*; Ctr, *Candida tropicalis*; Ec, *Escherichia coli*; Eg, *Euglena gracilis*; Hp, *Hansenula polymorpha*; Kl, *Kluyveromyces lactis*; Le, *Lodderomyces elongisporus*; Nc, *Naumovozyma castellii*; Nd, *Naumovozyma dairenensis*; Pf, *Pichia farinose*; Pg, *Pichia guilliermondii*; Pp, *Pichia pastoris*; Ss, *Scheffersomyces stipites*; Td, *Treponema denticola*; Tde, *Torulaspora delbrueckii*; Tp, *Tetrapisispora phaffii*; Vp, *Vanderwaltozyma polyspora*; Yl, *Yarrowia lipolytica*; Zr, *Zygosaccharomyces rouxii*.

5.8 Figures

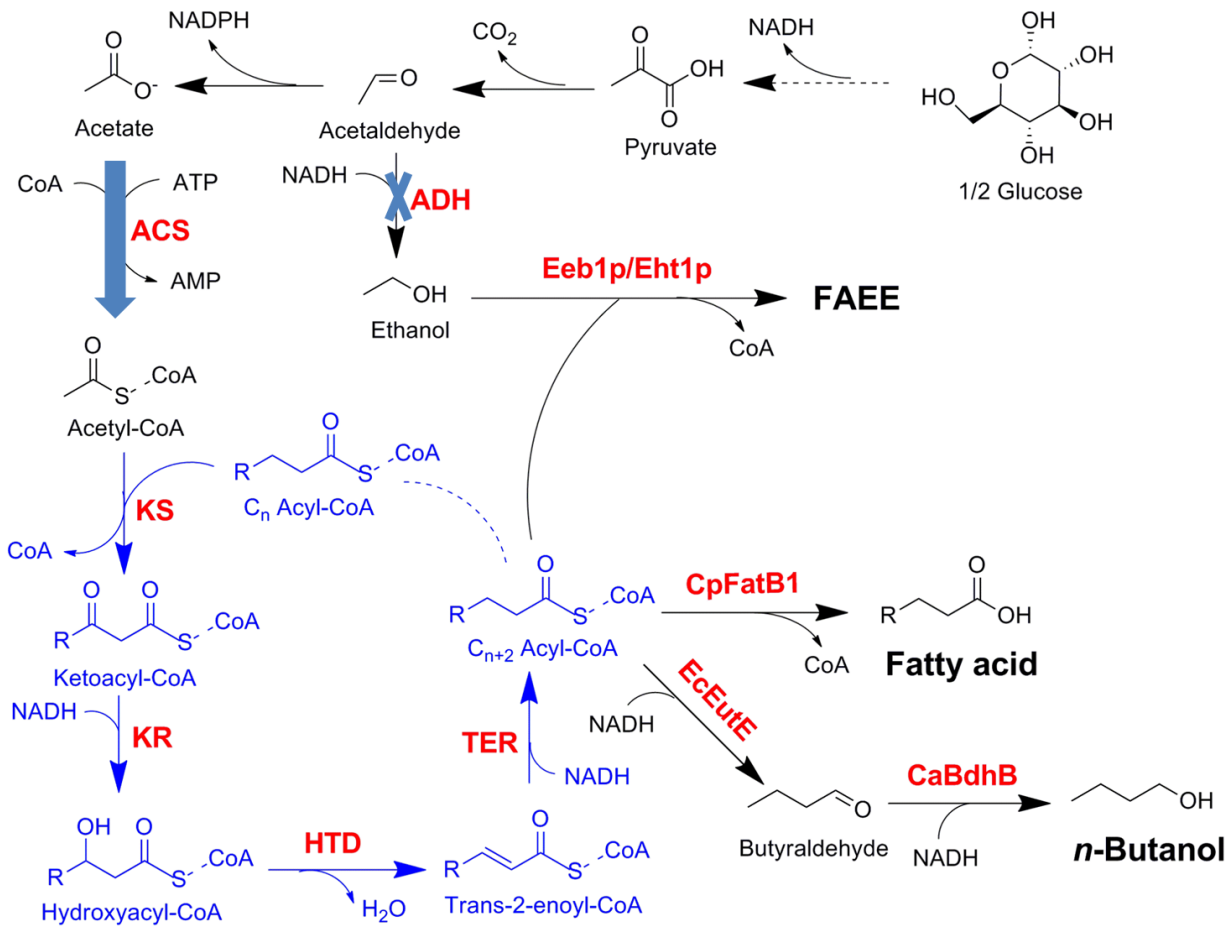

Figure 5.1 Overview of the synthesis of advanced biofuels by reversing the β-oxidation cycle in *Saccharomyces cerevisiae*. Reversed β-oxidation pathways were constructed via constitutive overexpression of the β-oxidation structural genes in the cytosol of yeast. To increase the cytosolic acetyl-CoA level, competing pathways for acetyl-CoA biosynthesis were inactivated and an acetyl-CoA synthetase mutant (ACS) free of feedback inhibition was overexpressed. KS, β-ketoacyl-CoA synthase; KR, β-ketoacyl-CoA reductase; HTD, β-hydroxyacyl-CoA dehydratase; TER, *trans*-2-enoyl-CoA reductase; CpFatB1, thioesterase from *Cuphea palustris*; EcEutE, CoA-acylating aldehyde dehydrogenase from *Escherichia coli*; CaBdhB, butanol dehydrogenase from *Clostridium acetobutylium*; EEB1/EHT1, acyl-CoA:ethanol *O*-acyltransferases; ADH, alcohol dehydrogenase; FAEE, fatty acid ethyl ester.

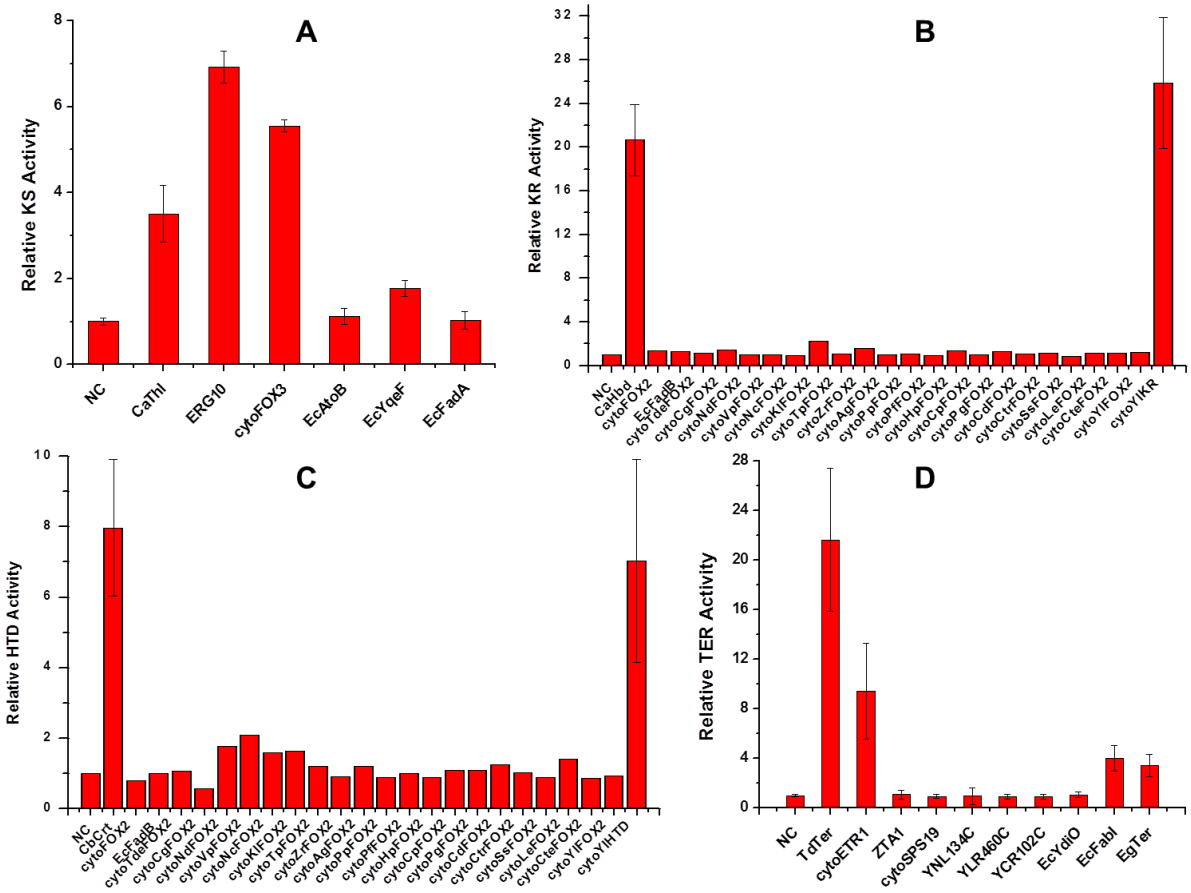

Figure 5.2 Enzyme activity assays of the reversed β-oxidation pathway enzymes, including KS (A), KR (B), HTD (C), and TER (D). The CoA-dependent *n*-butanol biosynthetic pathway enzymes including CaThl, CaHbd, CbCrt, and TdTer were used as positive controls for KS, KR, HTD, and TER activity assays, respectively.

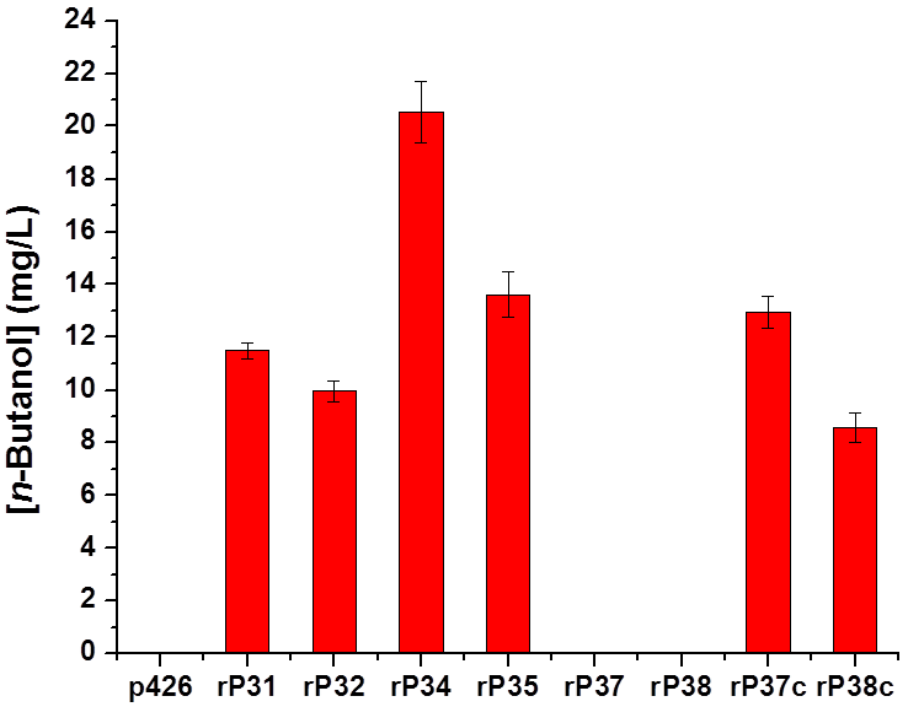

Figure 5.3 Detection and confirmation of *n*-butanol synthesis by the reversed β-oxidation pathways. The production of *n*-butanol could only be detected when a fully functional reversed β-oxidation pathway was present (rP31, rP32, rP34, and rP35). The failure of the control strains with either an empty vector (p426) or a nonfunctional pathway (rP37 and rP37) indicated the dependence of *n*-butanol production on the reversed β-oxidation pathways in *S. cerevisiae*. The production of *n*-butanol could be complemented by co-expressing cytoYlKR together with the incomplete pathway (rP37c and rP38c).

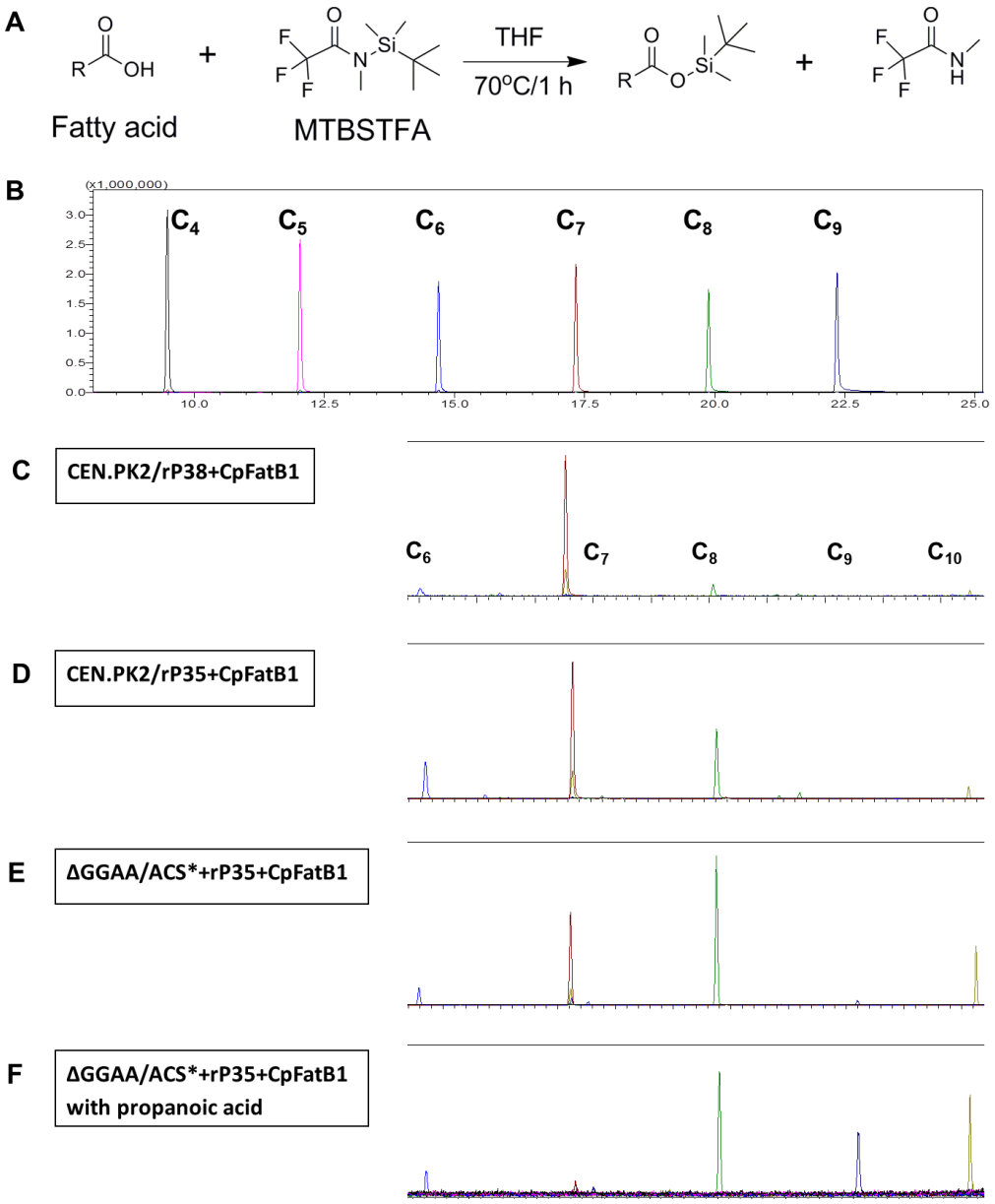

Figure 5.4 Production of MCFAs by the reversed β-oxidation pathway. (A) A protocol to derivatize and detect short-chain fatty acids by GC-MS was developed. MTBSTFA was chosen as the derivatiation reagents, since the derived fatty acid t-butyldimethylsilyl esters were less volatile and could be more accurately measured. (B) Using the developed GC-MS program, all short- and medium-chain fatty acids could be well separated and detected. (C) Extracellular fatty acid profiles of the wild-type strain expressing the thioesterase with an incomplete reversed β-oxidation pathway. (D) Extracellular fatty acid profiles of the wild-type strain expressing the thioesterase with a functional reversed β-oxidation pathway. (E) Extracellular fatty acid profiles of an acetyl-CoA overproducing strain expressing the thioesterase with a functional reversed β-oxidation pathway. (F) Production of odd-chain fatty acids with the supplementation of 0.1 g/L propanoic acid. 5 mg/L heptanoic acid was included as an internal standard (C, D, and E), except for D to show the full profiles of MCFAs produced by the engineered yeast strain.

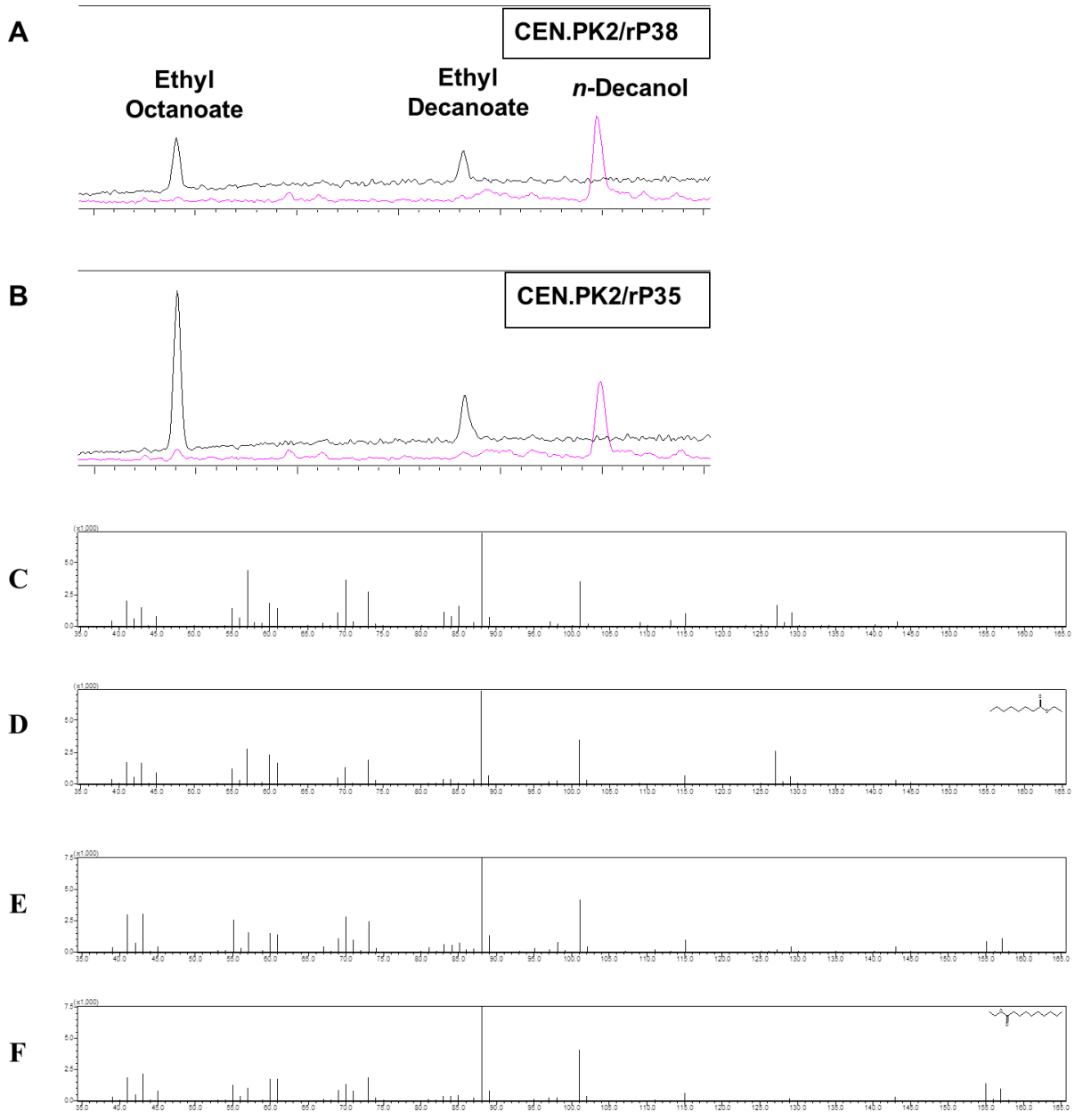

Figure 5.5 Increased production of MCFAEEs by the reversed β-oxidation pathway. Production of ethyl octanoate and ethyl decanoate was compared between the strains expressing either an incomplete (A) or a functional (B) reversed β-oxidation pathway. 1 mg/L n-decanol was included as an internal standard. The MS fragments of ethyl octanoate (C, D) and ethyl decanoate (E, F) were compared between the samples (C, E) and the standards (D, F).

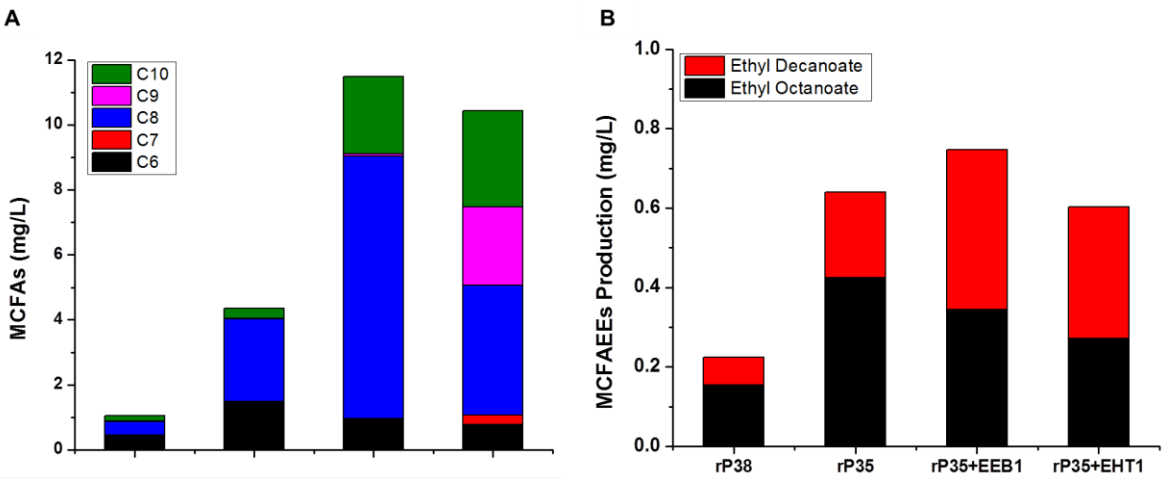

CEN.PK2	+	+	+	+
rP35	-(rP38)	+	+	+
CpFatB1	+	+	+	+
ΔGGAA/ACS*			+	+
Propanoic acid				+

Figure 5.6 Distribution of medium-chain fatty acids (A) and medium-chain fatty acid ethyl esters (B) produced by yeast strains with or without the reversed β-oxidation pathway.

Chapter 6 Modular Pathway Optimization at DNA Level: Induced Pathway Optimization by Antibiotic Doses

6.1 Introduction

Increasing attention has been drawn to convert renewable feedstocks into fuels, chemicals, and other value-added compounds, using microbial fermentation at large scales (1, 2). The introduction of biosynthetic pathways containing several heterologous genes is generally the first step to achieve microbial synthesis. In order to enable commercially viable production of these compounds, metabolic fluxes or protein levels in the heterologous multi-gene pathways must be carefully fine-tuned and balanced to maximize product titers, yields, and productivities (3, 4). The optimization of a multi-gene pathway can be achieved at DNA level (copy number (5, 6)), transcription and mRNA level (promoter engineering (7-9), intergenic region engineering (10), and terminator engineering (11)), translation and protein level (ribosome binding site engineering (12) and protein co-localization (13)), and metabolite level (dynamic control (14-16)). Notably, most of these synthetic biology tools are well developed for *Escherichia coli*. While in *Saccharomyces cerevisiae*, a preferred host for industrial applications, the development of these pathway optimization tools is far behind due to the complexity as a eukaryotic cell factory and limited to a few examples, such as the use of promoters (9, 17) and terminators (11) with different strength. Recently, RNA interference (RNAi) was also reconstituted in this eukaryotic host to modulate gene expression levels (18-20) and showed (potential) applications in metabolic engineering and synthetic biology. However, the use of RNAi for multi-gene pathway optimization has not been explored yet. Notably, gene expression levels and metabolic fluxes are mainly fine-tuned at the transcription and mRNA level, which was usually reported to have a limited dynamic range (~10 fold) (21). What is worse, lower expression or knock-down is

generally obtained using either promoter engineering or RNAi, while to achieve much higher expression level is more challenging (7, 9). Therefore, this work aimed to develop new synthetic biology tools to fine-tune protein expression levels and metabolic fluxes at DNA level, in the hope of further expanding the dynamic range of pathway optimization tools in *S. cerevisiae*.

Plasmids have been extensively used for both fundamental studies and metabolic engineering and synthetic biology applications, since they have the advantages of convenience and ease of use, flexibility of transferring to different hosts, high copy number to allow strong gene expression, and high transformation efficiency for library construction and high throughput screening (9, 11, 22). In *S. cerevisiae*, two sets of episomal plasmids have been developed, the so-called CEN/ARS-based low-copy plasmids (1-4 copies per cell) and 2μ-based high-copy plasmids (20-30 copies per cell with auxotrophic markers and 4-6 copies with antibiotic markers). These plasmids are constructed using a series of auxotrophic selection markers (such as HIS3, TRP1, LEU2, and URA3) and dominant antibiotic markers (such as KanMX, HygB, and Ble). Although widely used, the current system suffers from low copy numbers and a lack of dynamic range, making them rather limited for multi-gene pathway optimization. Previously, it was found that plasmid copy number (PCN) could be enhanced by weakening the expression of the selection marker genes (such as the use of heterologous or truncated promoters) (23-26) and destabilizing the marker proteins (such as fusion with a degradation tag) (22). This study aims to construct a series of 2μ-based plasmids with step-wise increased copy numbers, which can be used for modular optimization of multi-gene pathways. Assuming that promoter length may control the expression level of the marker gene, plasmids with different copy numbers can be obtained by truncating the promoter to different degrees in *S. cerevisiae*.

In the present study, the promoters driving the expression of selection marker genes, including HIS3, TRP1, LEU2, URA3, KanMX, and HygB, were truncated to different degrees and their effects on PCNs were systematically evaluated. By simply performing promoter truncation, plasmids with different copy numbers (as high as 100 copies per cell) were constructed, and a dynamic range of around 20 folds were achieved for engineered plasmids with KanMX and HygB markers, which endowed G418 and hygromycin resistance, respectively. More importantly, the copy number of the plasmids with engineered dominant markers (5-100 copies per cell) showed a positive correlation with the concentration of antibiotics supplemented to the growth media. Therefore, a simple method named iPOAD (induced pathway optimization by antibiotic doses) was developed for modular optimization of multi-gene pathways by different combination of antibiotic concentrations. The applications of iPOAD were demonstrated by modular optimization of the lycopene and *n*-butanol biosynthetic pathways, with the production of lycopene and *n*-butanol increased by 10- and 100-fold, respectively. Considering the strain stability and the requirement of antibiotic supplementation, the pathway optimized by iPOAD was integrated into chromosomes using delta integration. Multiplex double cross-over based integration at different loci of delta sequences was achieved by combining iPOAD and the CRISPR-Cas9 technology.

6.2 Results

6.2.1 Enhanced plasmid copy number via truncation of marker gene promoters

Previously it was found that the use of truncated promoters or partially defective promoters driving the expression of the marker genes (*LEU2* and *URA3*) led to significantly enhanced copy numbers of the 2μ-based plasmids (23, 24). Therefore, this simple strategy was also applied to other markers commonly used in *S. cerevisiae*, especially for those with dominant

antibiotic markers, which were reported to have very low PCNs (4-6 copies per cell) even though the 2μ-based backbone was used (11). Since plasmids with step-wise increased copy numbers are rather desirable for pathway optimization at DNA levels, promoter truncation at different levels (TP5, TP4, TP3, TP2, and TP1 corresponded to the use of 15 bp, 20 bp, 30 bp, 50 bp, and 100 bp sequences upstream of the start codon as the partially defective promoters, respectively) were performed for four auxotrophic markers (HIS3, TRP1, LEU2, and URA3) and two dominant markers (KanMX and HygB). The effects of promoter truncation on PCNs were systematically evaluated by using eGFP as a reporter (Figure 6.1). Using the dual marker system, all recombinant yeast strains were pre-cultured in SCD-LEU (non-selective media, except for those with LEU2 marker) to have a similar start point and then transferred to the corresponding selective media to study the effects of promoter truncation on PCNs. As shown in Figure 6.2A, no significant difference in eGFP fluorescence intensity was observed in non-selective media, which was gradually increased with a higher degree of promoter truncation in the corresponding selective media. For TRP1 and LEU2, PCNs were only slightly enhanced with partially defective promoters, while promoter truncation resulted in a step-wise increase of PCNs for HIS3, URA3, KanMX, and HygB, which showed a dynamic range around 5-10 fold (Figure 6.2B). By measuring PCNs with qPCR, it was found that PCNs followed the same pattern as those of eGFP intensity, and a strong linear correlation (R^2=0.87) between PCNs and eGFP intensities could be constructed (Figures 6.2C and 6.2D), indicating that eGFP intensity could be used as a reporter of PCNs in *S. cerevisiae*. Notably, dominant markers with full-length promoters (wild-type markers) showed rather low PCNs (lower than 5 copies per cell), even though the 2μ origin of replication was used, which agreed well with previous studies (11). Through promoter truncation, PCNs as high as 80 copies per cell could be achieved with either 200 mg/L G418 or hygromycin

supplemented to the growth media, which represented a 20-fold enhancement in PCNs. If mCherry was cloned instead of eGFP, the effects of promoter truncation could even be seen by naked eyes (Figure 6.2E). In addition, flow cytometry indicated that the enhanced PCNs were resulted from the redistribution of plasmids with different copy numbers (Figure 6.2F). Promoter truncation provided a selection pressure for plasmids with higher copy numbers and cells with higher PCNs would be enriched. Compared with those containing wild-type promoters which showed two peaks of eGFP fluorescence by flow cytometry, a single peak was observed for those with truncated promoters (engineered markers) (Figure 6.2F). In other words, besides the enhanced PCNs, the yeast population containing the engineered markers was more homogenous, which is another important feature useful for metabolic engineering and synthetic biology applications.

6.2.2 Dependence of PCNs on antibiotic concentrations

Since dominant markers with truncated promoters showed much higher PCNs, it was assumed that plasmids with these engineered markers might be more sensitive to the concentration of antibiotics. To prove this, G418 or hygromycin was supplemented to the growth media at different concentrations. Interestingly, as the antibiotic concentration increased, although PCNs were constant with the wild-type markers, a nice step-wise increase in PCNs could be obtained when engineered markers were used (Figure 6.3), especially for Kan20 (TP4) and Hyg30 (TP3). In other words, PCNs with engineered markers were antibiotic dose-dependent. Generally, PCNs were more sensitive to antibiotic concentrations with shorter promoters (higher degrees of truncation), leading to a larger dynamic range of PCNs. However, it was also found that the dynamic range of PCNs was lost if the promoter was truncated too much, such as the case with Hyg20 (TP4). Therefore, the promoter driving the expression of the

selection marker gene must be carefully engineered to achieve the best performance, such as the largest dynamic range for pathway optimization in this study. By combining promoter engineering and the optimal antibiotic concentration, PCNs as high as 120 copies per cell were achieved for both engineered KanMX and HygB markers.

6.2.3 Modular pathway optimization using plasmids with different copy numbers

Since a series of plasmids with step-wise increased copy numbers were obtained via promoter truncation, it was desirable to test whether they could be used to fine-tune the metabolic fluxes of a biosynthetic pathway at the DNA level. As a proof of concept, two fluorescent proteins (eGFP and mCherry) were cloned into HIS3 (HIS-CEN, HIS-WT, HIS100, HIS50, HIS30, and HIS15) and URA3 (URA-CEN, URA-WT, URA100, URA50, URA30, and URA15) based plasmids, respectively. As shown in Figures 6.4A and 6.4B, the eGFP and mCherry signals were almost distributed as expected, with eGFP mainly determined by HIS3 plasmids and mCherry by URA3 plasmids. Indeed, some interactions between the two series of plasmids were observed. For example, both eGFP and mCherry signals were significantly decreased when both were cloned into the plasmids with high copy numbers, probably due to the competition between these 2μ-based plasmids.

To further test whether antibiotic concentrations could be modulated to fine tune metabolic fluxes, eGFP and mCherry were cloned into Hyg30 and Kan20, respectively. Similarly, a nice distribution of eGFP and mCherry signals was obtained, with eGFP mainly determined by the concentration of hygromycin and mCherry by the concentration of G418, albeit not following a completely independent manner (Figures 6.4C and 6.4D).

Based on these results, plasmids with different copy numbers obtained by either promoter truncation at different levels or modulating antibiotic concentration could be used for pathway optimization at the DNA level. Especially for the latter, metabolic fluxes could be fine-tuned by simply modulating antibiotic concentration, representing a simplest strategy for pathway optimization. This method was named induced pathway optimization via antibiotic doses (iPOAD) for pathway optimization at the DNA level.

6.2.4 Increased lycopene production via iPOAD

To demonstrate that iPOAD could be applied for the optimization of multi-gene pathways, lycopene biosynthesis was chosen as the first example. The whole pathway involved more than 10 genes from acetyl-CoA was divided into two modules at the farnesyl diphosphate (FPP) branch, the FPP module with Hyg30 marker and Lyc module with Kan20 marker (Figure 6.5A). The FPP module contained several endogenous genes (*ERG10-ERG13*-t*HMGR-ERG12-ERG8-ERG20*) whose overexpression was confirmed to enable higher fluxes from acetyl-CoA to FPP (27), and the lycopene module contained genes (*CrtE-CrtB-CrtI*) that were responsible for the conversion of FPP to lycopene (28). By testing different combinations of G418 and hygromycin concentrations, it was found that lycopene production was increased at higher concentration of hygromycin, while G418 concentration had no effect (Figure 6.5B), indicating that the FPP module was the rate-limiting factor. Therefore, hygromycin was supplemented at higher concentration to further increase the metabolic fluxes towards FPP. Indeed, lycopene production continued to be improved as the hygromycin concentration was increased (Figure 6.5C). Compared with the system containing wild-type promoters, the production of lycopene was increased about 3 fold by promoter truncation and additional 3 fold by iPOAD, resulting in a total of around 10 fold improvement (Figure 6.5D).

6.2.5 Improved n-butanol fermentation via iPOAD

Although significant improvement in lycopene production was achieved, the balancing of metabolic fluxes at the DNA level was not clearly demonstrated, since the FPP module was rate-limiting. Therefore, another multi-gene pathway leading to the biosynthesis of *n*-butanol was tested. The whole pathway was divided into two modules at the butyryl-CoA branch, the upstream module (*Thl-Hbd-Crt-Ter*, from acetyl-CoA to butyryl-CoA) with Hyg30 marker and downstream module (*Bad-Bdh*, from butyryl-CoA to *n*-butanol) with Kan20 marker (Figure 6.6A). By testing different combinations of G418 and hygromycin concentrations, it was found that the optimal condition for *n*-butanol production was 800 mg/L of hygromycin and 400 mg/L of G418 (Figure 6.6B). Higher concentration of hygromycin before reaching the optimal level was better for *n*-butanol production, since the overall fluxes were controlled by the upstream module. The optimal G418 concentration was dependent on the upstream module, since the downstream module functioned to balance the overall fluxes. In other words, the concentration of hygromyin and G418 should be carefully adjusted to fine-tune the metabolic fluxes of both modules, since higher concentration would lead to cellular burdens and lower concentration would result in limited (upstream module) or unbalanced (downstream module) metabolic fluxes. Compared with the system containing wild-type promoters, the production of *n*-butanol was increased about 10 fold by promoter truncation (due to enhanced PCNs) and additional 10 fold by iPOAD (due to balanced metabolic fluxes), resulting in a total of around 100 fold improvement (Figure 6.6C).

6.2.6 Multiplex pathway integration via CRISPR-Cas9

Although iPOAD enabled the optimization of a multi-gene pathway at the DNA level by simply modulating the antibiotic concentration, its practical or industrial applications would be limited by the requirement for high concentration of antibiotics. Therefore, a final goal of this work was to transfer the iPOAD optimized pathway to chromosomes, since genome integrated strains were reported to have much higher stability and might eliminate the requirement of antibiotic supplementation to maintain the plasmids with high copy numbers. Assuming the engineered markers could control the copy numbers of plasmids, they might be able to control the copy numbers in the genome as well. To test this hypothesis, Kan20 with a 40 bp homology arm at both ends was integrated into delta sequences and the resultant strains were screened on plates with different G418 concentrations. As shown in Table 6.1, all the clones tested had only one copy integration at lower selection pressure, while delta integration with more than 30 copies could be achieved at higher G418 concentrations, indicating that the integration copy numbers were also follow a similar dose-dependent manner. Unfortunately, no colonies could be obtained if a large biosynthetic pathway was included together with the engineered marker, probably due to the lower transformation and/or integration efficiency of large DNA fragments. The introduction of a double strand break on the chromosome was reported to boost the efficiency of homologous recombination (HR) to a much higher level, with an improvement of at least 1000 fold (29). Therefore, the newly developed CRISPR-Cas9 system was employed to achieve multiplex delta integration (Di-CRISPR, Figure 6.7).

First of all, mCherry was cloned into the donor plasmid with Kan20 marker to optimize Di-CRISPR. As shown in Figure 6.8, the optimal condition to achieve highest delta integration efficiency is to place the CRISPR-Cas9 system on a super-high copy plasmid and three serial

transfers on integration medium and one transfer in plasmid rescue medium. Combined with counter selection, all donor plasmids were removed from the system, as confirmed by the inability of the 24 randomly picked up colonies to grow on SCD-URA (data not shown). After screening colonies on SCD plates containing different concentrations of G418, the fluorescence was found to be dependent on the selection pressure (higher antibiotic concentration resulted in more intensive fluorescence), confirming our assumption that the engineered markers were able to control the copy numbers of integrated cassettes on chromosome (Figure 6.9A).

Then the upstream module and downstream module of *n*-butanol biosynthetic pathway were cloned together with Hyg30 and Kan20, respectively, into the helper plasmids to construct two donor plasmids for Di-CRISPR. Using the optimal conditions for *n*-butanol production, 16 colonies were randomly picked up from the plates containing antibiotics with either non-optimal (Hyg200Kan200) or optimized conditions (Hyg800Kan400) and characterized for their ability to produce *n*-butanol. As shown in Figures 6.9B and 6.9C, higher *n*-butanol production was achieved with higher selection pressure (optimal condition), further confirming that the engineered markers could control the copy numbers of both plasmids and chromosomally integrated cassettes. Compared with the plasmid system, we found significant clonal variations in *n*-butanol production, which was commonly observed for delta integration (30-32), probably due to the difference in copy numbers and/or loci dependent pathway activities. As for the best performing strain (INT3), the production of *n*-butanol reached about 70% of the value achieved using the plasmid system. Then the copy numbers of the upstream module and downstream module in the four best performing strains (INT1, INT2, INT3, and INT4, respectively) were quantified by qPCR and compared with the strain containing plasmids, which were obtained under the same selection pressure (Figure 6.9D). Interestingly, although the exact copy numbers

were not the same, the ratio of the copy numbers of the upstream module and the downstream module was rather similar (~1:2.4 in the plasmid containing strain v.s. ~1:2.9 in the integration strains). These results indicated that the *n*-butanol biosynthesis pathway was also optimized in the integration strains through the use of the engineered markers. In other words, we were able to transfer the optimized pathway to the chromosome by combining iPOAD and CRISPR-Cas9 technologies.

Finally, the stability of the integration strain (INT3) was tested in media without antibiotics supplementation. After more than 20 rounds of cell division without selection pressure, the integrated strain still produced about 80% of the amount of *n*-butanol when antibiotics were supplemented, which was nearly undetectable in the plasmid based system (Figure 6.9E). Therefore, although the *n*-butanol titer was not as high as the plasmid containing strain, the integration strain demonstrated much higher stability without antibiotics supplementation, which promised potential applications of Di-CRISPR to construct yeast cell factories for industrial production of fuels and chemicals.

6.3 Discussion

Biological conversion of renewable feedstock into fuels and chemicals has been intensively investigated due to increasing concerns on sustainability and global climate change (1). Many chemicals, such as lactic acid, succinic acid, and *iso*-butanol, used to be produced by chemical processes are synthesized biologically with microbial fermentation. Microorganisms are able to convert a wide range of substrates, such as plant biomass and agricultural waste, to value-added chemicals and fuels, promising a low carbon economy and sustainable future. Biofuels and chemicals are preferred to be produced at large scales using industrially friendly hosts such as *E. coli* and *S. cerevisiae*. Besides these two model microorganisms, cyanobacteria

(33) and oleaginous yeasts (34) have also been explored as cell factories. Compared with its counterparts, *S. cerevisiae* is more industrially relevant thanks to the well-studied genetic and physiological background, the availability of a large collection of genetic tools, the compatibility of high-density and large-scale fermentation, the resistance to phage infection, and the high tolerance against toxic inhibitors and products (2). Therefore, *S. cerevisiae* is the most popular cell factory and has been successfully used in modern fermentation industry to produce a wide variety of products including but not limited to ethanol, organic acids, amino acids, enzymes, and therapeutic proteins (1, 2).

The development of microbial cell factory generally starts with the introduction of a biosynthetic pathway containing several heterologous genes, followed by optimization of the multi-gene pathway by balancing metabolic fluxes to maximize product titers, yields, and productivities (3, 4). The most powerful and well-developed method to achieve pathway optimization in *S. cerevisiae* is to use different promoters or promoter mutants with step-wise increased strengths. A method named COMPACTER using promoter mutants was developed in our previous studies to fine-tune the metabolic fluxes of multi-gene pathways. Although promoter mutants with different strengths could be generated by error-prone PCR, this method tended to generate promoter mutants with lower activities rather than higher ones and the dynamic range was very limited (~10 fold). Therefore, development of new tools at different levels of control (such as DNA level) was required to optimize multi-gene pathways. In this study, 2μ-based high copy plasmids were engineered to have different copy numbers through the use of partial defective promoters to drive the expression of both auxotrophic and dominant markers. Notably, promoter mutants used in COMPACTER tended to have lower activity than the wild-type, while the engineered marker containing plasmids tend to have higher copy

numbers than the traditional 2μ-based plasmids. Therefore, iPOAD and COMPACTER could be combined to further develop pathway optimization tools with expanded dynamic range in *S. cerevisiae*. From another perspective, the number of genes in a biosynthetic pathway could be optimized was limited by the library transformation efficiency. For example, assuming a transformation efficiency of 10^5 and 10 promoter mutants with step-wise increased strengths, a maximal of 5 genes could be optimized. This dramatically limited the application of COMPACTER to improve the production of many value-added compounds, whose biosynthetic pathways may generally involve more than 10 genes. Another advantage of combining iPOAD and COMPACTER is the possibility to divide a long synthetic pathway into different modules. In this case, each module containing around 5 genes could be optimized using COMPACTER (local or partial optimization), and further balancing the metabolic fluxes between different modules could be achieved using iPOAD (global or complete optimization) (Figure 6.10). Although the optimization of only two modules was demonstrated in this study, more engineered dominant markers such as Ble (bleomycin resistance) and Nat (natamycin resistance) could be achieved by following a similar strategy and included for the optimization of multi-module pathways.

Although plasmids possess the advantages mentioned above, they suffer from genetic instability due to segregational instability, structural instability, and allele segregation (32, 35). Clonal variations and PCN change at different growth stages are also associated with the plasmid-based expression systems. Therefore, genome integration to maintain the heterologous pathways during the long-time culture without selection pressure is preferred for industrial applications. A major challenge is to integrate several copies of the desired genes or pathways into the chromosome, especially for multi-gene pathways. In *E. coli*, a process named CIChE

(chemical induced chromosome evolution) was developed to evolve a chromosome with ~40 consecutive copies of a recombinant pathway (35). In *S. cerevisiae*, integration into the delta sequences (delta integration), which are positioned throughout the genome as the long terminal repeats of Ty retrotransposons, is generally used to construct genomic integrated yeast strains with multiple copies (30, 31). Interestingly, it was found that delta mediated integration tended to achieve high copy number integration by tandem (single cross-over) integration into the same locus rather than single (double cross-over) integration at different loci of delta sequences. One problem with genes in tandem repeat is their genetic instability, as shown in the CIChE engineered strains that the high copies could only be maintained under selection pressure or in a homologous recombination deficient strain (35). Recently, another study designed double cross-over based delta integration and only 6 copy integration was achieved, even hough the process was repeated several times with gradually increased selection pressures with a final antibiotic concentration as high as 20 g/L (32). In this study, much higher copy number integration was achieved at a lower antibiotic concentration, 200 mg/L of G418 to achieve 30 copies of integration (Table 6.1). In addition, by taking advantage of the CRISPR-Cas9 technology, we were able to integrate much larger DNA fragments (>10 kb) with high copy numbers into the chromosome. More importantly, by using the engineered markers, the copy numbers of the integrated cassettes could be controlled by the antibiotic concentrations, making the transfer of the iPOAD optimized pathway to chromosomes possible. In addition, although the production of *n*-butanol was slightly lower compared with the plasmid containing strain, the engineered strain obtained by Di-CRISPR showed much higher stability when antibiotics were not supplemented, an important feature for industrial applications. If even higher copies of integration were desired, Di-CRISPR could be repeated several cycles with gradually increased selection pressure as well.

The stability of the engineered strains obtained by Di-CRISPR that contained the same pathway at different loci should be further evaluated even without the supplementation of antibiotics.

6.4 Conclusions

Saccharomyces cerevisiae has increasingly been engineered as a cell factory for efficient and economic production of fuels and chemicals from renewable resources. We develop a new and simplest synthetic biology approach, named induced pathway optimization by antibiotic doses (iPOAD), to improve the performance of multi-gene biosynthetic pathways in *S. cerevisiae*. First of all, plasmids with step-wise increased copy numbers were constructed by engineering the expression level of selection marker proteins, including both auxotrophic and dominant markers. More importantly, the copy number of the plasmids with engineered dominant markers (5-100 copies per cell) showed a positive correlation with the concentration of antibiotics supplemented to the growth media. Based on this finding, iPOAD was developed for modular optimization of multi-gene pathways by different combinations of antibiotic concentrations. To demonstrate this approach, iPOAD was applied to optimize the lycopene and *n*-butanol biosynthetic pathways, with the production of lycopene and *n*-butanol increased by 10- and 100-fold, respectively. Finally, the pathway optimized by iPOAD was transferred to the chromosomes to increase the strain stability and eliminate the requirement of antibiotic supplementation, by taking advantage of iPOAD and the CRISPR-Cas9 technology for multiplex pathway integration.

6.5 Materials and Methods

6.5.1 Strains, media, and cultivation conditions

E. coli strain DH5α was used to maintain and amplify plasmids, and recombinant strains were cultured at 37°C in Luria-Bertani (LB) broth containing 100 μg/mL ampicillin. *S.*

cerevisiae INVSc1 strain (Life Technologies) was used as the host for homologous recombination based cloning and lycopene production. ΔGGAA strain constructed in Chapter 4 was used for *n*-butanol fermentation. Yeast strains were cultivated in complex medium consisting of 2% peptone and 1% yeast extract supplemented with 2% glucose (YPD) or galactose (YPG). Recombinant strains were grown on synthetic complete medium consisting of 0.17% yeast nitrogen base, 0.5% ammonium sulfate, and the appropriate amino acid drop out mix, supplemented with 2% glucose (SCD) or galactose (SCG). ΔGGAA derived recombinant yeast strains were pre-cultured in galactose medium under aerobic conditions (30ºC and 250 rpm) and inoculated to glucose medium for *n*-butanol fermentation under oxygen-limited conditions (30°C and 100 rpm) or micro-aerobic conditions (30ºC and 250 rpm with the top tightly capped). G418 (KSE Scientific, Durham, NC) and hygromycin (Roche, Indianapolis, IN) were supplemented to the growth media at specifically mentioned concentration. All restriction enzymes, Q5 polymerase, and the *E. coli*-*S. cerevisiae* shuttle vectors were purchased from New England Biolabs (Ipswich, MA). All chemicals were purchased from Sigma-Aldrich (St. Louis, MO) unless otherwise specified.

6.5.2 DNA manipulation

The yeast homologous recombination based DNA assembler method was used to construct the recombinant plasmids (28). Briefly, DNA fragments sharing homologous regions to adjacent DNA fragments were co-transformed into *S. cerevisiae* along with the linearized backbone to assemble several elements in a single step. All the recombinant plasmids constructed in this chapter are listed in Table 6.2. Wizard Genomic DNA Purification Kit (Promega, Madison, WI) was used to extract the genomic DNAs, according to the manufacturer's protocol. *HIS3*, *TRP1*, *LEU2*, *URA3*, *KanMX*, and *HygB* expression cassettes

with variable length of promoters were amplified from pRS423, pRS424, pRS425, pRS426, pUG6, and pXZ5, respectively, and then cloned into pH5 linearized by *Tth*111I (Figure 6.1). The lycopene biosynthetic pathway (*CrtE-CrtB-CrtI*) was amplified from pRS426-Zea, constructed in our previous study (28). Genes of the FPP module (*ERG10-ERG13-ERG8*-t*HMGR-ERG20-ERG12*) were amplified from *S. cerevisiae* CEN.PK2-1C genome. Upstream (rPu containing *ERG10*, cytoYl*KR*, cytoYl*HTD*, and cyto*ETR1*) and downstream (rPd containing Ec*EutE* and Ca*BdhB*) *n*-butanol biosynthetic pathways were amplified from rP34, constructed in Chapter 5. To confirm the correct clones, yeast plasmids were isolated using a Zymoprep Yeast Plasmid Miniprep II Kit (Zymo Research, Irvine, CA) and amplified in *E. coli* for verification.

6.5.3 Fluorescence intensity measurement

eGFP and mCherry fluorescence signals were measured at 488 nm-520 nm and 580 nm-620 nm, respectively, using a Biotek Synergy 2 Multi-Mode Microplate Reader (Winooski, VT). The fluorescence intensity was normalized to cell density that was determined by measuring the absorbance at 600 nm using the same microplate reader.

6.5.4 Plasmid copy number assays

Plasmid copy numbers were determined by quantitative PCR (qPCR) using the yeast total DNA extracts. As to the extraction process, 2 OD_{600} units of mid-log phase yeast culture were harvested by centrifuging at 15000 rpm for 1 min. After resuspending in 200 μL of lysis buffer (20 mM phosphate buffer at pH7.2, 1.2 M sorbitol, and 15 U Zymolase), the cells were incubated at 37°C for 20 minutes. Total DNAs were extracted from yeast cells by boiling the samples for 15 minutes, freezing at -80°C for 15 minutes, and then boiling again for another 15 minutes. After spinning at 15000 rpm for 5 min, the resulting supernatant containing the total DNA was

diluted by 10- to 100-fold and used for qPCR analysis. The ampicillin resistance gene (*Amp*^{r}) on the plasmids and *ALG9* gene on the chromosome were chosen as the target and reference genes, respectively. As for the quantification of PCNs of yeast strains containing more than one plasmid and the copy numbers of the integrated cassettes, the *KanMX* or *HygB* gene and *ALG9* gene were chosen as the target genes and reference gene, respectively. The copy numbers were quantified by comparing the C_q values of the target genes and the reference gene. qPCR was performed using LightCycler 480 SYBR Green Master on a Roche Light Cycler® 480 System (Roche).

6.5.5 Lycopene production and quantification

Lycopene producing strains were pre-cultured in SCD-HIS-URA medium for around 2 days and inoculated into SCD medium supplemented with different concentrations of hygromycin and G418 with an initial OD_{600} of 0.05. After growing into the stationary phase under aerobic conditions, 1 mL of yeast cells were collected by centrifuge at 15,000 rpm for 1 min and cell precipitates were resuspended in 1 mL of 3N HCl, boiled for 5 min, and then cooled in an ice-bath for 5 min. The cracked cells were washed with ddH_2O and resuspended in 400 μL acetone to extract lycopene. The cell debris was removed by centrifuge and the lycopene containing supernatant was analyzed for its absorbance at 472 nm using a Biotek Synergy 2 Multi-Mode Microplate Reader. Lycopene concentrations were determined by the standard curve method and normalized to cell density (dry cell weight).

6.5.6 n-*Butanol fermentation and quantification*

n-Butanol producing strains were precultured in SCG-LEU-URA medium under aerobic conditions for 2 days. For *n*-butanol fermentation under oxygen-limited condition, 200 μL seed culture was transferred into 10 mL fresh SCD medium supplemented with different

concentrations of hygromycin and G418 in a 50 mL unbaffled shaker flask; while for micro-aerobic fermentation, 200 μL seed culture was transferred into 5 mL fresh SCD medium supplemented with hygromycin and G418 in a 14 mL BD Falcon round bottom tube with the top tightly capped. Samples were taken every 24 h after inoculation until no further increase in *n*-butanol production was observed. Samples were extracted using the same volume of ethyl acetate and the top layer was analyzed by GC-MS as described in Section 4.5.4, except for the use of 100 mg/L of *2*-butanol as the internal standard.

6.5.7 Di-CRISPR

Considering the significant role of HR donors in delta integration, plasmid based donors which could be stably maintained under selection condition were designed for Di-CRISPR. To facilitate the construction of donor plasmids, two helper plasmids containing the left half (δ1) and the right half (δ2) of delta sequence with multi-cloning sites (MCSs) inserted in between (as shown in Figure 6.7B) were constructed. Then pathway of interest (rPu, rPd, or mCherry) and the engineered marker (Hyg30 or Kan20) were cloned into MCSs. The donor plasmids were based on pRS424 (TRP1 marker) and pRS426 (URA3 marker), which allowed counter-selection on 5-fluoroanthranilic acid (FAA) and 5-fluoroorotic acid (FOA) plates, respectively, to completely eliminate the donor plasmids from yeast cells. In addition, suicide sites were designed to flank the two halves of delta sequence on donor plasmids. Besides the delta sequences, crRNA arrays were designed to target the suicide sites on the donor plasmid as well. Therefore, the donor plasmids could be stably maintained during integration stage, and will be degraded and completely kicked out from the cell under non-selective and counter-selective conditions. A general protocol of Di-CRISPR was shown in Figure 6.11.

6.6 References

1. **Du J, Shao Z, Zhao H.** 2011. Engineering microbial factories for synthesis of value-added products. J. Ind. Microbiol. Biotechnol. **38:**873-890.
2. **Hong KK, Nielsen J.** 2012. Metabolic engineering of *Saccharomyces cerevisiae*: a key cell factory platform for future biorefineries. Cell Mol. Life Sci. **69:**2671-2690.
3. **Martin CH, Nielsen DR, Solomon KV, Prather KL.** 2009. Synthetic metabolism: engineering biology at the protein and pathway scales. Chem. Biol. **16:**277-286.
4. **Eriksen DT, Lian J, Zhao H.** 2014. Protein design for pathway engineering. J. Struct. Biol. **185:**234-242.
5. **Ajikumar PK, Xiao WH, Tyo KE, Wang Y, Simeon F, Leonard E, Mucha O, Phon TH, Pfeifer B, Stephanopoulos G.** 2010. Isoprenoid pathway optimization for Taxol precursor overproduction in *Escherichia coli*. Science **330:**70-74.
6. **Xu P, Gu Q, Wang W, Wong L, Bower AG, Collins CH, Koffas MA.** 2013. Modular optimization of multi-gene pathways for fatty acids production in *E. coli*. Nat. Commun. **4:**1409.
7. **Alper H, Fischer C, Nevoigt E, Stephanopoulos G.** 2005. Tuning genetic control through promoter engineering. Proc. Natl. Acad. Sci. U. S. A. **102:**12678-12683.
8. **Blazeck J, Alper HS.** 2013. Promoter engineering: recent advances in controlling transcription at the most fundamental level. Biotechnol. J. **8:**46-58.
9. **Du J, Yuan Y, Si T, Lian J, Zhao H.** 2012. Customized optimization of metabolic pathways by combinatorial transcriptional engineering. Nucleic Acids Res. **40:**e142.
10. **Pfleger BF, Pitera DJ, Smolke CD, Keasling JD.** 2006. Combinatorial engineering of intergenic regions in operons tunes expression of multiple genes. Nat. Biotechnol. **24:**1027-1032.
11. **Karim AS, Curran KA, Alper HS.** 2013. Characterization of plasmid burden and copy number in *Saccharomyces cerevisiae* for optimization of metabolic engineering applications. FEMS Yeast Res. **13:**107-116.
12. **Salis HM, Mirsky EA, Voigt CA.** 2009. Automated design of synthetic ribosome binding sites to control protein expression. Nat. Biotechnol. **27:**946-950.
13. **Dueber JE, Wu GC, Malmirchegini GR, Moon TS, Petzold CJ, Ullal AV, Prather KL, Keasling JD.** 2009. Synthetic protein scaffolds provide modular control over metabolic flux. Nat. Biotechnol. **27:**753-759.
14. **Zhang F, Carothers JM, Keasling JD.** 2012. Design of a dynamic sensor-regulator system for production of chemicals and fuels derived from fatty acids. Nat. Biotechnol. **30:**354-359.
15. **Dahl RH, Zhang F, Alonso-Gutierrez J, Baidoo E, Batth TS, Redding-Johanson AM, Petzold CJ, Mukhopadhyay A, Lee TS, Adams PD, Keasling JD.** 2013. Engineering dynamic pathway regulation using stress-response promoters. Nat. Biotechnol. **31:**1039-1046.
16. **Xu P, Li L, Zhang F, Stephanopoulos G, Koffas M.** 2014. Improving fatty acids production by engineering dynamic pathway regulation and metabolic control. Proc. Natl. Acad. Sci. U. S. A. **111:**11299-11304.
17. **Lee ME, Aswani A, Han AS, Tomlin CJ, Dueber JE.** 2013. Expression-level optimization of a multi-enzyme pathway in the absence of a high-throughput assay. Nucleic Acids Res. **41:**10668-10678.

18. **Crook NC, Schmitz AC, Alper HS.** 2014. Optimization of a yeast RNA interference system for controlling gene expression and enabling rapid metabolic engineering. ACS Synth. Biol. **3:**307-313.
19. **Si T, Luo Y, Bao Z, Zhao H.** 2015. RNAi-assisted genome evolution in *Saccharomyces cerevisiae* for complex phenotype engineering. ACS Synth. Biol. **4:**283-291.
20. **Williams TC, Averesch NJ, Winter G, Plan MR, Vickers CE, Nielsen LK, Kromer JO.** 2015. Quorum-sensing linked RNA interference for dynamic metabolic pathway control in *Saccharomyces cerevisiae*. Metab. Eng. **29:**124-134.
21. **Leavitt JM, Alper HS.** 2015. Advances and current limitations in transcript-level control of gene expression. Curr. Opin. Biotechnol. **34C:**98-104.
22. **Chen Y, Partow S, Scalcinati G, Siewers V, Nielsen J.** 2012. Enhancing the copy number of episomal plasmids in *Saccharomyces cerevisiae* for improved protein production. FEMS Yeast Res. **12:**598-607.
23. **Erhart E, Hollenberg CP.** 1983. The presence of a defective *LEU2* gene on 2μ DNA recombinant plasmids of *Saccharomyces cerevisiae* is responsible for curing and high copy number. J. Bacteriol. **156:**625-635.
24. **Okkels JS.** 1996. A URA3-promoter deletion in a pYES vector increases the expression level of a fungal lipase in *Saccharomyces cerevisiae*. Ann. N. Y. Acad. Sci. **782:**202-207.
25. **Kazemi Seresht A, Norgaard P, Palmqvist EA, Andersen AS, Olsson L.** 2013. Modulating heterologous protein production in yeast: the applicability of truncated auxotrophic markers. Appl. Microbiol. Biotechnol. **97:**3939-3948.
26. **Bao Z, Xiao H, Liang J, Zhang L, Xiong X, Sun N, Si T, Zhao H.** 2014. Homology-Integrated CRISPR-Cas (HI-CRISPR) System for One-Step Multigene Disruption in *Saccharomyces cerevisiae*. ACS Synth. Biol.**:**DOI: 10.1021/sb500255k.
27. **Ro DK, Paradise EM, Ouellet M, Fisher KJ, Newman KL, Ndungu JM, Ho KA, Eachus RA, Ham TS, Kirby J, Chang MC, Withers ST, Shiba Y, Sarpong R, Keasling JD.** 2006. Production of the antimalarial drug precursor artemisinic acid in engineered yeast. Nature **440:**940-943.
28. **Shao Z, Zhao H, Zhao H.** 2009. DNA assembler, an *in vivo* genetic method for rapid construction of biochemical pathways. Nucleic Acids Res. **37:**e16.
29. **Doudna JA, Charpentier E.** 2014. Genome editing. The new frontier of genome engineering with CRISPR-Cas9. Science **346:**1258096.
30. **Lee FW, Da Silva NA.** 1997. Improved efficiency and stability of multiple cloned gene insertions at the δ sequences of *Saccharomyces cerevisiae*. Appl. Microbiol. Biotechnol. **48:**339-345.
31. **Lee FW, Da Silva NA.** 1997. Sequential δ-integration for the regulated insertion of cloned genes in *Saccharomyces cerevisiae*. Biotechnol. Prog. **13:**368-373.
32. **Shi S, Valle-Rodriguez JO, Siewers V, Nielsen J.** 2014. Engineering of chromosomal wax ester synthase integrated *Saccharomyces cerevisiae* mutants for improved biosynthesis of fatty acid ethyl esters. Biotechnol. Bioeng. **111:**1740-1747.
33. **Lu X.** 2010. A perspective: photosynthetic production of fatty acid-based biofuels in genetically engineered cyanobacteria. Biotechnol. Adv. **28:**742-746.
34. **Ageitos JM, Vallejo JA, Veiga-Crespo P, Villa TG.** 2011. Oily yeasts as oleaginous cell factories. Appl. Microbiol. Biotechnol. **90:**1219-1227.
35. **Tyo KE, Ajikumar PK, Stephanopoulos G.** 2009. Stabilized gene duplication enables long-term selection-free heterologous pathway expression. Nat. Biotechnol. **27:**760-765.

6.7 Tables

Table 6.1 Copy numbers of *Kan20* cassette integrated to the chromosome under different selection pressure (G418 concentrations).

	25 mg/L	100 mg/L	400 mg/L
Clone 1	0.86	1.10	33.13
Clone 2	1.02	14.83	28.25
Clone 3	0.96	1.06	28.47

Table 6.2 Plasmids constructed in this chapter

Plasmids	Description
pRS413	*HIS3* marker with CEN/ARS4 origin
pRS416	*URA3* marker with CEN/ARS4 origin
pRS423	*HIS3* marker with 2 Micron origin
pRS424	*TRP1* marker with 2 Micron origin
pRS425	*LEU2* marker with 2 Micron origin
pRS426	*URA3* marker with 2 Micron origin
pH5	pRS425-*TEF1p-eGFP-TEF1t*
HIS-CEN	pRS413-*TEF1p-eGFP-TEF1t*
HIS-WT	pH5-*HIS3(*WT*)p-HIS3-HIS3t*
HIS100	pH5-*HIS3(*100bp*)p-HIS3-HIS3t*
HIS50	pH5-*HIS3(*50 bp*)p-HIS3-HIS3t*
HIS30	pH5-*HIS3(*30 bp*)p-HIS3-HIS3t*
HIS20	pH5-*HIS3(*20 bp*)p-HIS3-HIS3t*
TRP-WT	pH5-*TRP1(*WT*)p-TRP1-TRP1t*
TRP100	pH5-*TRP1(*100 bp*)p-TRP1-TRP1t*
TRP50	pH5-*TRP1(*50 bp*)p-TRP1-TRP1t*
TRP30	pH5-*TRP1(*30 bp*)p-TRP1-TRP1t*
TRP20	pH5-*TRP1(*20 bp*)p-TRP1-TRP1t*
LEU-WT (pH5)	p*LEU2(*WT*)p-LEU2-LEU2t-TEF1p-eGFP-TEF1t*
LEU100	p*LEU2(*100 bp*)p-LEU2-LEU2t-TEF1p-eGFP-TEF1t*
LEU50	p*LEU2(*50 bp*)p-LEU2-LEU2t-TEF1p-eGFP-TEF1t*
LEU30	p*LEU2(*30 bp*)p-LEU2-LEU2t-TEF1p-eGFP-TEF1t*
URA-WT	pH5-*URA3(*WT*)p-URA3-URA3t*
URA100	pH5-*URA3(*100 bp*)p-URA3-URA3t*
URA50	pH5-*URA3(*50 bp*)p-URA3-URA3t*
URA30	pH5-*URA3(*30 bp*)p-URA3-URA3t*
URA15	pH5-*URA3(*15 bp*)p-URA3-URA3t*
URA-CEN-R	pRS416-*TEF1p-mCherry-TEF1t*
URA-WT-R	URA-WT with *eGFP* replaced by *mCherry*
URA100-R	URA100 with *eGFP* replaced by *mCherry*
URA50-R	URA50 with *eGFP* replaced by *mCherry*
URA30-R	URA30 with *eGFP* replaced by *mCherry*
URA15-R	URA15 with *eGFP* replaced by *mCherry*
KanWT	pH5-Ag*TEF1(*WT*)p-KanMX*-Ag*TEF1t*
Kan100	pH5-Ag*TEF1(*100 bp*)p-KanMX*-Ag*TEF1t*
Kan50	pH5-Ag*TEF1(*50 bp*)p-KanMX*-Ag*TEF1t*
Kan30	pH5-Ag*TEF1(*30 bp*)p-KanMX*-Ag*TEF1t*
Kan20	pH5-Ag*TEF1(*20 bp*)p-KanMX*-Ag*TEF1t*
HygWT	pH5-*HXT7(*WT*)p-HygB-FBA1t*
Hyg100	pH5-*HXT7(*100 bp*)p-HygB-FBA1t*
Hyg50	pH5-*HXT7(*50 bp*)p-HygB-FBA1t*
Hyg30	pH5-*HXT7(*30 bp*)p-HygB-FBA1t*
Hyg20	pH5-*HXT7(*20 bp*)p-HygB-FBA1t*

Table 6.2 (cont.)

Plasmids	Description
Kan20-R	Kan20 with *eGFP* replaced by *mCherry*
pRS426-Zea	pRS426-*CrtE-CrtB-CrtI-CrtY-CrtZ*
FPP	pRS423-*Hyg30-ERG10-ERG13-ERG8-tHMGR-ERG20-ERG12*
Lyc	pRS426-*Kan20-CrtE-CrtB-CrtI*
rP34	pRS426-*ERG10*-cytoYl*KR*-cyto*ETR1*-cytoYl*HTD*-Ec*EutE*-Ca*BdhB*
rPu	pRS426-*Hyg30-ERG10*-cytoYl*KR-cytoETR1*-cytoYl*HTD*
rPd	pRS425-*Kan20*-Ec*EutE*-Ca*BdhB*
DiH1	pRS424-suicide1-δ1-MCS-δ2-suicide2
DiH2	pRS426-suicide1-δ1-MCS-δ2-suicide2
Di-rPu	pRS424-δ1-*Hyg30-ERG10*-cytoYl*KR-cytoETR1*-cytoYl*HTD*-δ2
Di-rPd	pRS426-δ1-*Kan20*-Ec*EutE*-Ca*BdhB*-δ2
pCRCT	p*URA3(*47bp*)p-URA3-SNR52p-crRNA-TEF1p-iCas9-RPR1p-tracrRNA*
pLH-CRCT	pCRCT with URA3 marker replaced with LEU2 and HIS30
Di-CRISPR	crRNA(delta)-crRNA(suicide) inserted into pLH-CRCT

6.8 Figures

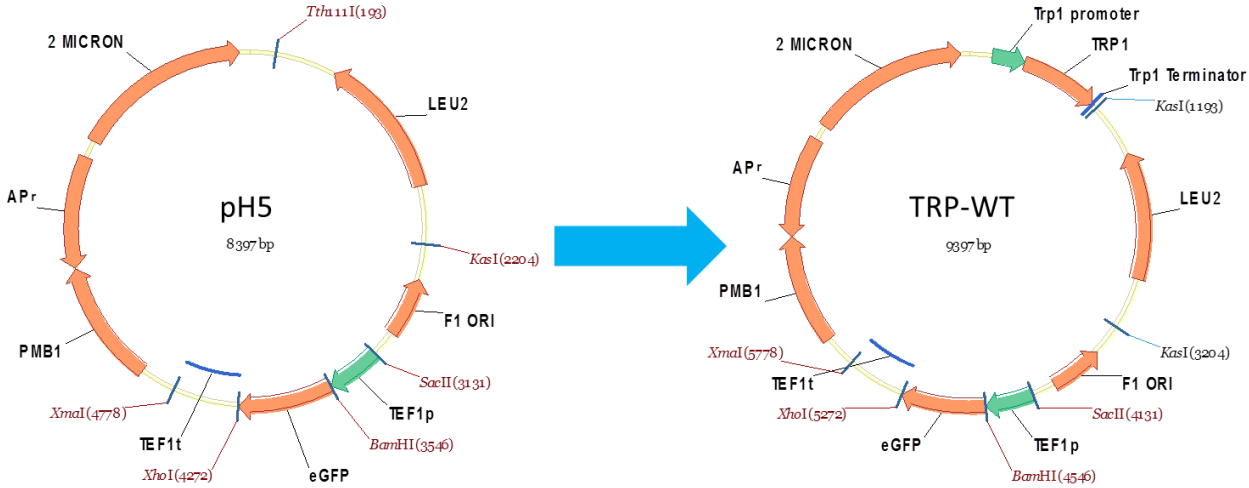

Figure 6.1 Development of an eGFP reporter system for quantification of plasmid copy numbers (PCNs). *HIS3*, *TRP1*, *LEU2*, *URA3*, *KanMX*, and *HygB* expression cassettes with variable length of promoters were inserted into the *Tth*111I site via DNA assembler.

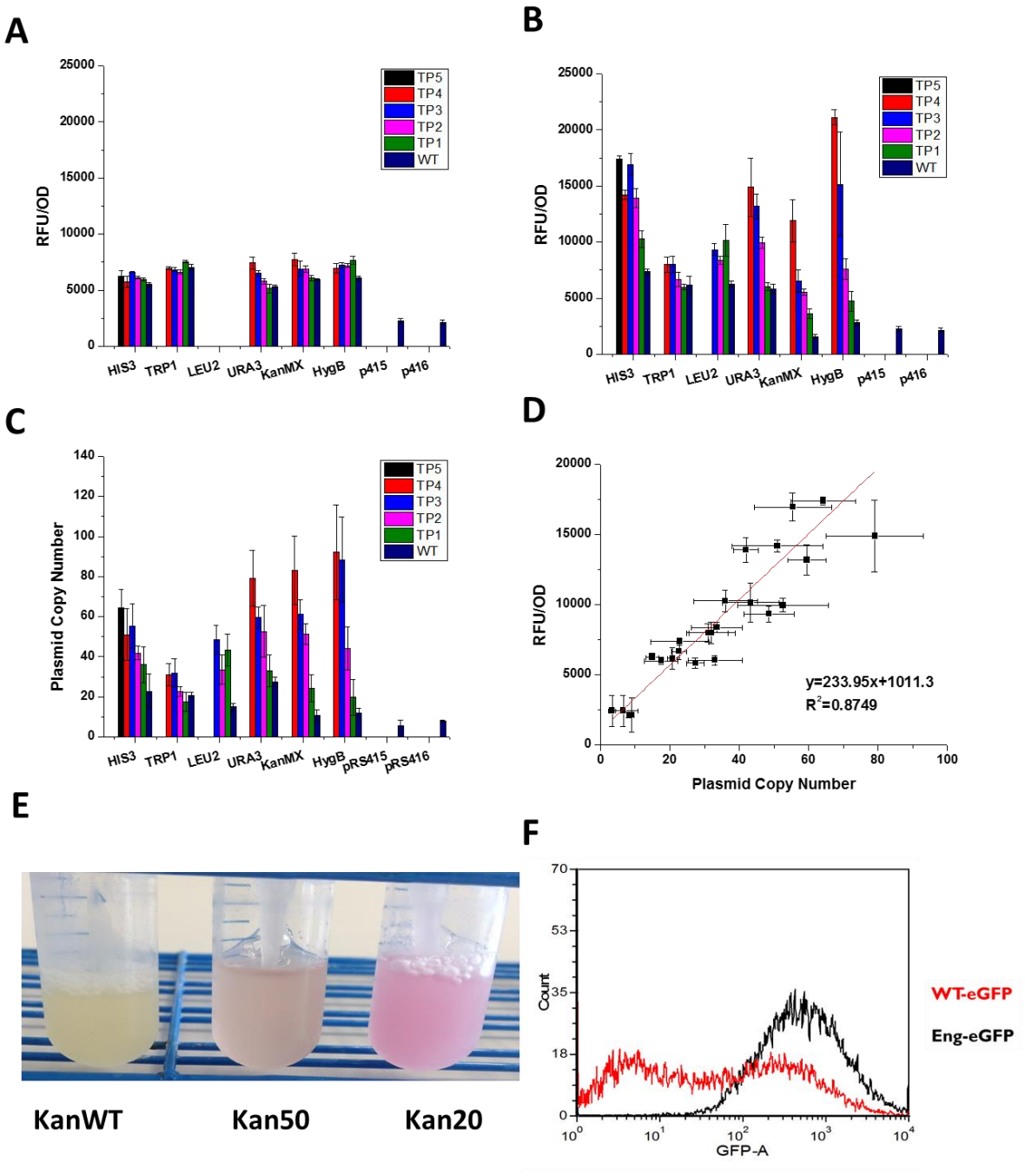

Figure 6.2 Systematic evaluation of promoter truncations on PCNs. Fluorescence intensity of plasmids with different level of promoter truncations cultured in non-selective media (cloning media, A) and selective media (B).PCNs of the engineered plasmids on selective media was quantified by qPCR (C). The use of eGFP as a reporter of PCNs was confirmed by their strong linear correlation (D). The effects of promoter truncation on PCNs could be seen by naked eyes (E) and flow cytometry (F).

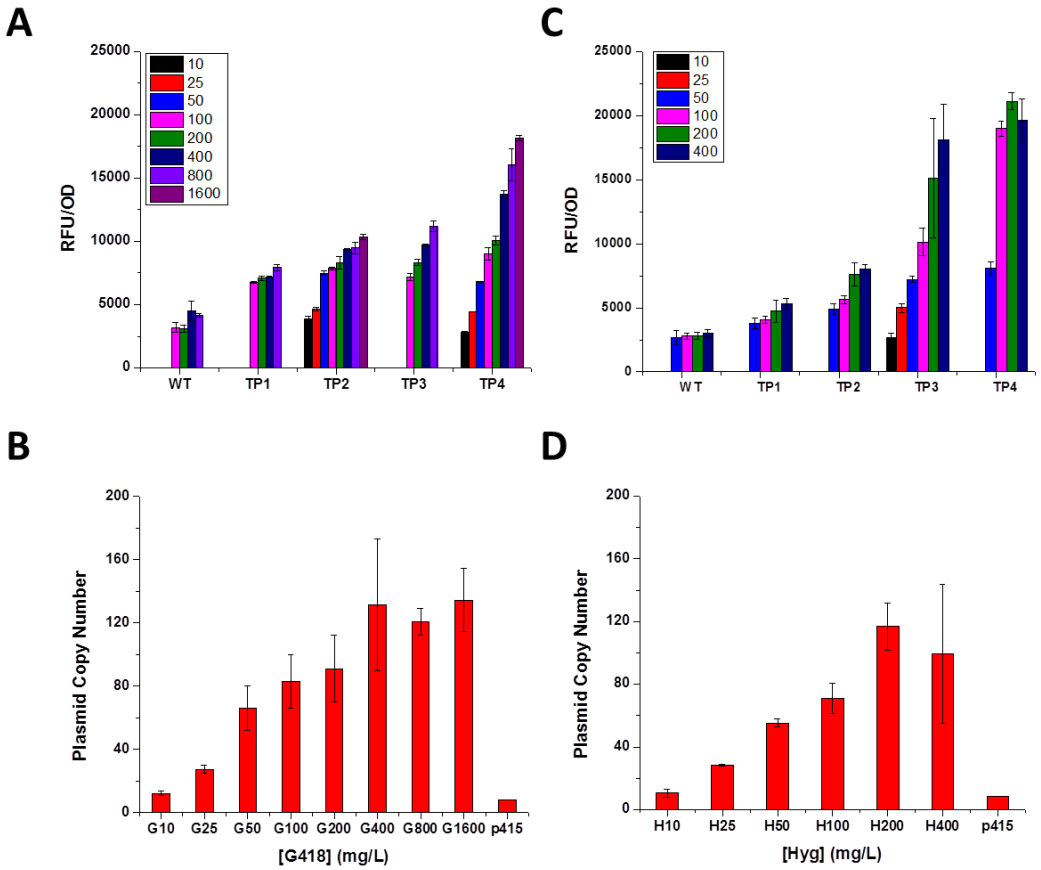

Figure 6.3 Dose dependence of PCNs with KanMX (A and B) and HygB (C and D) markers. Plasmids with different levels of truncation showed variable sensitivity to antibiotic concentration (A and C). TP4 and TP3 worked the best for KanMX and HygB, respectively, whose PCNs were quantified by qPCR (B and D).

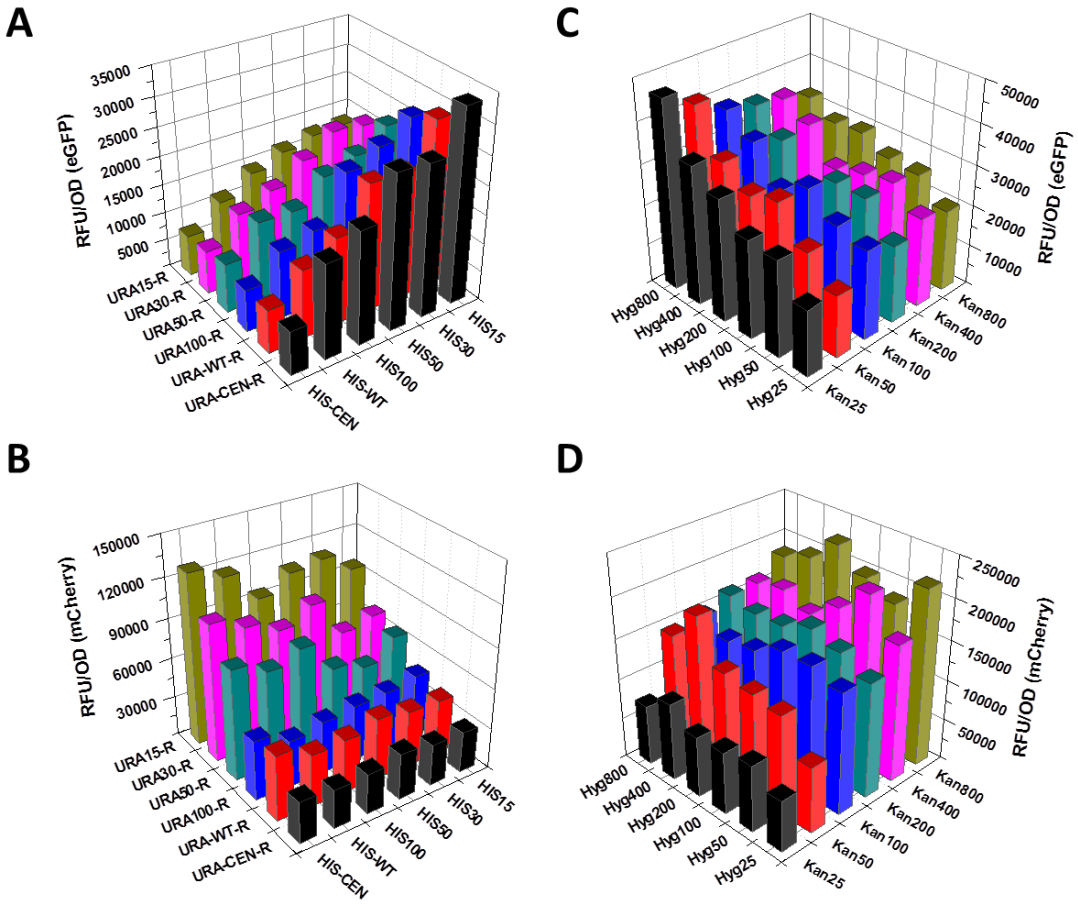

Figure 6.4 Demonstration of iPOAD using fluorescent proteins. iPOAD could be achieved by using either multi plasmids containing auxotrophic markers with different degrees of promoter truncations (A and B) or a single plasmid containing dominant markers with different antibiotic concentrations (C and D). The fluorescence intensities of eGFP (A and C) and mCheery (B and D) were distributed as expected.

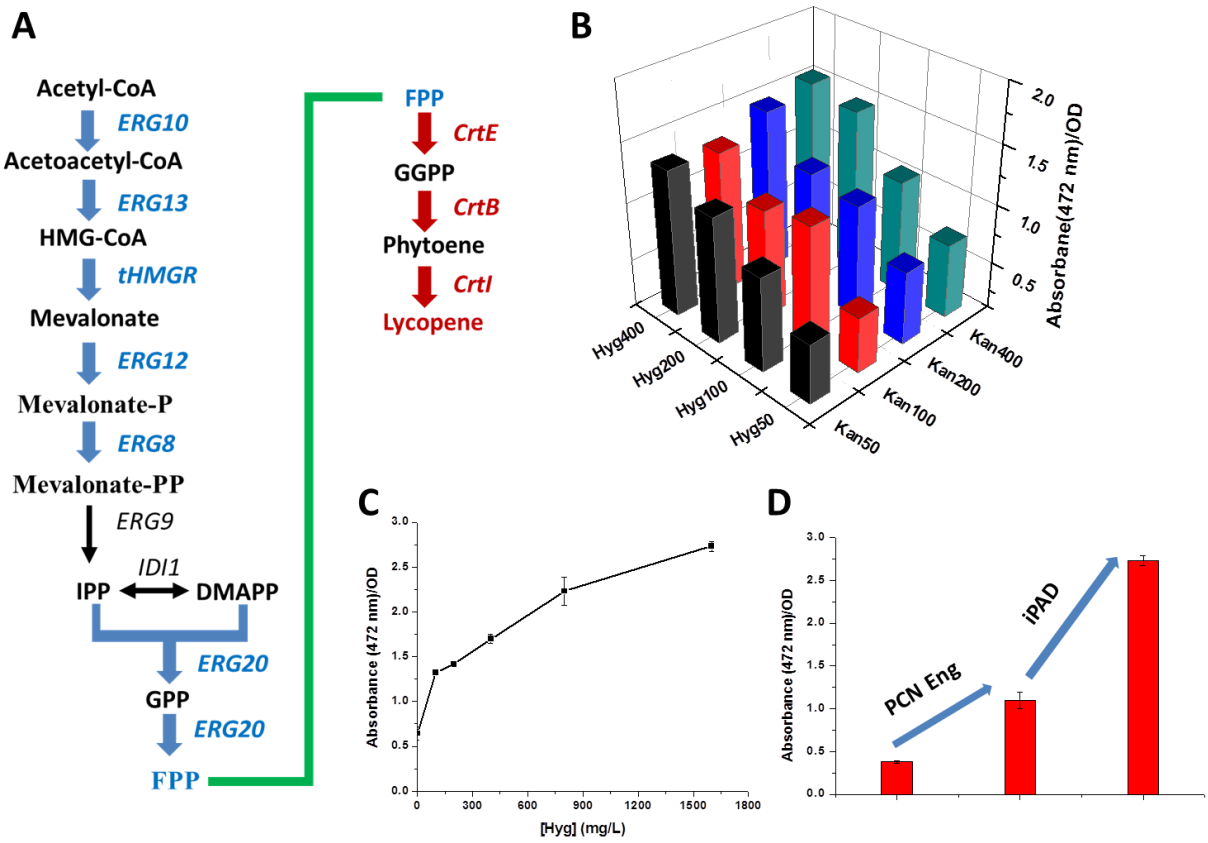

Figure 6.5 iPOAD for lycopene biosynthesis. A) The multi-gene lycopene biosynthesis pathway was divided into two modules, the FPP module (blue) and Lyc module (red). B) Optimization of lycopene production by testing combination of G418 and hygromycin concentrations. C) Further improvement of lycopene production by increasing the concentration of hygromycin. D) A summary of the engineering efforts to increase lycopene production.

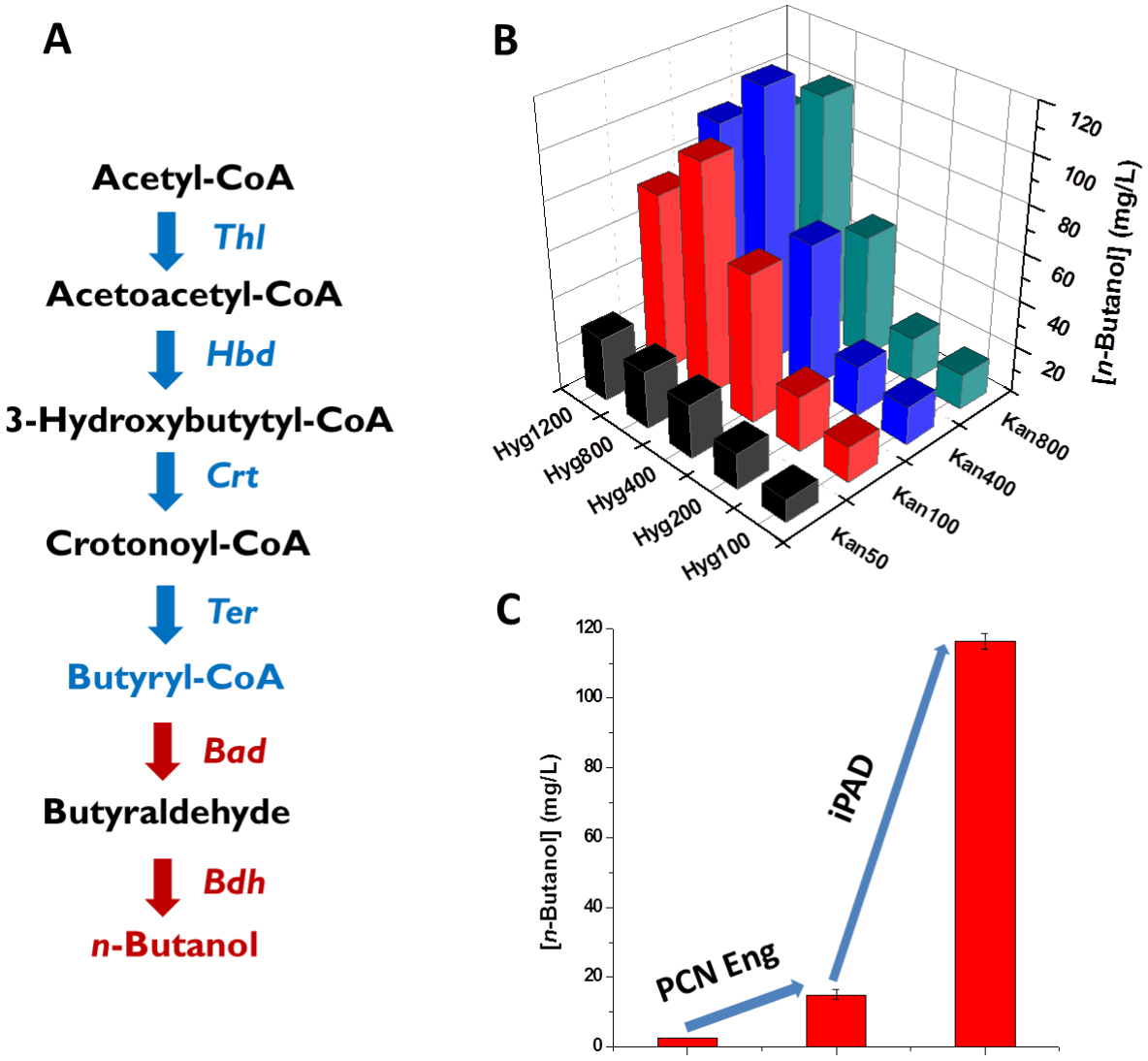

Figure 6.6 iPOAD for *n*-butanol production. A) The multi-gene *n*-butanol biosynthesis pathway was divided into two modules, the upstream module (blue) and the downstream module (red). B) Optimization of *n*-butanol production by testing combination of G418 and hygromycin concentrations. C) A summary of the engineering efforts to increase lycopene production.

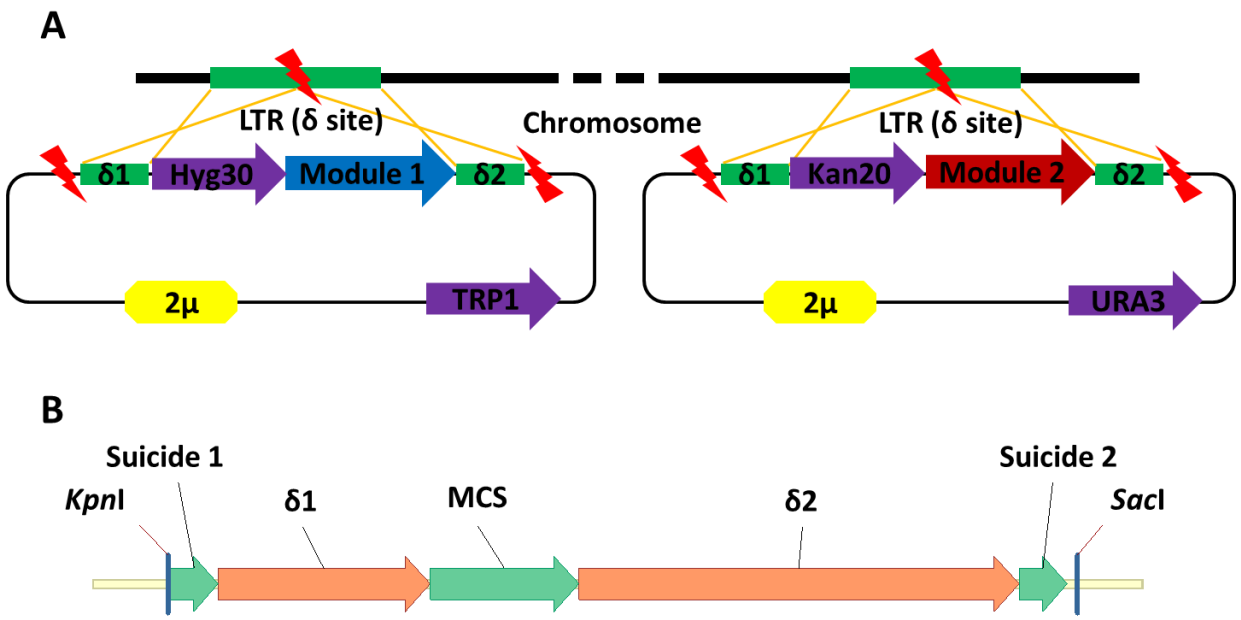

Figure 6.7 Design of Di-CRISPR. A) Multiplex pathway integration into the delta sites was achieved by taking advantage of the CRISPR-Cas9 technology to introduce a double strand break on the chromosome. To supply the HR donors for delta integration continuously, plasmid-based donors were designed, which allowed to be completely removed from yeast cells by Cas9 cutting and counter selection. B) The design of helper plasmids to facilitate the construction of donor plasmids.

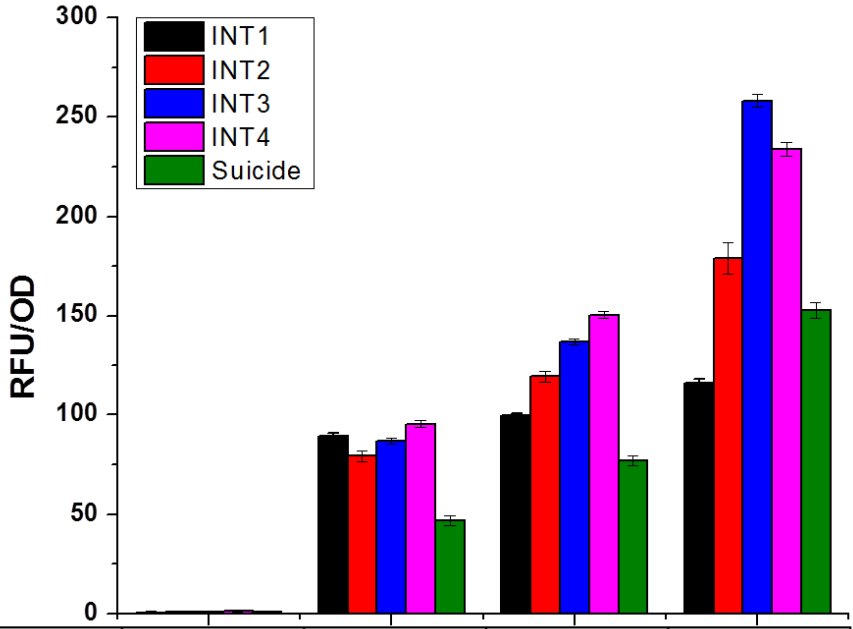

Donor Plasmid	-	+	+	+
crRNA	-	-	+	+
Cas9-tracrRNA	-	+	+	+
Copy number of Di-CRISPR	-	-	**High**	**Super-high**

Figure 6.8 Optimization of Di-CRISPR using a fluorescent protein.

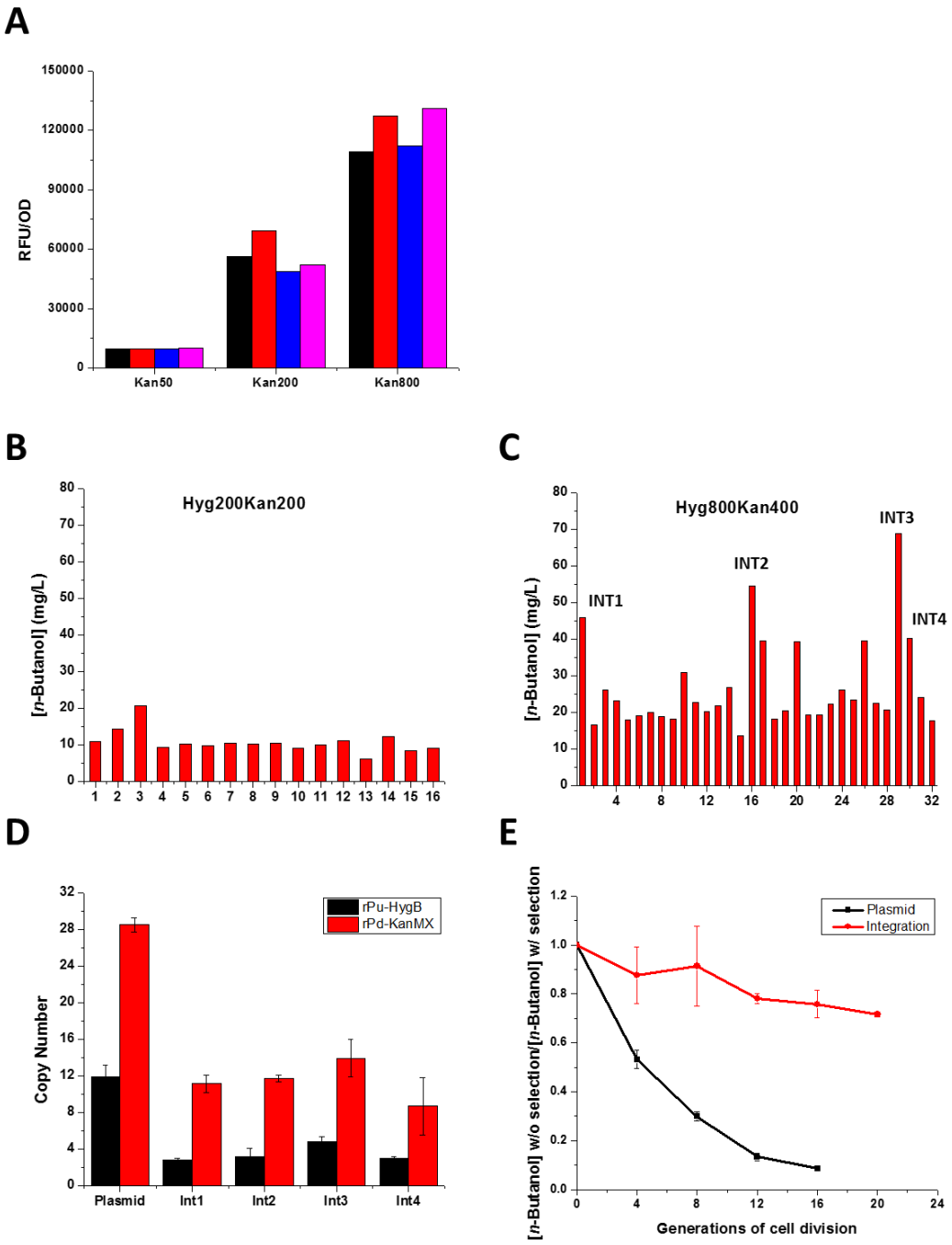

Figure 6.9 Dose-dependence of the copy numbers of the chromosomally integrated cassettes, including mCherry (A) and *n*-butanol biosynthetic pathway (B and C). Colonies were randomly picked up from the Di-CRISPR library with different selection pressures (antibiotic concentrations) and characterized for their fluorescence intensities (A) or *n*-butanol production levels (B and C). D) The copy numbers of the upstream module (rPu) and downstream module (rPd) on both plasmids and chromosomes, which were obtained under the same selection pressure, were determined by qPCR. E) Compared with the plasmid containing strain, the integration strain showed much higher stability under no selection pressure condition.

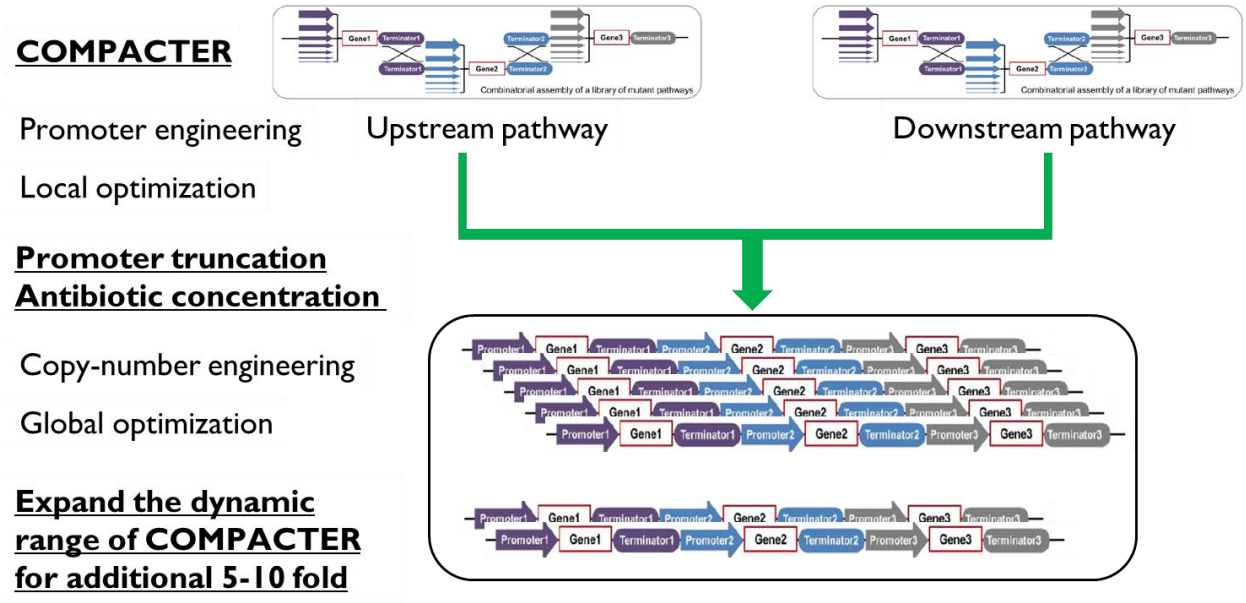

Figure 6.10 Combination of iPOAD and COMPACTER for the optimization of long biosynthetic pathways. The combined strategy shows advantages of expanding the dynamic range of pathway optimization tools and achieving global optimization of the desired biosynthetic pathway.

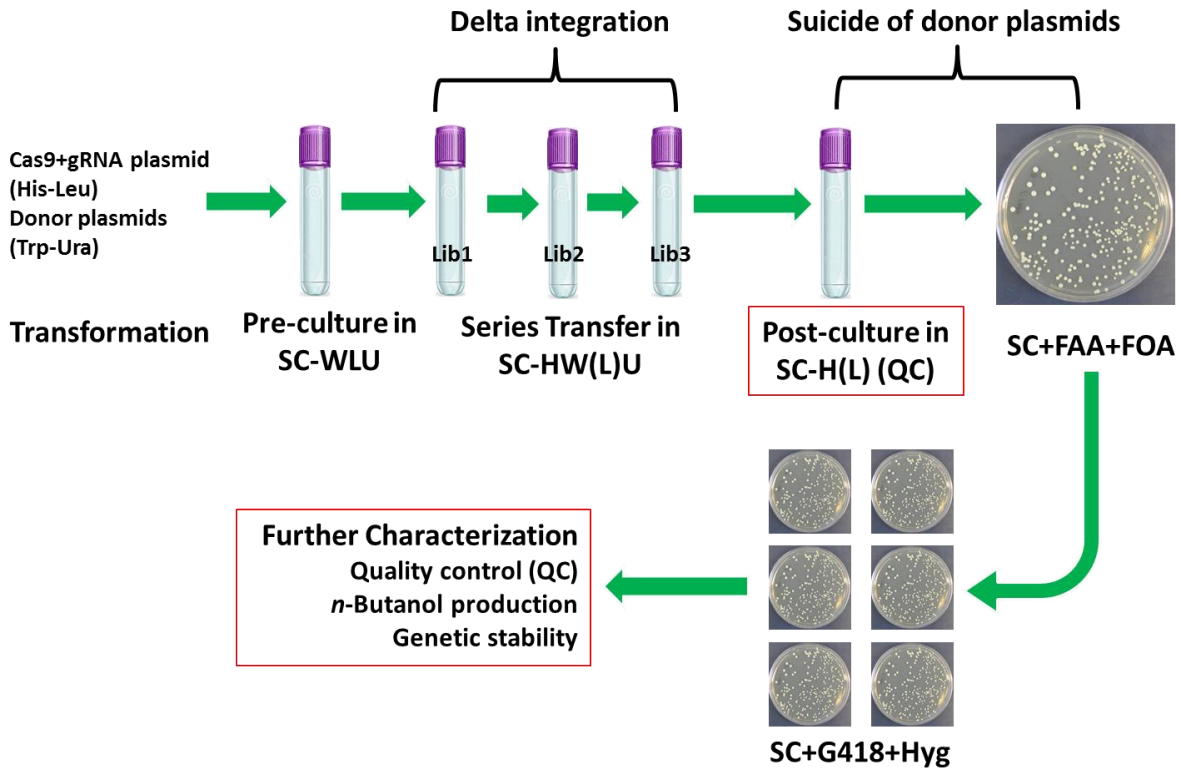

Figure 6.11 Protocol of Di-CRISPR for multiplex integration of long pathways. Cas9 plasmid and donor plasmids were co-transformed into ΔGGAA strain, and the resultant recombinant strain was pre-cultured in SC-WLU containing 10 g/L galactose for 2 days. Then 100 μL culture was transferred to fresh SC-HW(L)U containing 20 g/L galactose to increase the copy number of the Cas9 plasmid for efficient delta integration. After three serial transfers, the yeast cells were transferred to SC-H(L) containing 20 g/L galactose to suicide the donor plasmids. To completely eliminate the donor plasmids, yeast cells were spread into plates containing both FAA and FOA. Then the cells were collected and re-spread into plates containing different concentrations of G418 and hygromycin. Quality control (QC) was performed as indicated to confirm the elimination of donor plasmids.